Firth of Thames water quality and ecosystem health

Waikato
REGIONAL COUNCIL
Te Kaunihera ā Rohe o Waikato

Peer reviewed by:
Hilke Giles (WRC)
Pete Wilson (WRC)
Tom Stephens (DairyNZ)
David Burger (DairyNZ)   Date   June 2015

Approved for release by:
Dominique Noiton   Date   August 2015

Preface

This technical report describes the current state of knowledge on the environmental state of the Firth of Thames and identifies information gaps. It provides critical information required for effective decision-making on the future management of the Firth of Thames. It also provides valuable, scientifically robust, information for communities, stakeholders and iwi.

This technical report was commissioned following an independent yet coinciding requirement by Waikato Regional Council and DairyNZ to obtain an agreed baseline of understanding of the water quality and ecological health of the Firth of Thames. It was co-funded by Waikato Regional Council, DairyNZ and the National Institute of Water and Atmospheric Research (NIWA). While it focuses primarily on data collected and owned by NIWA, it also refers to some data sets held by other agencies.

This technical report is divided into two parts: Synthesis Report and Data Report.

The Synthesis Report presents key findings on water quality and ecosystem health in relation to sediment loading, nutrient loading, phytoplankton dynamics, dissolved oxygen dynamics and pH variability. It also identifies information gaps and priorities for future work that will enable more comprehensive assessments of water quality and ecosystem health of the Firth of Thames to be made in the future. All statements in the Synthesis Report are underpinned by data presented in the Data Report.

The Synthesis Report may be cited independently as:

> Green, M. and Zeldis, J. (2015) Firth of Thames Water Quality and Ecosystem Health – A Synthesis. NIWA Client Report No. HAM2015-016, prepared for Waikato Regional Council and DairyNZ.

The Data Report describes the data underpinning the Synthesis Report. It presents a description of available data sets and brief descriptions of the data and analyses that support the findings presented in the Synthesis Report. Some additional data are presented in the Data Report that are not presented in the Synthesis Report. This is to provide additional context and a comprehensive overview of available data. The Data Report does not attempt to discuss the ecological significance of the data or provide detailed interpretation of the results as this is presented in the Synthesis Report.

The Data Report may be cited independently as:

> Zeldis, J. et al. (2015) Firth of Thames Water Quality and Ecosystem Health – Data Report. NIWA Client Report No. CHC2014-123, prepared for Waikato Regional Council and DairyNZ.

Firth of Thames Water Quality and Ecosystem Health

A Synthesis

Prepared for Waikato Regional Council
and DairyNZ under separate contracts

April 2015

Prepared by:
Malcolm Green
John Zeldis

For any information regarding this report please contact:

Malcolm Green
Principal Scientist
Coastal and Estuarine Processes
+64-7-856 1747
malcolm.green@niwa.co.nz

National Institute of Water & Atmospheric Research Ltd
PO Box 11115
Hamilton 3251

Phone +64 7 856 7026

Quality Assurance Statement		
☐ Broekhuis	Reviewed by:	Niall Broekhuizen
☐	Formatting checked by:	Aarti Wadhwa
☐	Approved for release by:	Bryce Cooper

Contents

Key points

- Place names used in this report: the Firth of Thames, the extended Firth of Thames, and the Hauraki Gulf. The red triangle shows the location of the extended-Firth monitoring site.

Physical setting

- The Firth of Thames is an estuarine embayment occupying the Hauraki Depression bounded to the east and west by the Coromandel and Hunua Ranges, respectively.

- Prior to human habitation the Hauraki Plains was mainly native forest-clad. It is largely cleared of native forest today and dominated by agricultural landuse.

- The Firth receives runoff primarily from the Waihou River and the Piako River, which drain the Hauraki Plains.

- Tidal and wind-driven currents, mixing, and stratification are important hydrodynamic processes that influence all biogeochemical processes in the Firth of Thames and the wider Hauraki Gulf.

Sediments

- Fine sediments have already impaired and continue to affect ecosystem health in the Firth of Thames.

- Land clearance prior to the conversion of the Hauraki Plains for agriculture contributed much of the fine sediment in the Firth of Thames today.

- Present-day inputs of sediment from the Waihou and Piako Rivers account for only 40% of the estimated 430,000 t y-1 of sediment currently depositing in the southern Firth of

Thames. The apparent discrepancy is likely to be due to the reworking by waves and currents of legacy sediments deposited in the Firth during large-scale deforestation and mining activities that occurred during the late 1800s to early 1900s.

- Sediments are now accumulating at rates 2–10 times greater than 90 years earlier.

- Monitoring of intertidal regions of the southern Firth of Thames indicates little ongoing change to benthic fauna from changes to seabed mud content over the last decade.

Nutrients

- There are both oceanic and land sources of nitrogen to the Firth of Thames.

- At least when there is no strong ocean upwelling (which is the case for about 90% of the time), inputs from the land are the dominant source to the total nutrient loading of the Firth of Thames.

- Nitrogen loads in rivers draining to the Firth have been stable or increasing only slowly for at least 20 years, whilst phosphorus loads have reduced.

- Dissolved inorganic nitrogen and dissolved organic nitrogen at the extended-Firth monitoring site have increased over the past 15 years. Dissolved inorganic phosphorus has not changed but dissolved organic phosphorus has reduced over the past 15 years.

- The upward trend in nutrient runoff from the Waihou River is not large enough to fully explain the upward trend in nitrogen at the extended-Firth monitoring site. This points to a complex set of causes, possibly including changes to oceanic inputs, terrestrial inputs, physical oceanography and/or denitrification efficiency.

- Further work is needed to determine the nature and causes of the observed change in nitrogen levels within the extended Firth, including whether this is more widespread and continuing.

Phytoplankton and bacteria

- There is more phytoplankton in the Firth than in the extended Firth. Both of these areas contain more phytoplankton than the wider Hauraki Gulf. Primary production rates follow a similar pattern.

- Nitrogen from the land is one factor responsible for the higher phytoplankton levels in the Firth. Other factors are oceanic sources of nitrogen and physical processes such as mixing and water-column stratification that enhance phytoplankton production through effects on nutrient and light availability.

- Phytoplankton abundance and, to a lesser extent, biomass at the extended-Firth monitoring site have increased over the past 15 years. These changes are consistent with the trend in nitrogen at the extended-Firth monitoring site over the same period.

- Phytoplankton composition has also changed, resulting in more small phytoplankton and more large diatoms.

- The decay of phytoplankton and bacterial respiration are linked to seasonal oxygen depletion and pH depression.

Dissolved Oxygen

- The available data show that the Firth of Thames is generally well oxygenated.

- There are seasonal (autumnal) low-oxygen (60–70% saturation) events in the bottom waters at the extended-Firth monitoring site. These events occasionally penetrate into the upper water column and shoreward into the Firth.

- At least two different processes are likely to be contributing to the low-oxygen events in the bottom waters at the extended Firth of Thames: upwelling of high-salinity, low-oxygen cold water from offshore, and the mineralisation of organic matter in the water column, which consumes oxygen. We believe that latter to be the dominant driver of the autumnal DO decline.

pH

- pH has only been measured in the extended Firth of Thames since 2009, which limits our understanding of long-term change.

- Seasonal patterns indicate a pH minimum of 7.9 during autumn low-oxygen events, rising to pH 8.1 in spring.

Assessments of water quality and ecosystem health

The available information allows us to draw the following conclusions:

- Fine sediments in the Firth of Thames are largely the legacy of past human activities. As a result there are limited opportunities to mitigate sediment effects.

- The almost-complete collapse by the late 1960s of hard, biogenic reefs in the Firth composed of bivalves, sponges, ascidians, bryozoans and cnidarians, has been well documented. The modern sediment macrobenthic community of the Firth of Thames is adapted to the muddier post-reef-collapse conditions and is likely to be quite resilient to ongoing deposition of fine sediment.

- Even if catchment sediment inputs were to be turned off instantly, the prospects for a natural recovery of the Firth benthic ecosystem to a pre-reef-collapse state would be slim.

- The Firth and the extended Firth are sensitive to nutrient enrichment, meaning that symptoms of eutrophication are not likely to be suppressed by physical factors (such as turbid water/low light, short water residence time, and strong vertical mixing of the water column).

- The Firth and the extended Firth are now mesotrophic.

- The Firth of Thames will at least have been "less mesotrophic" prior to catchment deforestation and subsequent development in the catchment. Some simple figuring suggests the Firth may have been oligotrophic.

- Ocean-side loading prior to the historical land clearance and development of the Hauraki Plains was likely to have contributed a much larger percentage to a much lower overall nutrient load to the Firth.

- Denitrification is likely to be an important ecosystem service in the Firth that reduces the risk of eutrophication.

- A reduction in land-side nutrient inputs will reduce the organic-matter load of the Firth and the consequent oxygen depletion that occurs in the extended Firth towards the end of the phytoplankton growth season (late summer to early autumn).

- However, we cannot yet make any quantitative predictions of what changes might ensue following any specific reduction in land-side nutrients.

- Without a return to the former sediment macrobenthic community a full recovery to the pre-catchment-development pattern of nutrient cycling and water quality in the Firth seems unlikely.

The data are not available to make a full assessment of water quality and ecosystem health. This report identifies gaps and priorities for future work that will enable more comprehensive assessments to be made in the future.

Executive summary

Waikato Regional Council and DairyNZ share questions around water quality in the Firth of Thames. The questions relate to sediments, nutrients, phytoplankton/bacteria, dissolved oxygen and pH (acidification).

The objective of this report is to assess, where possible, the water quality and ecological health of the Firth of Thames, identify information gaps and recommend priorities for future work.

This report is complemented by a data report (Zeldis et al., 2015, NIWA Client Report No. CHC2014-123, prepared for Waikato Regional Council and DairyNZ), which describes the data that NIWA has collected in the Firth of Thames and Hauraki Gulf over the last 20 years.

Geographic zones

- Place names used in this report: the Firth of Thames, the extended Firth of Thames, and the Hauraki Gulf. The red triangle shows the location of the extended-Firth monitoring site.
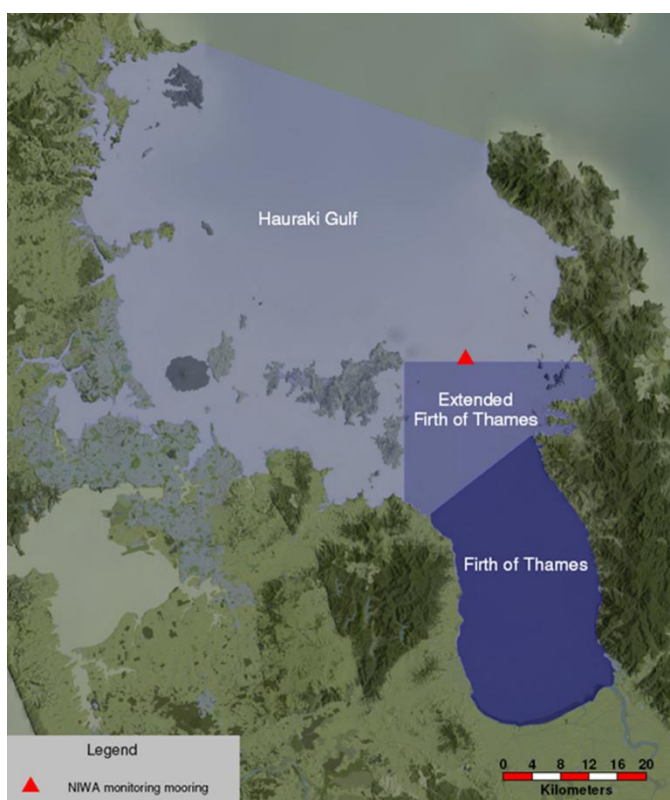
Sediments

- Intertidal flats in the southern Firth have been accreting for the last 90 years at rates that are an order of magnitude greater than rates that have been observed in intertidal regions of other North Island estuaries.

- Accumulation of mud has permitted widespread mangrove expansion.

- Intertidal flats appear to be accreting "legacy" sediments that are being transported shoreward from the subtidal zone by waves and currents.

- Needham et al.'s (2014) review of the inner Firth's intertidal benthic macrofauna and surface sediment concluded there was no evidence of ecologically significant changes to either sediment characteristics or indicator taxa over the past 10 years of monitoring.

- The inner, subtidal Firth is depauperate in macrofauna and infauna relative to the central Firth. The most likely reason for this is that the inner Firth is muddier.

Nutrients

- 15 years of measurements at the extended-Firth monitoring site show that dissolved inorganic nitrogen (DIN; the sum of nitrate and ammonium) is abundant in the upper water column only during winter and spring. The most likely reason is that uptake of DIN by primary production is limited by low light at those times. In summer and autumn, when there is plenty of light, DIN in the upper water column is drawn down, which is most likely because of uptake by primary production.

- Over the 15-year measurement period, DIN integrated over the water column increased at a rate of about 5% y^{-1}.

- We looked at possible reasons for the trend in DIN. One candidate was that the upwelling regime has changed (upwelling, driven by westerly winds, brings cool, nutrient-laden oceanic water onto the shelf), however a preliminary analysis yielded no evidence for that. Another possibility was that there has been a change in the nutrient runoff from the land. There does not appear to have been a sufficient upward trend in nutrient runoff from the Waihou River to fully explain the upward trend in nitrogen at the extended-Firth monitoring site.

- A possible contributor to the trend in nitrogen at the extended-Firth monitoring site is that there has been a change in denitrification efficiency, caused by increased organic matter loading to the seabed, and resulting in a decreased capacity of the system to vent nitrogen to the atmosphere.

- We view our analysis of the water-column-integrated data as only a first step towards identifying and understanding trends. The nutrient data exhibit vertical structure over the water column, which is lost by depth-integrating the data.

Phytoplankton and bacteria

- Phytoplankton biomass is generally greatest in spring and least in winter. Biomass is widely distributed in spring, but becomes progressively restricted to inshore areas (especially the Firth) from summer through winter. In the extended Firth, biomass is greatest in the upper water column in spring, but increases noticeably at depth in autumn. Primary production rates follow a similar pattern.

- Chlorophyll *a* and phaeopigment in the lower water column (greater than 20 m below the water surface) at the extended-Firth monitoring site increased over a 15-year monitoring period. There was no trend for chlorophyll *a* or phaeopigment in the upper water column (down to 20 m below the water surface).

- Cell counts (integrated over the water column) of total microphytoplankton showed a significant increasing trend of 6.9% y^{-1} over the 15-year monitoring period.

- Biomass (integrated over the water column) of total microphytoplankton also showed an increasing trend, about 2.5% y^{-1}, over the 15-year monitoring period, although this trend, with an associated *p* value of 0.07, was not statistically significant at the 95% confidence level.

- A community change has occurred over the 15-year period which includes more numerous smaller phytoplankton and also more numerous large diatoms.

- The overall changes (increasing abundance and, to a lesser extent, biomass of total microphytoplankton) are consistent with what might be anticipated if nutrients have become more abundant.

Dissolved oxygen

- Whilst we have long time series of dissolved oxygen (DO) at one site (in the extended Firth), we have fewer data from other sites. Thus, we cannot make conclusive statements about the oxygen status of the entire region. Nonetheless, the data do reveal temporal and spatial patterns, in particular, of occurrences of low dissolved oxygen at the extended-Firth monitoring-site.

- At the extended-Firth monitoring site, where we have 15 years of data, the upper 20 m of the water column was generally well oxygenated, with greater than 90% DO saturation for much of the year. In summer and autumn, when the water column was stratified, DO typically reduced to about 60–70% saturation at levels in the water column greater than 20 m below the surface. Occasionally, 40% DO saturation has been measured.

- These low-DO events occasionally penetrate into the upper water column and shoreward into the Firth.

- The autumnal subsurface DO depletion is more intense at the extended-Firth monitoring site than it is in the Firth. A likely explanation is that the shallower water in the Firth is better mixed.

- We attribute the seasonal depletion of DO at the extended-Firth monitoring site to a combination of at least two factors: strong stratification of the water column in late summer and autumn that inhibits oxygen exchange with the atmosphere, which otherwise would replenish the DO in the lower water column; and consumption of oxygen by microbial respiration of sinking organic matter that has accrued from primary production in the immediately preceding spring and early summer.

- The cold, high-salinity water that sometimes upwells from deep in the ocean onto the coastal shelf also tends to have low oxygen concentrations. Nonetheless, we do not believe that this is the driver of the annual oxygen depletion that occurs in late summer/early autumn.

- We have conducted a trend analysis of the DO data divided into two depth bins: an upper bin (the top 20 m of the water column) and a lower bin (everything below that). Both exhibited no statistically significant trend over time.

pH

- pH in the water column varies seasonally and is at its lowest in autumn. The pH minimum coincides with autumnal maxima in oxygen depletion and respiration. From this, we can infer that the same combination of physical and metabolic processes that we believe to be driving DO is also driving the carbonate system.

- We have been observing carbonate system dynamics since 2009 but complete records started only with the 2010 survey. This is too short a record to say anything about trends in the carbonate system.

Mineralisation of organic matter

- At all sites that we have made measurements (which includes the Firth, the extended Firth and the inner Hauraki Gulf), there was net oxygen consumption by the sediments. This means that the bed sediments are net heterotrophic, that is, respiration exceeds production. This was found to be the case regardless of water depth or bed-sediment type. Bed sediments in the Firth were about twice as heterotrophic as bed sediments in the extended Firth.

- Measurements of pelagic oxygen demand in autumn also showed strong net heterotrophy, with the rate of oxygen drawdown by respiration at inner-Firth sites being about twice the rate at extended-Firth sites.

- Comparing our data (measured fluxes of O_2 and, by implication, CO_2) with data reported from numerous Australian estuaries, we infer that denitrification efficiency (proportion of the nitrogen entering the seabed that is subsequently denitrified) may be maximum in the extended Firth and close to maximum in the inner Firth. Denitrification efficiency is dependent on the rate of input of organic matter to the bed sediments and can be suppressed by excessive loading. Denitrification measurements are required to assess if further increases in organic matter loadings to the seabed would have an effect on denitrification efficiency.

Budgets

- We developed a water budget, a salt budget and a carbon/nutrient budget for the Hauraki Gulf, extended Firth, and Firth of Thames. These help us to understand the relative importance of sources and the exchanges between different parts of the system.

- Because of data limitations, the budgets for the Gulf are valid for spring, summer and winter, while those for the Firth are valid for spring, summer and autumn. The budgets represent the conditions that prevailed during 2000–2001 surveys; at this time river flows were either close to average (for spring and autumn) or about 60% of average (for summer and winter). Sampling did not include conditions of strong upwelling.

- The budgets show that:
  - Rivers that drain to the Firth contribute 57% of total N inputs (DIN + DON + PON) and 87% of DIN inputs to the Firth, with the remainder coming from offshore.
  - For the Firth, the excess of respiration over production (i.e., the net heterotrophy) must be subsidised by net import of substantial amounts of labile organic carbon from the land and/or from offshore.
  - The Firth appears to be a large denitrifier. About 73% of the total nitrogen export from the Firth appears to be as N_2 gas that results from denitrification. This may help to buffer the system against nitrogen loading from terrestrial and marine sources.
  - On average, nitrogen in the Firth cycles about four times through the production–decomposition cycle before being lost to denitrification or (to a lesser extent) hydrographic export. This "amplifies" the effects of nitrogen imported to the Firth.

Assessments of water quality and ecosystem health

Sediments

- The almost-complete collapse by the late 1960s of hard, biogenic reefs composed of bivalves, sponges, ascidians, bryozoans and cnidarians, which has been attributed to dredge fishing

during about 1910 to 1968 that removed extensive reefs of green-lipped mussels, has been well documented. Despite dredging never recommencing, the reefs have not recovered.

- The modern sediment macrobenthic community of the Firth is adapted to the muddier post-reef-collapse conditions and is likely to be quite resilient to ongoing deposition of fine sediment. Even if catchment sediment inputs were to be turned off instantly, the prospects for a natural recovery of the Firth ecosystem to a pre-reef-collapse state would be slim.

The current trophic state of the system

- The Firth and the extended Firth are sensitive to nutrient enrichment (meaning that symptoms of eutrophication are not likely to be suppressed by physical factors such as turbid water/low light, short water residence time, and strong vertical mixing of the water column). This makes the Firth more susceptible to adverse effects from sediment and/or nutrient inputs from the land than either shallower, more rapidly flushed estuaries or coastal waters along an energetic, open coastline.

- Our data show that the Firth of Thames seasonally exceeds the NOAA ASSETS 5 mg m^{-3} chlorophyll a threshold for "medium impacts". This threshold is rarely exceeded at the extended-Firth monitoring site but it is frequently approached. Both regions are below the 20 mg m^{-3} "high impact" threshold. Thus, the ASSETS classification places the Firth in the "medium impacts" category while the extended Firth is at the upper end of "low impacts".

- Based primarily on our primary-production data, we would describe the current state of the Firth and the extended Firth as mesotrophic, where mesotrophic is the intermediate state between oligotrophic and eutrophic.

The pre-development trophic state of the system

- In our opinion, the Firth of Thames will at least have been "less mesotrophic" and may have been oligotrophic prior to catchment deforestation and subsequent development in the catchment. We have no direct data to support our estimation of any previous trophic state of the Firth (that is, we do not have any actual measurements from the pre-historic period).

The contribution of land runoff to nutrients

- It is likely that the balance between land-side and ocean-side nutrient loading was different prior to the historical land clearance and landuse intensification of the Hauraki Plains, specifically that ocean-side loading was likely to have contributed a much larger percentage to a much lower overall nutrient load to the Firth.

Cause(s) of the nitrogen trend at the extended-Firth monitoring site

- The cause of the trend in nitrogen at the extended-Firth monitoring site is likely to be complex, possibly including changes to oceanic inputs, terrestrial inputs, physical oceanography and/or denitrification efficiency.

Effects of low dissolved oxygen

- Oxygen minima below 6 mg L^{-1} in the lower water column at the extended-Firth monitoring site (with penetration into the upper water column on occasion), when combined with the uncertain response of kingfish/hapuka to oxygen status, warrant further investigation vis-à-vis management of the Coromandel Fish Farm Zone, which is approximately 2 km ESE of the extended-Firth monitoring site.

Effects of acidification

- The respiration of organic matter generates CO_2 which decreases pH (acidification). Acidification can have detrimental effects on species such as shellfish, kina and coralline algae that use carbonate for their solid structures, particularly in the juvenile life stages. pH has also been shown to have an influence upon the behaviour/physiology of non-calcareous organisms.

- Continued monitoring is required to identify any trends in pH (our records are currently too short for trend testing).

Reversibility and remediation

- Since the total nitrogen load to the Firth is dominated by land-side nutrient inputs (at least when there is no strong ocean upwelling, which is the case for about 90% of the time) and nutrients fuel primary production, we expect that a reduction in land-side nutrient inputs will reduce the organic-matter load of the Firth and the consequent oxygen depletion that occurs in the extended Firth towards the end of the phytoplankton growth season (late summer to early autumn).

- However, we cannot make any quantitative predictions of what changes might ensue following any specific reduction in land-side nutrients until we have a more thorough understanding of the dynamics of the system.

- Without a return to the former sediment macrobenthic community a full recovery to the pre-catchment-development pattern of nutrient cycling and water quality in the Firth seems unlikely.

The data are not available to make a full assessment of water quality and ecosystem health. This report identifies gaps and priorities for future work that will enable more comprehensive assessments to be made in the future.

Introduction

Waikato Regional Council and DairyNZ share questions around water quality in the Firth of Thames. The questions relate to sediments, nutrients, phytoplankton/bacteria, dissolved oxygen and pH (acidification).

The objective of this report is to assess, where possible, the water quality and ecological health of the Firth of Thames, identify information gaps and recommend priorities for future work.

This report is complemented by a data report (Zeldis et al., 2015[1]) that describes the data that NIWA has collected in the Firth of Thames and Hauraki Gulf over the last 20 years.

---

[1] Zeldis, J. et al. (2015) *Firth of Thames Water Quality and Ecosystem Health – Data Report*. NIWA Client Report No. CHC2014-123, prepared for Waikato Regional Council and DairyNZ.

1 Geographic zones

The Firth of Thames is a large mesotidal estuary on the east coast of the North Island (Figure 1-1). It is approximately 30 km long and 20 km wide, covering an area of about 730 km^2.

The extended Firth of Thames is an area of about 360 km^2 that is further north of the true Firth of Thames.

The Hauraki Gulf is the area north and west of the extended Firth of Thames. It contains the Waitemata Harbour, extending from Rodney in the west to the Coromandel Peninsula in the east.

Figure 1-1: **Geographic zones and place names.** The red triangle shows the location of the extended-Firth monitoring site.

2   Physical setting

Water depth in the Firth of Thames increases from very shallow in the southern half (<5 m) to 40 m in its northern approaches (Figure 2-1). The wider Hauraki Gulf reaches a depth of about 60 m in the north, before extending to the continental shelf edge (>200 m depth).

The Firth of Thames drains a combined area of 4200 km^2, which comprises the three major river catchments of the Waihou River (1980 km^2 area), Piako River (1461 km^2) and Kauaeranga River (132 km^2). Approximately 65% of the 4200 km^2 total catchment is in pasture, and about 20% is in native bush. The catchments of the Piako and Waitoa Rivers are mostly covered in pasture (90%), and most of that pasture is used for dairy farming. Approximately 60,000 people live in the Hauraki rivers catchment.
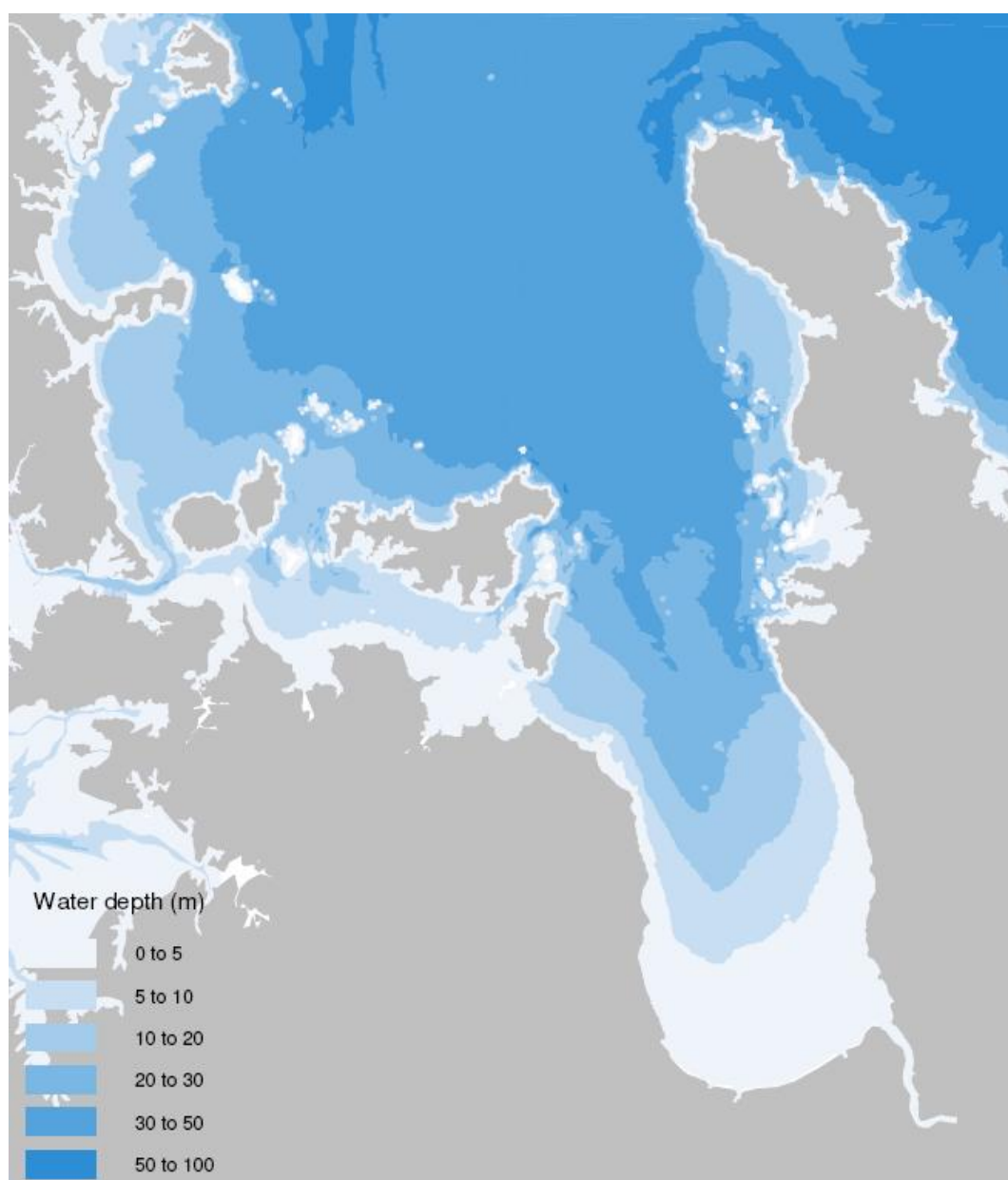

Figure 2-1:   Bathymetry. Data sourced from LINZ[2].

---

[2] https://data.linz.govt.nz/layer/447-depth-area-polygon-hydro-190k-1350k/

Prior to Māori and European land clearance, catchment landcover consisted of podocarp–hardwood forests on the Coromandel and Hunua Ranges. For much of the last 10,000 years, the Hauraki Plains have comprised freshwater marshes and swamp forests dominated by kahikatea, manuka and flax. Forest clearance by Maori was localised around settlements. European settlers arrived in the mid-1800s and large-scale deforestation began shortly after in the Coromandel Ranges, which was associated with timber logging and gold mining.

Early maps show that muds were accumulating in the Firth before large-scale catchment deforestation by European settlers had begun. Hydrographic surveys indicate that between 1882 and 1918 an estimated 7×10^6 m^3 of sediment was deposited within a 16 km^2 area of the lower Waihou River and its tidal delta and an estimated 37×10^6 m^3 was deposited in a 210 km^2 area of the Firth south of Tararu. Much of this sediment would have been associated with land clearance that preceded the development of pastoral agriculture in the Hauraki Plains. Prior to the construction of flood protection works following a large storm in 1938, floods deposited large quantities of sediment across the Hauraki Plains. Since the flood protection works, with floodwaters constrained to the river channels, sediment delivery to the Firth is likely to have been increased.

The Firth's tides are semi-diurnal with spring and neap tidal ranges of 3.2–3.5 m and 2.0–2.2 m, respectively. Northerly winds typically generate the largest waves, with periods less than 10 s and heights typically <1 m. Tidal currents may agitate bottom sediments and disperse suspended sediments.

The circulation of the open shelf adjacent to the Hauraki Gulf is strongly wind forced, which causes upwelling and downwelling (Figure 2-2). Upwelling is caused by persistent offshore (westerly) winds and brings cooler, nutrient-rich, low-oxygen oceanic water onto the shelf. Persistent onshore (northeasterly and easterly) winds cause downwelling, which transports nutrient-rich water away from the coast and depletes the continental shelf of nutrients. Upwelling is most frequent in winter and spring; downwelling in summer and autumn. During El Niño periods of the ENSO[3] weather cycle (indicated by a negative value of the Southern Oscillation Index, or SOI), westerly winds are more persistent (these reinforce upwelling of nutrient-rich, low-oxygen water). During La Niña periods of the ENSO weather cycle (indicated by a positive value of the SOI), northeasterly winds are more persistent (these reinforce downwelling).
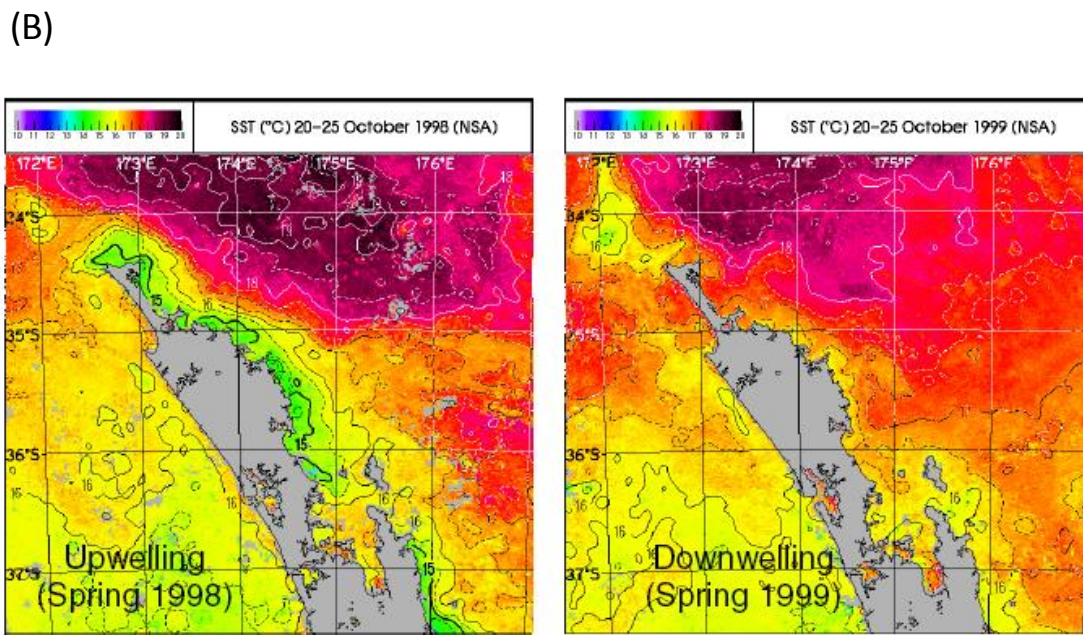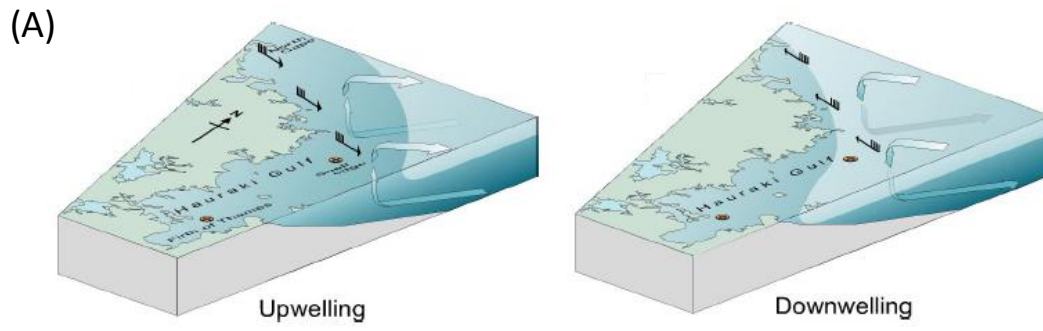
---

[3] El Niño Southern Oscillation.

(A)

(B)

Figure 2-2:   **Characteristics of upwelling and downwelling.**

3 Sediments

3.1 Sedimentation rates

Intertidal flats in the southern Firth have been accreting for the last 90 years at rates that are an order of magnitude greater (~25 mm y^{-1}) than rates that have been observed in intertidal regions of other North Island estuaries.

Sedimentation rates in subtidal areas of the southern Firth of Thames and in the extended Firth are much lower (2 mm y^{-1}) than on the intertidal flats, which we expect would be the case. However, this rate (2 mm y^{-1}) is much larger than rates obtained by Pocknall et al. (1989) from cores collected in water depths greater than 30 m in the extended Firth. Pocknall's cores gave sedimentation rates in the range 0.1–0.2 mm y^{-1} for the most recent interglacial, marine muddy fine sands that overlie early Holocene Last Glacial peats and coastal sediments (11,900–14,000 calendar years BP).

3.2 Mangrove expansion

Accumulation of mud has permitted widespread mangrove expansion, although this does not appear to occur continuously. Instead, successful mangrove recruitment – and therefore expansion – requires particular weather conditions, which only occur episodically.

3.3 Sediment budget

We have compared sedimentation rates to sediment inputs to develop a sediment budget (Table 3-1).

Table 3-1: **Sediment budget for the southern Firth of Thames.** Key: (1) Area per linear metre of shoreline; (2) SAR (m y^{-1}) is the present-decade average sedimentation rate ["SAR" stands for sediment accumulation rate or, more simply, just sedimentation rate]; (3) SAR (t y^{-1}) calculated per linear metre of shoreline using dry-bulk sediment density of 0.5 kg m^{-3}; (4) SAR-m is the total annual sediment-mass accumulation rate between the Piako and Waitakaruru Rivers (9.4 km); (5) SAR-m2 is the total annual sediment-mass accumulation rate in the Piako–Waitakaruru compartment per km^2.

Environment/ source	Compartment	Area (m^2)	SAR (m y^{-1})	SAR (t y^{-1})	SAR-m (t y^{-1})	SAR-m2 (t km^{-2} y^{-1})
Present day						
Mangrove forest	Old forest	260	0.01	1.3		
	Scrub forest	249	0.058	7.2		
	Fringe	116	0.056	3.3		
	Total-mangrove			11.8	110,900	18,860
Intertidal flat-1km	Upper intertidal	1000	0.025	12.5	117,500	12,500
Lower intertidal - subtidal flats	Area south of Tararu – Kaiaua	210 $x10^6$	0.002		200,000	1000
Waihou & Piako Rivers					190,000	–
Historical						
Southern Firth	as above (period 1882–1918)				18.3 x 10^6	2,427

Sedimentation rates indicate that ~110,000 t y^{-1} of fine sediment is accumulating in the mangrove forest and a similar amount is accumulating in the upper intertidal flat that is immediately adjacent (on the seaward side of the mangroves). By comparison, an estimated 200,000 t y^{-1} of fine sediment is accumulating in the 210 km^2 lower intertidal – shallow subtidal zone of the southern Firth. The present-day annual suspended-sediment loads of 160,000 t y^{-1} and 30,000 t y^{-1} for the Waihou and Piako Rivers, respectively, represent only about 40% of sediment depositing in the southern Firth. We think that the apparent discrepancy between sediment delivery by rivers and sedimentation in the Firth is due to the reworking by waves and currents of legacy sediments deposited in the Firth during large-scale deforestation and mining activities that occurred during the late 1800s to early 1900s. Under this scenario, intertidal flats are currently accreting legacy sediments that are being transported shoreward from the subtidal zone by waves and currents. WRC, DNZ and NIWA are currently researching this proposition.

3.4   Subtidal seabed sediments

Subtidal sediments have been mapped previously by Carter and Eade (1980), who depict the surficial sediments as being predominantly sandy muds (<0.063 mm grain diameter) and clays, with a minor coarse carbonate gravel (>2 mm) component (Figure 3-1).
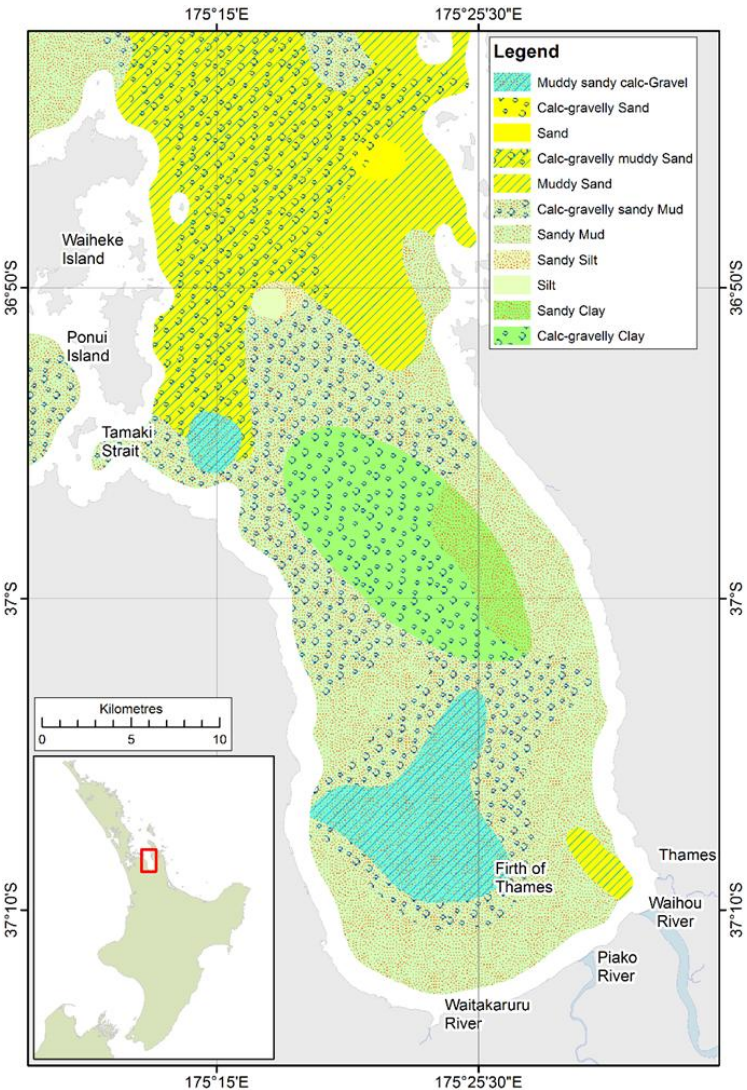

Figure 3-1:   **Carter and Eade's (1980) sediment map.**

Our more recent data (voyages in 2002, 2003 and 2012) confirm that subtidal sediments in the Firth of Thames are very muddy (70–100 % mud), and moving from inshore to offshore sediments become sandier.

At one of our measurement sites in the extended Firth, the mud content of the seabed appears to have increased over the period 1999–2003. Data from 2012 suggest a continuation of that trend, but a change in analysis methods between 2003 and 2012 means we cannot be sure of that result. We do not have comparable data for other areas of the Firth so cannot extrapolate this result to other locations.

Subtidal seabed sediments are moderately rich in organic carbon, but nothing outstanding compared to other New Zealand estuaries.

3.5   Benthic fauna

Needham et al. (2014) provided a comprehensive review of monitoring over the past 10 years by Waikato Regional Council of the inner Firth's intertidal benthic macrofauna and surface sediment. Needham et al. concluded there was no evidence of ecologically significant changes to either sediment characteristics or indicator taxa over the past 10 years of monitoring. We comment on that result below in section 3.7.

We have information on subtidal benthic infauna in the Firth and the extended Firth, but the data are limited, and do not tell us anything about trends. The data include information on bacteria (using phospholipids as a proxy), meiofauna and macrofauna abundance, chlorophyll *a* and associated pigments. The data suggest that the inner, subtidal Firth is depauperate in macrofauna and infauna relative to the central Firth. The most likely reason for this is that the inner Firth is muddier.

3.6   Numerical modelling

We have done numerical modelling to map dispersal of sediment discharged from river sources into the Firth. The modelling is limited in a couple of important ways: firstly, the sediment-transport model is not calibrated and, secondly, we have used the model to look at only a limited number of "scenarios" (different combinations of tide, wind and freshwater runoff).

The modelling shows that the three largest rivers (Waihou, Piako and Kauaeranga) deposit sediment in the southern Firth close to their respective mouths, with little river-borne sediment escaping from the entrance of the Firth to the wider Hauraki Gulf. Southwesterly winds steer sediment plumes along the western shore of the Coromandel Peninsula and northeasterly winds steer plumes along the southern and southwestern shores of the Firth.

3.7   Effects of sediments

The almost-complete collapse by the late 1960s of hard, biogenic reefs in the Firth composed of bivalves, sponges, ascidians, bryozoans and cnidarians has been well documented[4]. The reef collapse is likely to have reduced the overall biotic resilience and filtration capability of the Firth, and has been

---

[4] McLeod et al. (2012) ascribed the collapse of biogenic reefs in the Firth of Thames to dredge fishing from about 1910 to 1968 that removed extensive reefs of green-lipped mussels. They noted that, even though dredging never recommenced, the mussel reefs have not recovered. They investigated two potential reasons for this: (1) increased sedimentation and associated suspended sediments, which have a negative effect on the survival of mussels on the seafloor, (2) limited recruitment due to low larval supply or reduction in habitat that is suitable for larval settlement and post-larval survival. McLeod, I.M., Parsons, D.M., Morrison, M.A., Le Port, A., Taylor, R.B. (2012) Factors affecting the recovery of soft-sediment mussel reefs in the Firth of Thames, *New Zealand Marine and Freshwater Research*, 63: 78–83.

accompanied by a shift in the sedimentary regime to an overall muddier system. **The modern sediment macrobenthic community of the Firth that has developed post-collapse under the muddier conditions is likely to be quite resilient.**

The monitoring reported by Needham et al. (2014), which showed little evidence of ecologically significant changes in intertidal benthic macrofauna over the past 10 years of monitoring, supports this view.

3.8   Reversibility and remediation

Even if catchment sediment inputs were to be turned off instantly, the prospects for a natural recovery of the Firth benthic ecosystem to a pre-reef-collapse state would be slim. If recovery were to occur, it is likely to be very slow.

We take this view because it is not likely that the Firth could "naturally" cleanse itself of the large sediment burden, even though internal transfers of legacy sediments are today occurring.

4 Overview – nutrients, phytoplankton, bacteria, dissolved oxygen and pH

In the remainder of this report we discuss nutrients, phytoplankton, bacteria, dissolved oxygen, and pH. The terms "autotrophy" and "heterotrophy" are defined in this section.

Phytoplankton[5] form the base of the planktonic foodweb. They use the energy from sunlight to synthesize simple sugars from dissolved inorganic carbon and water. As a side effect of this synthesis, free oxygen is liberated from the water molecules. The process of sunlight-driven sugar synthesis is known as "photosynthesis".

The sugars produced by photosynthesis are combined with dissolved inorganic nutrients (notably, nitrogen, phosphorus and, in some taxa, silicon) to build more complex molecules and entire cells. Overall, this net conversion of inorganic materials into organic material is called "autotrophy" or "primary production".

Phytoplankton growth tends to be restricted to the near-surface layers of the water column because light levels reduce with depth below the water surface.

Ultimately, much of the organic matter produced by photosynthesis sinks through the water column and is consumed (or "respired") by heterotrophic[6] organisms that include bacteria and zooplankton. When oxygen is present, respiration is "aerobic". Oxygen is consumed and carbon dioxide (CO_2) is liberated. In the marine environment, nitrogen in the substrate material is released as ammonium (NH_4^+), which may be oxidised to nitrate (NO_3^-).

Heterotrophic organisms draw oxygen from the pool of oxygen dissolved in the water column. If the heterotrophic drawdown of dissolved oxygen is greater than the combined rate of reoxygenation of the local water by diffusion from the overlying atmosphere and the rate of autotrophic production of oxygen then the dissolved oxygen in the local water will become "depleted".

Depletion of dissolved oxygen typically occurs at depth in the water column where atmospheric oxygen is slow to reach and low light levels limit autotrophic production (and associated oxygen generation). When the water column is density stratified, the situation is worse because the stratification inhibits the mixing and overturn of the water column. (Mixing and overturn help to reaerate the water column.) In these conditions, oxygen can reach levels that are low[7] enough to inhibit the activities of, or even harm, aerobic organisms. To remain healthy, more active and complex organisms (notably fish and decapods) tend to require higher oxygen concentrations than less complex/active ones.

When CO_2 is released into water it dissociates into carboxyl ions. In turn, these encourage the water molecules (H_2O) to dissociate into OH^- and H^+ ion pairs. Acidity (pH) is related to the hydrogen ion (H^+) concentration. Hence, aerobic respiration in water, which generates CO_2, will cause the water to become more acidic (that is, the pH will drop).

It is widely known that few organisms can withstand extremes of pH, but even small to moderate drops in pH can be harmful to some organisms. This is especially true of marine organisms that build

---

[5] Phytoplankton, also known as microalgae, are microscopic marine plants. They contain chlorophyll and require light to grow.
[6] Heterotrophic organisms cannot manufacture their own food; in essence they eat autotrophic organisms.
[7] Hypoxia is a low level of oxygen; anoxia is no oxygen.

carbonate-based exoskeletons (molluscs, crustacean, corals, urchins, etc.) because carbonate tends to dissolve more readily as the pH drops.

There are two primary "external" sources of nutrients to the Firth. Firstly, upwelling of oceanic bottom water onto the coastal shelf (that occurs during prolonged periods of offshore [westerly] winds) brings cooler, low-oxygen, naturally nutrient-rich water into the Firth[8]. Secondly, freshwater runoff provides nutrients from the land to the coastal zone.

Nitrogen is typically the limiting nutrient in coastal marine waters, hence, excessive nitrogen in the water column can stimulate excessive organic matter production by autotrophs (i.e., phytoplankton). Subsequent decay of this locally produced organic material (together with decay of any organic material exported from the catchment) can induce oxygen depletion, with subsequent adverse effects on aerobic animals including fish and shellfish. Respiration of organic matter also produces CO_2, which can acidify the water, with adverse effects on creatures that build shells. This combination of nutrient enrichment and associated "symptoms" or adverse effects is called "eutrophication". Systems which have long flushing times (that is, limited or slow exchange of water with more pristine waters[9]) are more prone to eutrophication than well-flushed systems.

In healthy coastal ecosystems, any tendency towards eutrophication is countered by denitrification, which converts nitrate to gaseous N_2 (mainly in the sediments). The N_2 can then bubble to the sea surface and be vented to the atmosphere. Gaseous N_2 cannot be used as a nutrient by most autotrophs so, effectively, it is lost from the productive system.

Denitrification is driven by microbial processes at the oxic/suboxic boundary in the seabed sediments. Strictly, denitrification is the conversion of nitrate (NO_3^-) into free N_2, which occurs under anoxic conditions. The standing pool of NO_3^- is usually small and, if it were not replenished, rates of denitrification would quickly fall to zero.

Under aerobic conditions NH_4^+ (ammonium, which is often an end-product of respiration – see above) is converted to NO_3^- by specific bacteria. Therefore, successful conversion of ammoniacal nitrogen into free N_2 requires that aerobic and anaerobic processes occur in close proximity to one another, such that NO_3^- formed in the aerobic region can quickly move into the anaerobic zone where it may transform into N_2.

Hypoxia suppresses conversion of ammonium to NO_3^- and tends to increase the distance between aerobic and anaerobic zones, thus suppressing denitrification. Thus, hypoxia promotes retention of nitrogen in bioavailable forms (ammonium and nitrate) that are available to autotrophs. This leads to a positive feedback loop whereby the retained nitrogen fuels further production of organic matter, which fuels oxygen depletion, which suppresses denitrification, and so on.

Denitrification can thus be viewed as a valuable ecosystem service provided by coastal waters.

---

[8] Winds during winter and spring tend to blow more from the west than normal during El Niño phases of the Southern Oscillation; during La Niña phases winds tend to be northeasterly, which drives downwelling that in turn transports warmer shelf waters onshore.
[9] In this context, a "long flushing time" is likely to be around 10 days or greater.

5 Nutrients

5.1 Data

Nutrients were sampled at the extended-Firth monitoring site (the "Firth" in Figure 5-1) at 3-monthly intervals over the 15-year period 1998 to 2013. At the same time, phytoplankton and bacteria, dissolved oxygen and pH were measured, which we discuss in following sections.

Samples were collected by lowering a CTD that contained a sampling rosette (Figure 5-1) from a research vessel (usually the R/V *Kaharoa*, operated by NIWA). Typically, samples were collected at 6 depths in the water column. (These same samples were analysed for phytoplankton and bacteria.)
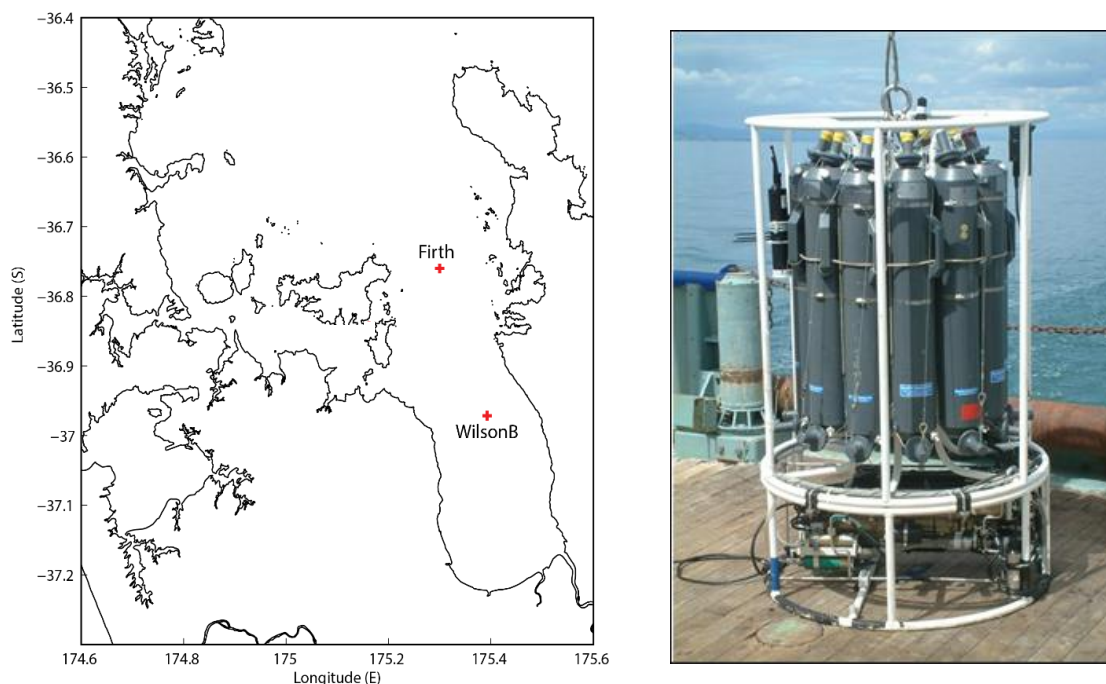
Figure 5-1: **(Left) Location of the extended-Firth monitoring site ("Firth" in the figure) and the Wilson B mooring site. T**he extended-Firth monitoring site is at 36^0 45.6' S, 175^0 18.0' E. The water depth is 40 m. The Wilson B site is adjacent to the Wilson Area B Marine Farm Zone (36^0 58.297' S, 175^0 24.116' E; 16 m depth). **(Right) The Conductivity–Temperature–Depth (CTD) instrument about to be deployed from the stern of NIWA RV *Kaharoa*.** The CTD is lowered though the water and used to sample parameters including temperature, salinity, oxygen and light, at various depths in the water column, using the electronic sensors at the base of the package. The bottles can be shut at specified depths to capture water for later laboratory analysis for nutrients and phytoplankton.

Some of the data are shown in Figure 5-2.

Figure 5-2: **15-year time series of nutrients (dissolved inorganic nitrogen), temperature and salinity at the extended-Firth monitoring site.**

The 15-year measurements of the different nutrient species reveal that dissolved inorganic nitrogen (DIN; the sum of nitrate and ammonium) is often most abundant in the upper water column during winter and early spring (indicated by times when temperatures are low: Figure 5-2A). The most likely reason is that uptake of DIN by primary production is limited by low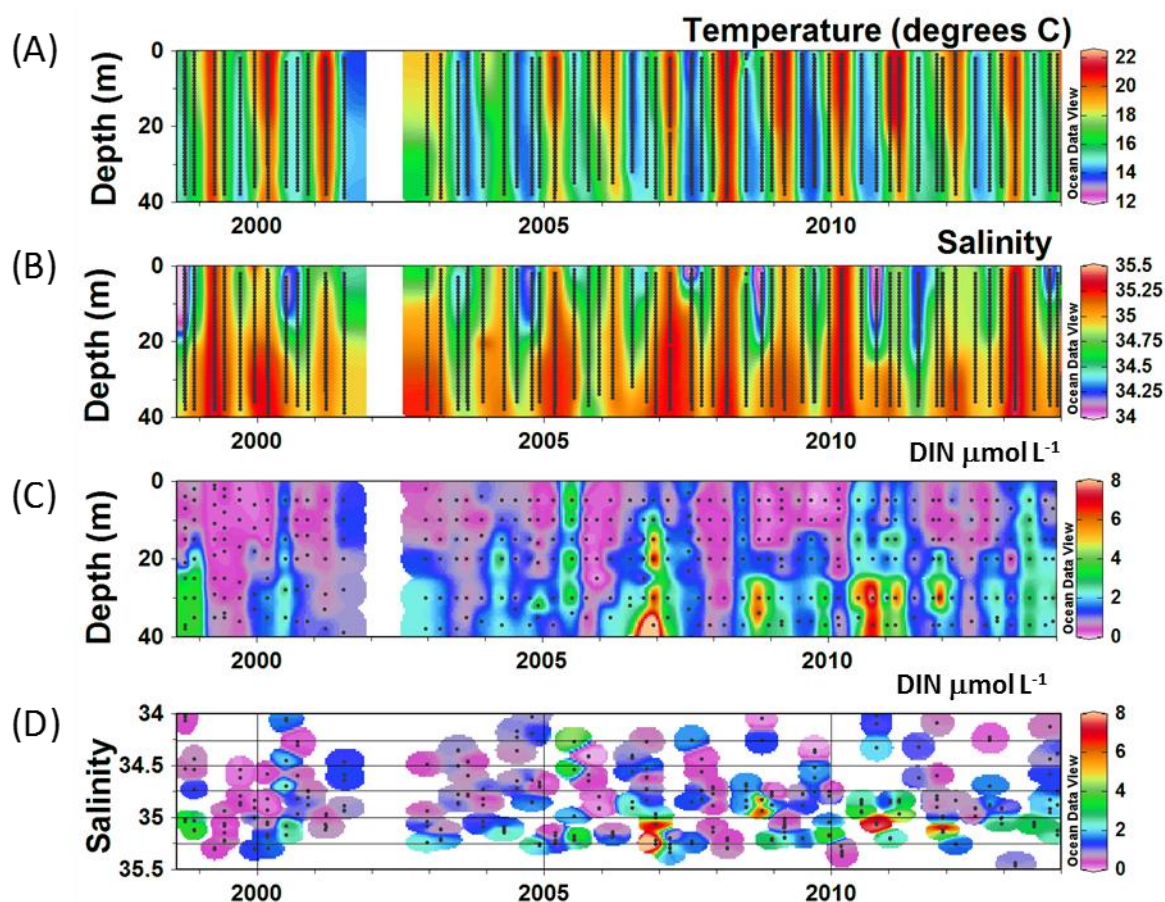 light at those times. In summer and autumn, when there is plenty of light and seasonal production is well-developed, DIN in the upper water column is reduced because of uptake by primary production.

5.2   Trends

We conducted trend analysis on the nutrient data after integrating it over depth in the water column. We used the non-parametric seasonal Kendall trend test (Jowett, 2014)[10] to detect trends in the water-column-integrated data. The water-column-integrated DIN concentration is shown as a time series in Figure 5-3, and the results of the trend analysis are tabulated in Appendix A.

---

[10] The seasonal Kendall trend test tests for a monotonic trend in data. It is a nonparametric test, meaning that data are not required to be normally distributed for the test to be valid. "Monotonic" means the data consistently increase or decrease over time. Any trend may or may not be linear. "Seasonality" implies that the data are differently distributed in different seasons. A "season" may or may not be a season in the normally understood sense; for example, three 8-hour periods in a day may constitute different seasons. In our analyses, "season" really does mean a traditional calendar season.
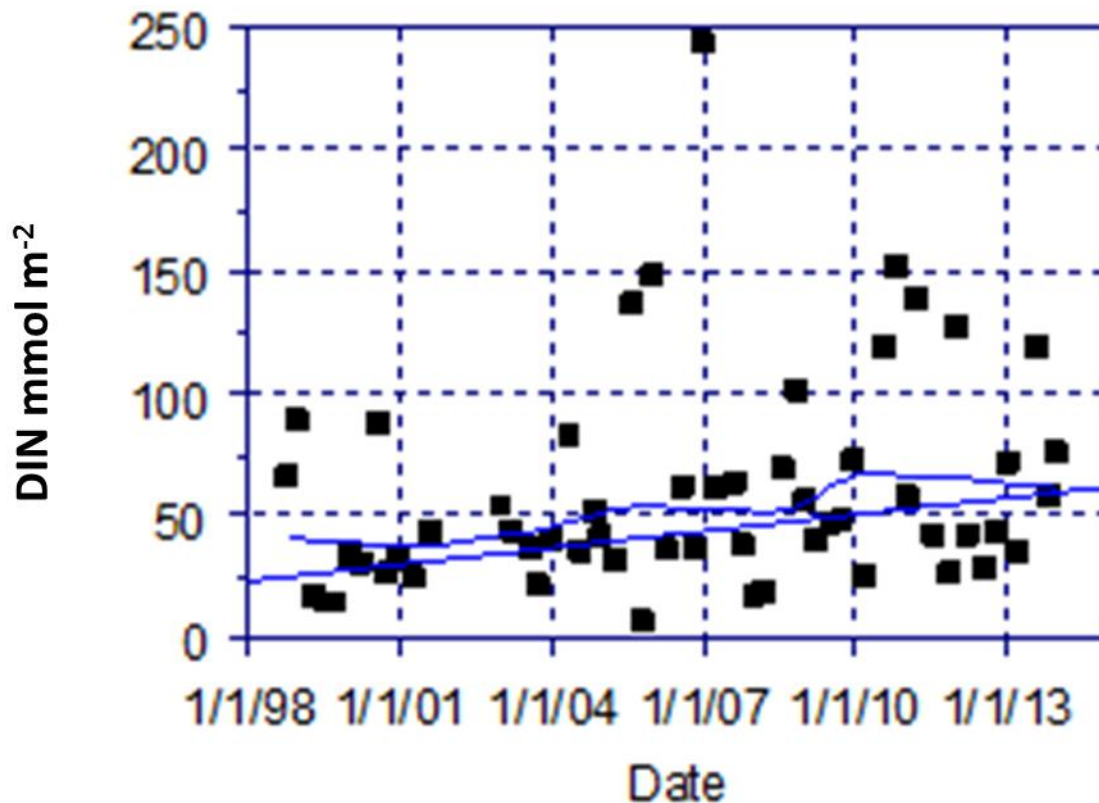
Figure 5-3: **Time series of water-column-integrated DIN concentration (units of mmole m^{-2}) at the extended-Firth monitoring site. Note that 1 mmol m^{-2} DIN = 14 mg m^{-2} DIN.** The blue curves show the fitted linear Kendall trend (the straight line) and a LOWESS moving average fit (the other line) that used 40% of the points in its fitting window.

The seasonal Kendall trend tests revealed:

- DIN had increased at a rate of 5.1% y^{-1} over the 15-year measurement period. This was a statistically significant[11] result ($p < 0.05$).

- Dissolved organic nitrogen (DON) was abundant relative to DIN, and also had a significant increasing trend (1.8% y^{-1}).

- In contrast, dissolved inorganic phosphorus (DIP) did not change significantly.

- Dissolved organic phosphorus (DOP) was less abundant relative to DIP, and decreased at a statistically significant rate of -5.5% y^{-1}.

- The ratio DIN/DIP increased at a statistically significant rate of 4.2% y^{-1}, indicating enrichment of N in the system relative to P.

These results are for water-column-integrated data and therefore represent the entire inventory of each dissolved nutrient at the extended-Firth monitoring site through time.

We have looked at what factors might be driving an increase in nitrogen at the extended-Firth monitoring site over the 15-year measurement period. The possible factors that we looked at divide broadly into two types: changes in oceanographic conditions, and changes in nutrient runoff from the land.

---

[11] This is statistical significance ($p < 0.05$), not that it necessarily has any particular or significant implication.

- There does not appear to have been a sufficient upward trend in nutrient runoff from the Waihou River to fully explain the upward trend in nitrogen at the extended–Firth monitoring site, as follows.

  Trends in river water quality in the Waikato region since 1993 have been described by Vant (2011) and Vant (2013). Many (67%) of the records showed no "important" trends, while 18% of the records showed improvements and 15% showed deteriorations.

  Vant (2013) gave trends for the Coromandel and Hauraki rivers, including patterns in the Waihou and Piako Rivers, which dominate riverine nutrient inputs to the Firth. For TP, improvements were found at most sites in both rivers. For TN, minor improvements or no change were found in the Piako River and deteriorations were found in the Waihou River.

  The Waihou River[12] showed flow-adjusted TN increasing at rates of 0.5, 1.0 and 1.7% y^{-1} at 3 monitoring sites, the latter two of which were considered to be "important". However, these rates are considerably less than the DIN trend that we see in the marine record. Furthermore, the site furthest downstream on the Waihou River, which we can reasonably expect to be most indicative of the loading into the Firth, actually had the slowest increase (0.5% y^{-1}) in TN. However, since DIN is just one component of TN, then if all of that 0.5% y^{-1} increase in TN at the site furthest downstream has occurred as an increase in DIN, then the % increase in DIN will actually exceed 0.5%. This needs to be explored.

  The Coromandel rivers contribute much lower nutrient loads and showed "important" increases for TN in the Kauaeranga (3.3% y^{-1}) and, for the Ohinemuri, no change at 2 sites and an "important" increase at one site (1.2% y^{-1}).

  To provide a more nuanced view on whether there are trends in nutrient runoff that could match the trend we have found in water-column-integrated DIN, the analysis of river loads should be repeated with a focus on "terminal reach" (i.e., at the location just before the river debouches at the coast) loads. Also, river trends in DIN, in addition to trends TN, need to be considered and understood.

- We have analysed the Southern Oscillation Index to see whether the upwelling regime may have changed (upwelling, driven by westerly winds, brings cool, nutrient-laden oceanic water onto the shelf). However, we found no significant shift in the SOI over the 15-year period. (The results are tabulated in Appendix A.) Satellite remotely-sensed sea-surface temperature data for the shelf north of the Gulf dating from 2003 also did not exhibit any long-term cooling trend, which could have resulted from a change in the upwelling regime.

  Further analyses need to be done on measurements of salinity and water temperature above and below the pycnocline[13], which could result from changed oceanographic conditions.

We view the seasonal Kendall trend test of the water-column-integrated data as a first step towards identifying and understanding trends. The nutrient data exhibit significant vertical structure over the

---

[12] Which, we estimate, via the budget shown in section 10, supplies about 60% of the total nutrient load to the Firth.

[13] The layer in the water column where the density gradient is greatest. Many properties of ocean water above and below a narrow pycnocline can be quite different.

Firth of Thames Water Quality and Ecosystem Health – Synthesis

water column (see Figure 5-2), that is, the water chemistry is markedly different between top and bottom water, which is lost by depth-integrating the data.

- For example, simple visual inspection of panel C in Figure 5-2 suggests that DIN has mostly changed in the water column at levels below about 20 m below the water surface. Furthermore, the change in DIN in the lower water column appears to have been driven by stronger "pulses" of DIN occurring later in the monitoring period. (Analysis is required to verify both of these casual observations.) This kind of detail, which may be important, is lost in the analysis of the water-column-integrated data.

One other possibility as a driver of the water-column-integrated DIN trend is that there has been a change in the way the seabed "processes" nitrogen, which could have resulted in a redistribution of nutrients across the various sediment, water and phytoplankton "compartments" that comprise the system. We talk further about this possibility in section 11.3 where we discuss trends.

6 Phytoplankton and bacteria

6.1 Data

Our data show that there are more phytoplankton in the Firth of Thames than in the extended Firth of Thames (Figure 6-1). Both of these areas contain more phytoplankton than the wider Hauraki Gulf. Rates of primary production (expressed as carbon fixed per time per area) follow a similar pattern (Figure 6-2).
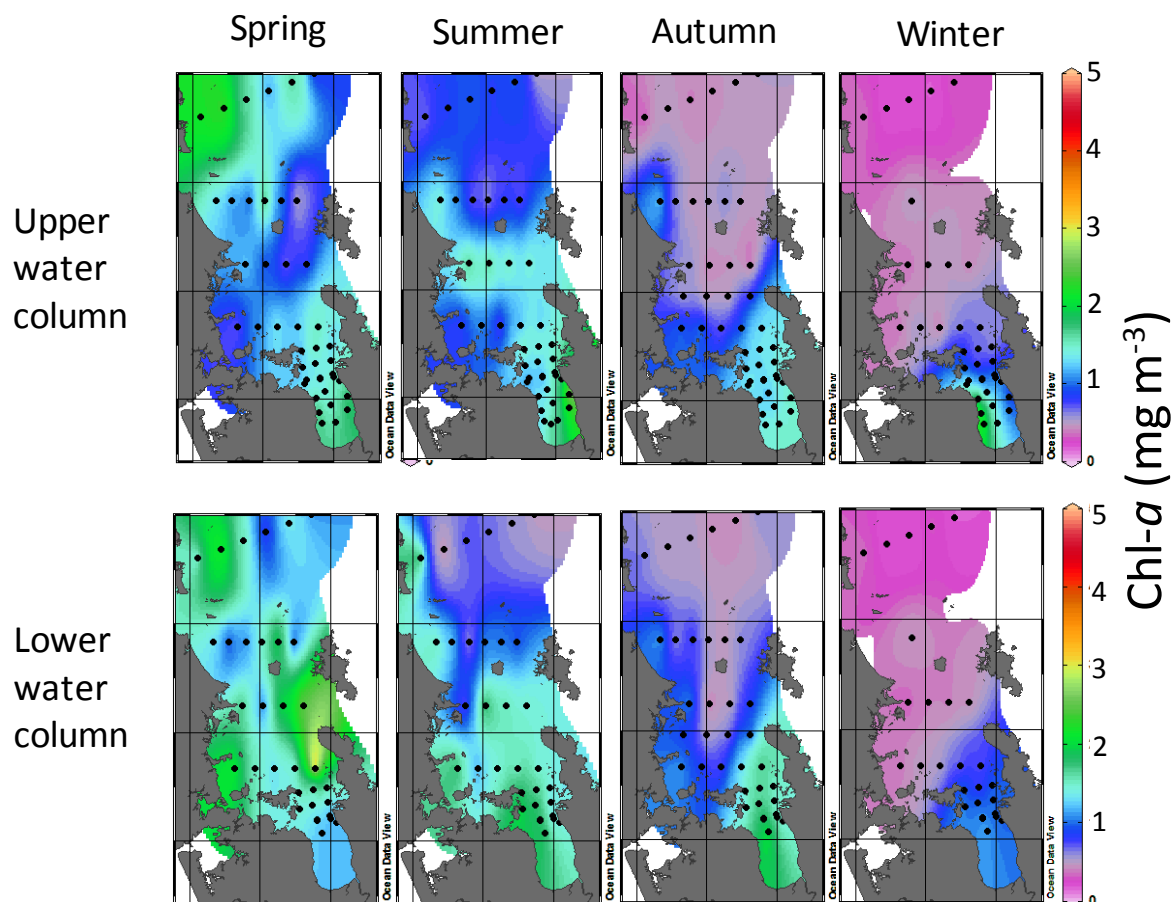
Figure 6-1: **Seasonal phytoplankton distributions in spring, summer, autumn and winter.** Chlorophyll *a* data were compiled from NIWA voyages made between 1996 and 2012. Values are averages for the upper water column (upper 15 m) and the lower water column (16–50 m), with sampling sites shown by black dots. Note that the inner Firth is shallower than 15 m hence no lower water column values were estimated.
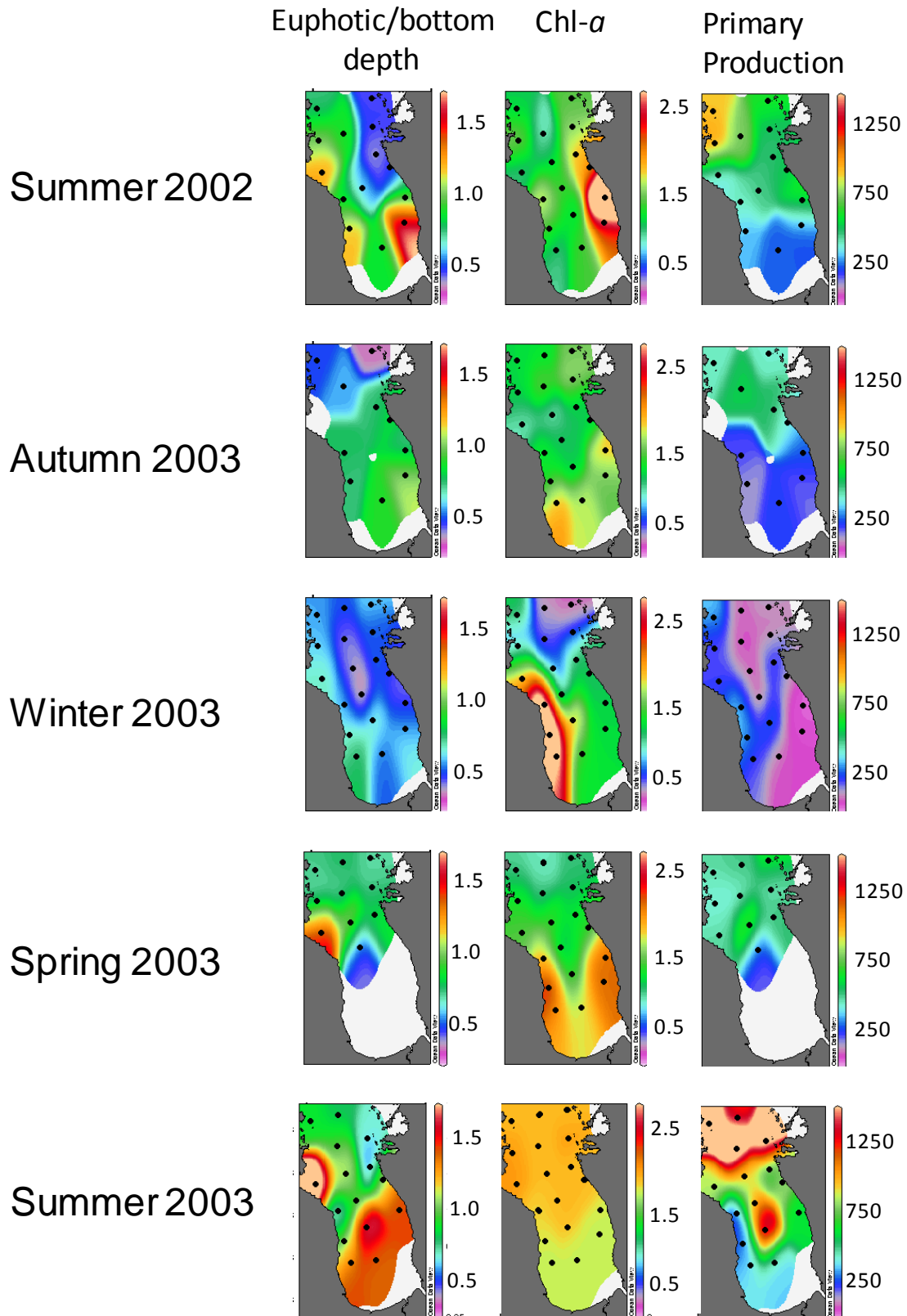
Figure 6-2: Primary production in Firth over 5 seasonal voyages, summer 2002–summer 2003. The columns show (left to right) the depth of light penetration (euphotic depth) relative to bottom depth, depth-integrated chlorophyll *a* concentration (mg m^{-2}) and primary production rate (mg C m^{-2} d^{-1}). Some light penetration data were lost in the spring voyage. The euphotic depth is the depth below the water surface where light first reaches 1% of the value incident at the water surface.

Figure 6-1, which is compiled from data collected during voyages made between 1996 and 2012, shows that phytoplankton biomass varies seasonally, being generally greatest in spring and least in winter. Biomass is widely distributed in spring, but becomes progressively restricted to inshore areas (especially the Firth) from summer through winter. In the extended Firth, biomass is greatest in the upper water column in spring, but increases noticeably at depth in autumn.

Seasonal variation in primary productivity has a great bearing on standing stocks of nutrients. Spatial surveys of the Firth in spring, summer, autumn and winter of 2003 and during 2012–13 (see Figure 6-2 and Figure 6-3) showed that phytoplankton growth reduced nitrate to low levels in all seasons except winter, while ammonium mineralisation[14] was evident in summer and autumn. It is in winter, when production is strongly light-limited (see primary production [pp] values in Figure 6-3), that the "conservative" spatial pattern of nutrients becomes evident. This is characterised by a gradient in nitrate concentrations, decreasing towards offshore from the inner Firth. **This suggests that catchment loading dominates DIN stocks.** We examine this suggestion in section 10 where we develop a budget for carbon/nutrients.

---

[14] "Mineralisation" is the breakdown by living organisms of organic matter into inorganic substances.

Figure 6-3: Transects of nutrient and chlorophyll a concentration from the inner Firth to the extended Firth (inset), by depth and season during seasonal voyages made in 2003 and 2012–13. Rates of primary production averaged across the Firth ("pp": mg C fixed m^{-2} d^{-1}) during the 2003 surveys are annotated on the 2003 chlorophyll *a* plots. **This page: spring and summer. Next page: autumn and winter.**

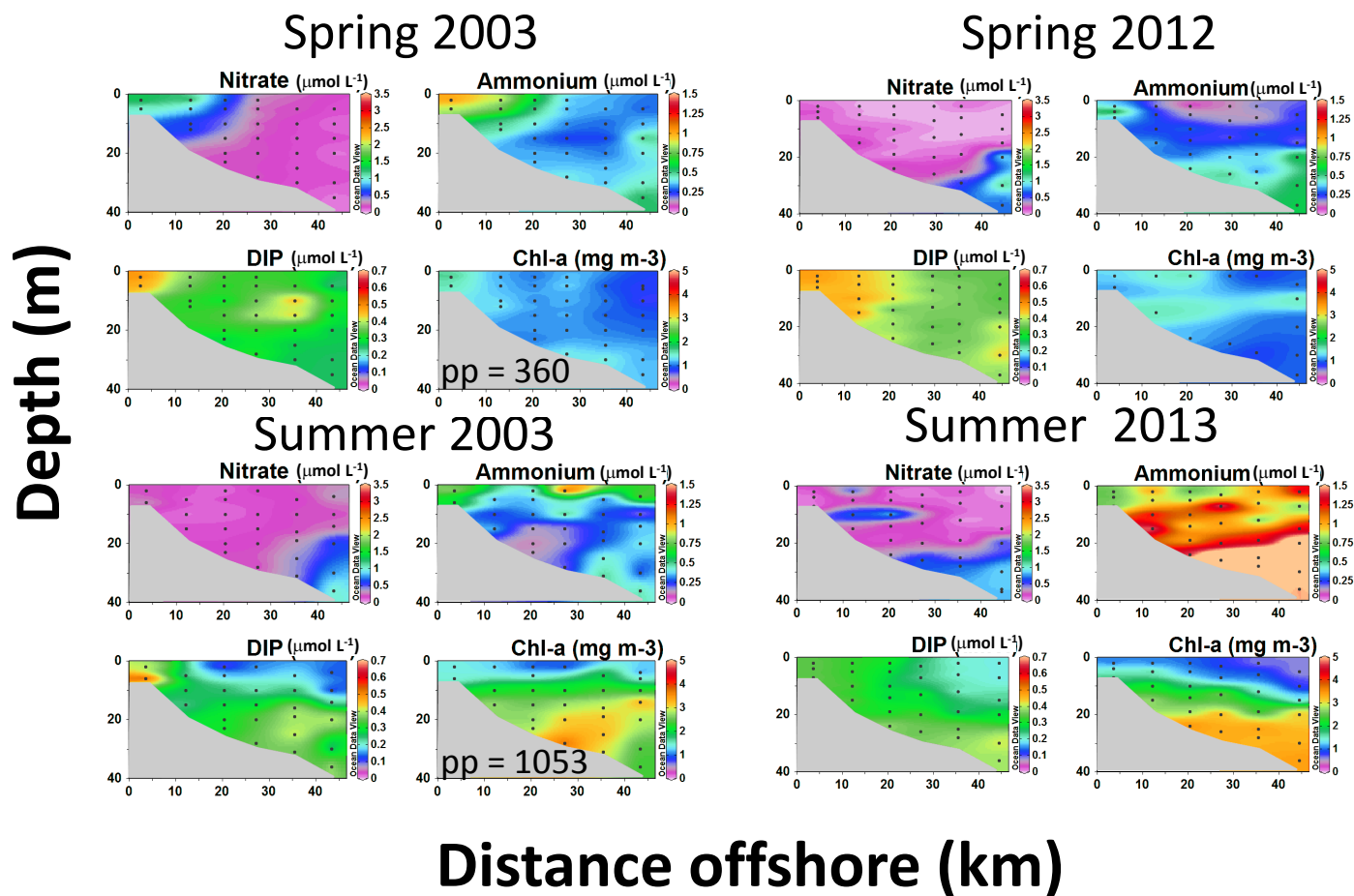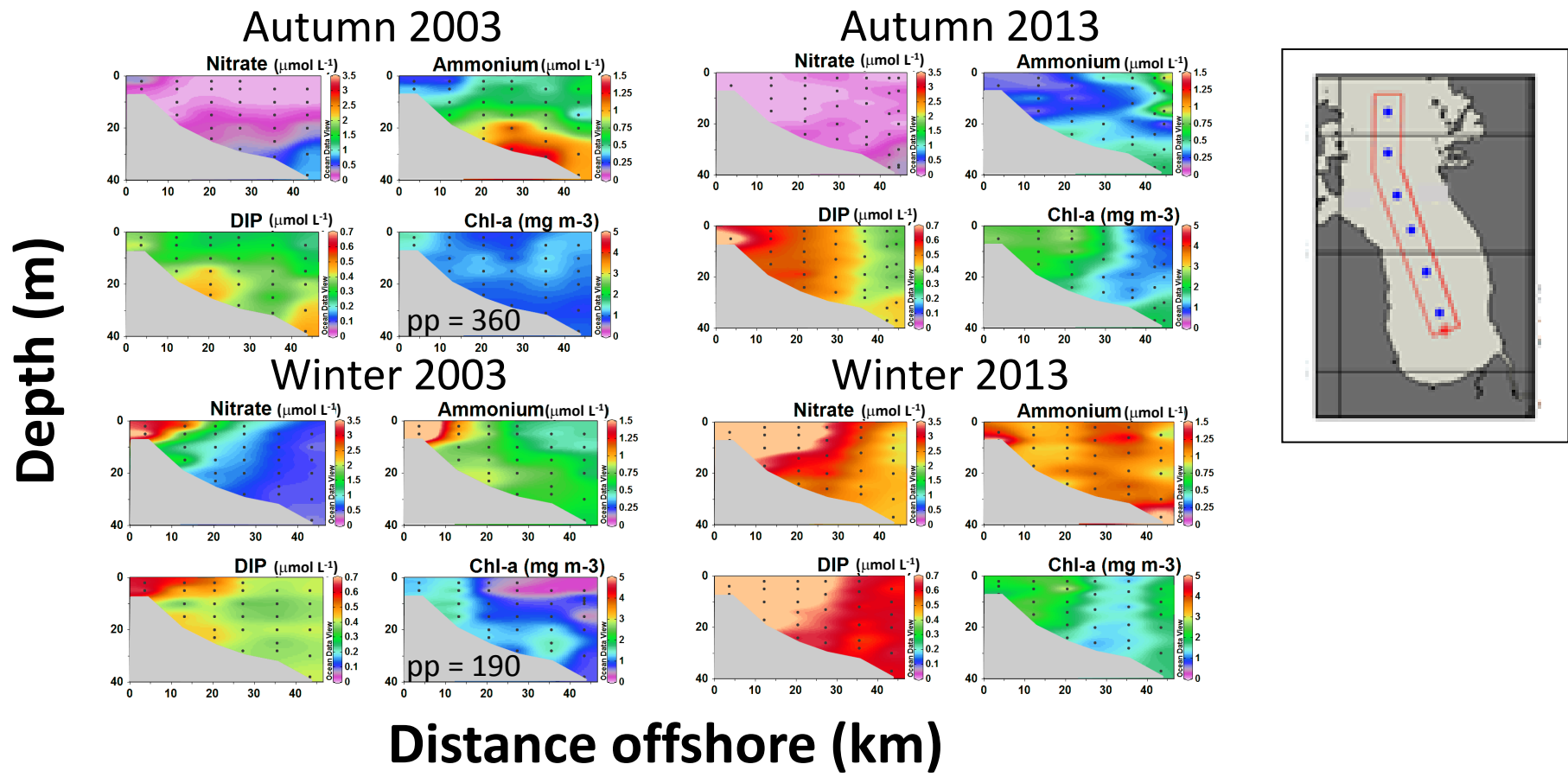**Figure 6-3:** **Transects of nutrient and chlorophyll a concentration from the inner Firth to the extended Firth (inset), by depth and season during seasonal voyages made in 2003 and 2012–13.** Rates of primary production averaged across the Firth ("pp": mg C fixed m^{-2} d^{-1}) during the 2003 surveys are annotated on the 2003 chlorophyll *a* plots. **This page: autumn and winter. Previous page: spring and summer.**

6.2   Trends

Phytoplankton pigment (chlorophyll *a* and phaeopigment[15]) and microphytoplankton cells (>2 µm cell size) have been sampled at the extended-Firth monitoring site at a 3-monthly interval over the 15-year period 1998 to 2013. The samples were collected by lowering a CTD-rosette from a research vessel. Typically samples were collected at 6 depths in the water column (these same samples were analysed for nutrients).

Plots of chlorophyll *a* and its breakdown product, phaeopigment, suggest increasing concentrations in the lower half of the water column over the 15-year measurement period (Figure 6-4).
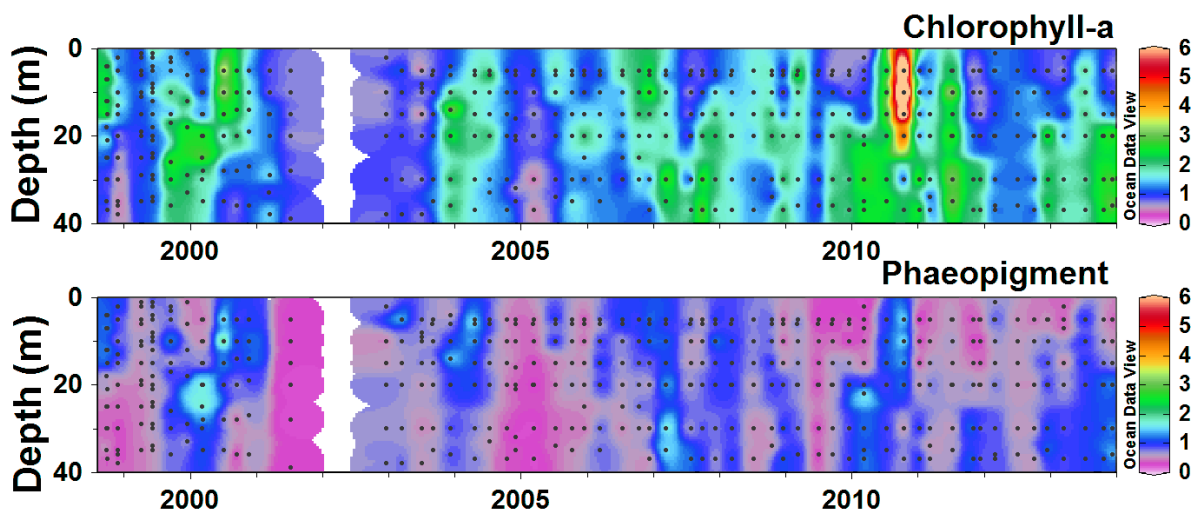
Figure 6-4:   Phytoplankton pigment concentrations (mg m^{-3}) plotted against depth below the water surface and time at the extended-Firth monitoring site.

We subjected the phytoplankton data to the seasonal Kendall trend test. For these tests, we divided some of data into two depth bins: from the water surface to 20 m below the surface (the "upper water column"), and from 20 m below the surface to 40 m below the surface (the "lower water column")[16]. This included the chlorophyll *a* and phaeopigment data. For other data, including cell counts and biomasses of different taxonomic groups, we analysed water-column-integrated data.

The results of the trend tests are tabulated in Appendix A. The results show a number of trends at the extended-Firth monitoring site over the 15-year measurement period.

- Chlorophyll *a* concentration and phaeopigment in the lower water column increased over the 15-year monitoring period. Chlorophyll *a* increased by about 4.2% y^{-1} and phaeopigment by about 2.5% y^{-1}. These were statistically significant increases.

- There was no trend for chlorophyll *a* or phaeopigment in the upper water column. This result has also been observed in monitoring data from Wilson Bay Area A (Stenton-Dozey and Zeldis, 2014) and is consistent with upper-water-column fluorometer data that we have collected.

---

[15] Phaeopigment is a product of the breakdown of chlorophyll *a*.
[16] These correspond to, roughly, above and below the pycnocline.

- Cell counts (integrated over the water column) of total microphytoplankton showed a significant increasing trend of 6.9% y^{-1} over the 15-year monitoring period (Figure 6-5). Total microphytoplankton comprises diatoms, dinoflagellates and "others" (a miscellaneous group of mostly small phytoplankton). Still in terms of cell numbers, the largest increases were in diatoms (4.6% y^{-1}) and others (6.7% y^{-1}). The cell numbers of large centric diatoms (which is a subgroup of diatoms) increased by 8.9% y^{-1}. All of these trends were statistically significant. Cell numbers of dinoflagellates showed a non-significant decreasing trend.
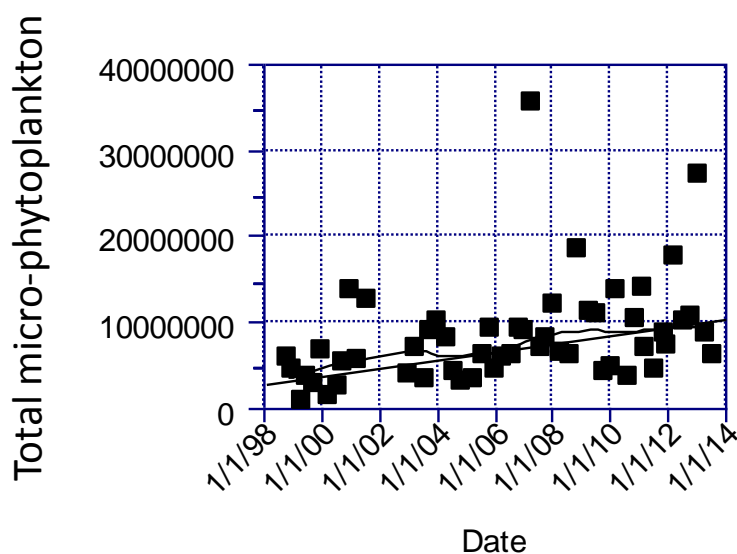

Figure 6-5: Time series of water-column-integrated total microphytoplankton cell counts (cells m^{-2} x 10^{-3}) at the extended-Firth monitoring site. The blue curves show the fitted linear Kendall trend (the straight line) and a LOWESS moving average fit (the other line) that used 40% of the points in its fitting window.

- Biomass of total microphytoplankton (integrated over the water column) increased by 2.5% y^{-1} over the 15-year monitoring period (Figure 6-6), however, this trend was not statistically significant at the 95% confidence level. (The trend had an associated *p* value of 0.07, whereas *p* < 0.05 is considered to be statistically significant.)[17] The following group trends were statistically significant: the bacteria group (7.0% y^{-1}, on a relatively high biomass), the "others" group (6.0% y^{-1}, on a relatively moderate biomass), and the prokaryotic picophytoplankton group (12.3% y^{-1}, on a relatively low biomass).

---

[17] The raw data that we have to work with are cell counts, and we convert these to biomass by assuming a certain biovolume per cell. This can lead to loss of precision in the data. For instance, we adjusted the assumed biovolume per cell through time from 1998–2013 depending on observed biovolume changes within taxa, which can occur as a consequence of maturity of the population, stage of growth cycle, etc. However, because it was impractical to make the conversion adjustments on every taxon for every sample, scope for error was introduced if the conversions were applied inappropriately through time. The effects of these errors can be substantial because the conversions generally involve cubic functions of cell dimensions.
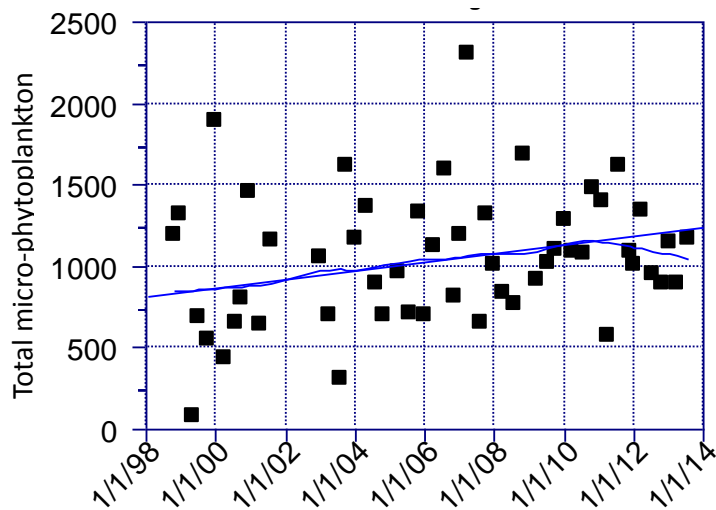
Figure 6-6: Time series of water-column-integrated total microphytoplankton biomass (mg C m^{-2}) at the extended-Firth monitoring site. The blue curves show the fitted linear Kendall trend (the straight line) and a LOWESS moving average fit (the other line) that used 40% of the points in its fitting window.

The overall changes to total microphytoplankton over the 15-year monitoring period are consistent with what might be anticipated if nutrients have become more abundant.

We looked for trends in toxin-producing phytoplankton counts and biomass.

- Potentially toxic genera were broken down into three groups; dinoflagellates, diatoms, and "others". The toxic dinoflagellates included the more prominent genera *Karenia*, *Alexandrium*, *Dinophysis*, *Gonyaulax*, *Lingulodinium*, and the less common *Ostreopsis* and *Gambierdiscus*. Toxic diatoms were limited to the genus *Pseudo-nitzschia*, which is capable of dominating the entire phytoplankton population at times. The toxic "others" group consisted of the raphidophytes including *Heterosigma*, *Fibrocapsa* and *Chattonella* as well as the occasionally observed *Oscillatoria/Trichodesmium* and *Prymnesium*.

- The only group to show a significant trend was toxic diatoms (11.3% y^{-1} increase in cell numbers), which was driven by an increase in numbers of *Pseudo-nitzschia*. However, toxic diatom biomass did not change, and neither did *Pseudo-nitzschia* biomass. This implies there was a shift to more numerous but smaller toxic diatom cells.

- *Pseudo-nitzschia* biomass makes up a small fraction of the total microphytoplankton biomass.

7   Dissolved oxygen

7.1   Data

Our primary datasets vis-à-vis dissolved oxygen (DO) derive from:

- 15 years of measurements made seasonally (every 3 months) over the period 1998–2013 at the extended-Firth monitoring site (Figure 5-1). The measurements were made using a CTD deployed from a research vessel. During this same sampling programme we were measuring nutrients and phytoplankton (reported in previous sections).

- Various spatial surveys using a CTD deployed from a research vessel.

- Moored dissolved-oxygen sensors at the extended-Firth monitoring site and at the Wilson B site, which is 25 km to the south (Figure 5-1). At both of these sites, sensors measured DO every 15 minutes.

    - The data at the extended-Firth monitoring site were collected with DO sensors mounted in the upper and lower water column at mean depths below the water surface of 10 and 33 m. Measurements were made over the period 2005–2014.

    - The Wilson B data, which were collected using a Seabird IDO MicroCAT at 5 m below the water surface, are from the period January to April, 2013[18].

7.2   Patterns in DO

Whilst we have long time series of DO at one site, we have fewer data from other sites. **Thus, we cannot make conclusive statements about the oxygen status of the entire region.** Nonetheless, the data do reveal temporal and spatial patterns, in particular, of occurrences of low dissolved oxygen in the water column.

Figure 7-1 shows temporal patterns in DO, temperature and water-column stratification at the extended-Firth monitoring site during the period 1998–2013. The data underlying Figure 7-1 were collected from a research vessel every 3 months (see caption to Figure 7-1).

---

[18] Another sensor type was also deployed at Wilson B: the "miniDOT" (Precision Measurement Engineering). We have subsequently determined that the miniDOT sensors were unacceptably affected by biofouling that rendered that data invalid. See Appendix B.
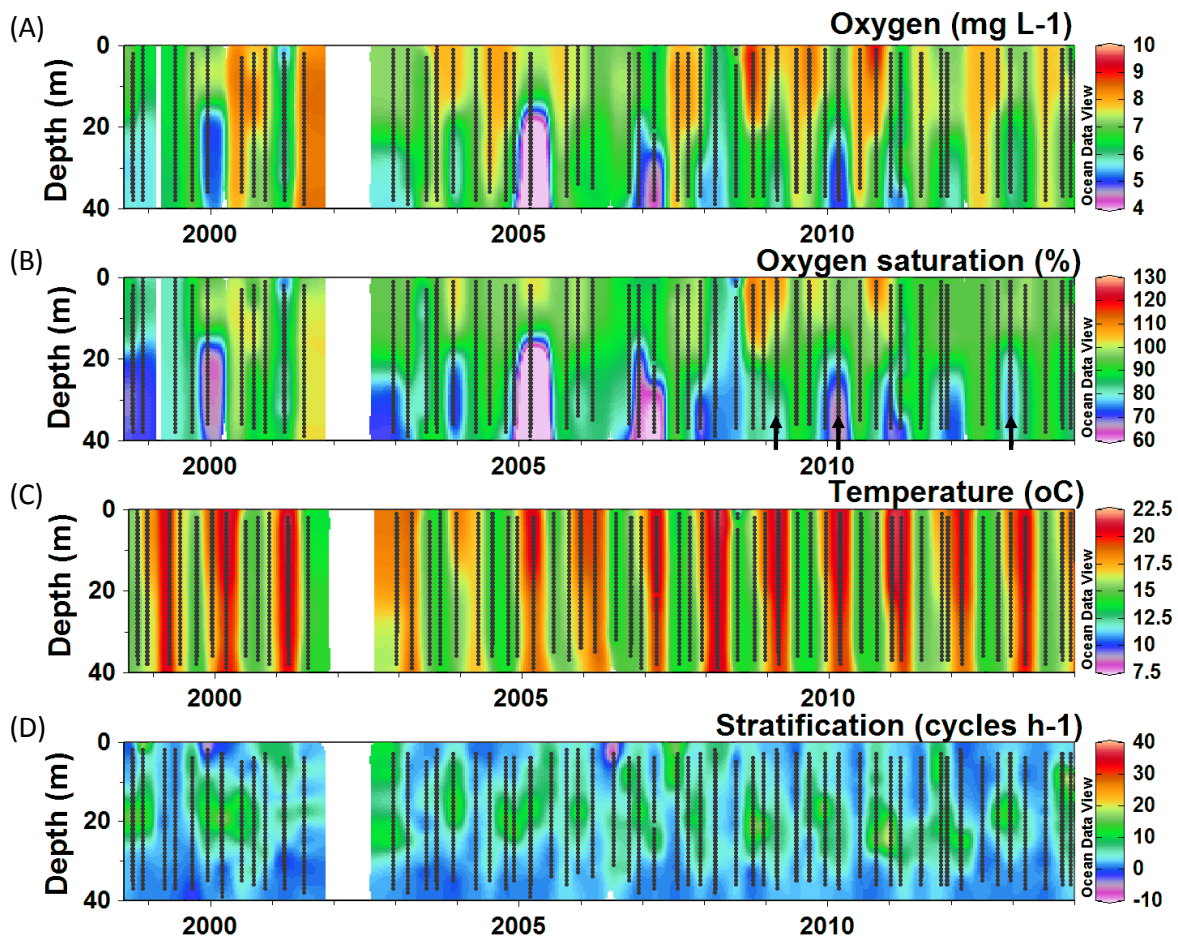
Figure 7-1: **Temporal patterns in DO, temperature and water-column stratification at the extended-Firth monitoring site inferred from measurements made by sensors mounted on a CTD and lowered through the water column from a research vessel. The vessel visited the site every 3 months during the period 1998–2013.** The black dots show the dates and vertical locations of DO records. The black arrows in panel (B) are referenced in Figure 7-2.

The data show:

- The upper 20 m of the water column at the extended-Firth monitoring site was generally well oxygenated (panels A and B), with greater than 90% DO saturation for much of the year.

- In summer and autumn (the higher temperatures in panel C), when the water column was stratified[19], DO typically reduced to about 60–70% saturation (4.9 and 5.7 mg L^{-1}, respectively) at levels in the water column greater than 20 m below the surface.

The data shown in Figure 7-1 were collected from a ship every 3 months. The moored instruments at the extended-Firth monitoring site and at Wilson B made measurements every 15 minutes, so they show more temporal detail.

The extended-Firth 15-minute data (2005–2014) (made with moored sensors) are quite consistent with the data shown in Figure 7-1. They show:

---

[19] Panel D shows the Brunt Väisälä frequency (*N*, units of cycles h^{-1}), which is indicative of water-column stratification: higher *N* means more strongly stratified.

- In two of six years where the 15-minute record is complete, subsurface[20] DO remained below 60% saturation for several weeks (Figure 7-2). The lowest recorded subsurface DO was about 40% saturation (2.7 mg L^{-1}).

- On rare occasions, and for periods of only a few days, surface[21] DO dropped as low as 40% saturation (Figure 7-3). DO was low at the surface less often and for shorter periods (maximum of about two weeks) than it was in the subsurface.

  Note that periods of lower DO nearly always occurred when the water column was stratified.

The Wilson B 15-minute data (January to April, 2013) show:

- At 5 m below the water surface, DO reached a minimum of 70–75 % saturation (Figure 7-4). At these times the water was colder and more saline, and subsurface DO at the extended-Firth monitoring site was also low (60% saturation).

Comparison of the extended-Firth 15-minute data with the Wilson B 15-minute data reveals an important detail:

- Less-than-saturation DO at Wilson B (5 m below the water surface) occurred just briefly (for between 40 and 60 minutes) on flooding tides and coincided with the appearance of colder and more saline water at the site. We interpret this as meaning that low-DO water that appears at Wilson B is the same low-DO bottom water that appears at the extended-Firth monitoring site, with currents transporting ("advecting") the water between the two sites.

---

[20] "Subsurface" here means at 33 m below the surface.
[21] "Surface" here means at 10 m below the surface.

Figure 7-2: **Time series from the extended-Firth monitoring site, 2005–2014.** The data are from the lower water column, 33 m below the surface. The circled data in the % saturation plot are coincident with the CTD oxygen data arrowed in Figure 7-1. At a salinity of 35, 100 µmol O_2 kg^{-1} ≈ 3.3 mg O_2 L^{-1}.
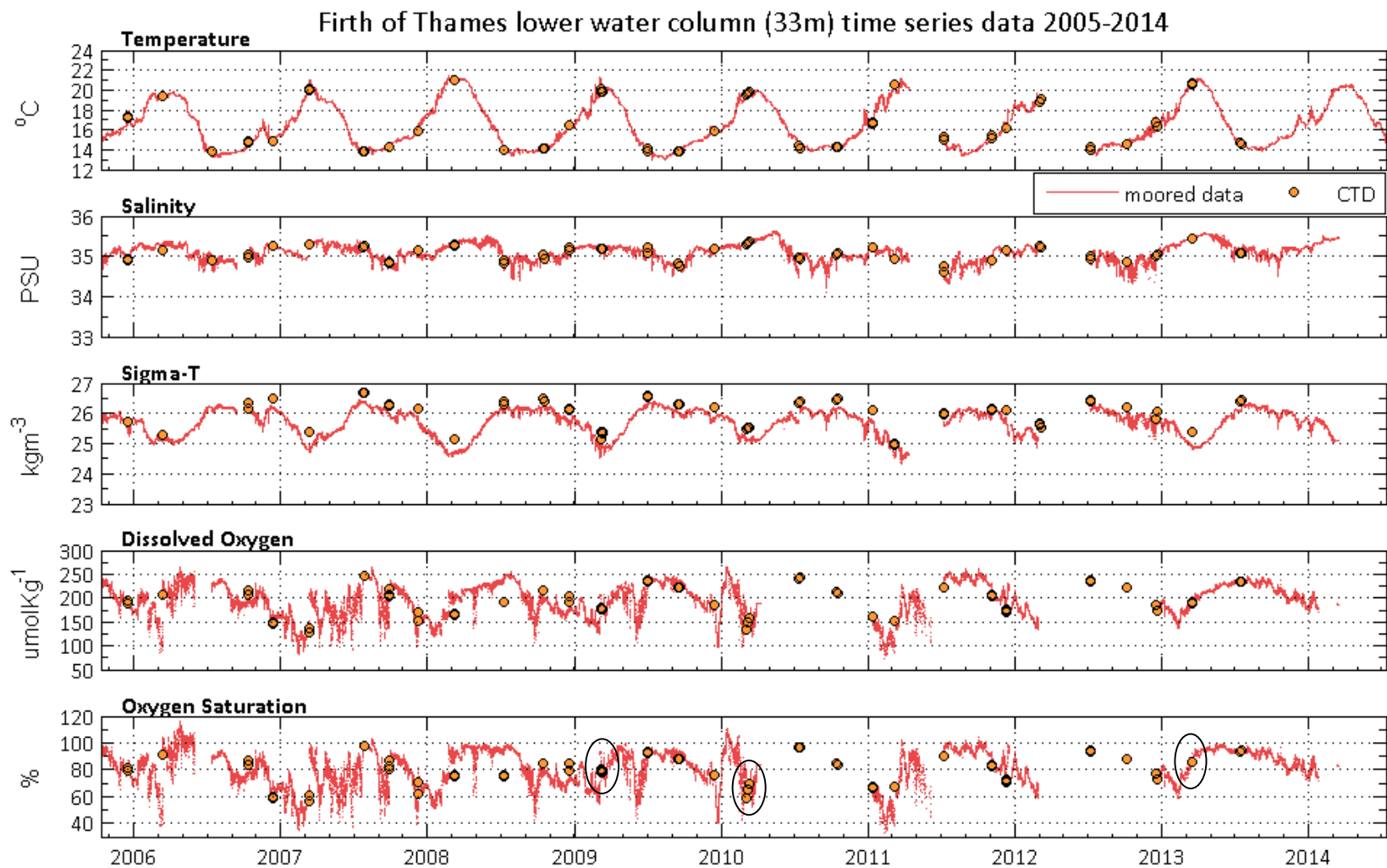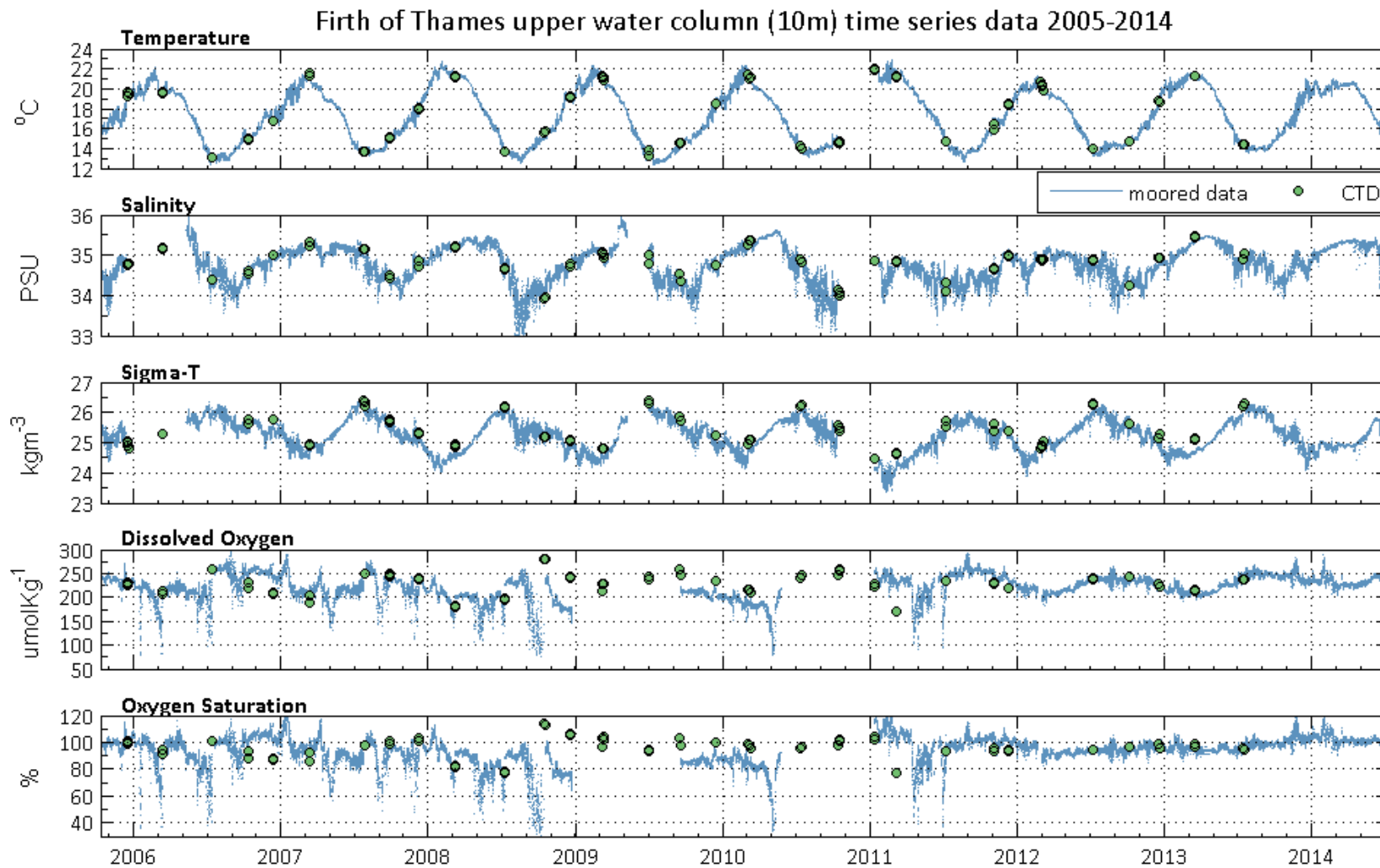
Figure 7-3: **Time series from the extended-Firth monitoring site, 2005–2014.** The data are from the upper water column, 10 m below the surface. At a salinity of 35, 100 μmol O$_2$ kg^{-1} ≈ 3.3 mg O$_2$ L^{-1}.
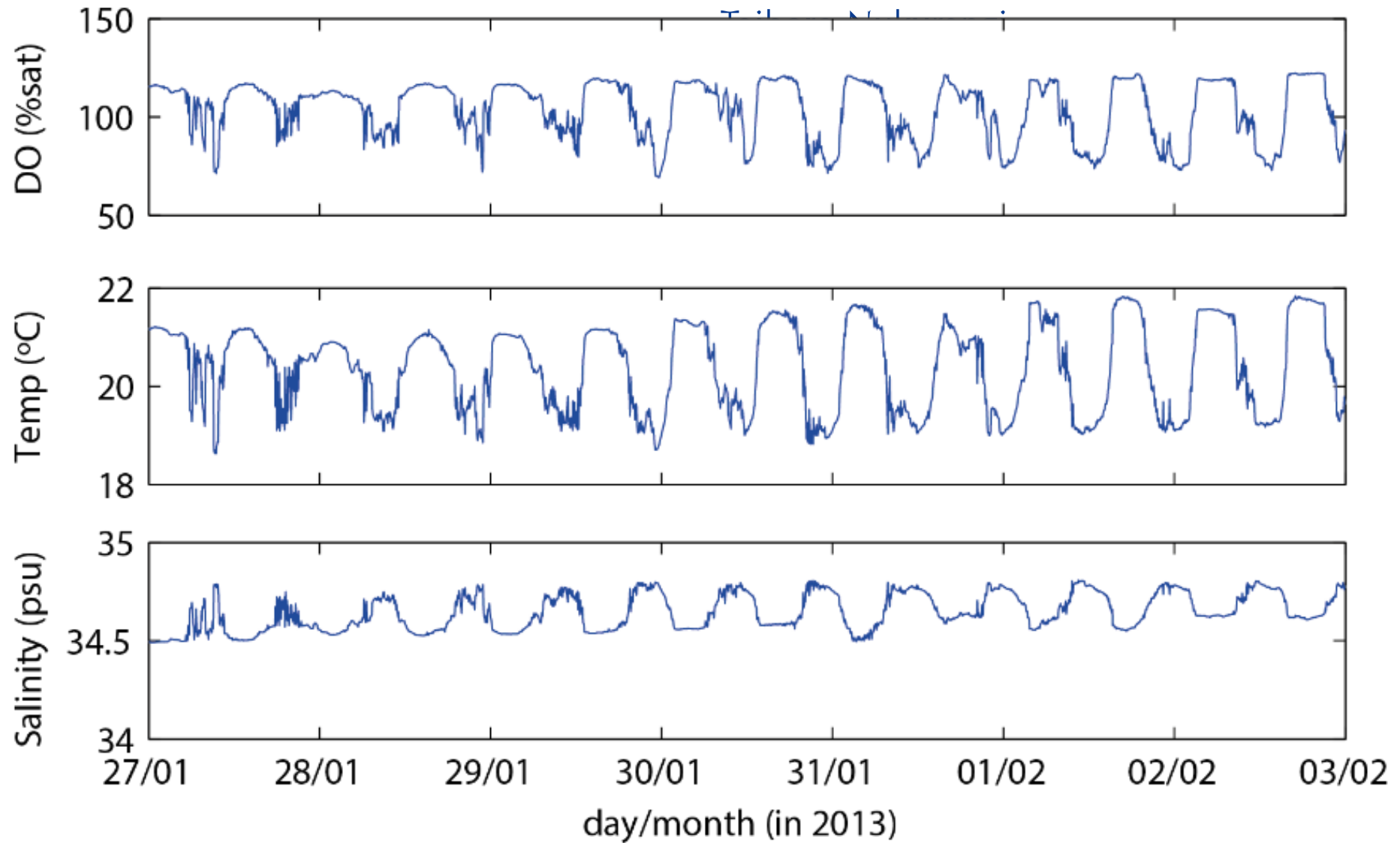
Figure 7-4: DO, temperature and salinity at Wilson B (5 m below the water surface) from January 27 to February 3, 2013.

Spatial surveys of DO conducted in autumn of each of three years show some further important features (Figure 7-5). For example, greatest oxygen depletion coincides with highest levels of phytoplankton deep in the water column (see, especially, the year 2010 in Figure 7-5). The extent of oxygen depletion is variable in strength from year to year[22]. Also, low DO, when it occurs, is contiguous between the extended-Firth monitoring site and Wilson B (not shown) but, moving into the Firth, the oxygen depletion becomes less pronounced. That is, the autumnal subsurface minimum is most intense in the extended Firth. A likely explanation is that the shallower water in the inner Firth inhibits water-column stratification, and this inhibition favours reoxygenation of the water column[23].

Figure 7-6, which shows oxygen data acquired in autumn in 3 separate years at 3 latitudes across the Gulf and Firth, provides more detail on the distribution of DO. For example, DO near the seabed reached 4.2 mg L^{-1} in the vicinity of Wilson Bay Areas A and B in autumn 2010. In autumn of 2009, DO near the seabed was 5.4 mg L^{-1}.

---

[22] Some of that variability may arise because we sampled on slightly different days in different autumns.
[23] Stratification hinders reoxygenation from the atmosphere by capping mixing and overturn of the water column, hence the absence of stratification favours reoxygenation. Water-column stratification breaks down in shallow water because, amongst other things, bottom-generated turbulence associated with tidal currents, wind-generated currents and waves is more effective at mixing the water column.
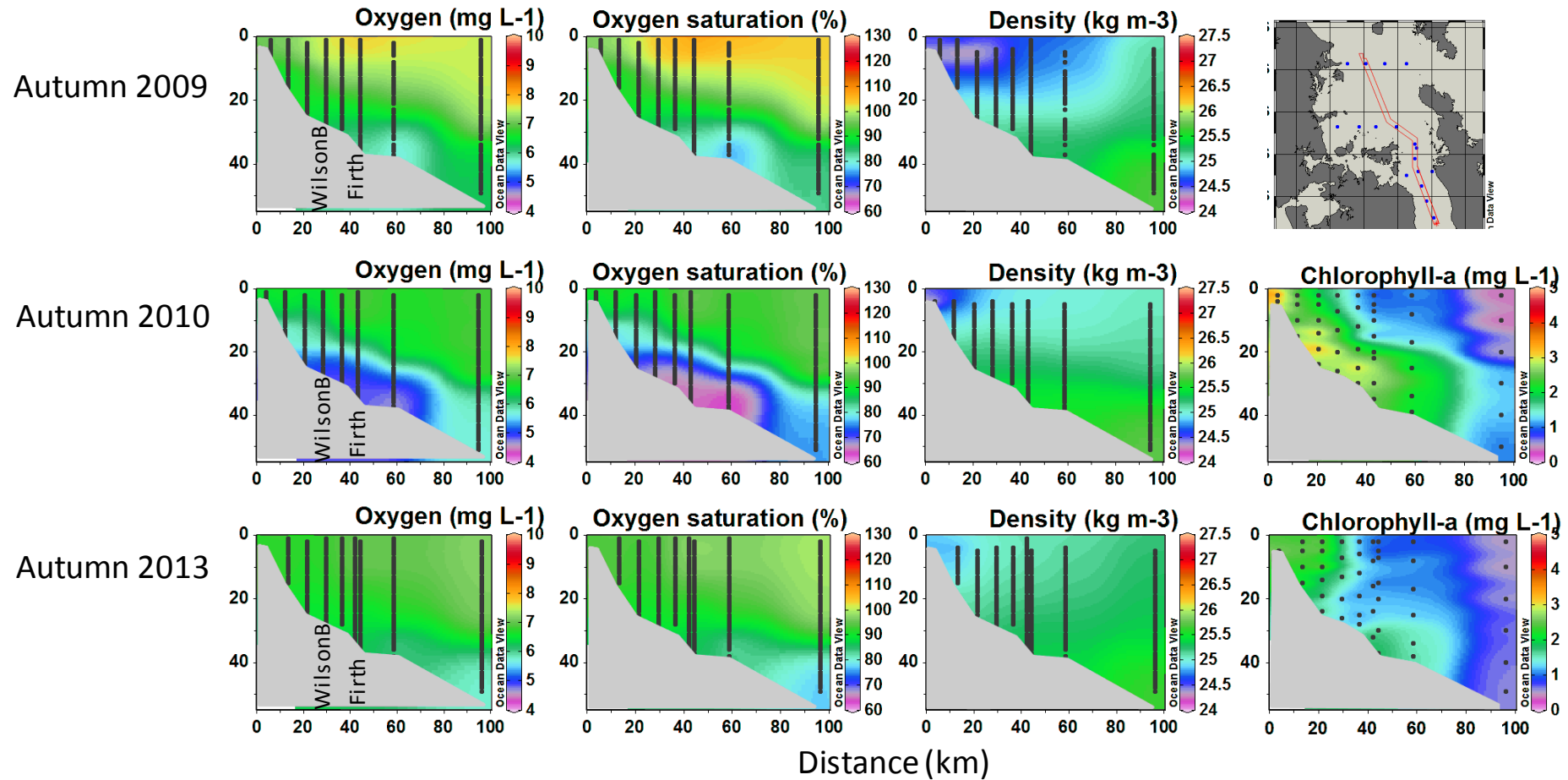
Figure 7-5: **Autumn survey data, 2009, 2010 and 2013.** Shown are oxygen concentration, oxygen saturation, seawater density and chlorophyll *a* at stations indicated in the inset map. The extended-Firth monitoring site and Wilson B mooring site are labelled in the left panels.
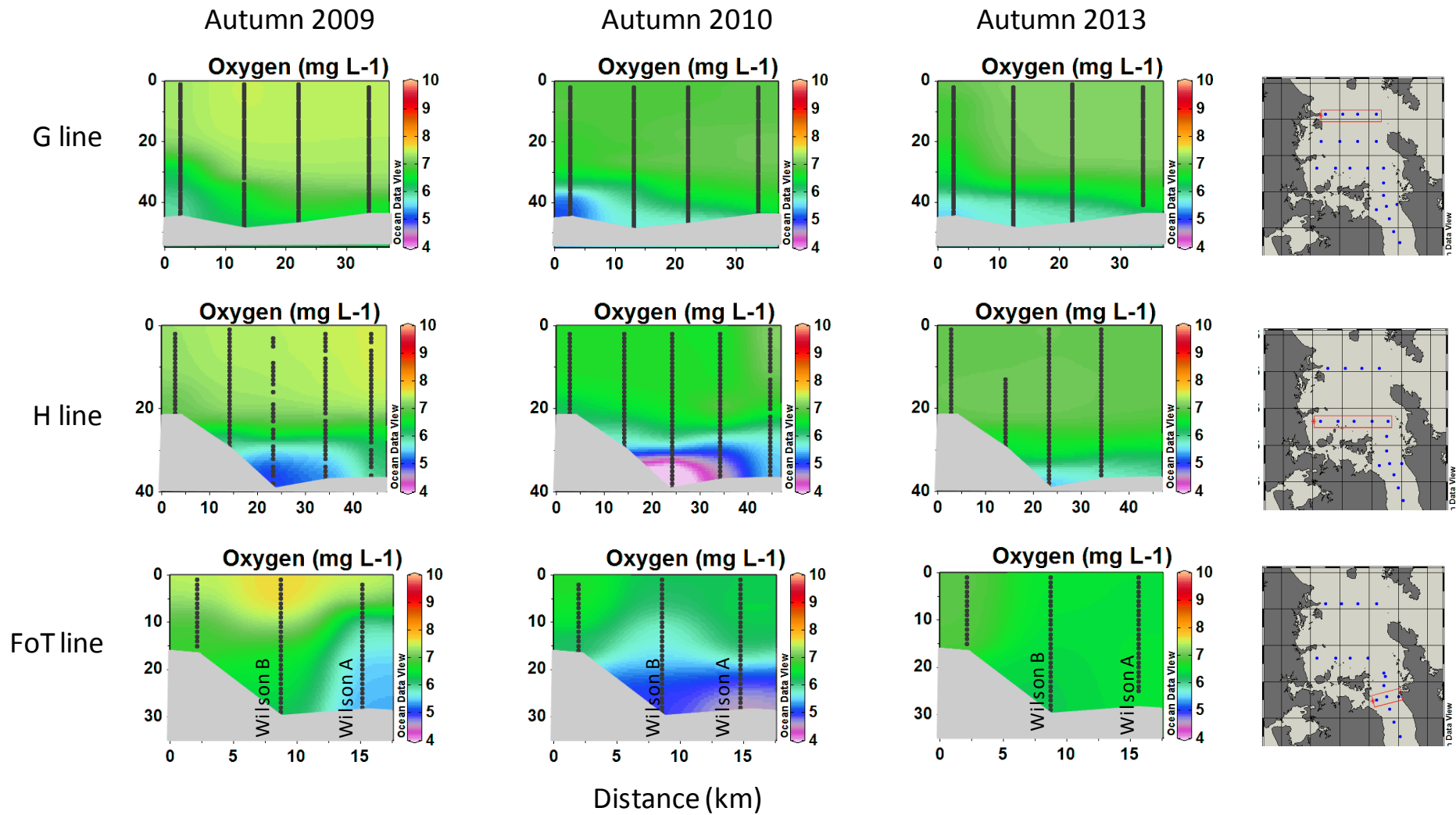
Figure 7-6: **Oxygen in the Firth and Hauraki Gulf in autumn 2009, 2010 and 2013.** Data are shown for 3 latitudinal sections.

Firth of Thames Water Quality and Ecosystem Health – Synthesis

7.3   Causes of oxygen depletion

We attribute the seasonal depletion of DO to a combination of at least two factors: strong stratification of the water column in late summer and autumn that inhibits oxygen exchange with the atmosphere which otherwise would replenish the DO in the water column; and consumption of oxygen by microbial respiration of sinking organic matter that has accrued from primary production in the immediately preceding spring and early summer.

The cold, high-salinity water that sometimes upwells from deep in the ocean onto the coastal shelf also tends to have low oxygen concentrations. **Nonetheless, we do not believe that this is the driver of the annual oxygen depletion that occurs in late summer/early autumn because upwelling is most frequent in late winter, spring and early summer.** Also, DO saturation in the upwelling water is rarely much below 80%. Thus, even if this water were to enter the extended Firth in the autumn, it could not, alone, be deemed to be the sole driver of the depressed oxygen.

7.4   Trends

We have conducted a trend analysis of the DO data shown in Figure 7-1. For this, we divided the DO data into two depth bins: the first bin was the top 20 m of the water column, and the second bin was everything below that, and we used the seasonal Kendall trend test for the analysis. **The result was that there was no trend in time in DO in either depth bin.** The results of the trend tests are tabulated in Appendix A.

Further analysis could examine relationships between water-column stratification and phytoplankton. The results might reveal more information on how stratification and organic matter influence oxygen depletion.

8 pH

8.1 Data

Carbonate system parameters (pH, partial pressure of CO_2 [pCO_2], dissolved inorganic carbon [DIC] and total alkalinity) were surveyed over the Firth and Hauraki Gulf during a voyage in autumn 2010 and during 4 seasonal voyages in 2012–13.

8.2 Results

The partial pressure of CO_2 was near or below atmospheric pressure in spring, reflecting spring-bloom consumption of CO_2 by actively growing phytoplankton. pCO_2 started to increase in summer and then peaked in autumn. Values were lowest in winter, being under-saturated with respect to the atmosphere over most of the region, when the water column was well mixed and phytoplankton were moderately abundant.

In summer and especially in autumn, there was a consistent decreasing seaward gradient in surface pCO_2, with maximal DIC oversaturation in the Firth of Thames, moderate oversaturation in the extended Firth of Thames, and values near neutral (atmospheric) in the Hauraki Gulf.

pH deep in the water column varies inter-annually. pH is near oceanic values (~8.05–8.1) in spring over the whole region, but starts dropping in summer. pH reaches its lowest value (~7.9) in autumn. pH increases in winter back toward oceanic values.

The pH minimum coincides with oxygen depletion. **From this, we can infer that the same combination of physical and metabolic processes that we believe to be driving DO is also driving the carbonate system.** That is, the same microbial respiration that consumes organic matter in the late summer and early autumn and produces CO_2 also pushes pH down to a minimum (most acidic) at the same time. Acidification lowers the calcium carbonate saturation state.

As further evidence of this connection we note that, at the extended-Firth monitoring site, higher pCO_2 and lower pH and saturation state occur near the seabed as opposed to near the sea surface (except in winter, when the water column is mixed). This indicates a metabolic association with oxygen consumption.

8.3 Trends

We have been observing carbonate system dynamics since 2009 but complete records started only with the 2010 survey. **This is too short a record to say anything about trends in the carbonate system.**

9   Mineralisation of organic matter

"Mineralisation" is the breakdown by living organisms of organic matter into inorganic substances. It is the opposite of the process of assimilation of inorganic nutrients into organic matter.

"Benthic" mineralisation occurs within and close to the seabed and "pelagic" mineralisation occurs in the water column.

Here we compare benthic and pelagic mineralisation, which have implications for the oxygen and carbonate system indicators of eutrophication (discussed in section 11.1 where we assess the trophic state of the Firth).

9.1   Benthic mineralisation

- The rate of benthic mineralisation of organic matter is highest in the inner Firth.

- At all sites that we have made measurements (which includes the Firth, the extended Firth and the inner Hauraki Gulf), there was net oxygen consumption by the sediments. That is, benthic respiration exceeded primary production at the seabed. Thus, the seabed was net heterotrophic. This was found to be the case regardless of water depth or bed-sediment type.

  Net heterotrophy means that more organic matter is mineralized than is synthesised. If the measurement period upon which this kind of conclusion is based is too short to accommodate natural cycles of production and destruction, then the "excess respiration" might be of stored organic matter generated within the system prior to the measurement period. However, in this case we believe that the necessary organic matter is fuelled by nutrients supplied from outside of the system, meaning from the ocean or supplied by rivers. We comment further on this in section 10.

- Net daily oxygen consumption by sediments was typically two times higher at sites in the inner Firth compared to sites in the extended Firth.

- Comparing measured fluxes of O_2 (and, by implication, CO_2) with corresponding flux and denitrification data from numerous Australian estuaries (reviewed in Eyre and Ferguson, 2002), we infer that denitrification efficiency (proportion of the nitrogen entering the seabed that is subsequently denitrified) may be maximum in the extended Firth and close to maximum in the inner Firth. Denitrification efficiency is dependent on the rate of input of organic matter to the bed sediments. **Hence, with efficiency already near or at maximum, further increases in organic matter to the seabed may reduce denitrification efficiency, depending on how close the system is to any threshold for decline in efficiency**.

  Denitrification measurements are required to assess if further increases in organic matter loadings to the seabed would have an effect on denitrification efficiency.

9.2   Pelagic mineralisation

- Measurements of pelagic oxygen demand in autumn showed strong net heterotrophy, with the rate of net O_2 drawdown (by respiration) at inner-Firth sites being about twice the rate at extended-Firth sites.

- Despite that, DO at inner-Firth sites remained high. We believe this is because the inner sites are in shallow water that does not stratify. Consequently, atmospheric oxygen is readily able to penetrate through the water column (see section 7). DO became depleted at extended-Firth sites, which were isolated from the atmosphere by water-column stratification.

- The ratio of water column-to-sediment respiration was 50:50 at inner-Firth sites and 90:10 at extended-Firth sites.

10   Water, salt and carbon/nutrient budgets

We developed a water budget, a salt budget and a carbon/nutrient budget for the Hauraki Gulf, extended Firth, and Firth of Thames. These help us to understand the relative importance of sources and the exchanges between different parts of the system.

We used the Land-Oceans Interaction in the Coastal Zone (LOICZ) biogeochemical budgeting procedure to produce the budgets. Each budget divides the region into 3 boxes (Figure 10-1).

The water and salt budgets are "conservative" meaning that water and salt do not change form. In contrast, the carbon/nutrient budget is non-conservative, reflecting the biogeochemical processes that transform these elements (e.g., assimilation of carbon into organic matter by autotrophs and the breakdown of organic matter into carbon dioxide by heterotrophs).

Net ecosystem metabolism (NEM) is the balance between primary production and decomposition of organic material by the system.
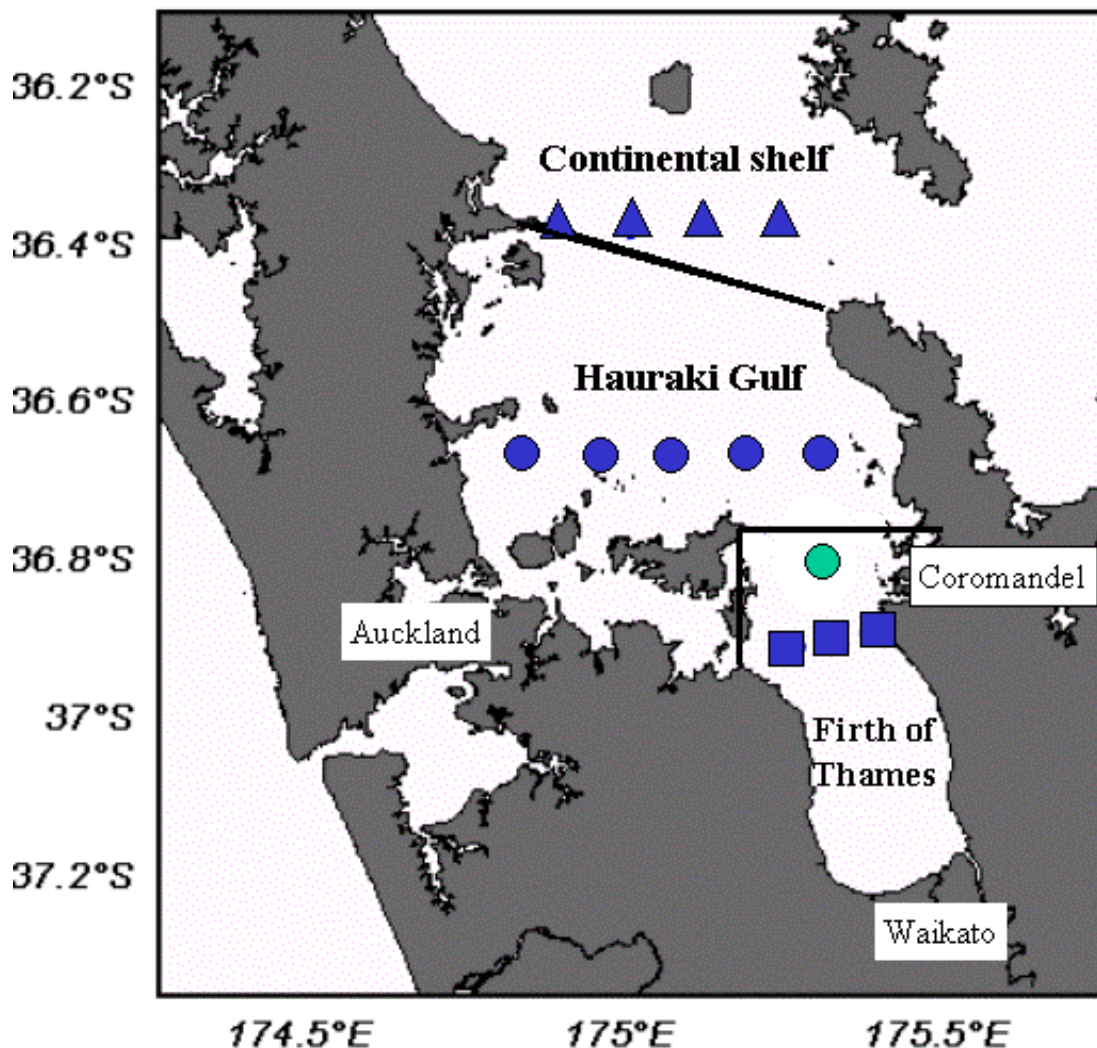

Figure 10-1:   Division of the region into 3 boxes for the purpose of developing budgets. Note that the Firth of Thames as defined for the purposes of the budgeting includes what we are calling in this report the Firth of Thames plus the extended Firth (see Figure 1-1).

We used a wide range of data to construct the budgets. These include NIWA's numerous surveys of water quality in the Firth, the extended Firth and the Hauraki Gulf, estimates of freshwater nutrient loadings, river flow, rainfall, evaporation, and discharges of treated sewage effluent.

Because of data limitations, the budgets for the Gulf are valid for spring, summer and winter, while those for the Firth are valid for spring, summer and autumn. The budgets represent the conditions that prevailed during 2000–2001 surveys; at this time river flows were either close to average (for spring and autumn) or about 60% of average (for summer and winter). Sampling did not include conditions of strong upwelling.

Some key results are:

- Rivers that drain to the Firth contribute 57% of total N inputs (DIN + DON + PON) and 87% of DIN inputs to the Firth, with the remainder coming from offshore.

- The average time required to exchange the water volume of the Firth with the Gulf is 20 days. The exchange time of the Gulf with the shelf and the Firth is 32 days.

- The Firth appears to be a net importer of organic phosphorus and a net exporter of inorganic phosphorus. The phosphorus flux shows net decomposition of organic matter to inorganic nutrients and net production of dissolved inorganic carbon (e.g., CO_2). These observations are consistent with the view that the Firth waters are net heterotrophic (more organic matter is mineralized than is created on a net basis).

- The nitrogen balance is also non-conservative. In this case, the system is a net exporter of organic nitrogen and a net importer of inorganic nitrogen. Overall, much more nitrogen is imported than is exported. In contrast to phosphorus, nitrogen does have a gaseous phase. We infer that much of the "excess" nitrogen is not retained within the system. Rather, we believe that it is being denitrified and exported as N_2. The denitrification rates predicted from the budget are consistent with N_2 losses inferred from direct carbon and nutrient flux measurements made in shipboard experiments in the Firth. Further measurements are required to better constrain rates.

- For the Firth, the rate of primary production is, on average, slower than the rate of respiration of organic matter. This causes the net ecosystem metabolism to be heterotrophic. In contrast, the Hauraki Gulf is nearly balanced between autotrophy and heterotrophy.

- For the Firth, the excess of respiration over production (i.e., the net heterotrophy) must be subsidised by net import of substantial amounts of labile organic carbon from the land and/or from offshore.

- The Firth is a large denitrifier. About 73% of the total nitrogen export from the Firth (total = denitrification plus DON export) appears to be as N_2 gas. This helps to buffer the system against nitrogen loading from terrestrial and marine sources.

- On average, nitrogen in the Firth cycles about four times through the production–decomposition cycle before being lost to denitrification or (to a lesser extent) hydrographic export. This "amplifies" the effects of nitrogen imported to the Firth in terms of generating primary production.

11 Assessments of water quality and ecosystem health

11.1 The current trophic state of the system

Phytoplankton biomass and growth are known to be related to nutrient loading but the relationships between nutrient loading and the actual expression of the symptoms of eutrophication (including phytoplankton blooms and depletion of dissolved oxygen) are governed by physiographic "filters". For instance, shallow estuaries with short water residence times flush phytoplankton to the sea before they can assume bloom proportions. Also, highly turbid systems limit light which in turn limits growth even under heavy nutrient loading.

The Firth and extended Firth are sensitive to nutrient enrichment (meaning that symptoms of eutrophication are not likely to be suppressed by physical factors such as turbid water/low light, short water residence time, and strong vertical mixing).

This makes the Firth more susceptible to adverse effects from sediment and/or nutrient inputs from the land than either shallower, more rapidly flushed estuaries or coastal waters along an energetic, open coastline.

Our reasons for this assessment are:

- the water is relatively clear[24], which means that light is available to drive primary production;

- the water residence time is long, which means the system is capable of supporting phytoplankton blooms that undergo complete life cycles of growth, retention and senescence;

- the water column is periodically stratified, which enhances the depletion of dissolved oxygen.

In this section, we look at the question of the trophic state of the system in a couple of different ways.

(a) It is not possible to evaluate trophic state simply by referring to nutrient concentrations in the water column. For one thing, physical factors such as light climate, water-column stratification, horizontal mixing and turbidity may all affect the expression of the actual symptoms of eutrophication[25]. Nevertheless, water-column nutrient concentrations have been used to assess "trophic state", meaning, broadly, the extent to which the symptoms of eutrophication are expressed.

- ANZECC (2000) guideline trigger levels give a threshold of 30 mg DIN m^{-3} for "slightly disturbed estuarine water"[26,], which is strictly relevant for southeast Australia only[27]. The current median value of DIN at the extended-Firth monitoring site is typically less than this (about 20 mg m^{-3}, based on Figure 5-3[28]).

---

[24] Despite the high turbidity in the inner Firth in particular, enough light generally reaches the bottom to generate primary production.
[25] Including depleted DO, acidification and reducing conditions in bed sediments.
[26] To aid conversion among units note that 1 μmol L^{-1} DIN = 14 mg m^{-3} DIN.
[27] These guideline figures were derived using data from estuaries in SE Australia. There is an implicit assumption that, were data available from NZ estuaries, they would point toward a similar threshold being applicable.
[28] This is calculated as the water-column-integrated value (from Figure 5-3) of about 55 mmol DIN m^{-2}, divided by the water depth (39 m) and converted to units of mg using the factor of 14.

- For southeastern USA estuaries Sheldon and Alber (2010) give limits of <25 mg DIN m^{-3}, 25–250 mg DIN m^{-3} and >250 mg DIN m^{-3} for water classified as "good", "fair" and "poor", respectively. The data in Figure 5-3 (roughly) place the waters at the extended-Firth monitoring site in the "good" category[29].

Further inshore, Vant (2011) measured nutrients and chlorophyll *a* in shallow subtidal Firth waters monthly at 3 sites during the period 2006–2007. Vant reported medians of 200–400 mg TN m^{-3} and 6–45 mg DIN m^{-3}. DIN varied over a very wide range of 6–940 mg m^{-3} with the high values (200–940 mg m^{-3}) occurring when phytoplankton growth became light-limited in winter. Vant's median values place the waters of the inner Firth approximately in the "fair" category of Sheldon and Alber (2010).

(b) The NOAA Assessment of Estuarine Trophic Status (ASSETS) is a protocol for evaluating eutrophication based on the National Estuarine Eutrophication Assessment (NEEA) database (Bricker et al., 2003). ASSETS is an integrated method for eutrophication assessment that combines an index of overall pressure from human influence (OHI), an assessment of eutrophication status, and an index of the level of management of the system. The OHI uses a simple mass-balance model based on nutrient loading from the land and system susceptibility.

NOAA developed thresholds for chlorophyll *a* with a group of regional experts (Sutula, 2011) and concluded that estuaries with chlorophyll *a* during "annual bloom periods" less than 5 mg m^{-3} appear to show "low impacts". Estuaries with annual-bloom chlorophyll *a* between 5 mg m^{-3} and 20 mg m^{-3} show "medium impacts" and estuaries with annual-bloom chlorophyll *a* in excess of 20 mg m^{-3} show "high impacts". These thresholds refer to bloom conditions (Table 2 in Bricker et al., 2003) and should not be confused with annual means, which would be, by definition, considerably lower. "Impacts" include decline in submerged aquatic vegetation, shift in phytoplankton community structure, high turbidity and low bottom-water oxygen.

Within the European Union, the Water Framework Directive uses phytoplankton biomass, taxonomic composition, and abundance and frequency of plankton blooms as "biological quality" elements in a framework to categorize waterbodies by ecological condition (Sutula, 2011). The WFD uses chlorophyll *a* thresholds that are similar to those used by ASSETS: <5 mg m^{-3} is considered undisturbed or slightly disturbed, and >30 mg m^{-3} is highly disturbed or hypereutrophic.

Eleven years of data from moored fluorometers (Figure 11-1) at the extended-Firth monitoring site show that chlorophyll *a* in excess of 4 mg m^{-3} is often experienced in both the upper water column (7 m below the water surface) and the lower water column (20 m below the water surface). These are seasonal highs, occurring from late spring/early summer to autumn each year. The data also show that chlorophyll *a* at the extended-Firth monitoring site has exceeded 5 mg m^{-3} on rare occasions at both levels in the water column. The 5 mg m^{-3} threshold is approached and seasonally exceeded in the inner Firth, as shown by chlorophyll *a* maps produced from underway sampling during 2012–13 (Figure 11-2).

Vant (2011) summarised water-quality data from three sites in the southern Firth of Thames. The sites were sampled monthly for 13 months. Median chlorophyll *a* concentrations ranged from 2.3–4.0 mg m^{-3} (range 0.4–9.3). The 5 mg m^{-3} threshold had been exceeded on several sampling occasions in the southern Firth. Vant concluded that there were no obvious grounds for concern, however he did

---

[29] It is typically the case that little guidance is given on how threshold figures like these should be calculated/used. For instance, do they refer to depth-averages or the surface layer? Are they annual averages and, if so, what "type" of average (mean, median, maximum)?

not have access to our extensive data from the extended Firth or to our 2012-13 underway sampling data, and based his conclusion upon his 13 months of southern Firth data alone.

To summarise, our data show that the Firth of Thames seasonally exceeds the NOAA ASSETS 5 mg m^{-3} chlorophyll a threshold for "medium impacts". This threshold is rarely exceeded at the extended-Firth monitoring site but it is frequently approached. Both regions are below the 20 mg m^{-3} "high impact" threshold. Thus, the ASSETS classification places the Firth in the "medium impacts" category while the extended Firth is at the upper end of "low impacts".

Figure 11-1:   Time series of chlorophyll a (mg m^{-3}) measured by INF fluorometers at the extended-Firth monitoring site from 2004 to 2014. The upper panel shows data from the INF deployed 7 m below the water surface and the lower panel shows data from the INF at 20 m below the surface.

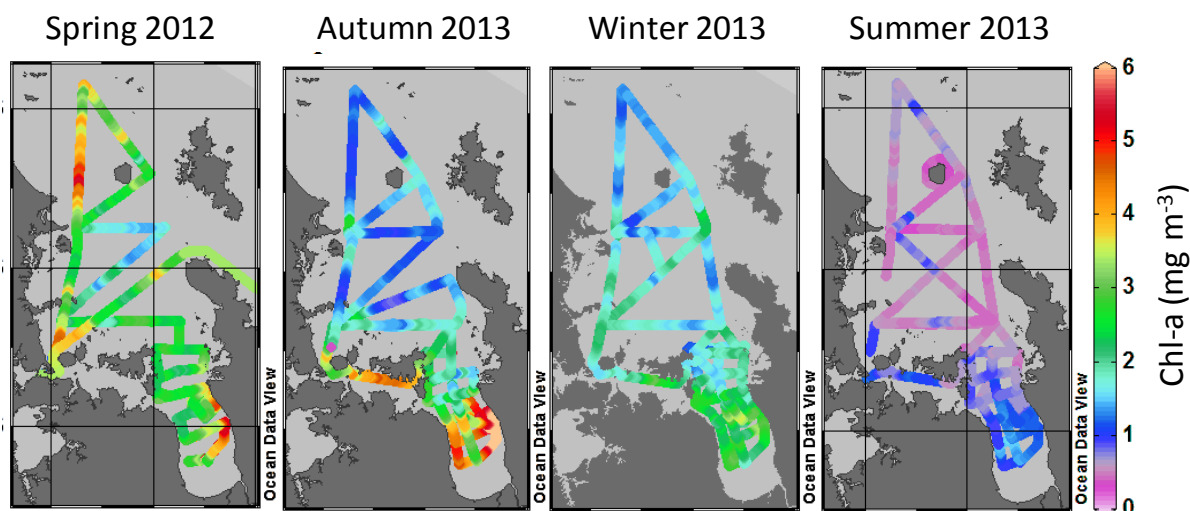| Spring 2012 | Autumn 2013 | Winter 2013 | Summer 2013 |

Figure 11-2: **Surface chlorophyll *a* concentration (mg m^{-3}) mapped using underway sampling 2012–2013.**

In a trophic rating system produced by Eyre and Ferguson (2009), sediments at extended and inner Firth sites are classified as "oligotrophic" and "approaching mesotrophic", respectively. This is based on our experimental measurements of benthic mineralisation, described in section 9, from which denitrification efficiency was inferred. However, Eyre and Ferguson's system applies strictly to Sydney metropolitan estuaries, and there appear to be issues in its application.

A commonly used trophic rating system for coastal waters based on water-column primary production rates (Nixon, 1995)[30], places the Firth and the extended Firth at the "mesotrophic" level of productivity. This is based on our experimental measurements of primary production averaged over all seasons from the inner Firth to the extended Firth (5 seasonal voyages) which found production to be about 191 g C m^{-2} y^{-1} (see Figure 6-2 for the voyage data). Systems with that level of productivity can be expected to export a high proportion (~45%) of production out of the upper water column to be degraded at depth by senescence and microbial processes.

Based primarily on our primary-production data, **we would describe the current state of the Firth and the extended Firth as mesotrophic**, where mesotrophic is the intermediate state between oligotrophic and eutrophic.

We comment below on what the pre-catchment-development trophic state of the Firth of Thames might have been.

11.2   The contribution of land runoff to nutrients

Our nutrient budget for the Firth (which is based on measurements collected during spring, summer and autumn during 2000–2001 only – see section 10) shows that the total nitrogen load to the Firth is dominated by land inputs (87% of DIN and 57% of TN)[31].

---

[30] Nixon (1995) defined eutrophication as a process which increases the rate of supply of organic matter to an ecosystem. The Nixon (1995) trophic classification designates oligotrophic as <100, mesotrophic as 100–300, eutrophic as 301–500 and hypertrophic as >500 g C m^{-2} y^{-1} primary production.

[31] The budget does not apply to periods of strong ocean upwelling, which will bring more nutrients into the system, in which case the dominance of land inputs will be less. However, MacDiarmid et al. (2009) showed that upwelling-favourable conditions occur for only 11% of the time. MacDiarmid et al. (2009), OS2020 Bay of Islands Coastal Project: Phase 1 – Desktop study. NIWA Client Report WLG2009-3, 396 pp.

Cooper and Thomsen (1988), in comparing adjacent pasture, pine and native-forest clad catchments, found that leaching from pasture averaged about 3 times that from native-forested catchments. For the developed catchments of the Hauraki Plains, Vant (2011) estimated that point and diffuse human sources contribute 8% and 70% of the TN load to the major rivers, respectively, with "natural" sources making up the remainder.

Hence, we think it is likely that the balance between land-side and ocean-side nutrient loading was different prior to the historical land clearance and landuse intensification of the Hauraki Plains, specifically that **ocean-side loading was likely to have contributed a much larger percentage to a much lower overall nutrient load to the Firth**.

11.3 Trends

11.3.1 Cause(s) of the nitrogen trend at the extended-Firth monitoring site

We noted in section 5.2 that water-column-integrated DIN had increased at a rate of about 5% y^{-1} over the 15-year measurement period at the extended-Firth monitoring site. We looked at changes in an indicator of upwelling patterns and land-side nutrient runoff as possible explanations, but our analysis could find nothing that might fully explain the DIN trend. (We noted that the analysis of land-side nutrient runoff should be repeated with a focus on "terminal reach" river nutrient loads to provide a more nuanced view on whether there are trends in nutrient runoff that could match the trend we have found in water-column-integrated nitrogen, and river trends in DIN, in addition to trends in TN, need to be considered and understood. We also noted that further analyses need to be done on measurements of salinity and water temperature above and below the pycnocline, which could result from changed oceanographic conditions associated with changes to the upwelling regime.)

We mentioned that another possibility as a driver of the DIN trend is that there has been a change in the nitrogen dynamics of the system, which could result in a redistribution of nutrients across the various sediment, water and phytoplankton "compartments" that comprise the system. What we are talking about here is a possible change in denitrification efficiency, resulting in a decreased capacity of the system to vent nitrogen to the atmosphere. We briefly explore that possibility now.

- Studies in coastal systems have shown that denitrification efficiency drops with increased carbon loading (Eyre and Ferguson, 2002) and the attendant anoxia in bottom waters. This results in the system becoming less able to vent N_2 to the atmosphere, and a corresponding reduction in its resistance to eutrophication (Seitzinger, 1988). The mechanism by which this can occur was summarised by Sutula (2011) and described by Boynton and Kemp (2008). In essence, organic enrichment of sediments and low bottom-water oxygen result in sediment recycling of nitrogen becoming more "efficient", meaning that more of the organic nitrogen deposited to sediments is returned to the water column as ammonium (Kemp et al., 1990), which then is available to further fuel primary production. Given the importance of denitrification in the Firth (described in sections 9 and 10), this kind of shift in the seabed nitrogen dynamics could explain an increase in the water-column-integrated DIN.

  Further data and analysis are required to enable a more comprehensive assessment of the possible importance of this process.

We conclude that the cause of the trend in DIN at the extended-Firth monitoring site is likely to be complex, possibly including changes to oceanic inputs, terrestrial inputs, physical oceanography and/or denitrification efficiency.

11.3.2 Toxic and nuisance algae

The increases of large, predominately centric diatoms in the Firth has included increases in species known to be grazer-resistant. *Coscinodiscus wailesii* is one such example. This species has been recorded worldwide, developing blooms and damaging shellfish and macroalgal aquaculture and commercial fisheries[32] (Nagai et al., 1995; Nehring, 1998). Its distribution was first restricted to the tropical Pacific and West Atlantic oceans, but has spread to Europe, the USA and Japan in recent years (Rick and Dürselen, 1995; Nehring, 1998; Lange et al., 1992). In culture, *Coscinodiscus wailesii* has been shown to impede grazing by the copepods *Temora longicornis* and *Calanus helgolandicus* (Roy et al., 1989), which are genera with members that are commonly found in the Hauraki Gulf zooplankton community (Zeldis and Willis, 2014). We have not yet looked at whether *Coscinodiscus wailesii* in the Firth is approaching or has reached levels that are a concern.

Whilst toxic algae remain rare in the Firth, one genus (*Pseudo-nitzschia*) has become more abundant. Evidence linking changed nutrient loading and nutrient ratios with harmful algal blooms (HABs) is accumulating (Smayda, 1990; Smayda, 1997a and 1997b; Anderson et al., 2002; Glibert et al., 2005a; Glibert and Burkholder, 2006; Glibert et al., 2005b). In the Gulf of Mexico, the sedimentary record of *Pseudo-nitzschia* spp. shows increases in cell counts that parallel increased nitrate loading over the past several decades (Turner and Rabalais, 1991; Parsons et al., 2002). Although cell numbers of the toxin-producing diatom *Pseudo-nitzschia* have increased in the Firth, analysis of more than a decade of monitoring data from New Zealand waters by Rhodes et al. (2013) has not revealed any increase in frequency or magnitude of toxic events.

11.4 The pre-development trophic state of the system

In our opinion, **the Firth of Thames will at least have been "less mesotrophic" and may have been oligotrophic prior to catchment deforestation and subsequent development in the catchment**. We have no direct data to support our estimation of any previous trophic state of the Firth (that is, we do not have any actual measurements from the pre-historic period).

The reason for our opinion that the trophic state has <u>shifted</u> is simple: the total nitrogen load to the Firth is dominated by land-side inputs[33] and nutrient runoff from the land will have increased since catchment deforestation and subsequent development.

We are less sure what the shift in trophic state has been <u>from</u>. However, a very simple calculation suggests that primary productivity could have been about half what it is today. We arrive at that by simply reducing the land-side nitrogen loading by the amount we think is anthropogenic (about 75% according to Vant, 2011) and then multiplying that by the component of the marine DIN that we think is riverine (rivers supply about 87% of DIN to the total DIN load – see the nutrient budget in section 10), which gives a reduction in marine DIN of about 65%. Assuming the primary production is about proportional to the DIN loading (which we acknowledge is inexact), the primary productivity could be expected to reduce by about half. This would reduce the 2002–03 rate of 191 g C m^{-2} y^{-1} to about 100, which is the oligotrophic state of Nixon (1995).

---

[32] The damage occurs through the likes of fouling of nets and clogging of filtration systems, not by any toxic effects.

[33] At least when there is no strong ocean upwelling; strong ocean upwelling occurs for about 10% of the time, as explained previously.

11.5   Effects of low dissolved oxygen

11.5.1 Recent meta-analyses

There are recognised guidelines for dissolved oxygen to protect marine life, and organism responses to oxygen stress have been summarised in recent meta-analyses by Gray et al. (2002) and Vaquer-Sunyer and Duarte (2008) – see box, next page.

Referring to Figure 11-3 (panel A), fish and crustaceans had the highest lethal concentration thresholds, meaning that they were most susceptible to oxygen stress, followed by bivalves. Sublethal thresholds (where life-giving factors such as reduced growth and reproduction, increased physiologic stress, forced migration, reduction of suitable habitat, increased vulnerability to predation, and disruption of life-cycles were found to be highest) were greatest for fish and crustacea, followed by molluscs. Taxa with higher thresholds were generally also those with greatest potential mobility. Lethal times after exposure to acute hypoxia were shortest for crustacea and fish (order of few hours to a few days) while times for molluscs were a few hundred hours.

Vaquer-Sunyer and Duarte (2008) questioned the widespread use of the 2 mg DO L^{-1} threshold in conventional applications and recommended its upward revision. They showed that the 2 mg L^{-1} threshold is below the empirical sublethal and lethal thresholds for half the species they tested. They recommended 4.6 mg DO L^{-1} as "a precautionary limit to avoid catastrophic mortality events, except for the most sensitive (e.g., crab) species, and to effectively preserve biodiversity". Based on this information, Horizons Regional Council recommended 70% DO saturation in its One Plan for estuary management subzones.

Guidelines for dissolved oxygen to protect marine life include:

- Sheldon and Alber (2010) designated 3 mg DO L^{-1} as the "fair/poor" threshold and 5.5 mg DO L^{-1} as the "good/fair" threshold for Georgia (USA) estuaries.

- Batiuk et al. (2009) designated DO criteria for Chesapeake Bay for protection of individual ecological values (e.g., fisheries, habitat protection including larval recruitment, bivalve fisheries) in individual sub-regions of the Bay. Criteria include a 30-day mean of 5 mg DO L^{-1} applied to open-water habitats, with a 7-day mean of 4 mg DO L^{-1} and an instantaneous minimum of 3.2 mg DO L^{-1}.

Organism responses to oxygen stress have been summarised in recent meta-analyses by Gray et al. (2002) and Vaquer-Sunyer and Duarte (2008):

- Gray et al. (2002) outlined a taxonomic progression of decreasing sensitivities to DO stress, progressing from fish to crustaceans to annelids to bivalves. They tabulated their findings qualitatively for these groups in terms of DO concentrations that elicit various effects (Table 11-1).

- The findings of Vaquer-Sunyer and Duarte (2008) were largely in agreement with those of Gray et al. (2002) but were conducted within a formal statistical framework that used 872 experimental assessments across 206 marine benthic organisms. Figure 11-3 summarises their findings.

Type of organism	Effect	Conc. (mg l^{-1})
Actively swimming fish	Growth	6
Actively swimming fish	Metabolism	4.5
Bottom-living fish	Metabolism	4
Most fishes	Mortality	2
Crabs, shrimps, lobsters, isopods	Growth	2–3.5
Bottom-living isopods	Mortality	1–1.6
Bivalve molluscs	Growth	1–1.5
Annelids	Growth	1–2
Mudskippers	Mortality	1

Table 11-1: Results of Gray et al. (2002) for DO concentrations eliciting different effects in different taxonomic groups.
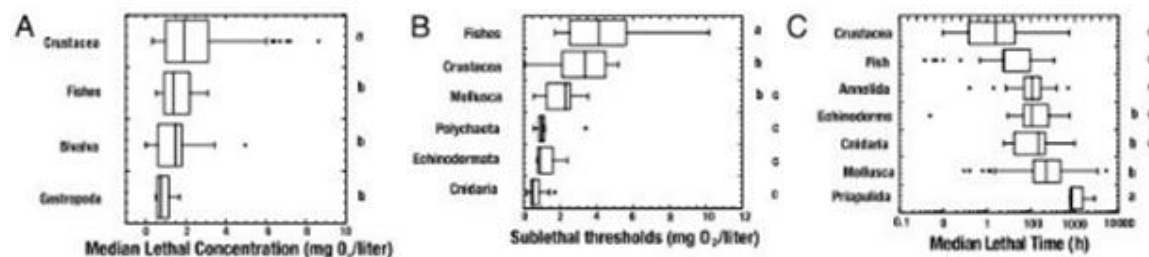

Figure 11-3: Box plot showing the distributions of oxygen thresholds among taxa. (A) Median lethal concentration (mg DO L^{-1}). (B) Median sublethal concentration (mg DO L^{-1}). (C) Median lethal time (h). The letters indicate the results of the Tukey HSD test, whereby the property examined did not differ significantly for taxa with the same letter. Adapted from Vaquer-Sunyer and Duarte (2008).

11.5.2 Green-lipped mussel farming

The meta-analyses indicate that bivalve molluscs are among the most resilient invertebrates to low oxygen, which is relevant to the observations of depleted DO in the vicinity of the Wilson Bay Marine Farm Zone.

Measurements made at Wilson B in 2013 (January 27 to February 3) showed DO at the surface dropping to 75% saturation, which is equivalent to 6 mg DO L^{-1} (Figure 7-4). The limited amount of data available suggest that the period sampled at Wilson B in Figure 7-4 was not an example of a particularly low autumn DO minimum. In autumn 2009 and autumn 2010 DO at the seabed dropped to 5.4 and 4.2 mg DO L^{-1} (Figure 7-6). Figure 7-2 also shows oxygen minima below 6 mg L^{-1} occurring in the lower water column at the extended-Firth monitoring site. Given that settled spat, rather than larvae, are used in farming operations, this may mean a reduced risk to operations arising from low DO in the farm area, although effects on farmed spat should be further investigated[34]. The vertical distribution of DO concentration should also be monitored.

Hence, oxygen conditions appear to be sufficient for green-lipped mussel farming in the Wilson Bay Marine Farm Zone. However, two factors need to be taken into account:

(1) We are unaware of information specific to oxygen tolerances of cultured *Perna canaliculus* adults. However, *P. canaliculus* are known to be resilient to low oxygen in intertidal habitats and are able to sustain themselves through long emersed periods (Marsden and Weatherhead, 1998), although this does incur a metabolic cost. The size of this cost has not been evaluated for immersed individuals experiencing low DO, and should be further investigated.

(2) Data do exist for *P. canaliculus* larvae and juveniles (spat) (Alfaro, 2005) which show significant and large negative effects on larval survival and settlement at 6 mg DO L^{-1}, with greatest negative effects occurring at low water flows (1 or 5 cm s^{-1}) in the experimental tanks. This oxygen level (6 mg DO L^{-1}) did not affect spat survival or settlement.

11.5.3 Fish farming

The most sensitive group to low oxygen in terms of sublethal effects is fish (Table 11-1, Figure 11-3), particularly active swimmers (Gray et al., 2002).

- This is relevant to fish farming in the Coromandel Fish Farm Zone, for which farming of yellowtail kingfish (*Seriola lalandi*) and hapuka (*Polyprion oxygeneios*) has been proposed. Bowyer et al. (2014) investigated interactive effects of water temperature (21, 24, 27°C) and DO (normoxic vs. hypoxic) on the growth rate, feed intake and digestive enzyme activity of yellowtail kingfish. The oxygen regimes used were highly variable ("hypoxic" conditions ranged from 3.3–5.3 mg DO L^{-1}) so it is difficult to draw firm conclusions from their results, but they did show a 13% decrease in specific growth rate under these oxygen conditions at 21°C. We know of no data for adult kingfish or hapuka performance.

Tolerances for farmed salmon can be discussed for comparison.

- As active swimmers, salmon have high oxygen requirements. The recommended minimum DO concentration is 6 mg L^{-1} (Sim-Smith and Forsythe, 2013) and concentrations below that

---

[34] Furthermore, the extent to which low autumnal DO might influence farming operations will depend upon the timing of spat seeding and the duration of the presumed sensitive-age-span period.

are defined as hypoxic for salmon because they cause a decrease in blood oxygen, chronic stress and reduced growth. Even temporary fluctuations below 6 mg L^{-1} have been shown to adversely affect salmon performance in terms of appetite, stress responses and growth. These results indicate that the minimum DO concentration should be >70% saturation for optimal salmon growth, and should be >60 % saturation for the welfare of the fish.

We conclude that observations of oxygen minima below 6 mg L^{-1} in the lower water column at the extended-Firth monitoring site (with penetration into the upper water column on occasion – see section 7), when combined with the uncertain response of kingfish/hapuka to oxygen status, warrant further investigation vis-à-vis management of the Coromandel Fish Farm Zone, which is approximately 2 km ESE of the extended-Firth monitoring site.

11.5.4 Further comments

The biogeochemical environment itself is also subject to identifiable gradients of response to oxygen minima. For instance, there is a consistent decrease in denitrification efficiency (i.e., less N$_2$, and more NH$_4$, produced per unit nitrogen entering the seabed) as benthic DO decreases. In a review of the literature, Boynton and Kemp (2008) showed that more than 50% (up to about 80%) of the sedimented nitrogen is denitrified when bottom-water DO exceeds 6 mg L^{-1}, but only about 20% of the sedimented nitrogen is denitrified when bottom-water DO is in the range 3-5 mg L^{-1}. Bottom-water DO concentrations as low as 3–5 mg L^{-1} (approx. 90–150 µmol kg^{-1}) are not the norm in the Firth, but they have occurred intermittently (for periods of days to weeks) in most years at the extended Firth monitoring site (see Figure 7-2). Kemp et al. (2005) concluded that time scales of recovery from de-oxygenation range from weeks to months for denitrifying bacteria communities to years for macrofaunal bio-irrigators. Both are necessary for healthy denitrifying benthic systems.

11.6 Effects of acidification

Ocean acidification decreases the saturation state of calcium carbonate and solid carbonate structures as a result become less stable and prone to dissolution. Thus, acidification can have detrimental effects on species such as shellfish, kina and coralline algae that use carbonate for their solid structures, particularly in the juvenile life stages. pH has also been shown to have an influence upon the behaviour/physiology of non-calcareous organisms. Fish behaviour can be adversely affected and physiological effects have also been noted, especially for fish larvae. Some photosynthetic species, such as seagrasses, benefit from the increased presence of CO$_2$ and H$_2$CO$_3$ (rather than HCO$_3^-$) that accompanies falling pH. These changes, as well as directly affecting specific species, may also result in change in the ecosystem structure.

Work in New Zealand on local molluscan responses to acidification was recently reported at the "Future proofing New Zealand's shellfish aquaculture: Monitoring and adaptation to ocean acidification" workshop in Nelson (Capson and Guinotte, 2014). It was reported (N. Ragg, Cawthron Institute) that *P. canaliculus* larvae underwent significant (nearly 50%) reductions in growth rate in water with pH of 7.7 compared to water with pH of 8.0. Large effects on shell thickness were also demonstrated, though pH ranges were not detailed. V. Cummings (NIWA) reported responses for adult (5–14 months old) cockles, abalone, and flat oysters in terms of survival, respiration (abalone), growth, reburial (cockles), physical condition, weight loss, physiological condition and righting behaviour (abalone). The experimental scenarios tested were based on temperature predictions for oceanic New Zealand for 2050 and 2100 (range 11–21°C) and a decline of 0.3–0.4 pH units by 2100. It was found that, for each species, the scenarios tested affected almost all of the response variables assessed. Interactive effects of temperature and pH were noted for abalone and cockles. Negative

influences on responses were observed even when aragonite saturation states were above 1, indicating cause for concern before environmental conditions reach under-saturation.

Management of the Firth needs to consider climate change effects and effects of resource use on pH. Continued monitoring is required to identify any trends in pH.

11.7   Reversibility and remediation

Since the total nitrogen load to the Firth is dominated by land-side nutrient inputs (at least when there is no strong ocean upwelling, which is the case for about 90% of the time) and nutrients fuel primary production, **we expect that a reduction in land-side nutrient inputs will reduce the organic-matter load of the Firth and the consequent oxygen depletion that occurs in the extended Firth towards the end of the phytoplankton growth season (late summer to early autumn)**.

However, **we cannot make any quantitative predictions of what changes might ensue following any specific reduction in land-side nutrients** until we have a more thorough understanding of the dynamics of the system. (This is the subject of ongoing and proposed research.)

Without a return to the former sediment macrobenthic community a full recovery to the pre-catchment-development pattern of nutrient cycling and water quality in the Firth seems unlikely.

12 Overview of NIWA data used in this report

12.1 Sediments

- GPS Monitoring of Rod Surface Elevation Table (RSET) benchmarks located along the Appletree Transect B since 2008.

- Aerial photographs of the southern Firth dating to the 1940s and early 1950s.

- Sediment cores collected from 12 sites collected in February 2005 along Appletree Transect B. Cores dated and analysed for bulk density and particle size.

- Sediment cores collected in February 2006 from the intertidal flats along a 1 km long, north–south transect aligned with the Appletree Transect B. Cores dated and X-rayed.

- Annual sediment budget estimated for the mangrove forest at the Appletree transect, a 1000 m transect seaward of the mangrove-forest fringe, and the lower intertidal and shallow subtidal.

- Voyage SEA0201, December 2002, occupying a total of 29 stations along transects in the Firth and extended Firth.

- Voyage KAH0310 in December 2003, occupying a reduced number of sites on the same transects.

- Voyage KAH1202 in March 2012, occupying one site ("outer") in the extended Firth and two sites ("inner") in the Firth.

- Voyage TAN9915 north of the Mokohinau Islands in a water depth of 125 m (site 5, 35° 48.83'S, 175° 1.83'E).

12.2 Nutrients

- 15 years (1998–2013) of measurements of nutrient concentrations across a suite of nutrients every 3 months at the extended-Firth monitoring site. Measurements by CTD containing a rosette sampler lowered from a research vessel. Samples typically from 6 levels in the water column.

- Surveys of nutrient concentrations across the Hauraki Gulf and Firth of Thames in spring, summer, autumn and winter of 2003 and also during 2012–13.

- Southern Oscillation Index (SOI) state and seasonal wind directions in the northeast North Island.

- Satellite remotely-sensed sea surface temperature (SST) data for the shelf north of the Gulf dating from 2003.

12.3 *Phytoplankton and bacteria*

- Phytoplankton pigment (chlorophyll a and phaeopigment) has been measured and microphytoplankton cells (>2 μm cell size) have been collected at the extended-Firth monitoring site seasonally (every 3 months) over the 15-year period 1998–2013. Water samples for analysis by CTD containing a rosette sampler lowered from a research vessel. Samples typically from 6 levels in the water column. Picophytoplankton (<2 μm cell size) and bacteria cells have been collected at the extended-Firth monitoring site since December 2002

- Chlorophyll *a* samples at CTD sites in the greater Hauraki Gulf and Firth that have been occupied at various times, dating from 1996. This includes chlorophyll *a* measurements from a grid pattern of stations from inner to extended Firth waters occupied in December (summer) 2002, March (autumn), July (winter), October (spring) and December (summer) 2003.

- Photosynthesis–irradiance determinations made onboard ship during primary-production experiments over 6 voyages from spring 1999 to summer 2000 at the extended-Firth monitoring site and at a site on the continental shelf.

- Data from two Integrating Natural Fluorometers (INFs) at the extended-Firth monitoring site. INFs positioned at 7 m and 20 m below the surface. Data were first collected in mid–2004, but most consistently after mid–2005.

- Chlorophyll *a* determined spatially using underway fluorometry during 4 seasonal voyages, 2012–13.
    - Spring – voyage KAH1209. Summer – voyage KAH1311. Autumn – voyage KAH1304. Winter – voyage KAH1306.

12.4 Dissolved oxygen

- 15 years (1998–2013) of measurements every 3 months at the extended-Firth monitoring site. Measurements by CTD lowered from a research vessel.

- Spatial surveys of DO conducted in autumn of each of three years.

- Measurements every 15 minutes at two depths in the water column on a fixed mooring at the extended-Firth monitoring site over the period 2005–2014.

- Measurements every 15 minutes at the Wilson B site at 5 m below the water surface over the period January to April, 2013

12.5 pH

- Voyage in autumn 2010 (KAH1002), comprising underway sampling and sampling with a CTD at stations. Variables sampled included carbonate parameters, oxygen, chlorophyll, dissolved organic matter, turbidity, temperature and salinity.

- 4 seasonal voyages in 2012–13, comprising underway sampling and sampling with a CTD at stations, collecting the same variables as in 2010.
    - Spring – voyage KAH1209. Summer – voyage KAH1311. Autumn – voyage KAH1304. Winter – voyage KAH1306.

12.6 Benthic and pelagic mineralisation

- Voyages KAH0310 in December 2003 and KAH1202 in March 2012 visiting subtidal sites around the Firth and extended Firth, examining nutrient and oxygen sediment fluxes and concentrations, sediment bulk properties and structure, porewater chemistry, benthic microalgae and infauna.

- Voyage TAN9915 from the inner Firth to the outer NE continental shelf examining sediment oxygen fluxes.

- NIWA biogeochemical study in the Firth in May 2012, inner and extended Firth sites examining sediment bulk properties and structure, porewater chemistry.

13 Recommendations for further research and data collection

13.1 Trends

- Trend analyses should be revisited using new methods that eschew the use of the *p* statistic to infer significance (McBride, G.B., Cole, R.G., Westbrooke, I., Jowett, I. (2013) Assessing environmentally significant effects: a better strength-of-evidence than a single *p* value? *Environmental Monitoring and Assessment*. 10.1007/s10661-013-3574-8).

13.2 Sediments

- Sediment loads in the Waihou and Piako Rivers need to be better measured to determine what fraction of the sediment burden in the Firth is related to present-day land sources.

- Further analysis of the Appletree dataset as part of an ongoing PhD research project (Andrew Swales, NIWA) is aimed at distinguishing between resuspension of sediments by waves and sediment delivered in river plumes to the southern Firth.

- The Appletree experiments, which are located in central southern Firth, could be repeated at sites along the eastern and western margins to quantify cross-Firth differences in the physical environment.

- In order to better understand the effects sediments are having on subtidal infaunal communities, community analyses using multivariate statistics could be undertaken on existing datasets, combining information from the bulk sediment and biogeochemical properties with the composition of the meiofaunal community. Meiofaunal indices for eutrophication and pollution could also be investigated (e.g., nematode to copepod ratios), as could information on environmental adaptations, which could be derived from more detailed speciation of the meiofaunal (and macrofaunal polychaete) samples.

- The Deltares sediment-transport model should be calibrated. The calibrated model should be used to simulate a wide and systematically-defined range of scenarios to confirm and quantify the tentative modelling results presented herein.

- An integrated freshwater–seawater monitoring network could be set up to collect baseline information and enable assessment of the effectiveness of any future catchment landuse change.

13.3 Nutrients

- Update nutrient budgets with new data collected in replicates during all seasons.

- More seasonally resolved data on pelagic and benthic nutrient metabolism are needed.

- Biogeochemical modelling of Gulf and Firth should be done to help develop our understanding of nutrient dynamics and enable predictions of system responses to nutrient loading.

- Direct or indirect measurements of denitrification efficiency would provide actual denitrification rates. Ongoing monitoring of denitrification would help determine

seasonal and long-term changes to this likely important ecosystem service. Long-term (months) chamber experiments examining denitrification as function of organic matter loading, DO, bioturbation, etc.

- Terminal reach monitoring of nutrient loading from rivers would help quantify the land-derived loading to the Firth of Thames. Currently monitoring stations are located approximately 30 km upstream of Piako and Waihou River mouths, thus only providing indicative loads. Ongoing monitoring would provide better information on the degree of changes in loads.

- Analysis of existing datasets to elucidate drivers of nutrient dynamics.

- Measurements and ongoing monitoring in the Firth of Thames to fill information gaps.

13.4 Primary production

- Continued monitoring of the nutrient and phytoplankton trends at the extended-Firth monitoring site is needed to understand their past and potential future trajectories. This should be extended into the Firth.

- More seasonally resolved data on pelagic and benthic nutrient metabolism are needed.

- Datasets of HAB incidence collected at marine farms in the region could be assessed in the context of the results presented here.

- Other datasets available from NIWA but not analysed here include large data sets on micro- and mesozooplankton which could be assessed in the context of the results presented here.

13.5 Dissolved oxygen and pH

- Monitor DO and pH in the Firth of Thames

- Improve understanding of vertical distribution of oxygen concentration at the extended-Firth monitoring site and at Wilson Bay Area A and B and connectivity between these areas.

- Prioritise studies of low DO and carbonate state tolerances of adult and especially larval stages of Firth of Thames aquaculture species and larval/juvenile snapper and any key bentho-pelagic species.

- Continue monitoring and analysis of data from the extended-Firth monitoring site and associated spatially extensive surveys to enhance our present understanding of fundamental drivers of the Hauraki Gulf and Firth of Thames environment.

- Investigate whether remotely sensed data for total suspended solids, CDOM and chlorophyll a can provide a synoptic multi-year data set to compare with the oxygen and pH time series shown here.

- Look into the drivers of inter-annual variations in strength, duration and spatial extent of stratification.

- Biophysical modelling of oxygen and carbonate system dynamics could be used for scenario testing, e.g., of oceanic and catchment loading conditions.

14 Data catalogue

14.1 Sediments

- Dated sediment cores enable annual–decadal-scale patterns of sedimentation the intertidal flats and in the mangrove forests of the southern Firth to be reconstructed.

- Dated sediment cores collected by Bentley et al. (in prep) enable annual–decadal-scale patterns of sedimentation in the intertidal zone of the southern Firth to be reconstructed.

- Dated sediment cores collected by Nodder et al. (in prep) enable annual–decadal-scale patterns of sedimentation in the subtidal zones of the Firth and Hauraki Gulf to be reconstructed.

- Sediment surveys across the Firth and Gulf collected in NIWA research describe the distributions of bulk properties and biogeochemical character of Firth sediments.

- Remotely sensed data (MODIS / Aqua) describe time and space distributions of fine suspended material in the upper water column of the entire Hauraki region from 2003 to the present.

- Modelling of sediment dispersal by the Deltares modelling platform is available. The Deltares model is presently uncalibrated for sediments.

14.2 Nutrients

- Water, salt and nutrient mass-balance modelling and loading estimates.

- Sediment and water-column biogeochemistry, including oxygen, carbon and nutrient flux rates.

- Nutrient concentrations through the water column at the Firth of Thames monitoring site 1998–2014, measuring decadal-scale changes at seasonal frequencies across a suite of nutrients.

- Surveys of nutrient concentrations measured broadly across the Hauraki Gulf and Firth of Thames.

14.3 Primary production

- Ship surveys of phytoplankton biomass and production across the northeast continental shelf, Hauraki Gulf and the Firth of Thames, with high spatial resolution in the Firth.

- Phytoplankton and bacteria cell counts, biomass and community composition at the Firth of Thames monitoring site (1998–2014), showing decadal-scale changes at seasonal frequencies with high taxonomic resolution.

- Phytoplankton abundance measured by the biophysical mooring at the Firth monitoring site (2004–2014) at daily frequency and measured across the region using underway surveys (2012–13).

- Expert knowledge available to describe the status, changes and causes of change in phytoplankton and bacteria.

14.4 Dissolved oxygen and pH

- 13 years of oxygen profiling at the extended-Firth monitoring site, accompanied by a wide array of physical and biological co-variables.

- Numerous spatially extensive surveys over the region using CTD.

- 9 years of moored oxygen data with accompanying current, temperature, salinity and phytoplankton fluorescence data.

- 5 years of carbonate system dynamical information from ship-based underway and CTD sampling.

- Expert knowledge available to describe the status, changes and causes of change in the oxygen and carbonate systems.

15 Data assessment

15.1 Sediments

- Data cover all geomorphic regions of the Firth (from old mangrove forest to the subtidal Firth approaches). Numerous aspects of sedimentary structure and sediment accumulation rates are covered, in representative spatial distributions.

- More information on subtidal conditions, especially sediment accumulation rates in the inner Firth, is needed.

- Conditions preventing the recolonization of biogenic reefs in the subtidal environment warrant better understanding, including past biotic conditions and changes that limit current recruitment.

- More information is needed on likelihood of negative feedback effects on nutrient cycling from continued elevated rates of sedimentation, inputs of organic-carbon enriched sediment to the western Firth, and inputs of sediment enriched in total organic-matter to the eastern Firth.

- We have placed much reliance on interpretation of sediment cores that were collected along Appletree Transect B, which is located mid-way between the Waitakaruru and Piako Rivers. Transect B was selected for coring because sediments deposited here should preserve changes in physical conditions on the intertidal flats that are representative of the southern Firth in general, which is a relatively linear shoreline. Closer to the river mouths, sedimentation rates are likely to be more spatially variable, being influenced by strong gradients in sediment transport and deposition rates associated with hydrodynamic conditions characteristic of the more complex tidal-river channel, deltaic and levee environments.

15.2 Nutrients

- The sediment and pelagic chemistry findings describe mainly summer and autumn conditions and could be extended to other seasons.

- Further analysis of spatial and temporal aspects of nutrient distributions is possible using data collected over the last 12 years and in particular the last 3 years.

- New water, salt and nutrient mass-balance modelling is possible with existing data collected in the last 2 years.

15.3 Primary production

- The datasets described above are one-of-a-kind in New Zealand and very unusual overseas for their detail and breadth in time and space.

- Remote sensing of coastal-zone phytoplankton chlorophyll is still being developed for the Hauraki Gulf/Firth of Thames. This could greatly expand our views of phytoplankton dynamics of the region over weekly to decadal time scales and spatial scales of 100s of m to 100s of km.

- It would be advantageous to explore datasets of HAB incidence collected at marine farms in the region and to assess them in the context of the results presented herein.

- Other datasets available from this research but not analysed here include large datasets on micro- and mesozooplankton, which would be advantageous to assess in the context of the results presented herein.

15.4 Dissolved oxygen and pH

- Further investigation of the movement of low-oxygen waters should be undertaken.

- Better understanding of high-frequency variability in pH and saturation state is required, which is approachable with moored sensors (for pH) and ongoing carbonate system parameter sampling.

- Better understanding of sensitivity of local biota to low DO and acidification effects is needed, including aquaculture species (mussels, oysters, kingfish), wild fisheries species (especially larval snapper) and the key benthic burrow formers and bioturbators (planktonic and post-settlement life-cycle stages).

- Hydrodynamic and biogeochemical modelling should be applied to investigate oxygen and carbonate dynamics, including scenario testing of various oceanographic and landuse conditions. Various modelling platforms are available for this, some of which are already developed for this region.

Acknowledgements

16 References

Alfaro, A.C. (2005) Effect of water flow and oxygen concentration on early settlement of the New Zealand green-lipped mussel, Perna canaliculus. *Aquaculture*, 246: 285–294.

Anderson, D., Glibert, P., Burkholder, J. (2002) Harmful algal blooms and eutrophication: Nutrient sources, composition, and consequences. *Estuaries and Coasts*, 25: 562–584.

Batiuk, R., Breitburg, D., Diaz, R., Cronin, T., Secore, D., Thursby, G. (2009) Derivation of habitat-specific dissolved oxygen criteria for Chesapeake Bay and its tidal tributaries. *Journal of Experimental Marine Biology and Ecology*, 381: S204–S215.

Boynton, W., Kemp, W. (2008) Estuaries. 809–856 In: D. Capone, Bronk, D., Mulholland, M., and Carpenter, E., editors. *Nitrogen in the Marine Environment*. Elsevier, Burlington, Massachusetts.

Bowyer, J.N., Booth, M.A., Qin, J.G., D'Antignana, T., Thomson, M.J.S., Stone, D.A.J. (2014) Temperature and dissolved oxygen influence growth and digestive enzyme activities of yellowtail kingfish *Seriola lalandi* (Valenciennes, 1833). *Aquaculture Research,* 45: 2010–2020.

Bricker, S., Ferreira, J., Simas, T. (2003) An integrated methodology for assessment of estuarine trophic status. *Ecological Modelling*, 169: 39–60.

Capson, T., Guinotte, J. (2014) F*uture proofing New Zealand's shellfish aquaculture: monitoring and adaptation to ocean acidification.* ISSN 1179-6480 (online), ISBN 978-0-478-43763-8 (online).

Carter, L., Eade, J.V. (1980) Hauraki sediments. *New Zealand Oceanographic Institute (now NIWA) Chart, Coastal Series*, 1: 200 000.

Cooper, A., Thomsen, C. (1988) Nitrogen and phosphorus in streamwaters from adjacent pasture, pine, and native forest catchments. *New Zealand Journal of Marine and Freshwater Research*, 22: 279–291.

Eyre, B., Ferguson, A.P. (2009) Denitrification efficiency for defining critical loads of carbon in shallow coastal ecosystems. *Hydrobiologia*, 629: 137–146.

Eyre, B.D., Ferguson, A.J.P. (2002) Comparison of carbon production and decomposition, benthic nutrient fluxes and denitrification in seagrass, phytoplankton, benthic microalgae- and macroalgae-dominated warm-temperate Australian lagoons. *Marine Ecology Progress Series*, 229: 43–59.

Gray, J.S., Wu, R.S.-S., Or, Y.Y. (2002) Effects of hypoxia and organic enrichment on the coastal marine environment. *Marine Ecology Progress Series*, 238: 249–279.

Glibert, P., Burkholder, J. (2006) The complex relationships between increasing fertilization of the earth, coastal eutrophication and proliferation of harmful algal blooms: 341–354, In: E. Graneli and Turner, J., editors. *Ecology of Harmful Algae*. Springer.

Glibert, P., Seitzinger, S., Heil, C., Burkholder, J., Parrow, M., Codispoti, L., Kelly, V. (2005a) The role of eutrophication in the global proliferation of harmful algal blooms. *Oceanography and Marine Biology - an Annual Review*, 18: 198–209.

Glibert, P., Trice, T., Michael, B., Lane, L. (2005b) Urea in the tributaries of the Chesapeake and coastal bays of Maryland. *Water Air Soil Pollut.,* 160: 229–243.

Jowett, I. (2014) Time Trends Software. http://www.jowettconsulting.co.nz/home/time-1

Kemp, W., Sampou, P., Cafrey, J., Mayer, M., Henriksen, K., Boynton, W. (1990) Ammonium recycling versus denitrification in Chesapeake Bay sediments. *Limnology and Oceanography*, 35: 1545–1563.

Kemp, W., Boynton, W.R., Adolfi, J.E., Boesch, D.F., Boicourt, W.C., Brush, G., Cornwell, J.C., Fisher, T.R., Glibert, P.M., Hagy, J.D., Harding, L.W., Houde ,E.D., Kimmel, D.G., Miller, W.D., Newell, R.I.E., Roman, M.R., Smith, E.M., Stevenson, J.C. (2005) Eutrophication of Chesapeake Bay: Historical trends and ecological interactions. *Marine Ecology Progress Series*, 303: 1–29.

Lange, C., Hasle, G., Syvertsen, E. (1992) Seasonal cycle of diatoms in the Skagerrak, North Atlantic, with emphasis on the period 1980–90. *Sarsia*, 77: 173–187.

Marsden, I.D., Weatherhead, M.A. (1998) Effects of aerial exposure on oxygen consumption by the New Zealand mussel *Perna canaliculus* (Gmelin, 1791) from an intertidal habitat. *Journal of Experimental Marine Biology and Ecology*, 230: 15–29.

Nagai, S., Hori, Y., Manabe, T., Imai, I. (1995) Morphology and rejuvenation of *Coscinodiscus wailesii* gran (bacillariophyceae) resting cells found in bottom sediments of Harima-Nada, Seto inland sea, Japan. *Nippon Suisan Gakk,* 61: 179–185.

Needham, H., Singleton, N., Giles, H., Jones, H. (2014). *Regional Estuary Monitoring Programme 10 Year Trend Report: April 2001 to April 2011.* TR 2014/41, Waikato Regional Council, http://www.waikatoregion.govt.nz/Services/Publications/Technical-Reports/TR-201441/

Nehring, S. (1998) Non-indigenous phytoplankton species in the North Sea: Supposed region of origin and possible transport vector. *Arch. Fish. Mar. Res.* 46: 181–194.

Nixon, S. (1995) Coastal marine eutrophication: A definition, social causes, and future concerns. *Ophelia*, 41: 199–219.

Parsons, M., Dortch, Q., Turner, R. (2002) Sedimentological evidence of an increase in pseudo-*Nitzschia* (bacillariophyceae) abundance in response to coastal eutrophication. *Limnology and Oceanography*, 47: 551–558.

Pocknall, D.T., Gregory, M.R., Greig, D.A. (1989) Palynology of core 80/20 and its implications for understanding Holocene sea level changes in the Firth of Thames, New Zealand. *Journal of the Royal Society of New Zealand* 19(2): 171–179.

Rhodes, L., Jiang, W., Knight, B., Adamson, J., Smith, K., Langi, V., Edgar, M. (2013) The genus pseudo-*Nitzschia* (bacillariophyceae) in New Zealand: Analysis of the last decade's monitoring data. *New Zealand Journal of Marine and Freshwater Research*, 47: 490–503.

Rick, H., Dürselen, C. (1995) Importance and abundance of the recently established species *Coscinodiscus wailesii* gran et angst in the German bight. *Helgolander Meeresun*, 49: 355–374.

Reigman, R. (1995) Nutrient-related selection mechanisms in marine phytoplankton communities and the impact of eutrophication on the planktonic food web. *Water Science and Technology*, 32: 63–75.

Roy, S., Harris, R., Poulet, S. (1989) Inefficient feeding by *Calanus helgolandicus* and *Temora longicornis* on *Coscinodiscus wailesii*: Quantitative estimation using chlorophyll-type pigment and effects on dissolved free amino acids. *Mar. Ecol. Prog. Ser.*, 52: 145–153.

Seitzinger, S. (1988) Denitrification in freshwater and coastal marine ecosystems: Ecological and geochemical significance. *Limnology and Oceanography,* 33: 702–724.

Sheldon, J., Alber, M. (2010) *The Condition of Georgia's Coastal Waters: Development and Analysis of Water Quality Indicators*. Georgia Coastal Research Council, University of Georgia, Athens GA, for the Georgia Department of Natural Resources, Coastal Resources Division. 173pp

Sim-Smith, C., Forsythe, A. (2013) *Comparison of the International Regulations and Best Management Practices for Marine Finfish Farming*. NIWA Client Report AKL2013-013, 85 pp.

Smayda, T. (1990) *Novel and Nuisance Phytoplankton Blooms in the Sea: Evidence for a Global Epidemic.* Elsevier, New York.

Smayda, T. (1997a) What is a bloom?: A commentary. *Limnol. Oceanogr.*, 42: 1132–1136.

Smayda, T. (1997b) Harmful algal blooms: Their ecophysiology and general relevance to phytoplankton blooms in the sea. *Limnol Oceanogr.*, 42: 1137–1153.

Stenton-Dozey J., Zeldis J. (2014) *Wilson Bay Marine Farming Zone Area A Water Quality Monitoring Biennial Report: April 2012 to April 2014*. NIWA Client Report No. CHC2014-073, prepared for Wilson Bay Group A Consortium, June 2014, 29 pp.

Sutula, M. (2011) *Review of Indicators for Development of Nutrient Numeric Endpoints in California Estuaries.* Southern California Coastal Water Research Project Technical Report No. 646, 269pp.

Turner, R., Rabelais, N.N. (1991) Changes in Mississippi River water quality this century: Implications for coastal food webs. *BioScience*, 41: 140–147.

Vant, B. (2011) *Water Quality of the Hauraki Rivers and Southern Firth of Thames, 2000–09*. Waikato Regional Council Technical Report, TR 2013/20.

Vant, B. (2013) *Trends in River Water Quality in the Waikato region, 1993–2012*. Waikato Regional Council Technical Report: TR 2013/20.

Vaquer-Sunyer, R., Duarte, C.M. (2008) Thresholds of hypoxia for marine biodiversity. *Proc. Natl. Acad. Sci. USA*, 105: 15452–15457.

Zeldis, J., Willis, K. (2014) Biogeographic and trophic drivers of mesozooplankton distribution on the NE continental shelf and in Hauraki Gulf, New Zealand. *New Zealand Journal Marine and Freshwater Research*. DOI: 10.1080/00288330.2014.955806

Appendix A   Tabulation of results of trend tests

Table A-1:   Non-parametric seasonal Kendall tests for time trends in water-column-integrated nutrient concentrations (mmol m^{-2}) and ratios. Data from the extended-Firth monitoring site, October 1998 to July 2013. Data are grouped by season (seasons used were: Sep – Nov, Dec – Feb, Mar – May, Jun – Aug for spring, summer, autumn and winter, respectively).

Nutrient variable	Sample size	Median value	p	Median slope (annual)	5 % confidence limit for slope	95 % confidence limit for slope	Percent annual change
DIN	57	43.3	0.01	2.22	0.78	3.26	5.14
NO$_3$- N	57	24.7	0.10	0.83	-0.1	1.91	3.37
NH$_4$ -N	57	18.6	0.03	0.85	0.11	1.45	4.55
DIP	57	14.6	0.69	-0.1	-0.31	0.17	-0.68
DIN/DIP	57	3.1	0.04	0.13	0.05	0.24	4.15
DRSi	47	408.0	0.25	-8.69	-18.23	3.49	-2.13
DON	53	278.7	0.02	4.92	1.49	8.31	1.76
DOP	51	6.9	0.04	-0.38	-0.7	-0.08	-5.48

Table A-2:   Non-parametric seasonal Kendall tests for time trend in the Southern Oscillation Index. Data are from October 1998 to July 2013. Data are grouped by month.

Physical variable	Sample size	Median value	p	Median slope (annual)	5% confidence limit for slope	95% confidence limit for slope	Percent annual change
SOI	201	0.4	0.20	0.03	-0.01	0.06	7.14

Table A-3:   Non-parametric seasonal Kendall tests for time trends in chlorophyll *a* and phaeopigment concentrations (mg m^{-2}) integrated over the water column. Data from the extended-Firth monitoring site, October 1998 to July 2013. Data are grouped by season (seasons used were: Sep – Nov, Dec – Feb, Mar – May, Jun – Aug for spring, summer, autumn and winter, respectively).

Chlorophyll variable	Sample size	Median value	p	Median Slope (annual)	5 % confidence limit for slope	95 % confidence limit for slope	Percent annual change
Chl-*a* >= 20 m	56	28.50	0.00	1.20	0.58	1.87	4.22
Chl-*a* < 20 m	56	24.08	0.51	-0.22	-1.02	0.46	-0.91
Phaeo >= 20 m	55	13.78	0.02	0.34	0.07	0.64	2.49
Phaeo < 20 m	55	12.79	0.11	-0.37	-0.73	0.02	-2.92

Table A-4   **Non-parametric seasonal Kendall tests for time trends in cell counts (cells m^{-2} x 10^{-3}) integrated over the water column.** Data from the extended-Firth monitoring site, October 1998 to July 2013. Data are grouped by season grouped by season (seasons used were: Sep – Nov, Dec – Feb, Mar – May, Jun – Aug for spring, summer, autumn and winter, respectively).

Counts	Sample size	Median value	p	Median slope (annual)	5 % C.L. for slope	95 % C.L. for slope	Percent annual change
All micro phyto	53	6938291	0.00	477211	223557	646149	6.9
Diatoms	53	1129149	0.03	51870	14361	96930	4.6
Dinoflagellates	53	237451	0.39	-5096	-18291	4258	-2.2
Others	53	5374044	0.00	361234	175643	477743	6.7
Large centric diatoms	53	341824	0.01	30252	8796	55277	8.9

Table A-5:   **Non-parametric seasonal Kendall tests for time trends in cell biomass (mg m^{-2}) integrated over the water column.** Data from the extended-Firth monitoring site, October 1998 to July 2013. Data are grouped by season (seasons used were: Sep – Nov, Dec – Feb, Mar – May, Jun – Aug for spring, summer, autumn and winter, respectively).

Biomass	Sample size	Median value	p	Median slope (annual)	5 % C.L. for slope	95 % C.L. for slope	Percent annual change
All micro phyto	53	1050	0.07	26.33	0.98	42.67	2.51
Diatoms	53	358	0.36	9.4	-6.17	21.84	2.62
Dinoflagellates	53	301	0.33	-9.45	-25.17	4.74	-3.15
Others	53	232	0.01	13.94	6.98	21.43	6.02
Eukaryotic picos	42	724	0.65	10.64	-25.95	50.2	1.47
Prokaryotic picos	42	83	0.01	10.19	4.91	19.85	12.34
Bacteria	42	1287	0.01	90.53	35.77	140.11	7.03
Centric diatoms	53	207	0.07	8.8469	0.6135	21.8612	4.27

Table A-6: **Non-parametric seasonal Kendall tests for time trends in toxic diatom cell counts (cells m^{-2} x 10^{-3}) and biomass (mg m^{-2}) integrated over the water column.** Data from the extended-Firth monitoring site, October 1998 to July 2013. Data are grouped by season (seasons used were: Sep – Nov, Dec – Feb, Mar – May, Jun – Aug for spring, summer, autumn and winter, respectively).

Toxic Counts/Biomass	Sample size	Median value	p	Median slope (annual)	5 % C.L. for slope	95 % C.L. for slope	Percent annual change
Diatom counts	53	51012	0.00	5777	3126	10726	11.33
Diatom biomass	53	23.79	0.88	0.18	-2.18	1.42	0.75
Dinoflagellate counts	53	88289	0.06	-5868	-10661	-490	-6.65
Dinoflagellate biomass	53	52.4	0.30	-2.1	-4.94	0.88	-4.01

Table A-7: **Non-parametric seasonal Kendall tests for time trends in oxygen concentrations (mg L^{-1}).** Data from the extended-Firth monitoring site, October 1998 to July 2013. Data are grouped by season (seasons used were: Sep – Nov, Dec – Feb, Mar – May, Jun – Aug for spring, summer, autumn and winter, respectively).

Oxygen variable	Sample size	Median value	p	Median slope (annual)	5 % C.L. for slope	95 % C.L. for slope	Percent annual change
Oxygen <20 m depth	53	224.6	0.98	-0.05	-1.10	1.18	-0.03
Oxygen ≥ 20 m depth	53	198.2	0.66	0.21	-0.60	0.98	0.11

Appendix B Observations of depleted oxygen reported by O'Callaghan (2013)

Data from a miniDOT dissolved oxygen sensor deployed at Wilson B that were reported by O'Callaghan (2013) showed oxygen depletion in surface waters. This included the observation that during late winter through to spring 2012 surface waters in the Firth of Thames had dissolved oxygen levels of less than 4.1 mg L^{-1} over a period of 28 days.

We have subsequently determined that the miniDOT sensors were unacceptably affected by biofouling that rendered the data invalid.

As a result, we do not stand by the miniDOT data and observations based on that data presented in O'Callaghan (2013).

O'Callaghan, J. (2013) Dissolved oxygen variability in Hauraki Gulf. NIWA Client Report, WLG2013-42, 21 pp.

Firth of Thames Water Quality and Ecosystem Health

Data Report

Prepared for Waikato Regional Council
and DairyNZ under separate contracts

May 2015

Prepared by:
John Zeldis
Andrew Swales
Kim Currie
Karl Safi
Scott Nodder
Craig Depree
Fiona Elliott
Mark Pritchard
Mark Gall
Joanne O'Callaghan
Daniel Pratt
Steve Chiswell
Matt Pinkerton
Drew Lohrer
Sam Bentley

For any information regarding this report please contact:

John Zeldis
Principal Scientist
Marine Ecosystems and Aquaculture
+64 3 343 7813
john.zeldis@niwa.co.nz

National Institute of Water & Atmospheric Research Ltd
10 Kyle Street
Riccarton
Christchurch 8011

Phone +64 3 348 8987

Contents

Reviewed by   Approved for release by

Malcolm Green   Bryce Cooper

1   Introduction

Waikato Regional Council and DairyNZ share questions around water quality in the Firth of Thames. The questions relate to sediments, nutrients, phytoplankton/bacteria, dissolved oxygen and pH (acidification). For each of these questions Green and Zeldis (2015)[35] synthesised and interpreted data from the Hauraki Gulf and Firth of Thames collected largely over the last 20 years. The synthesis was augmented with data and findings from other New Zealand regions and from overseas.

This report provides a description of the data NIWA has collected in the Firth of Thames and Hauraki Gulf over the last 20 years that informed the synthesis by Green and Zeldis.

2   Geographic zones

The Firth of Thames (in this report sometimes also referred to as "the Firth") is a large mesotidal[36] estuary on the east coast of the North Island (Figure 2-1). The Firth of Thames as defined by WRC for the purpose of marine farming policy[37] and also as defined by Terry Hume for the NIWA estuary classification[38] is approximately 30 km long and 20 km wide, covering an area of about 730 km^2.

Within this report, the "extended Firth of Thames" (Figure 2-1) refers to an area of about 360 km^2 that is further north of the true Firth of Thames. This distinction is made to avoid confusion arising from past reports describing both regions inter-changeably under the one name.

Sample sites in the northern area are usually referred to as being situated in the extended Firth of Thames, including the intensively sampled extended-Firth monitoring site (Figure 2-1).

"Hauraki Gulf" refers to the area north and west of the extended Firth of Thames (Figure 2-1). It contains the Waitemata Harbour, extending from Rodney in the west to the Coromandel Peninsula in the east.

---

[35] Green, M. and Zeldis, J. (2015) *Firth of Thames Water Quality and Ecosystem Health – A Synthesis.* NIWA Client Report No. HAM2015-016, prepared for Waikato Regional Council and Dairy NZ.
[36] Mesotidal refers to a class of coastal waters in which tidal influence is strong, but not necessarily dominant, and the tide range is 2–4 m.
[37] http://www.waikatoregion.govt.nz/Council/Policy-and-plans/Rules-and-regulation/Regional-Coastal-Plan/Regional-Coastal-Plan/APPENDIX-VI-Glossary/
[38] The estuary area was derived from the coastline of the 1:50000 LINZ DTDB which is high water. The accuracy of this number depends on how well LINZ defined the high water line from the aerial photographs.
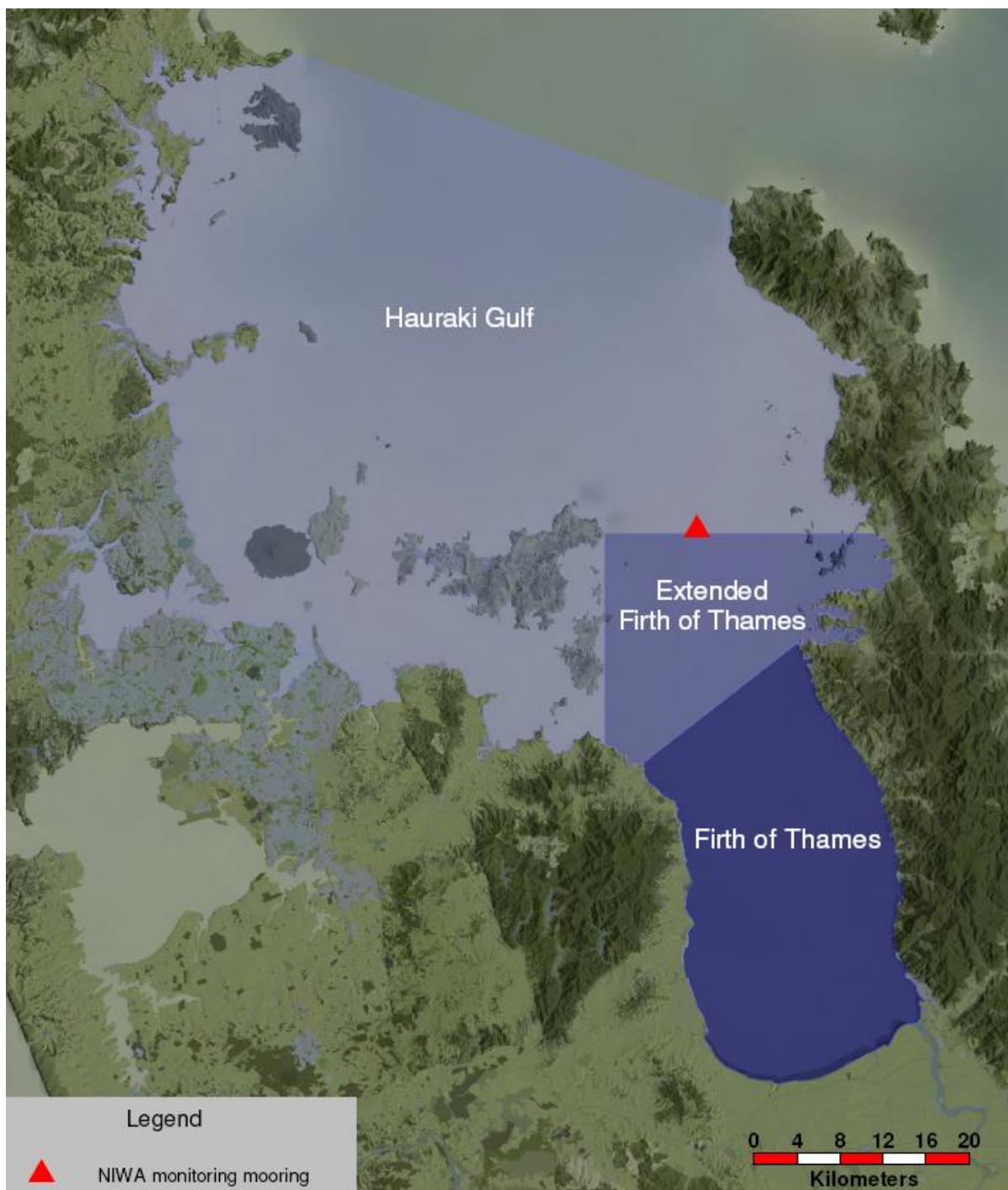
Figure 2-1: **Geographical zones and place names used in this report.** The red triangle denotes the location of the extended-Firth monitoring site.

3 Firth of Thames physical setting

3.1 Geology

The Firth of Thames occupies the Hauraki Depression, which is a structural rift-graben (Hochstein and Ballance, 1993; Healy, 2002), bounded to the east and west by the Coromandel and Hunua Ranges, respectively. To the south are the low-lying Hauraki Plains, which are underlain by Holocene estuarine and older Tertiary–Quaternary sediments (Woodroffe et al., 1983).

North–south trending faults are associated with the Hauraki Depression and are known to be active. Transverse faults across the Hauraki lowlands cause horizontal offsets. The rift structure is infilled with soft Tertiary and weakly consolidated Quaternary sediments to a maximum thickness of about 3 km (Figure 3-1). Onshore, the land slopes up gently towards the south, reaching an elevation of +3 m mean sea level (MSL) some 25 km inland.
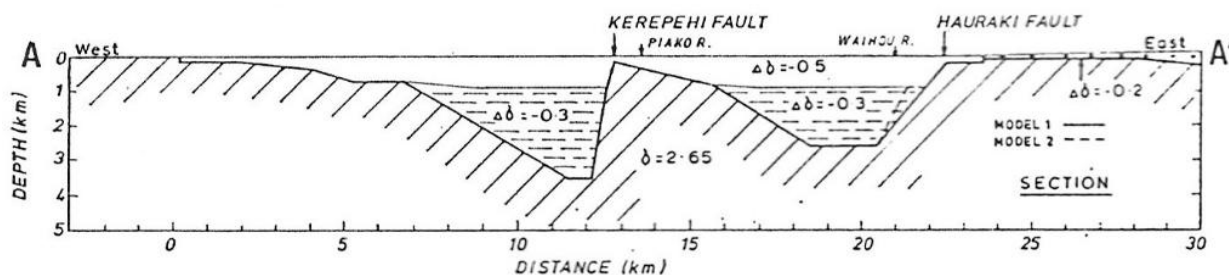

Figure 3-1: **Southern Firth of Thames southwest–northeast geophysical transect (A–A'), interpreted from observed and computed Bouguer and observed magnetic anomalies.** The geometry of the sedimentary basins and bulk densities of the greywacke basement (2.65 t m^{-3}) and unconsolidated Tertiary–Quaternary sediments (2.65 t m^{-3}) are shown. The location of transect A–A' is south of and approximately parallel with the stop bank flanking the southern Firth. Reproduced from Hochstein and Nixon (1979).

The best-known active geological structure within the Hauraki Depression is the Kerepehi Fault (Figure 3-1) (de Lange and Lowe, 1990), with the submarine section comprising a NNW-striking normal fault located down the central axis of the Firth of Thames (Chick et al., 2001).

3.2 Landcover history

Prior to Māori and European land clearance, catchment landcover consisted of podocarp–hardwood forests on the Coromandel and Hunua Ranges (McGlone et al., 1984; Newnham et al., 1995). For much of the last 10,000 years, the Hauraki Plains have comprised freshwater marshes and swamp forests dominated by kahikatea (*Dacrycarpus dacrydioides*), manuka (*Leptospermum scoparium*) and flax (*Phormium tenax*).

Early Māori arrived ~1,000 years ago and settled the higher levee along the banks of the Waihou and Piako Rivers (Phillips, 2000). Forest clearance was mainly restricted to the immediate areas around settlements (Phillips, 2000). European settlers arrived in the mid-1800s and large-scale deforestation began shortly after in the Coromandel Ranges, which was associated with timber logging and gold-mining (Brownell, 2004).

The Austrian geologist Ferdinand von Hochstetter's 1859 map of the Auckland-Waikato regions include the Firth of Thames (Figure 3-2). His map clearly shows the presence of extensive intertidal

flats and river deltas in the southern Firth. The German text *Weicher schlamm* shown on the intertidal flats translates to *soft mud*. This is significant because it suggests that muds were accumulating in the Firth before large-scale catchment deforestation by European settlers had begun.
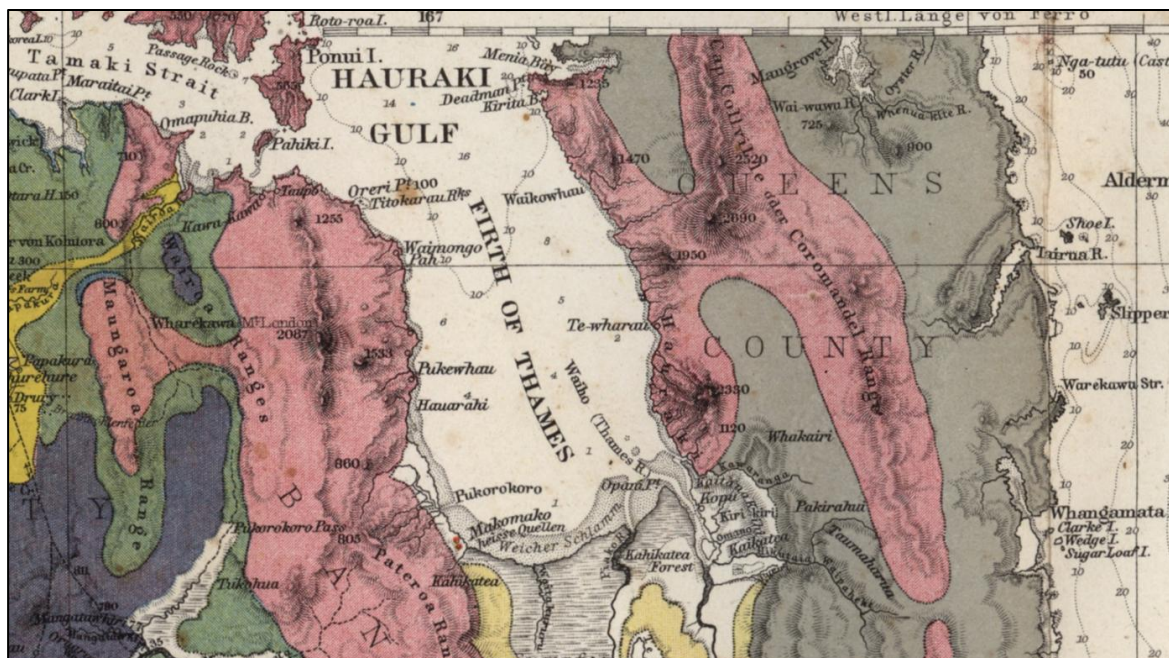

Figure 3-2:   **Hochstetter's 1859 map of the Auckland – Waikato regions.** Acknowledgement: University of Auckland Libraries and Learning Services and the Early New Zealand Book Collection. Map cropped to Firth of Thames – Coromandel region.

Hydrographic surveys conducted by the Public Works Department in 1882 and 1918 indicate that over that 36-year period an estimated 7×10^6 m^3 of sediment was deposited within a 16 km^2 area of the lower Waihou River and its tidal delta (Figure 3-2) and an estimated 37×10^6 m^3 was deposited in a 210 km^2 area of the Firth south of Tararu (these numbers are very approximate). Much of this sediment would have been associated with land clearance prior to the conversion of the Hauraki Plains for pastoral agriculture, which was delayed until drainage works began in 1905 to construct a stopbank along the southern shore of the Firth and the tidal reaches of the Waihou and Piako Rivers. By 1920 some 162 km^2 of swamp had been converted to pasture (Brownell, 2004).

The 1938 storm (4–5 May) flooded 35,000 Ha of the lower Hauraki Plains, through a combination of the perigean-spring tide coinciding with northeasterly gales and a wave set-up of +3 m MSL. As a result, the shoreline stopbank from Waitakaruru to Kopu was breached. Subsequent engineering works to raise the stopbank have constrained floodwaters to the river channels. Prior to the flood protection works, large flood events such as that in 1938 deposited large quantities of sediment across the Hauraki Plains. Since the flood protection works, with floodwaters constrained to the river channels, sediment delivery to the Firth is likely to have been increased.

3.3   Bathymetry

Water depth in the Firth of Thames increases from very shallow in the southern half (<5 m) to 40 m depth in its northern approaches. Thus, the Firth possesses a wedge-shaped bathymetry (Figure 3-3). The wider Hauraki Gulf reaches a depth of about 60 m in the north, before extending to the continental shelf edge (>200 m depth).
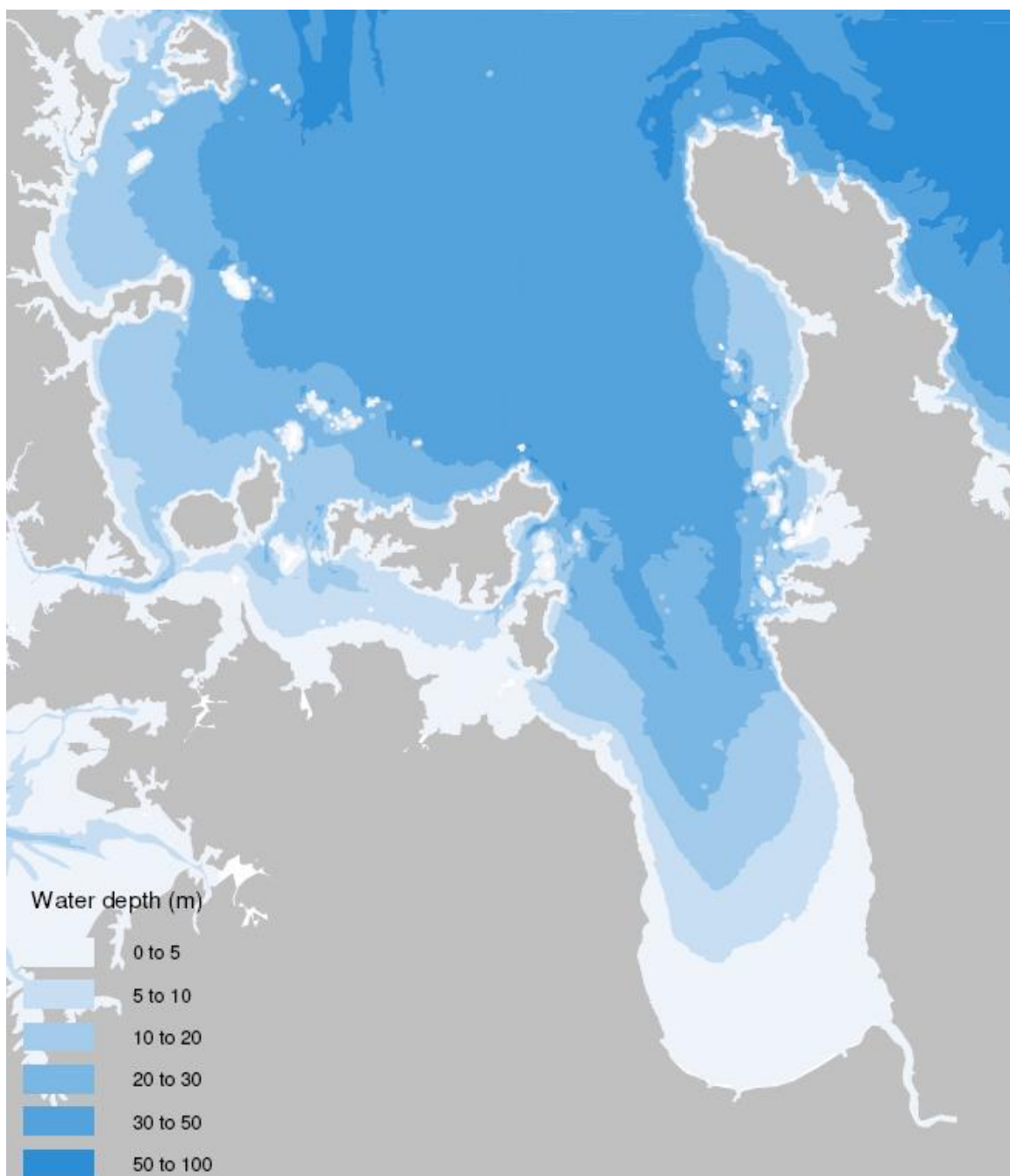
Figure 3-3: **Water depth in the Hauraki Gulf (m below MSL).** Data sourced from LINZ[39].

3.4   River inflow and catchment characteristics

There are three moderately-large rivers that flow into the southern part of the Firth of Thames: the Waihou, Piako and Kauaeranga Rivers (Figure 3-4, Figure 3-5). Additional important rivers include the Waitoa River, which joins the Piako River about 40 km upstream of its mouth, and the Ohinemuri River, which is a major tributary of the Waihou River. These rivers are sometimes collectively referred to as the "Hauraki rivers". Monitoring information and analysis of Hauraki river water quality have been presented by Vant (2011, 2013).

---

[39] https://data.linz.govt.nz/layer/447-depth-area-polygon-hydro-190k-1350k/

Figure 3-4: **River input locations (centres of circles) and mean annual flows (red circles) determined from the NIWA WRENZ tool.** The area of the red circles is proportional to the mean annual flow with the largest circle equal to 67.35 $m^3 s^{-1}$ for the Waihou River (lower right). Figure sourced from Knight and Beamsley (2013).

Figure 3-5:   The Firth of Thames and the main rivers that flow into it. Shown are the 5 sites for which average flows and catchment information are given in Table 3.1. Numerals are annual average flows ($m^3\ s^{-1}$). Data sourced from Waikato Regional Council (refer to Table 3-1).

The Firth of Thames drains a combined area of 4200 km^2 (NIWA Estuary Classification), which comprises river catchment areas of 1980 km^2 (Waihou River), 1461 km^2 (Piako River) and 132 km^2 (Kauaeranga River). Approximately 65% of the 4200 km^2 total catchment is in pasture and about 20% is in native bush (Turner et al. 2006, Figure 3-6).
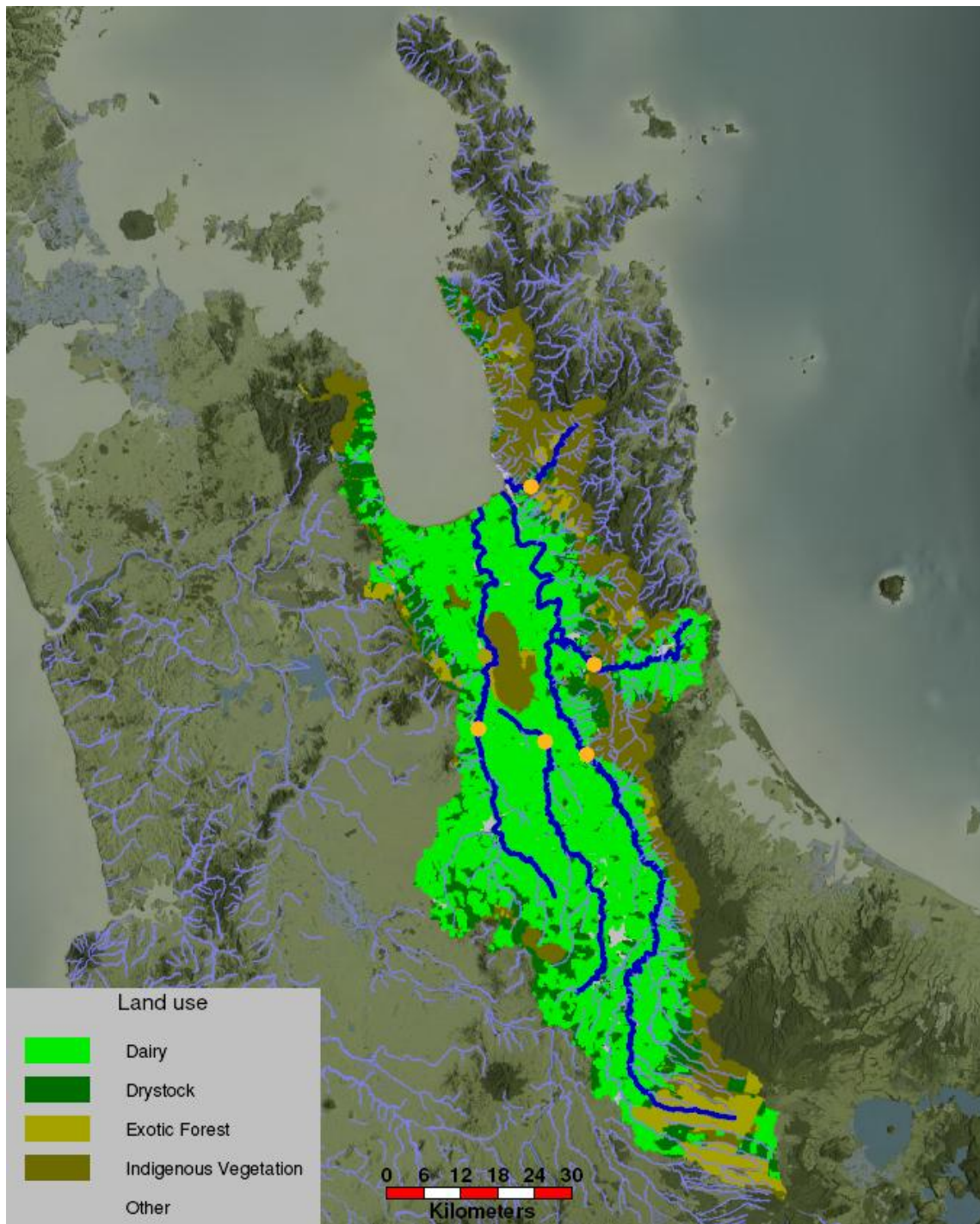
Figure 3-6:   Firth of Thames catchment land cover and main rivers (see Figure 3-5). Data sourced from Waikato Regional Council (refer to Table 3.1).

Table 3-1 lists important characteristics of the five Hauraki river catchments, showing that they differ markedly. At one extreme the catchment of the Kauaeranga River is mostly covered by indigenous vegetation (89%). By contrast, the catchments of the Piako and Waitoa Rivers are mostly covered in pasture (90%; mainly dairy). This information is reproduced from Vant (2011), who also provides information on the number of moderate-to-large point sources discharging to each river.

Table 3-1: Average river flows during 2000–09 and important catchment characteristics at key sites on the rivers (see Figure 3-5). Table reproduced from Vant (2011).

|	Kauaeranga at Smiths	Piako at Paeroa-Tahuna Rd	Waitoa at Mellon Rd	Ohinemuri at Karangahake	Waihou at Te Aroha
Flow ($m^3 s^{-1}$)	5.8	6.9	4.8	11.1	37.2
Catchment area (km^2)	120	540	410	285	1100
Indigenous vegetation	89%	5%	3%	47%	24%
Exotic forest	5%	<1%	<1%	<1%	16%
Dairy pasture	0%	66%	69%	32%	44%
Drystock pasture	5%	25%	21%	14%	14%
Other	1%	4%	7%	6%	3%

Approximately 60,000 people live in the Hauraki rivers catchment; many of them (~60%) in one of seven moderate-sized towns (3500–7000 people each).

3.5   Winds and circulation[40]

Field data (Sharples, 1997; Sharples and Grieg, 1998; Zeldis et al., 2000; Zeldis et al., 2001) and simulation results (Black et al., 2000; Proctor and Greig, 1989) have demonstrated a strong link between northeastern New Zealand continental shelf hydrodynamics and the regional winds.

Winds with a strong along-shelf component from the northwest cause upwelling, and those with southeast components cause downwelling (Figure 3-7A) (Zeldis et al., 2004). Satellite sea surface temperature pictures (Figure 3-7B) demonstrate changes to water temperatures on the northeastern shelf under differing conditions of upwelling and downwelling. Upwelled water is colder, richer in nitrogen but depleted in oxygen (Zeldis, 2004). Upwelled water fertilises the continental shelf while downwelling conditions transport nutrient-rich water away from the coast and deplete the continental shelf of nutrients. These conditions can significantly alter nutrient availability irrespective of changes to inputs from the Hauraki river catchments.

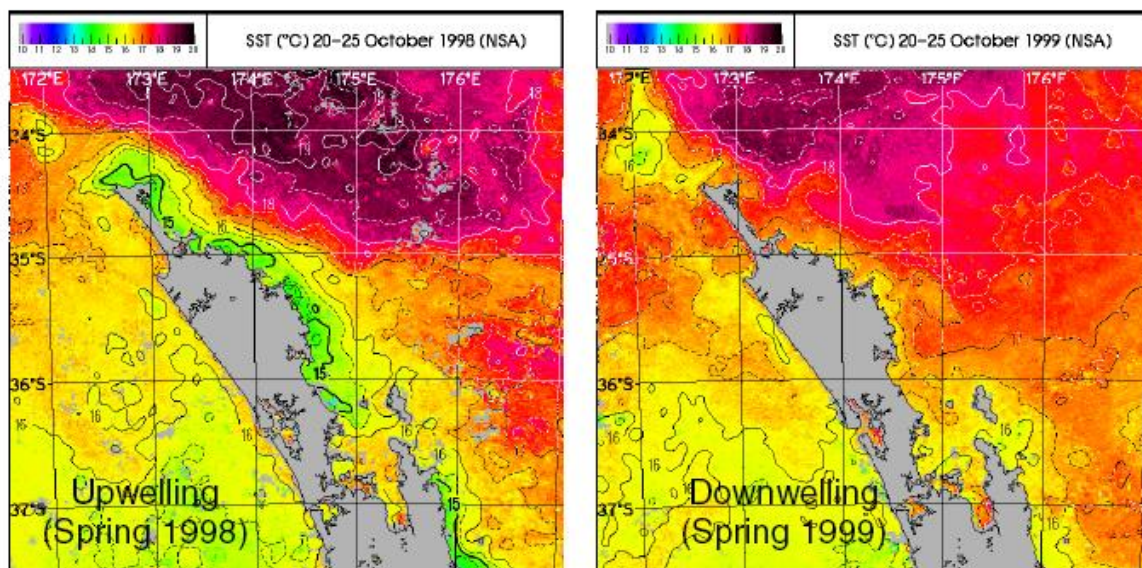[40] This section is reproduced from Broekhuizen et al. (2002).

(A)
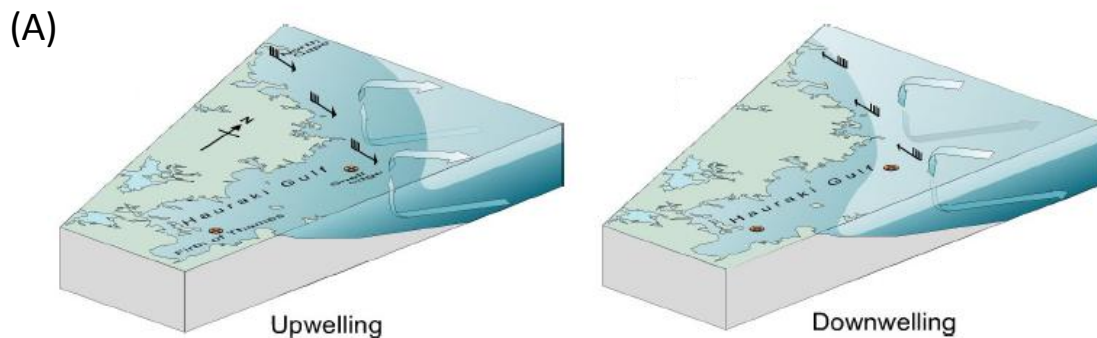
(B)

Figure 3-7: **Characteristics of upwelling and downwelling.** (A) This view up the coast to the north of the Hauraki Gulf shows two key wind-driven current patterns – upwelling and downwelling. Winds are shown as feathered arrows, surface water is shaded light blue, and deepwater is shaded dark blue. (B) Lower panels: These satellite images of sea surface temperature (SST) show snapshots illustrating up- and downwelling-related SST (cool water is coloured green).

Wind data recorded at Mokohinau Island (Figure 3-8) at the entrance to the Hauraki Gulf show that winds in the region are predominately from the southwest. These winds, however, have a significant along-shelf northwesterly component, especially in winter and spring. The other main winds are from the east, with a strong along-shelf component from the southeast. These are most common in summer. These seasonally variable winds cause a predominance of upwelling in winter and spring, but change to downwelling in summer when nutrient-poor, warm surface water is brought close to the coast (Sharples, 1997; Sharples and Grieg, 1998; Zeldis, 2004; Zeldis et al., 2004).
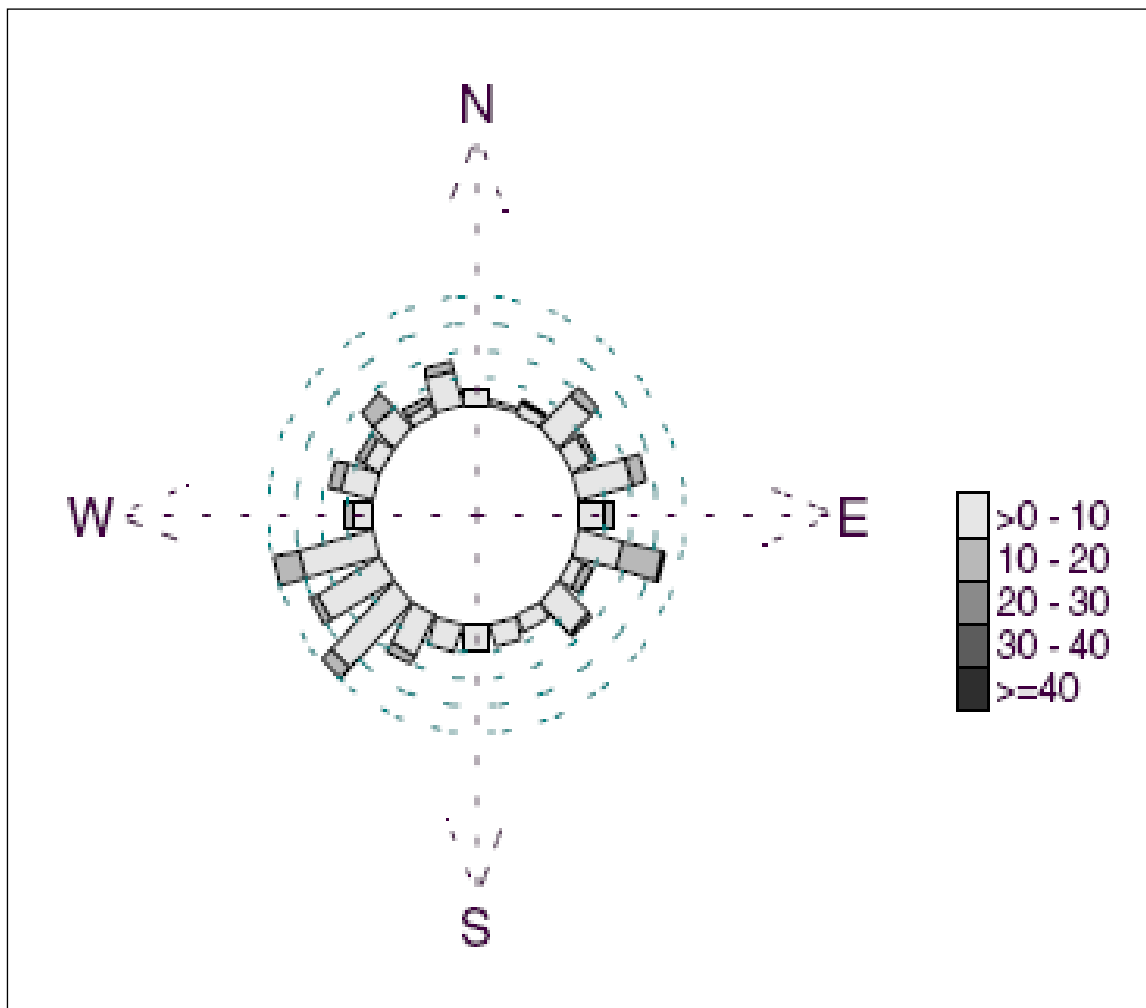
Figure 3-8: **Wind rose for Mokohinau Islands (data from January 1998 to July 2000).** Directions and shown by bars and wind speeds (km h^{-1}) by grey shades.

In addition to seasonal variation, there is important interannual variation in the prevalence of the alongshelf winds, which is related to the sign of the Southern Oscillation Index (SOI) (Figure 3-9). Westerly winds are typically predominant during El Niño periods (SOI negative). This is because anticyclones are more common over the Tasman Sea and winds blow from the west during this period. Easterly winds prevail during La Niña; this causes anticyclones to be more common on the east of the country. Thus, there is a relationship between SOI and the prevalence of upwelling and downwelling on the northeast shelf.
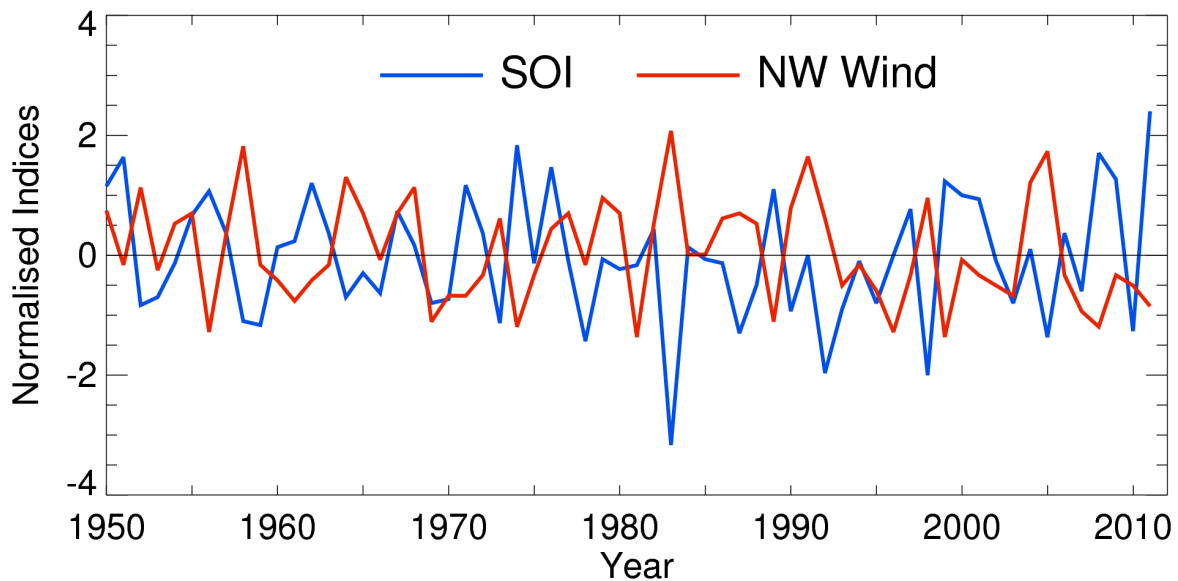
Figure 3-9: **Relationship between Southern Oscillation Index (SOI) and winds from the northwest measured in the northern Hauraki Gulf region (Mokohinau Island).** Positive values of SOI indicate La Niña and negative values El Niño. Positive values of wind indicate alongshelf winds from the NW and negative values from the SE. There is a frequent anti-correlation between SOI and NW winds in the region (data from Brett Mullan, NIWA, 2012).

3.6   Currents, waves and sea level

Currents in the Firth are forced primarily by tides, winds and river flows.

Solar and freshwater inputs alter hydrodynamic properties by stratifying the water column, that is, by isolating deeper bottom waters from less dense surface waters (Stephens, 2003).

The Firth's tides are semi-diurnal with average spring and neap tidal ranges of 3.2–3.5 m and 2.0–2.2 m, respectively (Healy, 2002). Tidal currents within the Firth of Thames are typically ≤ 0.3 m s^{-1} on an average tide although speeds of up to 1.4 m s^{-1} have been recorded (Black et al., 2000; Proctor and Greig, 1989).

Field data, model results and satellite images indicate that the flood tide enters the Hauraki Gulf through the Colville Channel and north of Great Barrier (de Lange[41], pers. comm.). This generates a gradient that pushes water down into the Firth of Thames. The water flow tends to deviate to the left of the direction of travel, so the flood flow is stronger (the thalweg) down the eastern side of the Firth of Thames. The water in the southern Firth of Thames shallows and the effects of winds increase, and the thalweg can sometimes migrate westwards. The overall effect is a clockwise eddy in the southern Firth of Thames, and sometimes there is an anticlockwise eddy in the middle to northern Firth of Thames.

The residual tidal current is weak (0.01–0.02 m s^{-1}) because ebb and flood phases are typically symmetrical (Broekhuizen et al., 2002; Liu, C., Waikato Regional Council, unpublished results). However, within approximately 5 km of the Waihou River mouth, the residual currents are about

---

[41] The information provided in this and the following paragraph was provided by Dr. Willem de Lange, Faculty of Science and Engineering, The University of Waikato. The general pattern of tidal current flow has also been confirmed through WRC in-house modelling studies.

0.05–0.08 m s^{-1} resulting from the river discharge (Liu, C., Waikato Regional Council, unpublished results).

Wind-forcing can cause large changes to the net movement of water in the Hauraki Gulf, including the Firth of Thames (Proctor and Greig, 1989; Bell et al., 2003; Liu, C., Waikato Regional Council, unpublished results). Under moderate to strong winds, substantial wind-driven currents can be generated, particularly in the surface layer (Broekhuizen et al., 2002). Persistent winds from the north to east cause a clockwise residual circulation, while the prevailing winds from the south and west produce an anti-clockwise circulation.

Northerly winds typically generate the largest waves, with periods less than 10 seconds and height typically <1 m. Gorman and Heydenrych (2004) developed a 20-year wave-climate hindcast for the Firth of Thames (1979 to 1998). Table 3-2 presents the results of this wave-climate hindcast for Kaiaua (western Firth of Thames) and the central Firth of Thames.

Table 3-2: Firth of Thames 20-year wave-climate hindcast statistics. H_{sig} is significant wave height, T_{peak} is the period of the peak wave energy and T_m is the average wave period. Wave direction is that from which the predominant wave energy arrives in descending order (source: Gorman and Heydenrych, 2004).

Site	Mean H_{sig} (m)	Max H_{sig} (m)	Mean T_{peak} (s)	Max T_m (s)	Direction
Kaiaua [5 m depth]	0.26	1.25	4.3	8.5	N, NNE
Central Firth [9.7 m depth]	0.41	1.49	5.3	8.6	NNW, N

Extreme significant wave heights are seldom >1.5 m. Wave heights are likely to be further attenuated in the southern Firth due to bed friction over intertidal mud flats. Wave periods indicate the sea state is mostly local wind-sea, with occasional penetration of swell from the Hauraki Gulf during extreme low-pressure cyclonic storms. Swell attenuation will be more pronounced due to the longer wavelength (Gorman and Heydenrych, 2004).

Tidal currents may agitate bottom sediments and disperse suspended sediments. In addition, tidal and residual currents trap river-borne suspended sediments that are deposited in the Firth of Thames (Healy, 2002). Consequently, substantial mud resuspension and transport by waves and currents onto the southern shorelines of the Firth of Thames has contributed to delta formation (e.g., at major river mouths and along intertidal flats).

Over the period 2004–2006, mean sea level[42] in the Firth was approximately 0.1 m above the local Moturiki Vertical Datum–1953 (Swales et al., 2007). The historical rate of relative sea level rise at the Port of Auckland (1899–2005) has averaged 1.4 mm y^{-1} based on the results of Hannah and Bell (2012) up to 1999 and extended to include the years 2000–2005. Sea level has been rising in the southern Firth of Thames at a similar rate to Auckland, based on a comparison with the short 1993–2006 sea level record at Tararu (Bell and Goodhue, 2007).

---

[42] The mean level of the sea (MLOS) is the actual average sea level which varies from year to year and is also increasing due to global warming. This should not be confused with mean sea level datum (MSL) which is a fixed survey datum across a region.

3.7　References

Bell, R.G., Oldman, J.W., Stephens, S.A. (2003) Recent applications of 3Dwind-driven circulation modelling to a semi-enclosed sea: Hauraki Gulf, New Zealand. In: Spaulding, M.L. (Ed.). Estuarine and Coastal Modelling. Proceedings of the *Eighth International Conference*, Monterey, 3-5 November 2003. American Society of Civil Engineers, Reston, Virginia USA: 288–307.

Bell, R.G., Goodhue, N. (2007) Mean level of the sea at Tararu: 1993–2006. *NIWA Client Report* HAM2007-084, prepared for Environment Waikato.

Black, K.P., Bell, R.G., Oldman, J.W., Carter, G.S., Hume, T.M. (2000) Features of 3-dimensional barotropic and baroclinic circulation in the Hauraki Gulf, New Zealand. *New Zealand Journal of Marine and Freshwater Research,* 34(1): 1–28.

Broekhuizen, N., Zeldis, J., Stephens, S., Oldman, J., Ross, A., Ren, J., James, M. (2002) Factors related to the Sustainability of Shellfish Aquaculture Operations in the Firth of Thames: A Preliminary Analysis. *NIWA Client Report EV202243*, prepared for Environment Waikato and Auckland Regional Council.

Brownell, B. (2004) *Muddy feet: Firth of Thames RAMSAR-site update 2004*. Ecoquest Education Foundation, Pokeno, New Zealand: 198.

Chick, L., de Lange, W.P., Healy, T.R. (2001) Potential tsunami hazard associated with the Kerepehi Fault, Firth of Thames, New Zealand. *Natural Hazards*, 24: 309–318.

de Lange, P.J., Lowe, D.J. (1990) History of vertical displacement of Kerepehi Fault at Kopouatai bog, Hauraki Lowlands, New Zealand, since c. 10 700 years ago. *New Zealand Journal of Geology and Geophysics*, 33(2): 277–283, doi: 10.1080/00288306.1990.10425685.

Gorman, R.M., Heydenrych, C. (2004) Hauraki Gulf wave climate simulation. *NIWA Client Report* HAM2004-092, prepared for Auckland Regional Council.

Hannah, J., Bell, R.G. (2012) Regional sea-level trends in New Zealand. *Journal of Geophysical Research*, 117: C01004, doi:10.1029/2011JC007591.

Healy, T. (2002) Muddy coasts of mid-latitude oceanic islands on an active plate margin – New Zealand: 347-374. In: Healy, T., Yang, J.-A. Healy, (*eds*.) *Muddy coasts of the world: processes, deposits and function.*

Hochstein, M.P., Ballance, P.F. (1993) Hauraki Rift: a young, active, intra-continental rift in a back-arc setting. *Sedimentary basins of the world,* 2: 295–305.

Hochstein, M.P., Nixon, I. M. (1979) Geophysical study of the Hauraki Depression, North Island, New Zealand. *N.Z. Journal Geology and Geophysics,* Vol. 22, No. 1: 1–19.

Knight B.R., Beamsley, B. (2013) *3-D Hydrodynamic and Aquaculture Effects Models: Firth of Thames and Hauraki Gulf Calibration Report*. Cawthron Report No. 2372.

McGlone, M., Nelson, C., Todd, A. (1984) Vegetation history and environmental significance of pre-peat and surficial peat deposits at Ohinewai, Lower Waikato Lowland. *Journal of Royal Society of NZ*, 14: 233-244.

Newnham, R., de Lange, P., Lowe, D. (1995) Holocene vegetation, climate and history of a raised bog complex, northern New Zealand based on palynology, plant macrofossils and tephrochronology. *The Holocene*, 5: 267–282.

Phillips, C. (2000) *Waihou Journeys. The Archaeology of 400 years of Māori Settlement*. Auckland University Press.

Proctor, R., Greig, M.J.N. (1989) A numerical model of the Hauraki Gulf, New Zealand. *New Zealand Journal of Marine and Freshwater Research*, 22: 379–390.

Sharples, J. (1997) Cross-shelf intrusion of subtropical water into the coastal zone of northeast New Zealand. *Continental Shelf Research,* 17: 835–857.

Sharples, J.; Greig, M.J.N. (1998) Tidal currents, mean flows and upwelling on the northeast shelf of New Zealand. *New Zealand Journal of Marine and Freshwater Research,* 32: 215–231.

Stephens, S. (2003) *Ecological Sustainability assessment for Firth of Thames shellfish aquaculture: Task 1-Hydrodynamic modelling*. NIWA Client Report HAM 2003-113, prepared for Auckland Regional Council, Environment Waikato and the Western Firth Consortium.

Swales, A., Bell, R.G., Ovenden, R., Hart, C., Horrocks, M., Hermansphan, N., Smith, R.K. (2007) Mangrove-habitat expansion in the southern Firth of Thames: sedimentation processes and coastal-hazards mitigation. *Environment Waikato Technical Report,* 2008/13, www.ew.govt.nz/Publications/Coastal/.

Turner, S., Hume, T., Gibberd, B. (2006) *Waikato Region Estuaries — Information and Management Issues*. Environment Waikato Internal Series 2006/09, Waikato Regional Council.

Vant, B. (2011) *Water Quality of the Hauraki Rivers and Southern Firth of Thames, 2000–09*. Waikato Regional Council Technical Report, TR 2013/20.

Vant, B. (2013) *Trends in River Water Quality in the Waikato region, 1993–2012*. Waikato Regional Council Technical Report: TR 2013/20.

Woodroffe, C.D., Curtis, R.J., McLean, R.F. (1983) Development of a chenier plain, Firth of Thames, New Zealand. *Marine Geology,* 53: 1–22.

Zeldis, J.R. (2004) New and remineralised nutrient supply and ecosystem metabolism on the northeastern New Zealand continental shelf. *Continental Shelf Research* (24): 563–581.

Zeldis, J.R., Gall, M., Uddstrom, M., Grieg, M.J. (2000) La Niña shuts down upwelling in Northeastern New Zealand. *Water & Atmosphere,* 8(2): 15–18.

Zeldis, J.R., Handley, S., Gall, M., Greig, M., Pinkerton, M., Richardson, K., Hooker, S., Moana, D., Siddal, V. (2001) From ENSO to Oysters. *Seafood New Zealand*, 9(11): 17–19.

Zeldis, J.R., Walters, R.A., Greig, M.J.N., Image, K. (2004) Circulation over the northeastern New Zealand continental slope, shelf and adjacent Hauraki Gulf, from spring to summer. *Continental Shelf Research (*24): 543–561.

4 Sediments

4.1 Overview of data sources

In this section we list sources of data presented in this chapter. Unless otherwise specified data were collected and are owned by NIWA.

4.1.1 Subsidence

- GPS Monitoring of Rod Surface Elevation Table (RSET) benchmarks located along the Appletree Transect B since 2008.

4.1.2 Mangrove forest expansion

- Aerial photographs of the southern Firth dating to the 1940s and early 1950s.

4.1.3 Recent sedimentation history of mangrove forests

- Sediment cores collected from 12 sites collected in February 2005 along Appletree Transect B. Cores dated and analysed for bulk density and particle size.

4.1.4 Unvegetated intertidal flats

- Sediment cores collected in February 2006 from the intertidal flats along a 1 km long, north–south transect aligned with the Appletree Transect B. Cores dated and X-rayed.

4.1.5 Sediment budget for the southern Firth of Thames

- Annual sediment budget estimated for the mangrove forest at the Appletree transect, a 1000 m transect seaward of the mangrove-forest fringe, and the lower intertidal and shallow subtidal.

4.1.6 Subtidal

- Voyage SEA0201, December 2002, occupying a total of 29 stations along transects in the Firth and extended Firth.

- Voyage KAH0310 in December 2003, occupying a reduced number of sites on the same transects.

- Voyage KAH1202 in March 2012, occupying one site ("outer") in the extended Firth and two sites ("inner") in the Firth.

- Voyage TAN9915 north of the Mokohinau Islands in a water depth of 125 m (site 5, 35° 48.83'S, 175° 1.83'E).

4.2 Intertidal-flat morphology

Intertidal-flat morphology is similar to that described for the muddy coast of Suriname, South America (Augustinus, 1980; Wells and Coleman, 1981). The lower–middle intertidal flat in the Firth is characterized by low-density mud deposits, with water content of ~50% per unit volume, while a "mud bastion" morphology of isolated consolidated-mud mounds ≤ 20 cm high has developed on the middle–upper intertidal flat above 0.7 m MSL (Figure 4-1). On the Suriname coast, these features have been interpreted as remnants of an eroded mudflat (Augustinus, 1980) as is the case in the southern Firth.

Figure 4-1: Location of the mud-bastion morphology characteristic of the middle–upper intertidal flat.
Photo taken ~800 m north of mangrove-forest fringe, Transect B 4-3; 14 March 2006. For scale, mud bastions ~10 cm high. For transect locations see Figure 4-3.

Above 0.8 m MSL, the mud bastions are replaced by a 300-m wide band of large-scale "mud forms" that resemble an irregular ridge–runnel system (Figure 4-2). These shore-normal, often bifurcating ridges are up to 0.25 m high with wavelengths $\leq$2 m and sinuous crests up to 50 m long. The features represent large-scale bedforms and similar bedforms are reported by Augustinus (1980) from Suriname's muddy coast. The southern Firth's intertidal morphology is characteristic of a mesotidal (2–4 m tidal range), moderately wave-exposed, muddy coast whose large mud supply results in high suspended-sediment concentrations (SSC) and rapid sedimentation. Notably, in similar muddy-coast environments, near-bed SSC in the range 10^3–10^4 mg L^{-1} increases fluid density sufficiently to attenuate shoaling waves (Wells and Coleman, 1981; Mehta, 2002) and further increase sedimentation rates.

Figure 4-2: **Ridge and runnel bedform morphology developed on the intertidal flat immediately seaward of the mangrove fringe, Appletree Transect B (30 March 2006).** Note mangrove tree at bottom right of photo. For scale, mudforms are up to 25-cm high and the runnels are 1–2 m apart. For transect locations see Figure 4-3.

4.3   Subsidence

GPS Monitoring of Rod Surface Elevation Table (RSET) benchmarks located along the Appletree Transect B since 2008 (Figure 4-3) show that the deep sedimentary basin west of the Kerepehi Fault is subsiding at 7.6–8.6 ±0.9 mm y^{-1} (1 sigma) (Swales, unpublished data). Rates of subsidence at all three RSET benchmarks within the mangrove forest at transect B are very similar, indicating that the entire intertidal-flat/mangrove forest complex in the southern Firth is subsiding. Notably, as the RSET benchmarks extend 18 m down into the sediment column, deep subsidence is occurring rather than any change associated with the dewatering of near-surface, recently deposited sediments.
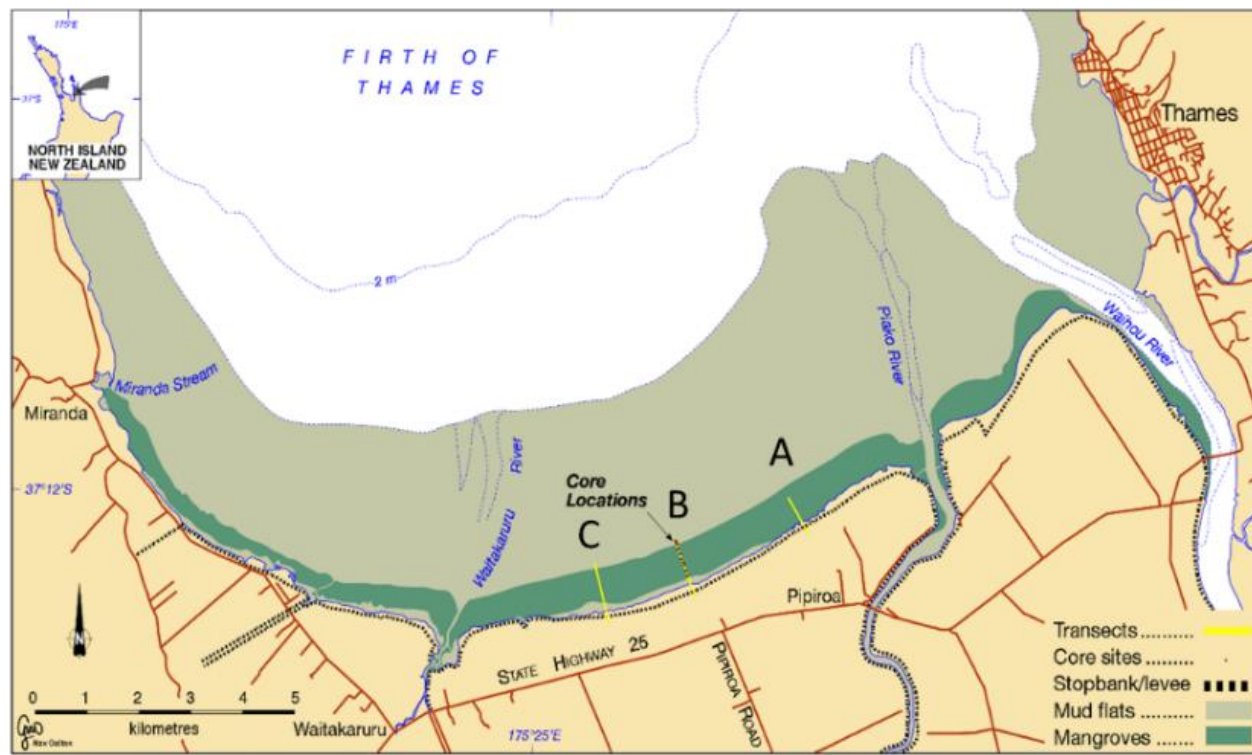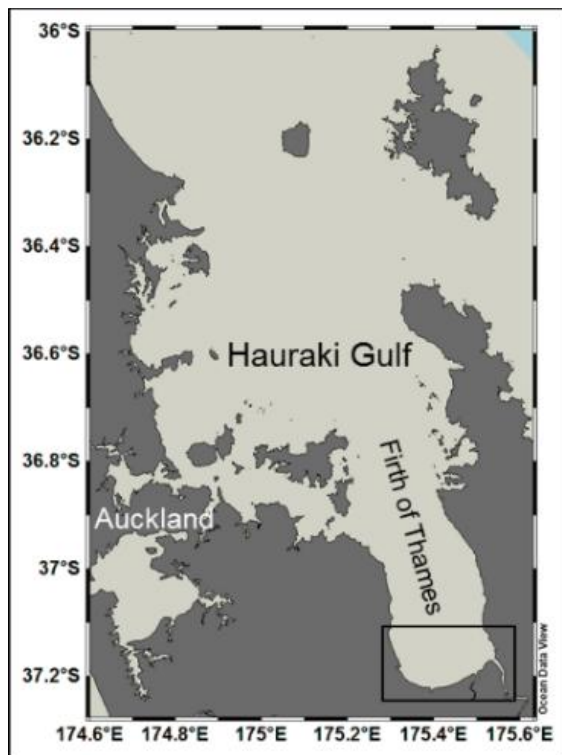
Figure 4-3: Location map, showing transects. Shore-normal elevation profiles (yellow lines) at Transects A (east), B (also called "Appletree", opposite Pipiroa Road) and C (west). Sediment cores were collected along the central Transect B.

4.4   Mangrove forest expansion

The surface elevation of intertidal flats is a first-order control on mangrove-forest development due to physiological constraints that, in the case of the grey mangrove *Avicennia marina* subspecies *australasica*, limit seedling establishment to areas above mean sea level. Seedling recruitment on open intertidal flats is also constrained by bed erosion, particularly in estuaries in which wave fetches exceed several kilometres (Swales et al., 2007b; Morrisey et al., 2010).

Although the mangrove, or Manawa, has rapidly colonised intertidal flats in the southern Firth of Thames since the 1960s, Captain James Cook noted the presence of mangroves along the banks of the lower Waihou River as early as 1769 (Beaglehole, 1968). Palynological evidence also suggests that mangroves were also present in the Firth at least 12,000 years ago (Pocknall et al., 1989). Pocknall et al. (1989) collected sediment cores on the 35-m isobath west of Manaia (Coromandel Peninsula) containing mangrove pollen, which marked an earlier shoreline that existed 12,000 to 14,000 years ago.

Aerial photographs of the southern Firth dating to the 1940s and early 1950s demonstrate that mangrove habitat was restricted to delta deposits, flanking the mouths of the Waitakaruru, Piako and Waihou Rivers. By contrast, today, mangroves occupy some 7 km^2 of former intertidal flat between the Piako and Waitakaruru Rivers and 11 km^2 in the southern Firth as a whole (Brownell, 2004).

Swales et al. (2007) analysed the historical aerial-photographic record for the southern Firth to reconstruct the pattern of mangrove-habitat expansion since the mid-1940s. Figure 4-4 and Figure 4-5 summarise the aerial photography as a 200-m wide swath centred on the Appletree Transect B, where sediment cores were collected for dating in 2005 (Swales et al., 2007). The 1944 aerial survey shows that saltmarsh occupied the upper-intertidal zone along the coast between the Piako and Waitakaruru Rivers, and that mangroves were confined to the river deltas. From 1944 to 1952 aerial surveys showed no substantial change in the mangrove-forest distribution, being localised to the mouths of the Waitakaruru, Piako and Waihou Rivers. By 1963, mangroves had colonised the entire section of coast between the river mouths, extending to the middle intertidal flat 300 m seaward of the stopbank. The mangrove stand at this time was approximately 50 m wide and ~10 m seaward of core site LC-3 (Figure 4-4). The 1944–1963 photo sequence also clearly shows that saltmarsh habitat was progressively colonising the upper intertidal flat. By 1977, mangrove forest had spread seaward and, to a more limited extent, landward, and occupied a 500-m wide zone along the entire coast of the southern Firth (Figure 4-5). At Transect B, the mangrove-forest fringe was located at core site LC-6. Mangrove forest has continued to spread seaward since the 1970s and by 2002 occupied a ~800-m wide zone and ~7 km^2 of former intertidal flat between the Waitakaruru and Piako River mouths.
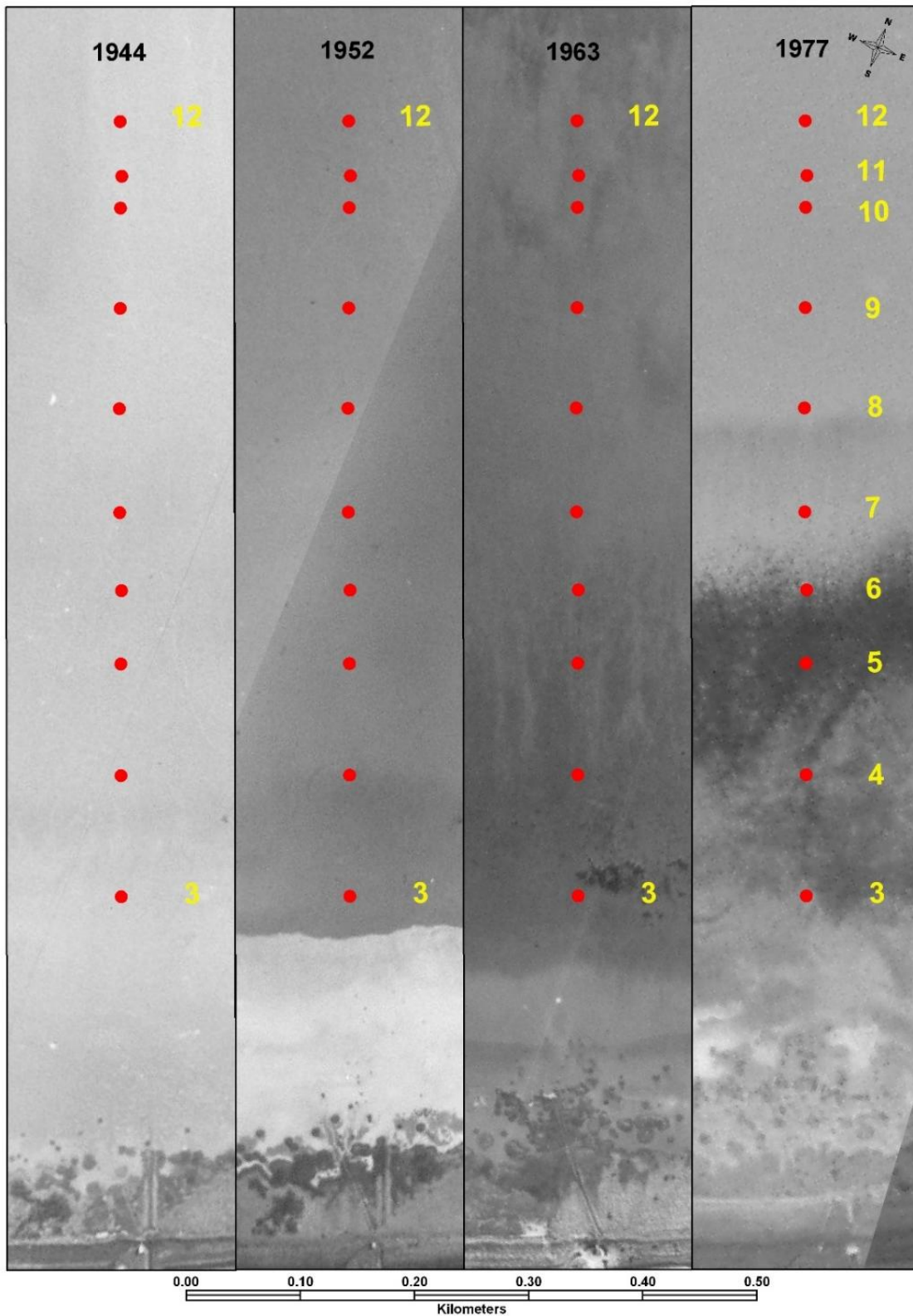
Figure 4-4: Aerial photographs of the intertidal flat ±100 metres east and west of Appletree Transect B (see Figure 4-3 for location): 1944, 1952, 1963 and 1977. The locations of the sediment cores (sites 3–12) collected in 2005 are also shown. Source: Swales et al. (2007).
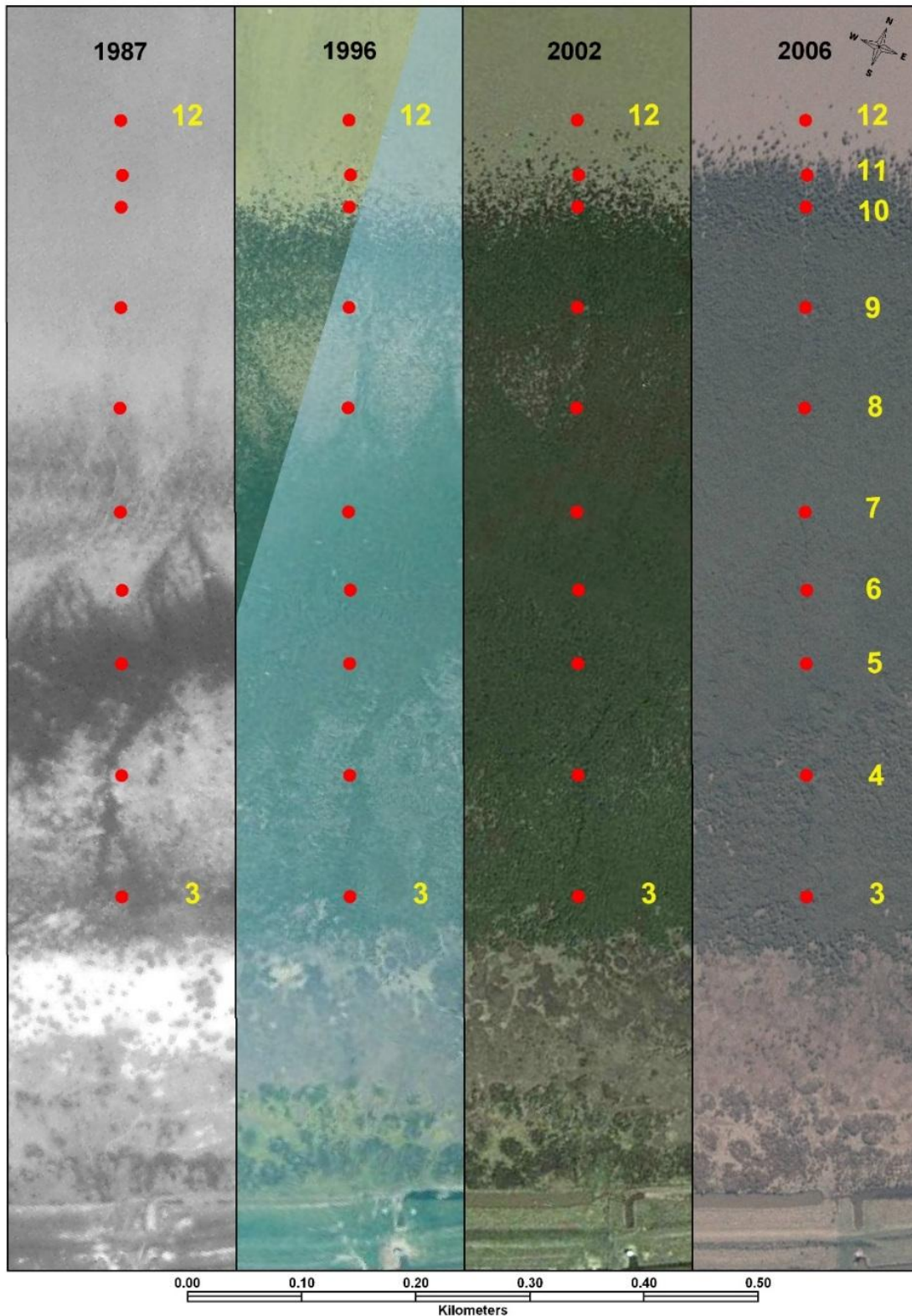
Figure 4-5: **Aerial photographs of the intertidal flat ±100 metres east and west of Appletree Transect B (see Figure 4-3 for location): 1987, 1996, 2002 and 2006.** The locations of the sediment cores (sites 3–12) collected in 2005 are shown. Source: Swales et al. (2007).

Mangrove-habitat expansion depends on successful annual recruitment of seedlings on the exposed intertidal flat. In the southern Firth, mangrove-seedling recruitment is constrained by frequent

---

erosion of the intertidal flat by waves. Observations suggest that most seedlings typically fail to establish and that large-scale habitat expansion is likely to coincide with rare periods of calm weather during the summer recruitment period (Swales et al., 2007b). Mangrove-seedling recruitment on the intertidal flats of the southern Firth is therefore an episodic rather than regular (i.e., annual) process. The aerial-photographic record indicates that at least four major mangrove-seedling recruitment events have occurred since the early-1950s during the time intervals 1952–1963, 1963–1977, 1977–1987 and 1987–1996 (Swales et al., 2007b). Figures 4-4 and 4-5 also show that the mangrove forest has not substantially increased its seaward extent since 1996, implying that no major seedling recruitment has occurred in the following decade.

4.5   Recent sedimentation history of mangrove forests

4.5.1   Data collection

Sediment cores were collected along Appletree Transect B (Figure 4-6), which is located mid-way between the Waitakaruru and Piako Rivers (Figure 4-3). Transect B was selected for coring because sediments deposited here should preserve changes in physical conditions on the intertidal flats that are representative of the southern Firth in general, which is a relatively linear shoreline. Closer to the river mouths, sedimentation rates are likely to be more spatially variable, being influenced by strong gradients in sediment transport and deposition rates associated with hydrodynamic conditions characteristic of the more complex tidal-river channel, deltaic and levee environments.
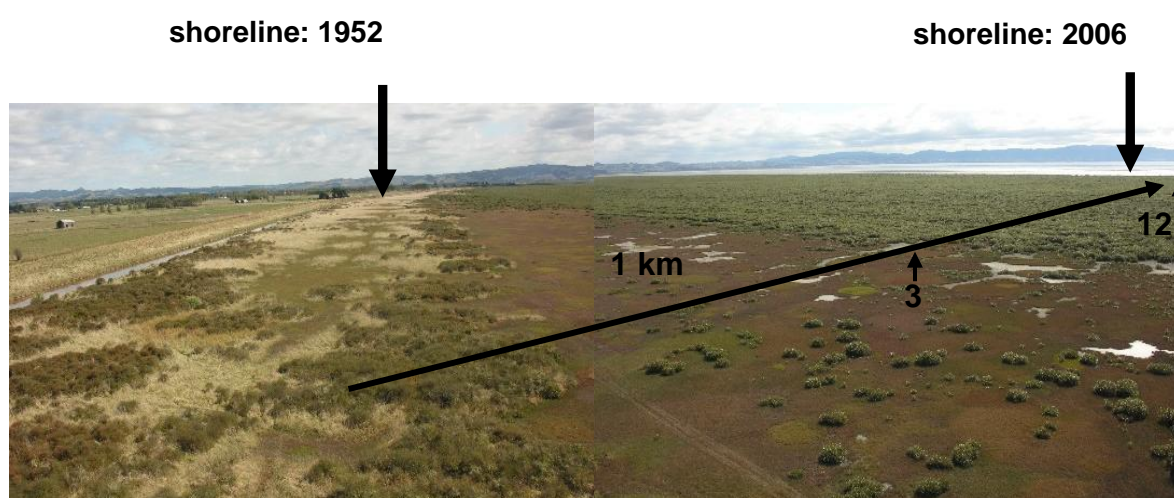

Figure 4-6:   View of Appletree Transect B looking west. The transect location is indicated by the black line. Core site 3 is close to the landward edge of the mangrove forest and site 12 is located ~50 m seaward of the seaward edge of the mangrove. Glasswort (*Sarcocornia quinqueflora*) saltmarsh occupies a 200-m wide zone between the mangrove forest and an area of saltmarsh ribbon wood (*Plagianthus divaricatus*). *Muehlenbeckia complexa* (scrub pohuehue) with tall fescue grass (*Schedonorus phoenix*) is adjacent to the stopbank. Source: Swales et al. (2007)**..**

Replicate sediment cores (7.5 cm in diameter and ≤1.9 m long) were collected during 22–24 February 2005 from the mangrove forest along Transect B using a Livingston piston corer (Table 4-1; sites LC-3 to LC-11; Figure 4-7). A 0.7 m long push core was collected from the mud flat 50 m seaward of the mangrove-forest fringe (site LC-12). Replicate short cores (40 cm long and 10 cm diameter) were also collected at sites LC-3 to LC-11. The cores were logged and sub-sampled at depth intervals in 2-cm

thick slices for radioisotope dating, bulk density and particle-size determination. Core compression was <5% at all sites.
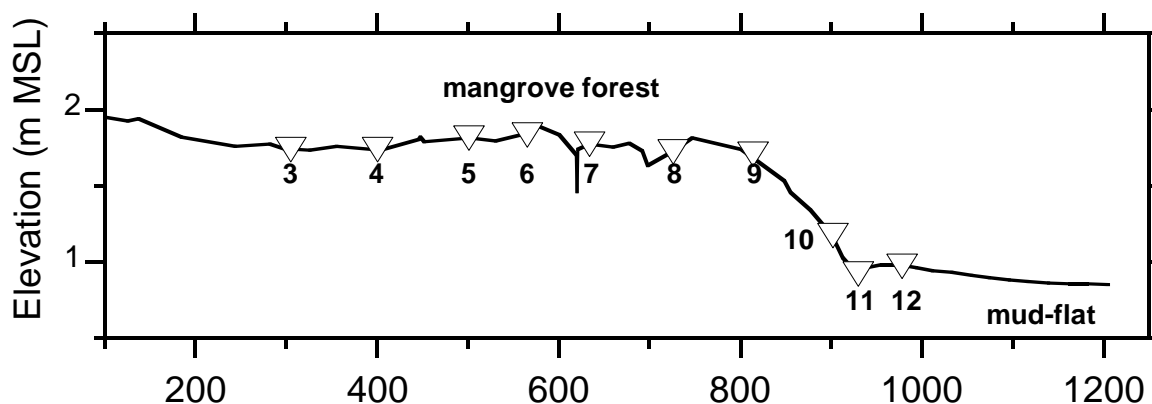

Figure 4-7: **Sediment core locations along Transect B (LC-3 to LC-12).** The mangrove-forest fringe (seaward edge) was at site LC-11 in February 2005. Bed elevations are relative to mean sea level (Moturiki Vertical Datum 1953).

Table 4-1: **Sediment core locations along Transect B collected from the mangrove forest (LC-3 to LC-10) and intertidal flat (LC-11 and LC-12).** Distance is relative to total station position on top of stopbank. Bed elevations are relative to mean sea level (Moturiki Vertical Datum 1953).

Core site	Distance (m)	Elevation (m MSL)	NZMG East	NZMG North
LC-3	305	1.74	2727954	6440321
LC-4	400	1.74	2727558	6440421
LC-5	501	1.81	2727524	6440513
LC-6	565	1.84	2727503	6440573
LC-7	634	1.77	2727478	6440637
LC-8	726	1.72	2727447	6440723
LC-9	814	1.71	-	-
LC-10	902	1.17	2727388	6440888
LC-11	930	0.92	2727380	6440915
LC-12	978	0.97	-	-

4.5.2   Dating methods

The sediment cores were dated using radioisotope and pollen techniques, and the results were used to reconstruct the recent sedimentation history of the shoreline. Sediment accumulation rates (SAR) were estimated from lead-210 (^{210}Pb, $t_{1/2}$ 22.3 y) and caesium-137 (^{137}Cs, $t_{1/2}$ 30 y) concentrations. Concentrations of the cosmogenic radioisotope beryllium-7 (^{7}Be, $t_{1/2}$ 53 days) were also measured in the core samples. ^{7}Be is particle reactive and tends to be concentrated in aquatic systems, making it a useful sediment tracer in fluvial–marine systems at seasonal timescales (Sommerfield et al., 1999). In the present study, ^{7}Be is used to provide information on the depth and intensity of sediment mixing. The radioisotope dating techniques used in the present study are described in 11.

4.5.3   Sediment properties

Sediment cores LC-3 to LC-8 collected from the mangrove forest growing on the upper-intertidal platform sample sediments down to approximately -0.1 m MSL elevation. The particle-size profiles show that sediments deposited in the mangrove forest are composed of homogenous muds, with median (D_{50}) and mean particle diameters of ≤ 20 µm (Figure 4-8). Wet-sediment bulk sediment densities vary between 1.0 and 2.4 g cm^{-3}. Dry-sediment bulk sediment densities (DBD) are uniformly low, with an average value of 0.5 g cm^{-3} (range 0.3–0.75 g cm^{-3}), indicating high *in situ* water content. An ~80% porosity or water content by volume is estimated assuming a quartz–feldspar mineral density of 2.6 g cm^{-3}.
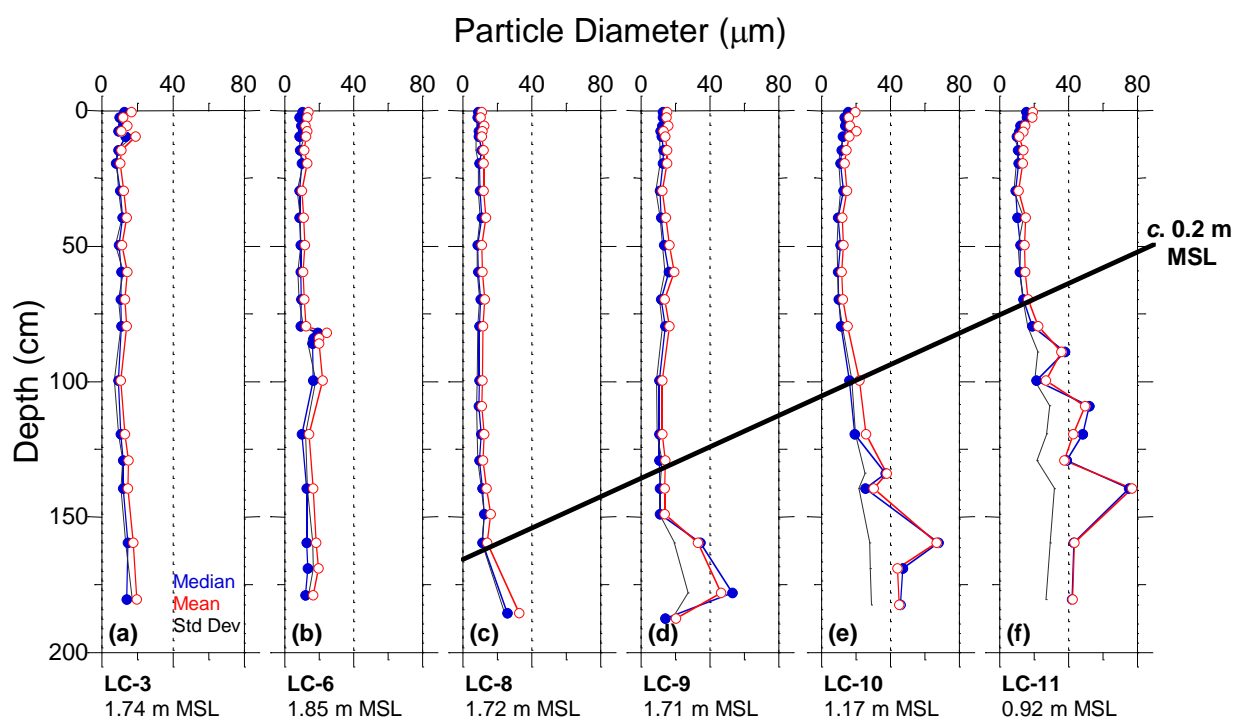

Figure 4-8:   **Particle-size profiles for selected cores from the mangrove forest (LC-3 to LC-9), seaward fringe (LC-10) and adjacent intertidal flat (LC-11).** "Depth" denotes distance below the surface of the core. The elevation of each core surface is shown relative to mean sea level (Moturiki Vertical Datum 1953).

Located near the seaward limit of the mud platform, core LC-8 shows an abrupt increase in particle size at 1.85 m depth (Figure 4-8c). These basal sediments at 1.85 m depth include muddy fine sands containing 10% fine sand ≤ 75 µm in diameter. Cores LC-9 to LC-11, which were collected from the seaward-sloping mud beach on the forest fringe, sample older sediments below ~0.2 m MSL. These cores also show abrupt increases in particle size and sand content, although at progressively shallower depths below the sediment surface for decreasing height above mean sea level (Figure 4-8f). The abrupt increase in particle size occurs at 1.6-m depth in core LC-9 and at 0.7-m depth in LC-11, located at the base of the mud beach. The transition from homogenous-mud deposition to muddy-sands consistently occurs at ~0.2 m MSL. These muddy fine sands are composed of ≤70% sand by volume and ≤165 µm diameter particles.

The shift from muddy-sand to pure-mud sedimentation indicates a fundamental change in the sedimentary regime of the southern Firth. [210]Pb dating shows that this transition from sand to mud occurred in the mid-1960s. Although this appears to coincide with mangrove-forest expansion during the 1952–1963 period (Swales et al., 2007), further analysis of the data from cores LC-7 to LC-11

highlights that increases in sedimentation rates on the intertidal flats predate mangrove colonisation at these core sites by years to decades (see below).

4.5.4   Sedimentation rates

The excess ^{210}Pb (^{210}Pb$_{ex}$) profiles preserved in the sediment cores display prominent changes in gradients that indicate changes in SAR over time and space (Figure 4-9).
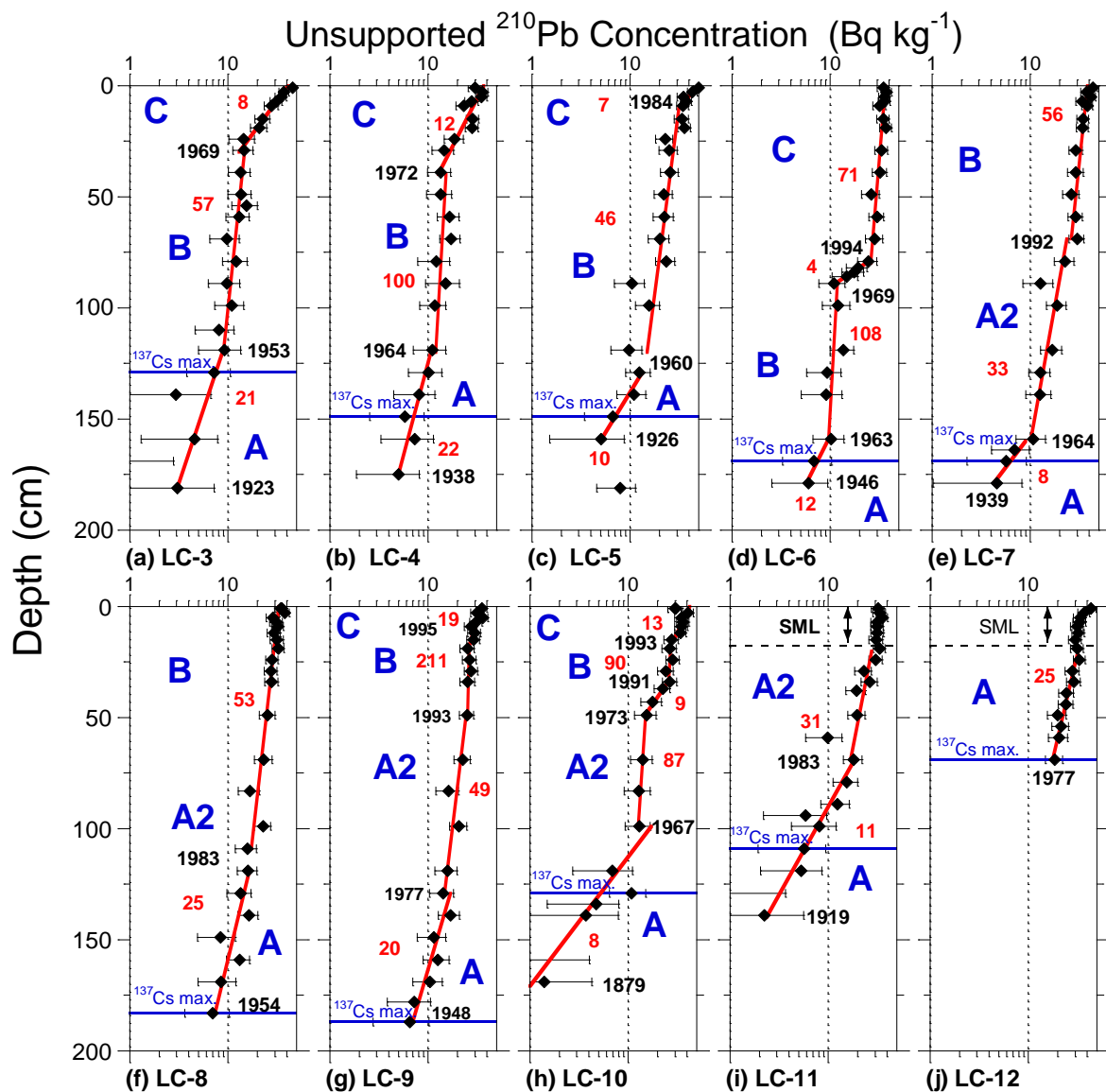

Figure 4-9: **Cores LC-3 to LC-12: unsupported ^{210}Pb concentrations, with 95% confidence intervals.** Time-averaged sediment accumulation rate (red text), maximum ^{137}Cs depth, and ages of the sediment deposit at inflection points in the ^{210}Pb profile are shown. Also shown are the sedimentation environments (blue text): (A) muddy sand or mud mangrove-free intertidal flat; (A2) rapid mud sedimentation in the absence of mangroves; (B) mangrove fringe; (C) mangrove forest.

The ^{210}Pb$_{ex}$ profiles are classified into two main types.

Type-one profiles (e.g., LC-3 to LC-5) exhibit a simple stair–step profile, with changes in sediment accumulation rate indicated by changes in the slope of the log–linear regression fitted to the ^{210}Pb$_{ex}$ data (Figure 4-9a–c). These cores show a transition from a muddy-sand or mud mangrove-free

intertidal flat (A) to a mangrove-fringe environment (B), which is identified by an abrupt increase in SAR, then a decline in SAR as old-growth forest develops and the forest fringe moves seawards (C). SAR declines as the old-growth forest is isolated from the supply of sediment. This occurs by a progressive reduction in hydro-period (i.e., frequency and duration of submergence) as the sediment surface rises and the open intertidal flat moves further seaward.

Type-two profiles differ from the simple stair–step sedimentation sequence. Some profiles, such as LC-6 and LC-10, display multiple stair-step forms and other profiles display progressive increases in SAR over time. An additional sedimentation phase A2 was identified by comparing the dated profiles to the chronology of mangrove-habitat expansion. The A2 represents a period of accelerated mud sedimentation in the absence of mangroves. Cores LC-7 to LC-11 clearly show that the intertidal flat seaward of LC-6 began to accrete mud 2–10 times more rapidly and as much as twenty years before the arrival of mangroves (Figure 4-9e–i; Table 4-2). The onset dates for increases in SAR at sites LC-7 to LC-11 and potential recruitment windows for mangrove colonisation of these cores sites are summarised in Table 4-3. We have confidence in these findings because of the high temporal resolution of the cores (i.e., SAR) and the comprehensive aerial-photographic record.

The sediment cores collected from the mangrove forest also preserve information about historical sediment accumulation rates on the intertidal flats prior to mangrove colonisation. The basal $^{210}Pb_{ex}$ profiles indicate that SAR typically varied from 8–25 mm y^{-1} (mean 16 mm y^{-1}) during the 1920s–1980s (Figure 4-9). Similarly, the present-day intertidal flat immediately seaward of the mangrove forest has accumulated sediment at a rate of ~25 mm y^{-1} since the mid-1970s (Figure 4-9 j). These data suggest that the intertidal flats have been rapidly accreting sediment over the last 90 years or more.

Table 4-2 summarises the chronology of the changes in the sedimentary environment of the southern Firth that have occurred since the 1880s. This chronology has been reconstructed from the Transect B sediment cores and the historical aerial photographs.

Table 4-2: **Chronology of changes in sedimentary environment of the intertidal flat at Appletree Transect B based on** [210]**Pb dating, historical aerial photographs, X-radiographs and sediment properties.** The estimated surface elevation of the tidal flat (metres relative to mean sea level – Moturiki Vertical Datum 1953) at the end of each time period is included in brackets.

	Sedimentary Environment				
Core	**Mangrove-free intertidal flat, muddy sand (A)**	**Mangrove-free intertidal flat, mud (A)**	**Rapid mud sedimentation, no mangroves (A2)**	**Mangrove fringe (B)**	**Mangrove forest (C)**
LC-3	-	pre-1953 (0.55)	-	1953–1969 (1.45)	post-1969
LC-4	-	pre-1964 (0.56)	-	1964–1972 (1.36)	post-1972
LC-5	pre-1926 (0.2)	1926–1960 (0.54)	-	1960–1984 (1.64)	post-1984
LC-6		pre-1963 (0.24)	-	-	-
LC-7	-	1939–1964 (0.17)	1964– 1992 (1.0)	post-1992 (1.1)	-
LC-8	pre-1965 (0.13)	1965–1983 (0.58)	post-1983	post-1983	-
LC-9	pre-1966 (0.21)	1966–1977 (0.42)	1977–1993 (1.21)	1993–1995 (1.51)	post-1995
LC-10	pre-1967 (0.17)	-	1967–1973 (0.67)	1991-1993 (1.02)	post-1993
LC-11	pre-1983 (0.23)	-	1983–	-	-
LC-12	-	pre-2005	-	-	-

Table 4-3: **Timing of the onset of increased sedimentation rate on the intertidal flats as indicated by the excess** [210]**Pb profiles in cores LC-7 to LC-11 and aerial-photographic record for the southern Firth.**

Core	Increase in SAR (^{210}Pb profile)	Mangrove recruitment window (aerial photographic record)
LC7	1964	1977–1987
LC8	1983	1987–1996
LC9	1977	1987–1996
LC10	1967	1987–1996
LC11	1983	1987–1996

4.6 Unvegetated intertidal flats

4.6.1 Data collection

Sediment push cores (diameter 10 cm, length 40 cm) were collected from the intertidal flats along a 1 km long, north–south transect aligned with the Appletree Transect B (Figure 4-3). The intertidal transect sampled each of the bed types seaward of the mangrove forest fringe. The push cores were collected in February 2006 at 50, 200, 400, 600, 800 and 1000 m from the forest fringe. Sediment accumulation rates and surface-mixed layers were estimated from ^{210}Pb and [7]Be profiles, respectively. Sediments were sampled from each core as 1 cm thick slices (up to 20 per core) for dating.

4.6.2   Sedimentation rates

Table 4-4 summarises the recent ^{210}Pb sedimentation rates across the intertidal-flat transect. The data suggest that there is an SAR maximum on the large-scale mud-form field immediately adjacent to the mangrove forest. The SAR maximum declines seaward of the mud-form field until it is uniform, averaging ~26 mm y^{-1} in the zone 600–1000 m from the 2006 seaward edge of the mangrove forest. This average rate is similar to the long-term rates (post-1920) indicated by the ^{210}Pb preserved in the mangrove-forest cores (Figure 4-9). Uniform [7]Be profiles, extending up to ~7-cm depth, also indicate rapid and deep mixing of near-surface sediments (Bentley et al., in prep).

Table 4-4:   Intertidal-flat sedimentation rates.

Core	[210]Pb SAR (mm y^{-1})	Time period
T200	43	1996–2006
T400	36	1994–2006
T600	26	1990–2006
T800	27	1990–2006
T1000	26	1990–2006

X-radiographs of the intertidal-flat cores clearly show fine-scale laminated clays, silts and fine sands overlaying abundant shell valves and hash of cockle (*Chione stuchburyi*) and estuarine trough shell (*Mactra ovata*) (Figure 4-10). These images, along with radioisotope data, indicate that post-depositional reworking of intertidal flat sediments is dominated by wave-driven bed erosion events and that bed disturbance occurs to a substantial depth. The sediment cores from the tidal flats are characterized by two distinct zones of contrasting sedimentary fabric. A surface layer, extending up to 7-cm depth, contains mm-to-cm scale bedding with sharp basal contacts, grading upward from coarser (light grey in X-radiographs) to finer (darker grey) sediments. These sediments have relatively high water content, as indicated by the dark shades in the X-radiographs, are largely unbioturbated, and finely laminated. A finely-laminated layer, consisting of re-deposited sorted sediments and which coincides with the maximum [7]Be penetration depth is characteristic of wave-reworked tidal flats (Yang et al., 2005). Below this relatively recently reworked surface layer, as indicated by [7]Be (i.e., 53-day ½ life), there is a range of biogenic structures, including clearly defined burrows. These biogenic structures have overprinted mm-to-cm-scale stratification that is similar to the surface layer, but less clearly preserved, due to post-depositional bioturbation.
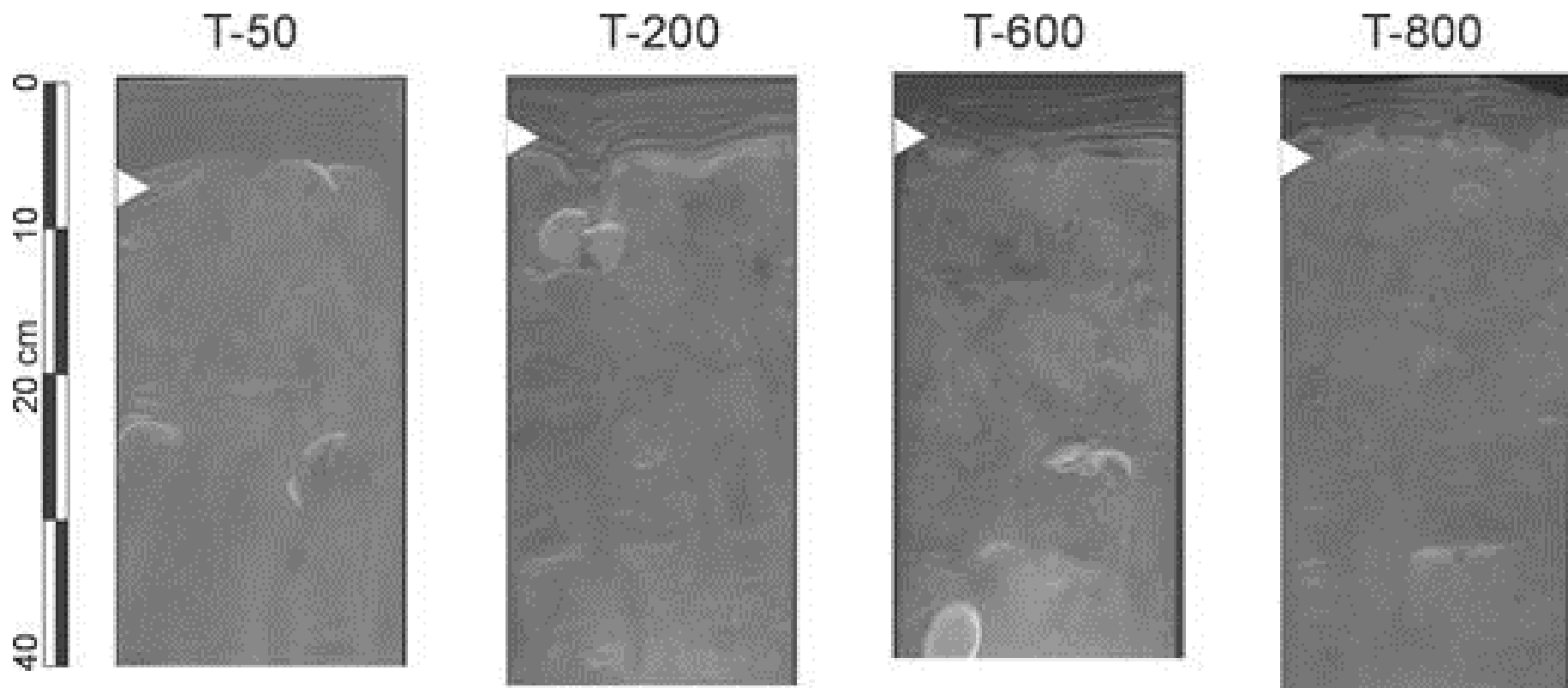
Figure 4-10: X-radiograph negatives of mudflat cores. Bright shades indicated high-density or coarser sediment, and dark shades indicate low-density or finer sediment. [7]Be penetration depth is indicated by white triangles. Shell valves are of *Mactra ovata*. Source: Reproduced from Swales et al. (2007b).

4.7   A sediment budget for the southern Firth of Thames

The sedimentation data presented to this point are now used to estimate a present-day sediment budget for the southern Firth of Thames.

The annual sediment budget is estimated for several sub-environments:

- mangrove forest at Appletree transect (core sites LC-3 to LC-11, 625 m transect; see Figure 4-3),

- intertidal flat, 1000 m transect seaward of the mangrove-forest fringe,

- lower intertidal and shallow subtidal.

Annual-average SAR over the last decade and historical volumetric estimates of sediment accumulation are converted to mass using a dry-bulk sediment density of 0.5 kg m^{-3}, which is characteristic of the under-consolidated muds deposited in the southern Firth of Thames (Swales et al., 2007).

Values of present-day SAR (i.e., the last decade) are used to develop the sediment budget.

Table 4-5 summarises the present-day sediment budget for the southern Firth as well as historical estimates for comparison. The sediment budget developed for the southern Firth indicates that ~110,000 t y^{-1} of fine sediment is accumulating in the mangrove forest. This is a very conservative estimate as it does not include mangrove forest west and east, respectively, of the Waitakaruru and Piako Rivers. A similar mass of sediment (~117,000 t y^{-1}) is accumulating in the same compartment on the 1-km wide upper intertidal flat immediately adjacent to the mangrove forest. By comparison, an estimated 200,000 t y^{-1} of fine sediment is accumulating on the 210 km^2 of lower intertidal – shallow subtidal zone of the southern Firth, south of Tararu–Kaiaua. The 2 mm y^{-1} SAR estimate is a conservative value at the lower end of average values for North Island estuaries (Swales et al., 2013) and is consistent with data from the extended Firth. This SAR value is also less than half the rate indicated by the sediment-mass deposition near the peak of the catchment deforestation and mining activities in the late 1800s to early 1900s (2,427 t km^{-2} y^{-1}, Table 4-5).

The present-day sediment loads for the Waihou and Piako Rivers are uncertain as sediment transport data are not available for hydrometric stations. Hicks et al. (2011) have estimated annual suspended-sediment loads of 160,000 t y^{-1} and 30,000 t y^{-1} for the Waihou (1966 km^2) and Piako (1476 km^2) Rivers, respectively. These numbers suggest that present-day suspended-sediment input from the two largest rivers represents only about 40% of the estimated ~430,000 t y^{-1} of sediment depositing in the southern Firth (Table 4-5). About half of this annual sediment deposition (53%, 228,000 t y^{-1}), is occurring in the upper-intertidal flat/mangrove-forest complex, which accounts for only 7% of the area of the 210 km^2 southern-Firth compartment. Furthermore, sedimentation in the upper-intertidal flat/mangrove-forest complex alone more than accounts for all of the annual river load. The importance of the mangrove forest as a sink for fine sediments is also shown by the mass deposition per square kilometre. Presently, the mangrove forest accumulates 18,900 t km^{-2} y^{-1} in comparison to 12,500 t km^{-2} y^{-1} on the upper intertidal mudflat and the estimated 1,000 t km^{-2} y^{-1} in the subtidal basin (Table 4-5). Therefore, the upper intertidal flat and mangrove forest are accumulating fine sediments at an order of magnitude higher rate than in the southern Firth as a whole.

The apparent discrepancy between sediment delivery by rivers and the (conservative) estimate of annual sedimentation in the Firth could be due to the reworking by waves and currents of legacy

sediments deposited in the Firth during large-scale deforestation and mining activities. The estimated 18.3 million tonnes deposited during the late 1800s to early 1900s (Table 4-5) only represents part of the total quantity of soil eroded from the catchment since the 1850s. Swales et al. (2007) suggested that the intertidal flats were largely built by muds reworked by waves from the shallow subtidal zone and transported onshore and deposited. The sediment core data suggest that this process has been occurring since at least the 1920s. This mechanism also explains the relatively recent development of the mangrove forest since the 1950s, as mangrove seedling establishment could occur after the intertidal flat had accreted above MSL elevation.

Table 4-5: Sediment budget for the southern Firth of Thames. Key: (1) Area per linear metre of shoreline; (2) SAR (m y^{-1}) is the present-decadal average; (3) SAR (t y^{-1}) calculated per linear metre of shoreline using dry-bulk sediment density of 0.5 kg m^{-3}; (4) SAR-m is the total sediment mass accumulation rate between the Piako and Waitakaruru Rivers (9.4 km); (5) SAR-m2 is the total annual sediment-mass accumulation rate in the Piako–Waitakaruru compartment per km^2.

Environment/ source	Compartment	Area (m^2)	SAR (m y^{-1})	SAR (t y^{-1})	SAR-m (t y^{-1})	SAR-m2 (t km^{-2} y^{-1})
Present day						
Mangrove forest	Old forest	260	0.01	1.3		
	Scrub forest	249	0.058	7.2		
	Fringe	116	0.056	3.3		
	Total-mangrove			**11.8**	110,900	18,860
Intertidal flat-1km	Upper intertidal	1000	0.025	12.5	117,500	12,500
Lower intertidal - subtidal flats	Area south of Tararu – Kaiaua	210 x10^6	0.002		200,000	1000
Waihou & Piako Rivers					190,000	–
Historical						
Southern Firth	as above (period 1882–1918)				18.3 x 10^6	2,427

4.8 Subtidal region

4.8.1 Data collection and analysis

Sediment samples were collected from the subtidal environment of the Firth and the extended Firth on three occasions: NIWA voyages SEA0201 in December 2002, KAH0310 in December 2003 and KAH1202 in March 2012 (Figure 4-11).

Samples were also collected across the Firth, extended Firth, Hauraki Gulf and on the NE shelf and slope on NIWA voyage TAN9915 in December 1999. This data and data collected on KAH0310 have been reported by Giles et al. (2007).
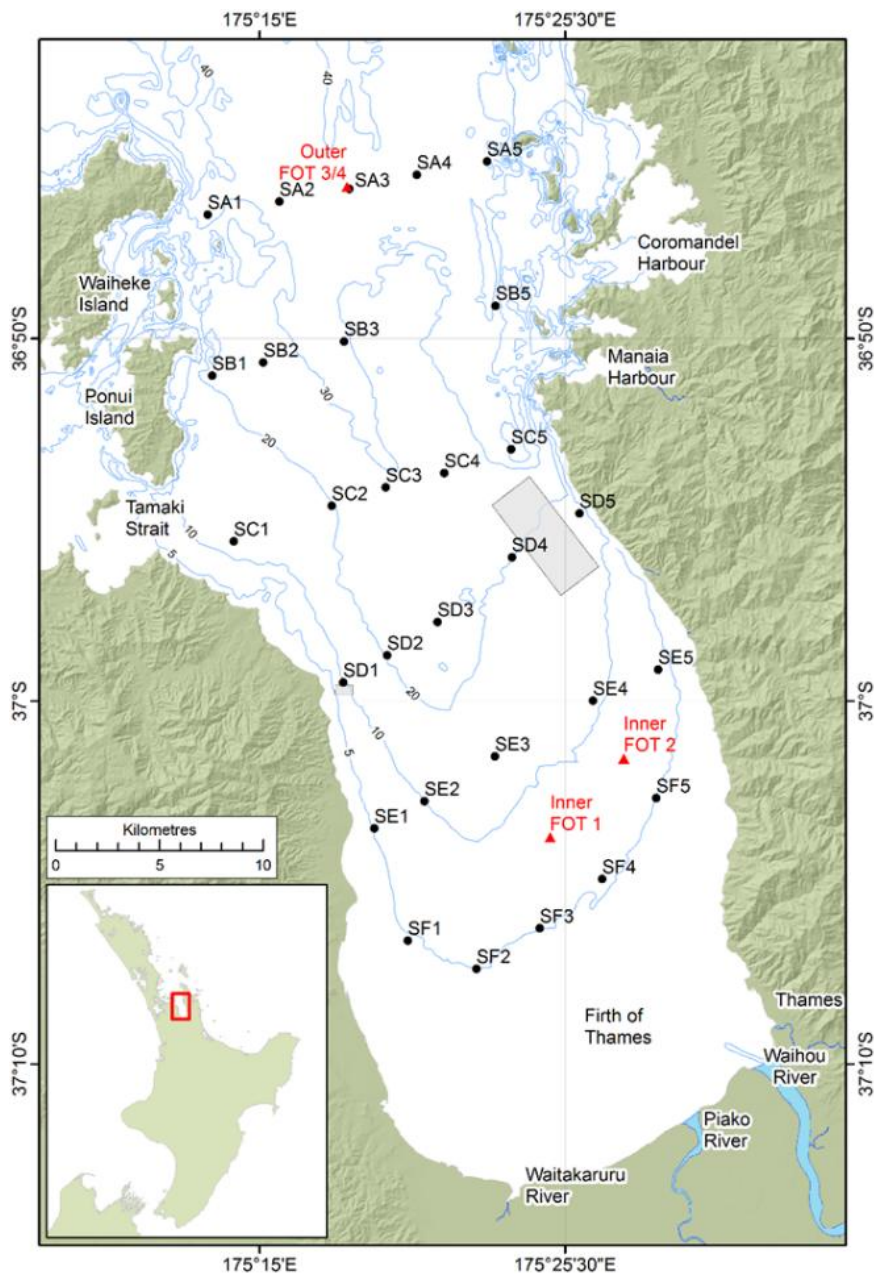
Figure 4-11: Subtidal bathymetry, sampling sites and mussel farms. Subtidal samples were collected on three voyages: SEA0201 (December 2002), KAH0310 (December 2003) (both shown as black dots on transects SA to SF) and KAH1202 (January 2013) (red triangles). The "outer" site is in the extended Firth. The grey box depicts the Wilson Bay Marine Farming Zone Area A.

On TAN9915, SEA0201 and KAH0310, samples were obtained using an Ocean Instruments MC-800 multi-corer with eight 10 cm diameter sampling tubes, which is designed to sample the sediment–water interface with minimal disturbance. On KAH1202, a similar diameter mini-multi-corer (KC Denmark Model 71.000) was used.

After siphoning off the overlying seawater, sediment samples were then either:

- sliced at set intervals (0.5 or 1 cm thick slices) for analysis of physical and biogeochemical parameters (e.g., grainsize, total organic matter, calcium carbonate content, organic carbon, nitrogen, phosphorus and phytopigments);

- subsampled for biological components of the seabed community (e.g., meiofauna, macro-infauna); and/or

- extruded into chambers and used in shipboard incubation experiments to derive fluxes of key biogeochemical elements (e.g., oxygen, nutrients, dissolved inorganic carbon).

On SEA0201, the main focus of the voyage was obtaining a spatial map of the surficial sediments by sampling a series of transects across and along the length of the Firth and the extended Firth. A total of 29 sites were occupied: these were sites SA1–5 and SB1–5 in the extended Firth, repeated on transects SC to SF moving into the Firth, except for no sampling at SB4. On KAH0310, sediment, biological and biogeochemical samples were obtained, although at a reduced number of key sites (SA3, SA5, SD1, SD3, SD5, SF2 and SF5), with SA1 also sampled for sediment properties only. On KAH1202, the voyage objectives were to obtain detailed information at a smaller number of sites (3 in total) (Figure 4-11) spanning observed gradients in carbonate parameters, with one site (SA3) in common with the two previous voyages.

For details of the sample processing and physical, chemical and biological laboratory analyses, refer to Nodder et al. (2003; 2007) and Giles et al. (2007). The macrofauna samples were sieved at 500 μm, rather than the 300 μm that was used in the deep-ocean studies. On KAH0310, a phospholipid proxy analysis was used to estimate sediment bacterial biomass at each of the sites (Findlay et al., 1989).

Sediment accumulation rates were determined using the radioisotope ^{210}Pb, as described in 11. This work was undertaken as part of an undergraduate MSc thesis project by de Baere (2006) at the University of Southampton (United Kingdom), with selected other measurements also presented in Sikes et al. (2009). de Baere's (2006) method used alpha spectrometry to determine the down-core concentrations of ^{210}Pb, following acid leaching and auto-deposition onto silver discs. Ten to fifteen depth intervals were sampled from cores collected at sites SA3, SD3 and SF5 from voyage KAH0310 (Figure 4-11). An additional sample was collected on the shelf during NIWA voyage TAN9915 north of the Mokohinau Islands in a water depth of 125 m (site 5, 35° 48.83'S, 175° 1.83'E).

Similar ^{210}Pb and ^{137}Cs analyses were conducted on additional samples from sites SA3 and SC3 (voyage KAH0310) by the National Radiation Laboratory (NRL, Christchurch, New Zealand), with the information from SA3 reported in Sikes et al. (2009); the ^{210}Pb data from SC3 are new and unpublished, and have been processed for the purposes of the present report (Andrew Swales, NIWA pers. comm.). Measurements were made using dried sediment samples embedded in an epoxy resin and analysed in a Hyper Pure Germanium gamma detector for a 30-day counting period. Results were processed using GENIE-2000 software by NRL. ^{210}Pb, ^{226}Ra and ^{137}Cs concentrations were highly variable (based on counting statistics) and/or below detection limits for several samples and, accordingly, the SAR for site SA3, determined using this method, should be regarded as tentative.

For graphical purposes, the sediment physical and biogeochemical properties were imported into a Geographic Information System (ArcGIS version 10.2) and the data interpolated between sites using a regularised spline function contoured at appropriate scales. Maps were produced using a Mercator projection with a Standard Parallel of 41° S on Geographic Coordinate System WGS84. The spline function in ArcGIS uses "an interpolation method that estimates values using a mathematical function that minimizes overall surface curvature, resulting in a smooth surface that passes exactly through the input points" (ArcGIS Help 10.2.1).

4.8.2 Sediment properties reported by Giles et al. (2007)

Sediment characteristics measured on TAN9915 and KAH0310 and reported by Giles et al. (2007) differed across the Firth, Hauraki Gulf and NE shelf, with Firth sediments being very fine-grained (76–90% silt/clay) and with low $CaCO_3$ content (less than 8.0%), high porosity and high water content. The Firth had highest total organic matter (7.7–18.5%), POC (1.7–2.6%) and PON (0.21– 0.33%) contents and lowest C:N ratios (8.9–9.9) of the 3 regions. The average chlorophyll *a* content measured at Firth sites was 5.7 times higher than values measured in the Hauraki Gulf (which included the extended Firth). These, in turn, were 6.4 times higher than values at the deep sites. The average phaeopigment content in the Firth was 2.5 times higher compared to the Hauraki Gulf, but the distinction between the Hauraki Gulf and the deep sites was not as clear. Carotenoid content was also elevated at most sites in the Firth.

4.8.3 Sediment properties from further datasets

Surface (top 0–1 cm) sediment bulk and biogeochemical properties were sampled over a wide grid of stations encompassing water depths from 5 to 40 m across the Firth and extended Firth (voyage SEA0201). The interpolated results are shown in Figure 4-12.
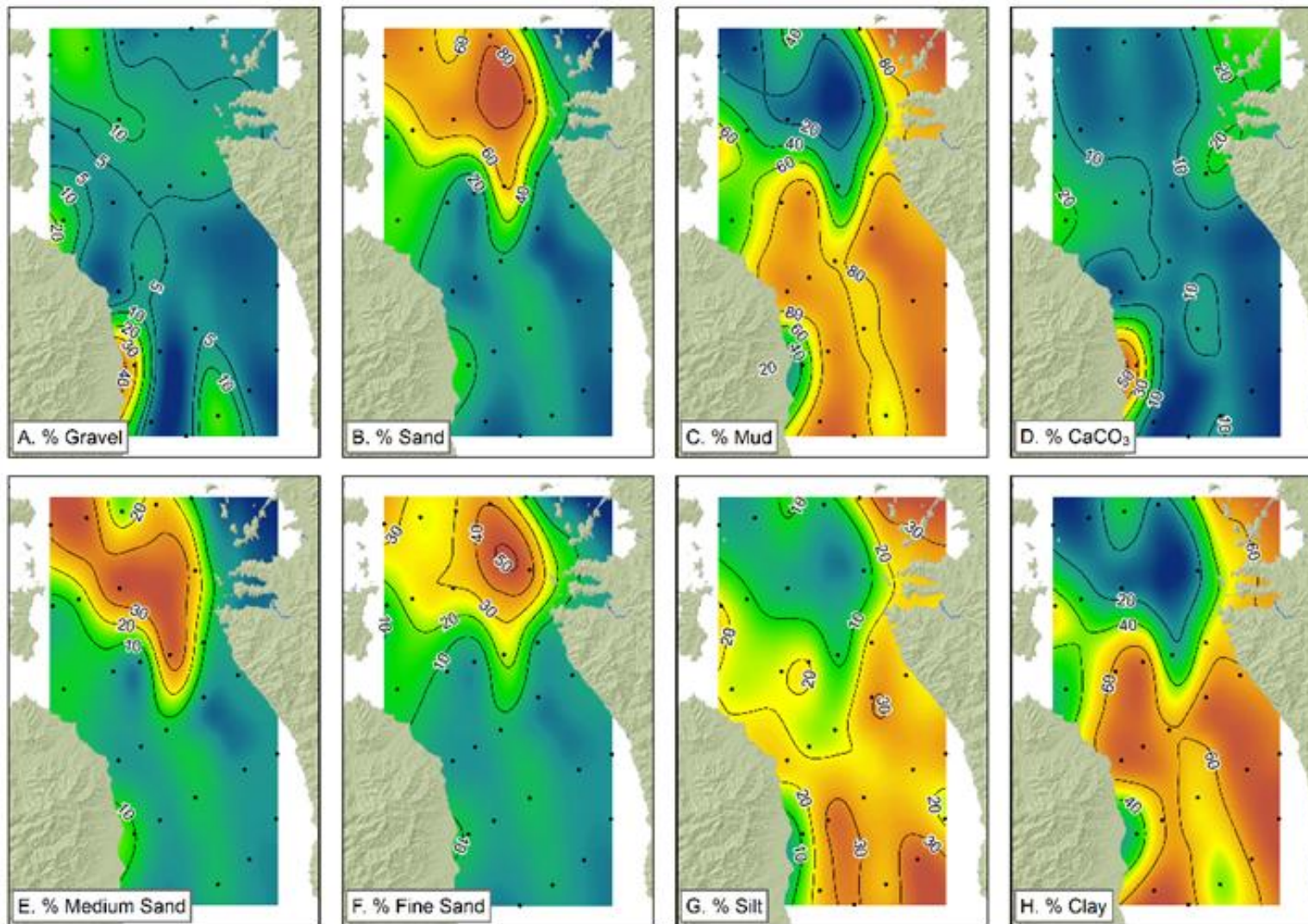
Figure 4-12: Surface sediment bulk physical properties sampled using the multi-corer on voyage SEA0201 (December 2002). Station locations shown by black dots. Colours indicate interpolated results. Refer to Figure 4-11 for site locations.

The inner Firth seabed comprises muddy sediments with a 60–70% contribution from clay-sized particles (<0.004 mm diameter). This zone of mud deposition extends out from the inner Firth to a latitude of ~36°52'S (between Ponui Island to Manaia Harbour) and off Coromandel Harbour to the northeast. Sandy sediments become dominant (>50% sand, <20% mud) further seaward, with a 60–70% sand component on the northernmost sampling transects in the extended Firth (SA and SB) comprising mostly fine to medium sands. This concurs with previous research (e.g., Carter and Eade, 1980; see Figure 4-13). The surface contouring to 80% sand in the central reaches of the extended Firth shown is an artefact of the gridded sampling strategy and the spline interpolation algorithm; the suggestion of high levels of sand in the surficial sediments in this area would need to be confirmed with additional sampling and should be treated with caution.
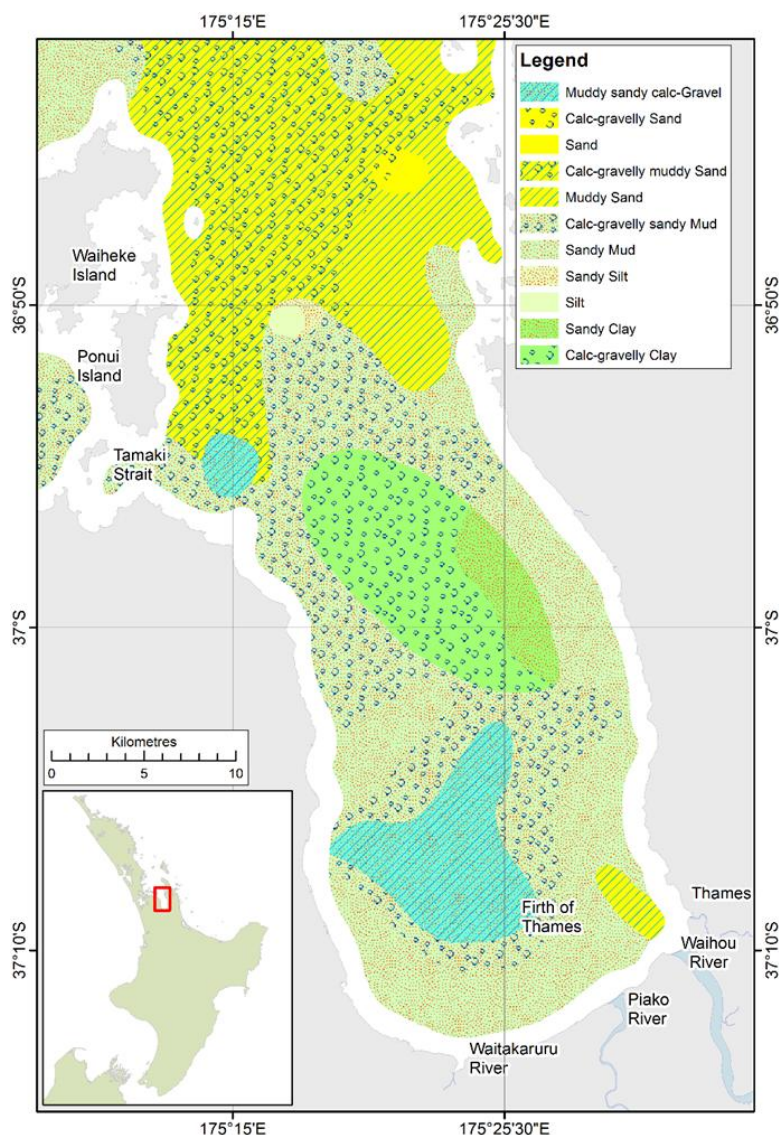

Figure 4-13:   Sediment map (from Carter and Eade, 1980). The subtidal sediments have been mapped previously by Carter and Eade (1980), who depict the surficial sediments as being predominantly sandy muds (<0.063 mm grain diameter) and clays, with a minor coarse carbonate gravel (>2 mm) component. An area of sandy muddy calcareous gravel is recognised by Carter and Eade (1980) in the southwestern Firth, but this interpretation is based on limited quantitative data. North of Coromandel Harbour, the sediments grade to muddy sands and carbonate sands (0.063–2 mm) with a pervasive calcareous gravel component (e.g., Smith and Nelson, 1994; Manighetti and Carter, 1999).

Localised patches of gravel-sized (>2 mm) sediment are also seen, with values of more than 15% gravel in the inner Firth (site SF3), on the southwestern margin of the central Firth (site SE1, ~30%) and in the western extended and northern Firth (sites SA2 and SC1). The spatial extent of these areas of coarse-grained sediment cannot be mapped with certainty due to their patchy and highly localised distribution, and would need to be corroborated with additional sampling for ground-truthing the acoustic seabed classification techniques, which are derived from more continuous side-scan sonar and multi-beam echo-sounder backscatter data and/or the application of QTC software on single-beam echo-sounder data (e.g., Eidem and Landmark, 2013). For example, during KAH1202, a coarse shell hash grading down to a poorly sorted calcareous-gravelly sandy mud was encountered in the surficial sediments at site FOT1 in the inner Firth in a water depth of ~7 m. Just ~6 km to the east and ~3 km to the south, fine-grained silty muds were encountered, which are more characteristic of the sediments in the southern end of the Firth (Figure 4-11, Figure 4-12).

The calcium carbonate content in inner-shelf sediments reflects the contributions from mineralogical sources and a myriad of potential *in situ* and allochthonous carbonate producers, including foraminifera (calcareous protozoa), bryozoans and molluscs (invertebrates), which are often associated with and/or constitute coarse-grained sediments in the Hauraki Gulf (e.g., Carter and Eade, 1980; Smith and Nelson, 1994; Manighetti and Carter, 1999). In the central reaches of the Firth and extended Firth, calcium carbonate percentages vary from <5% to 10%, with little evidence of a south-to-north gradient (Figure 4-12). Carbonate content increases to >20% moving into Tamaki Strait to the west and Coromandel Harbour to the east, with a very high value of 40% at a site dominated by coarse-grained gravelly sediments (site SE1) on the southwestern margin of the Firth (Figure 4-12).

The organic carbon (OC) content of surficial sediments exhibits a broad gradient from values of 1–2% in the south to lower values (<1%) in the north (Figure 4-14). There is a noticeable increase in OC along the western margin of the Firth (2.5–3.5%). A similar trend is observed for total organic matter (TOM), determined by loss-on-ignition, with high values of 10–12% in the southern Firth diminishing to 2–8% in the central Firth and extended Firth (Figure 4-14). However, one difference is that elevated TOM values of 14–16% also occur along the eastern margin of the Firth and there is a suggestion of values increasing north of the sampling domain (i.e., ~10% at two SA sites).

The distribution of total sediment nitrogen is more complex, including an area of higher concentration (>0.25%) in the central Firth and localised "hotspots" close to the Coromandel Peninsula and in Tamaki Strait (Figure 4-14). Otherwise total nitrogen concentrations are typically less than 0.2%.

The phosphorus content of the surficial sediments exhibits a decreasing trend from south to north, with values in the range of 0.4–0.5% in the inner Firth, grading to values of less than 0.2% in the extended Firth (Figure 4-14). Localised high values of 0.6–1.0% are found close to the entrance to Tamaki Strait, and on the eastern side off Coromandel Harbour.
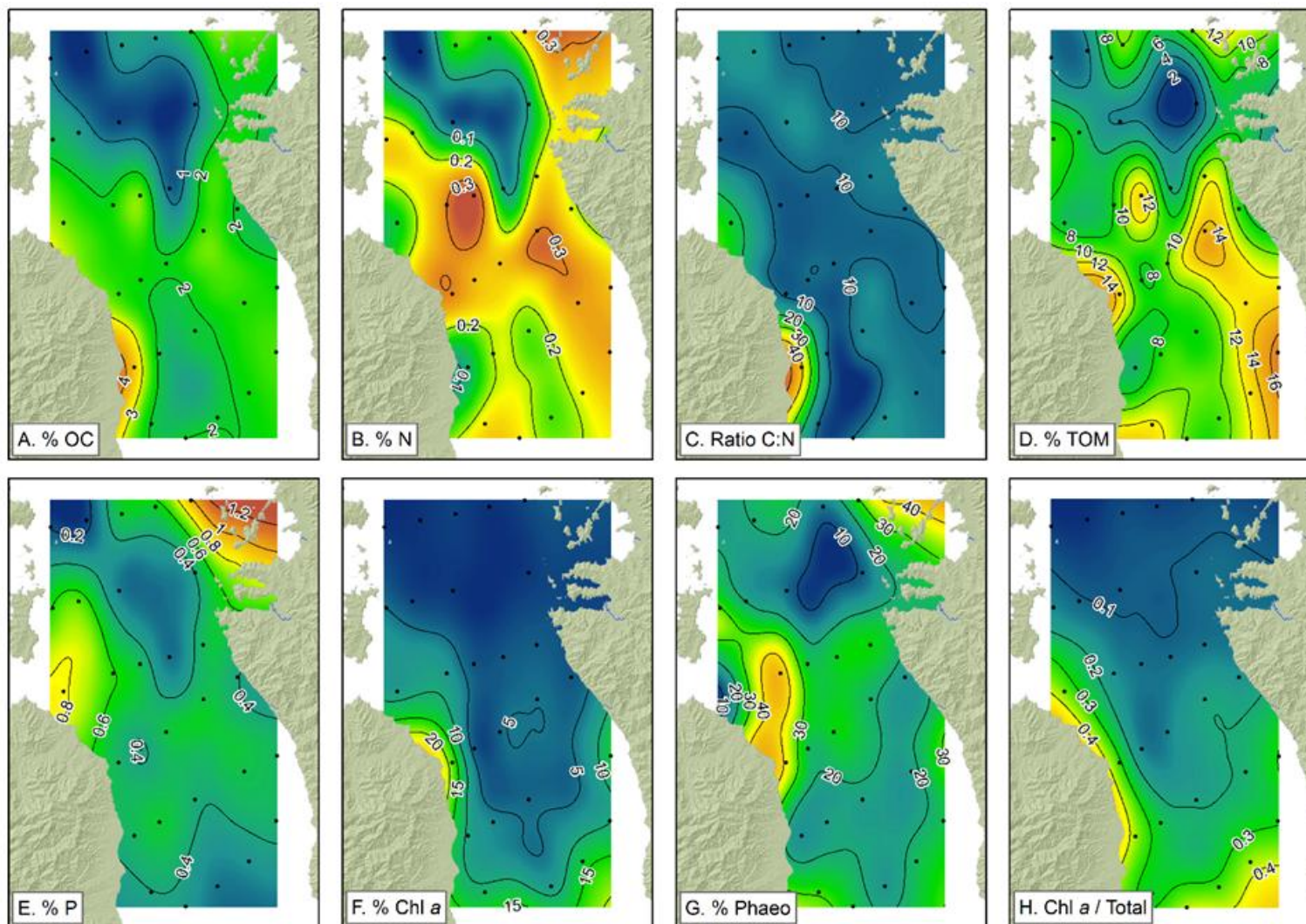
Figure 4-14: Surface sediment chemical and biological properties sampled using the multi-corer on voyage SEA0201 (December 2002). Station locations shown by black dots. Colours indicate interpolated results. Refer to Figure 4-11 for site locations.

The sediments approximately inshore of the 7-m isobath contain elevated levels of sediment chlorophyll *a*, with values typically more than 12 µg g^{-1} dry sediment, compared to values of less than 7–8 µg g^{-1} dry sediment in deeper water (Figure 4-14). Sediment phaeopigments, or degradation products of chlorophyll *a* (e.g., Vernet and Lorenzen, 1987), exhibit a less pronounced gradient with concentrations of between 10 and ~20 µg g^{-1} dry sediment throughout most of the system, except off the entrance to Tamaki Strait and Coromandel Harbour on opposite sides of the embayment where concentrations are 30–40 µg g^{-1} dry sediment (Figure 4-14).

Data collected during voyage KAH1202 suggest that organic carbon and chloro-phytopigments persist to moderately deep subsurface depths (at least 10 cm) in both the shelly and muddy sediments of the inner Firth and in the sandier sediments in the extended Firth off Coromandel Harbour (site SA3) (Figure 4-15). OC tends to remain at similar levels down-core, except for a peak at 4–7 cm sub-surface depth at the shelly FOT1 site that is also associated with anomalously high C:N ratios at the base of the upper shell hash layer (data not shown), suggesting that this peak is related to a layer of highly recalcitrant OC. In contrast, while the inner Firth site FOT1 has lower concentrations of sediment chlorophyll *a* than the other finer grained sites that were also sampled (i.e., FOT2, which is muddy, and FOT3, which is sandy), in all cases labile chloro-phytopigments decrease down-core to similar values of 1–3 µg g^{-1} at sub-bottom depths of about 8–9 cm (Figure 4-15). The one difference to note, however, is that at FOT1 the proportion of labile phytopigments in the near-surface sediments is almost twice that at the other sites, including the other inner Firth location FOT2 (see below).
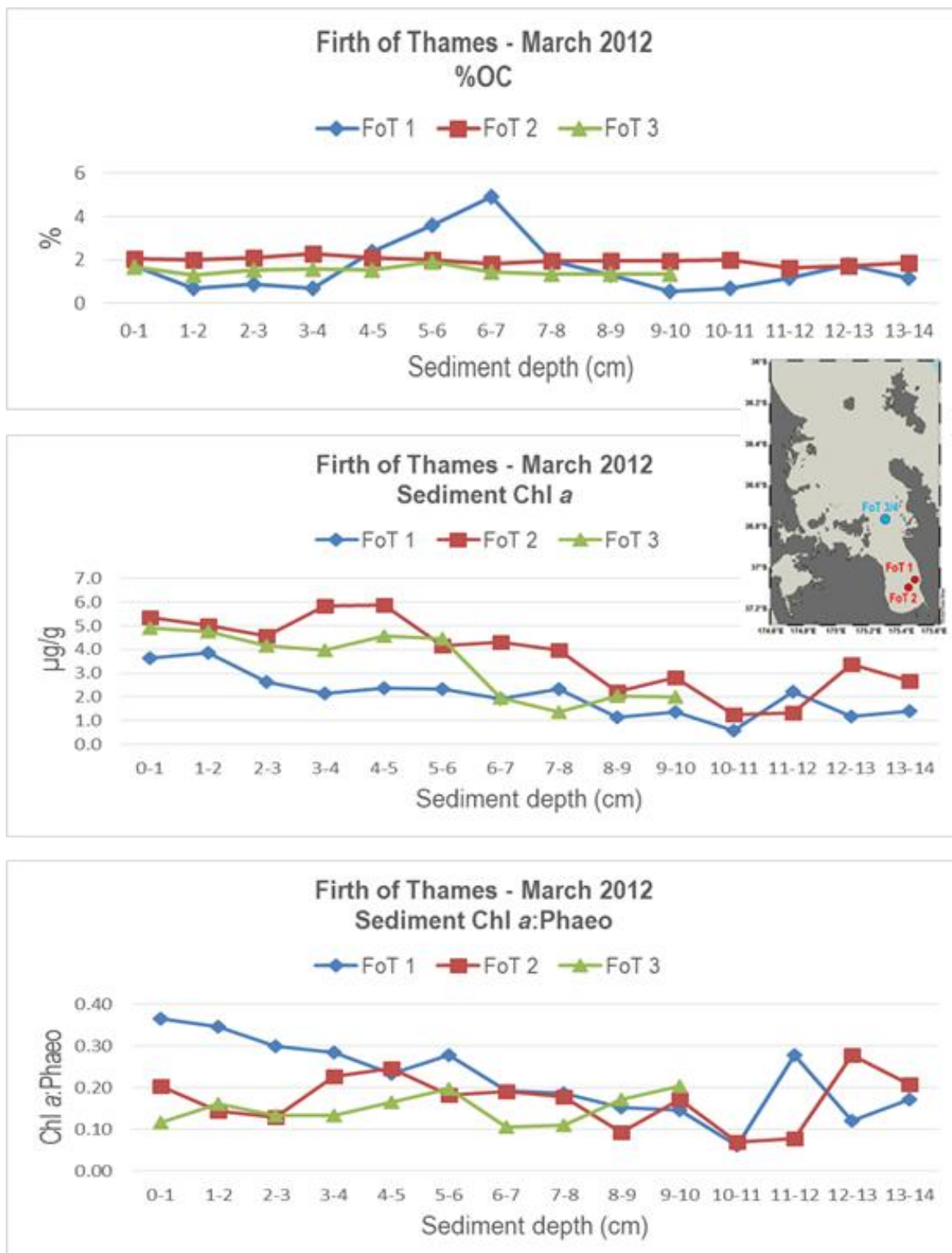
Figure 4-15:   Down-core variation in organic carbon and phyto-pigments collected at inner-Firth and extended-Firth subtidal locations (inset) on voyage KAH1202 (March 2012). Refer to inset and Figure 4-11 for site locations.Measures of organic matter lability provide a guide to the reactive nature of organic matter and the degree to which it has been degraded in the environment (e.g., Lancelot and Billen, 1985; Anderson and Sarmiento, 1994). Typically, marine primary producers, such as phytoplankton, exhibit average theoretical molar carbon to nitrogen (C:N) ratios of 6.6, known as the Redfield ratio (Redfield et al., 1963). Values above this ratio suggest varying degrees of degradation and

decomposition, related mainly to the preferential loss of nitrogen-based organic compounds such as proteins. In comparison, higher or vascular plants have C:N ratios greater than 20 (e.g., Meyers and Teranes, 2001). C:N ratios of mangrove detritus are in the range of 45–50, which decreases as carbon is lost and nitrogen becomes relatively enhanced during decomposition under estuarine conditions (Gladstone-Gallagher et al., 2014). Another measure of organic matter lability is the ratio of chlorophyll *a* to total chloro-phytopigments (chlorophyll *a* + phaeopigments), with high values suggesting greater amounts of "fresh" pigment contributions to the total phytopigment pool in the sediments.

The surficial sediments of the Firth have high molar C:N ratio values, all typically close to or greater than 10 (Figure 4-14). Very high outliers in C:N are observed at localities on the SC transect (westernmost site SC1, off Tamaki Strait, C:N ~20) and on the SE transect (southwestern site SE1, C:N ~40), suggesting highly refractory (degraded, low % N) organic matter sources at these locations. Both of these sites are also characterised by relatively elevated levels of calcareous gravelly sediments (Figure 4-12).

Chlorophyll *a*:total phytopigment ratios vary from 0.4 in the inner and western Firth, decreasing to less than 0.1 in the extended Firth (Figure 4-14).

4.8.4   Sediment accumulation rates

Sediment accumulation rates were measured at three subtidal sites (Figure 4-16). At SA3 in the extended Firth, the SAR was ~2.0 mm y^{-1}, similar to the value of ~2.2 mm y^{-1} determined from independent measurements undertaken on samples from the same site, as reported in Sikes et al. (2009). The SAR at SD3 (northern Firth) was slightly less at ~1.6 mm y^{-1}. SAR was not determined at SF5 (inner Firth) due to the deep surface-sediment mixed layer (~14 cm) (de Baere, 2006). Causes for the latter include bioturbation and physical processes (e.g., wave resuspension, tidal currents). In comparison, surface-sediment mixed layers were 3 cm and 4 cm at SA3 and SD3, respectively. These SAR values were higher than the SAR estimated at the shelf site (TAN9915 site 5, water depth of 125 m, 35° 48.83'S, 175° 1.83'E; SAR of ~0.9 mm y^{-1}), where a surface mixed layer ~2 cm was observed (de Baere, 2006).
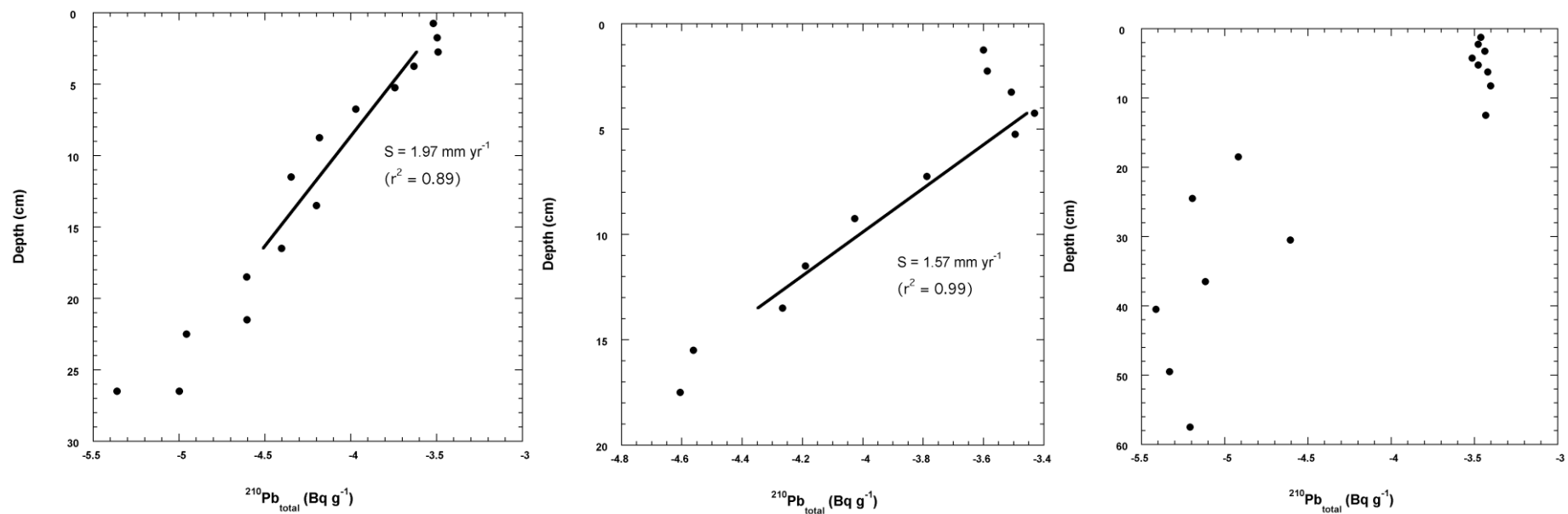
Figure 4-16: Radioisotope ^{210}Pb measurements in three cores. Left panel: site SA3. Centre panel: site SD3. Right panel: site SF2. (Figures from de Baere, 2006).Refer to Figure 4-11 for site locations.

New processing of radioisotope data from site SC3 was undertaken for the purposes of the present report. For site SC3, an SAR of 1.46 mm y^{-1} (r^2 = 0.97, n = 7) over 10–11 cm sediment depths is indicated by Figure 4-17 (Andrew Swales, NIWA, pers. comm.), which is consistent with similar radioisotope chronological information from other subtidal Firth sites (Figure 4-16). At SC3, no measurable surface mixed layer was observed. Combined, the data therefore indicate that subtidal SAR throughout the Firth and extended Firth is in the range of 1.5–2.0 mm y^{-1}.
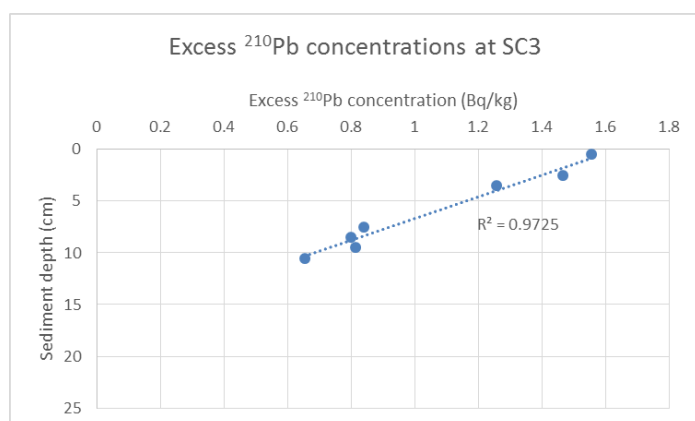
Figure 4-17: Radioisotope ^{210}Pb measurements from site SC3. Refer to Figure 4-11 for site location.

The subtidal sedimentation rates (1.5–2.0 mm y^{-1}) are up to an order of magnitude lower than those in fringing mangrove and intertidal areas of the inner Firth (ranging from 8–25 mm y^{-1} from 1920–1980 and reaching more than 25 mm y^{-1} immediately seaward of the mangrove forest since 1970). Pocknall et al. (1989) dated a series of cores from water depths greater than 30 m in the extended Firth that suggested sedimentation rates in the range 0.1–0.2 mm y^{-1} for the most recent Interglacial, marine muddy fine sands that overlie early Holocene Last Glacial peats and coastal sediments (11,900–14,000 calendar years BP).

Changes in pollen species with depth in shallow marine sediment cores can be used to infer changes in environmental and/or anthropogenic activities on the surrounding landscape (e.g., McGlone and Wilmhurst, 1999: Hope et al., 2004; Mildenhall and Orpin, 2010). In particular, transitions from times when forest cover was extensive on the landscape to partial or complete clearance and the establishment of agriculture can be recorded by pollen changes. The timing of variations in pollen can also be used as an independent measure to compare with sedimentation rates determined by other methods, such as radioisotope chronologies. Pollens contained in sediment cores collected at subtidal sites SF5, SD3, SC3 and SA3 on voyage KAH0310 (see Figure 4-11) indicate that at least the last 100 years of post-European habitation are recorded over sub-surface depths of 10–16 cm (D. Mildenhall, GNS Science, pers. comm., 2007). In the core from site SC3, the abundance of *Agathis* (kauri), a lack of grass and rare introduced pine pollen at 64–65 cm indicate an age immediately post-European occupation, as corroborated by the occurrence of known forest disturbance indicators such as *Coriaria* (tutu), *Pteridium* (bracken) and *Coprosma*. In contrast, the pollen assemblage in the deepest sample (57–58 cm) from the core at the shallowest site (SF2) suggests these deposits were formed in pre-European times (perhaps ~700 years ago), with a paucity of grass pollen and introduced pine pollen, and the presence of charcoal, the bryophyte family Anthocerotales (indicators of open, bare ground) and abundant bracken spores. Together, these data suggest subtidal sedimentation rates across the Firth in the range of 1–6.5 mm y^{-1}, which are comparable to the radioisotopic rates (1.5–2.0 mm y^{1}) determined for subtidal environments in the Firth.

4.8.5 Subtidal benthic infauna

Bacteria

In marine sediments, total phospholipid concentrations can be used as a proxy for bacterial biomass (Findlay et al., 1989), thereby negating the need for labour-intensive laboratory analyses using staining and enumeration (*cf*. Nodder et al., 2003; 2007). Unlike meiofauna and macrofauna biomass (see below) there appears to be a peak in total phospholipid concentration at site SD3 in the northern Firth. All sites host comparable concentrations (Figure 4-18), despite there being marked differences in the physical and biogeochemical sediment properties across these sites. As for meiofauna and macrofauna, the lowest average measurements of phospholipids were found at site SA3 in the extended Firth.
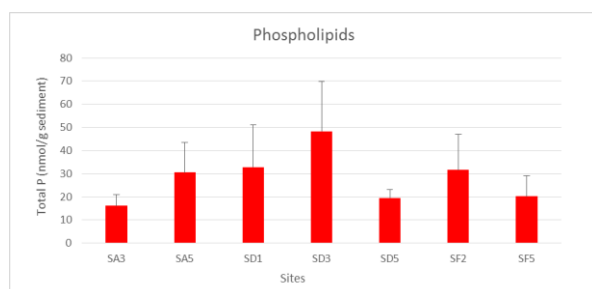

Figure 4-18:   Total phospholipid concentrations (average ± 1 standard deviation, *n* = 3) in surface sediments.
Sites SA3 and SA5 are in the extended Firth, SD1–SD5 are in the northern Firth and SF2 and SF5 are in the inner Firth. Refer to Figure 4-11 for exact site locations.

Meiofauna

Average meiofauna abundance is lowest at sites SA3, SF2 and SF5, with the highest abundances at the marginal sites in the northern Firth at SD1 and SD5 (Figure 4-19). On average (*n* = 2–3), nematodes dominate the meiofauna community (range 72–97% of total individuals across all sites), with the lowest proportions at the SF sites (72–80%) and SA sites (82–91%). Excluding nematodes, adult copepods are the next most abundant faunal group (25–60%), with bivalves being an important component of the community at the shallow SF sites (27–51%, *cf*. 1–17% at other sites). Annelids (1–25%, highest at the extended Firth sites), kinorhynchs (21%, with 38% at SD5) and ostracods (4–19%) are variously important across the system.
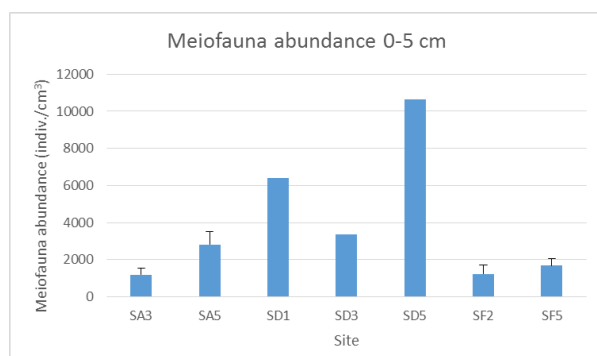

Figure 4-19:   Meiofauna abundance (average ± 1 standard deviation, *n* = 2–3) at 0–5 cm sediment depths.
Sites SA3 and SA5 are in the extended Firth, SD1–SD5 are in the northern Firth and SF2 and SF5 are in the inner Firth. Refer to Figure 4-11 for exact site locations.

Similar spatial trends in meiofauna (and macrofauna) biomass were observed during voyage KAH0310, with comparable values at the shallow inner (SF2, SF5) and deep extended-Firth (SA3, SA5) sites. There was consistently higher biomass at the northern-Firth sites (SD1, SD3, SD5), although this trend is not as apparent in the macrofauna biomass due to higher intra-site variability (Figure 4-20). A "margin" effect might explain these patterns, with higher average biomass at the sites nearer the terrestrial margin of the Firth (sites SD1 and SD5), although further testing is required to determine if this pattern does support the latter inference or that there is a local influence at some sites from the proximity to large mussel farms (Figure 4-11).

It is noted that there may also be reasonably high temporal variability in these samples since meiofauna biomass results from a muddy inner-Firth site sampled on voyage KAH1202, using the same analytical techniques, were an order of magnitude lower (inner FOT2: average 88.8 ± 57.2 µg 10 cm^{-2} *cf*. 650–670 ± 270-300 µg 10 cm^{-2} at SF2 and SF5), while comparable, if not higher, values were observed at the extended-Firth site SA03 (average 1865.0 ± 115.0 µg 10 cm^{-2} *cf*. 421 ± 97 µg 10 cm^{-2}). In fact, substantial small-scale spatial variability is present between inner-Firth sites. At inner-Firth site FOT1 on KAH1202, sample recovery was difficult due to the presence of a surficial very coarse shell hash, with polychaete worm tubes, in a sandy mud matrix. The meiofauna biomass over 0–5 cm sediment depths at this site was ~3420 µg 10 cm^{-2}, which was higher than the previously highest biomass measurements at the northern-Firth sites SD1 and SD5 of 1370 and 1200 µg 10 cm^{-2}, respectively (see Figure 4-11 for site locations). This estimate at the inner FOT1 site is almost two orders of magnitude higher than the biomass at the neighbouring inner FOT2 site (89 ± 57 µg 10 cm^{-2}), just 6 km to the east.
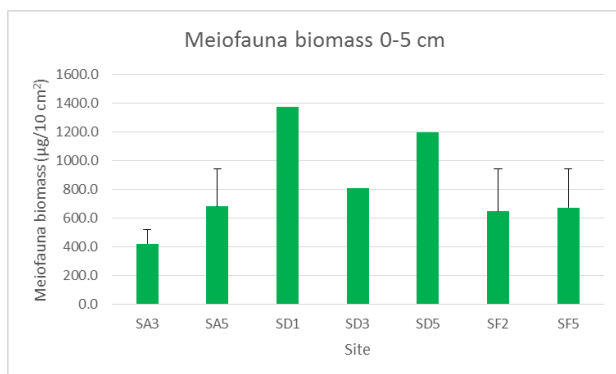

Figure 4-20:   Meiofauna biomass (average ± 1 standard deviation, *n* = 2–3) at 0–5 cm sediment depths. Sites SA3 and SA5 are in the extended Firth, SD1–SD5 are in the northern Firth and SF2 and SF5 are in the inner Firth. Refer to Figure 4-11 for exact site locations.

Macrofauna

As was the case for meiofaunal abundance, the macrofaunal community exhibited considerable intra- and inter-site variability, with replicate cores from sites often exhibiting very different proportions of animals comprising the community. At most sites, polychaetes were present and often dominant, with bivalves, amphipods, gastropods, ophiuroids and cumaceans occasionally dominating (up to 100%). For example, at extended-Firth site SA3 amphipoda and polychaetes constituted 100% of the macrofauna in each of two cores, with bivalves (92%) and polychaetes (8%) prominent in a third core from the same multi-corer deployment. In two other cores collected from the same site, but on another multi-corer deployment, polychaetes constituted 40–54% and amphipods 22–55%, with "unassigned' fauna 24% in one core and ophiuroids making up the remaining 5% in the second core.

However, if the polychaetes only are considered, then the lowest abundance of this faunal group occurs at site SF5, followed by the two sites on the SA transect and the other shallow site SF2 (Figure 4-21).
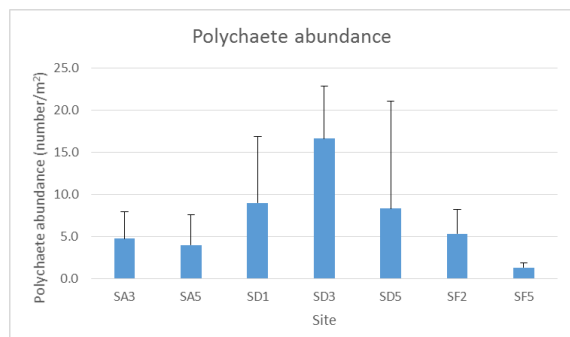

Figure 4-21:   Average polychaete abundance (±1 standard deviation, *n* > 2) in surface sediments. Sites SA3 and SA5 are in the extended Firth, SD1–SD5 are in the northern Firth and SF2 and SF5 are in the inner Firth. Refer to Figure 4-11 for exact site locations.

As was the case for meiofaunal biomass, macrofauna biomass from voyage KAH0310 was highest at sites located nearest the terrestrial margins of the Firth (SD1 and SD5), although the site nearest Coromandel Harbour (SA5) recorded the most variable, elevated biomass of all sites; conversely, this site corresponded to moderately low meiofaunal biomass (Figure 4-20). Lowest macrofaunal biomass was observed at the extended-Firth site SA3 and inner-Firth sites SF2 and SF5 (Figure 4-22). The high intra-site variability observed in macrofauna and meiofauna biomass, with single fauna often dominating individual core samples (up to 100%) from the same sites, reduce the ability to differentiate a broader spatial pattern.
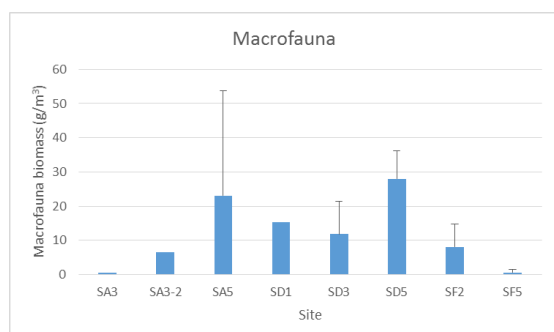

Figure 4-22:   Macrofauna wet weight biomass (average ± 1 standard deviation, *n* = 3) in surface sediments. Sites SA3 and SA5 are in the extended Firth, SD1–SD5 are in the northern Firth and SF2 and SF5 are in the inner Firth. Refer to Figure 4-11 for exact site locations.

Comments

There is limited information on subtidal benthic infaunal communities in the Firth of Thames, the extended Firth and the wider Hauraki Gulf, with the Firth and extended-Firth fauna sampled most widely on voyage KAH0310 (December 2003) at seven selected sites on transects SA, SD and SF (Figure 4-11). Only site SA3 has been sampled on several occasions since 1999; none of the other sites have been re-sampled for infauna. Meiofaunal data in the upper 5 cm collected from site SA3 during TAN9915 (December 1999) indicate average abundances of 3800 ± 1600 individuals per 10 cm^2, compared to 1200 ± 400 individuals per 10 cm^2 from KAH0310 (December 2003) and 10,400 ± 1700 individuals per 10 cm^2 observed during KAH1202 (January 2012). There are no comparable data

for macrofauna or bacteria abundance and biomass over the same time period (1999–2012) at site SA3 or from any other sites in the Firth .

In general, data from KAH0310 suggest that the benthic infauna communities of the inner Firth (i.e., sites on the SF transect) have similar abundance and biomass to those in the extended Firth (transect SA), with peaks in most parameters, except phospholipids (bacterial biomass), occurring either on the margins or across the northern Firth (transect SD). In addition, intra-site macrofauna abundance varies considerably, with consequent variability expected in biogeochemical and ecological functioning (e.g., Pratt et al., 2014a).

4.9   Satellite remote sensing of total suspended sediment

Remotely sensed data on total suspended sediment (TSS) concentration and distribution were acquired from NASA's MODIS-Aqua sensor and the NIWA X-band receiver.

Time series (Figure 4-23) show that TSS is concentrated within the inner Firth, before rapidly dropping to low levels seaward that are more typical of NZ's open-coastal waters. There is a weak seasonal pattern of increased TSS seaward extent in winter (i.e., during low seasonal sea-surface temperature), probably associated with greater winter river flows.
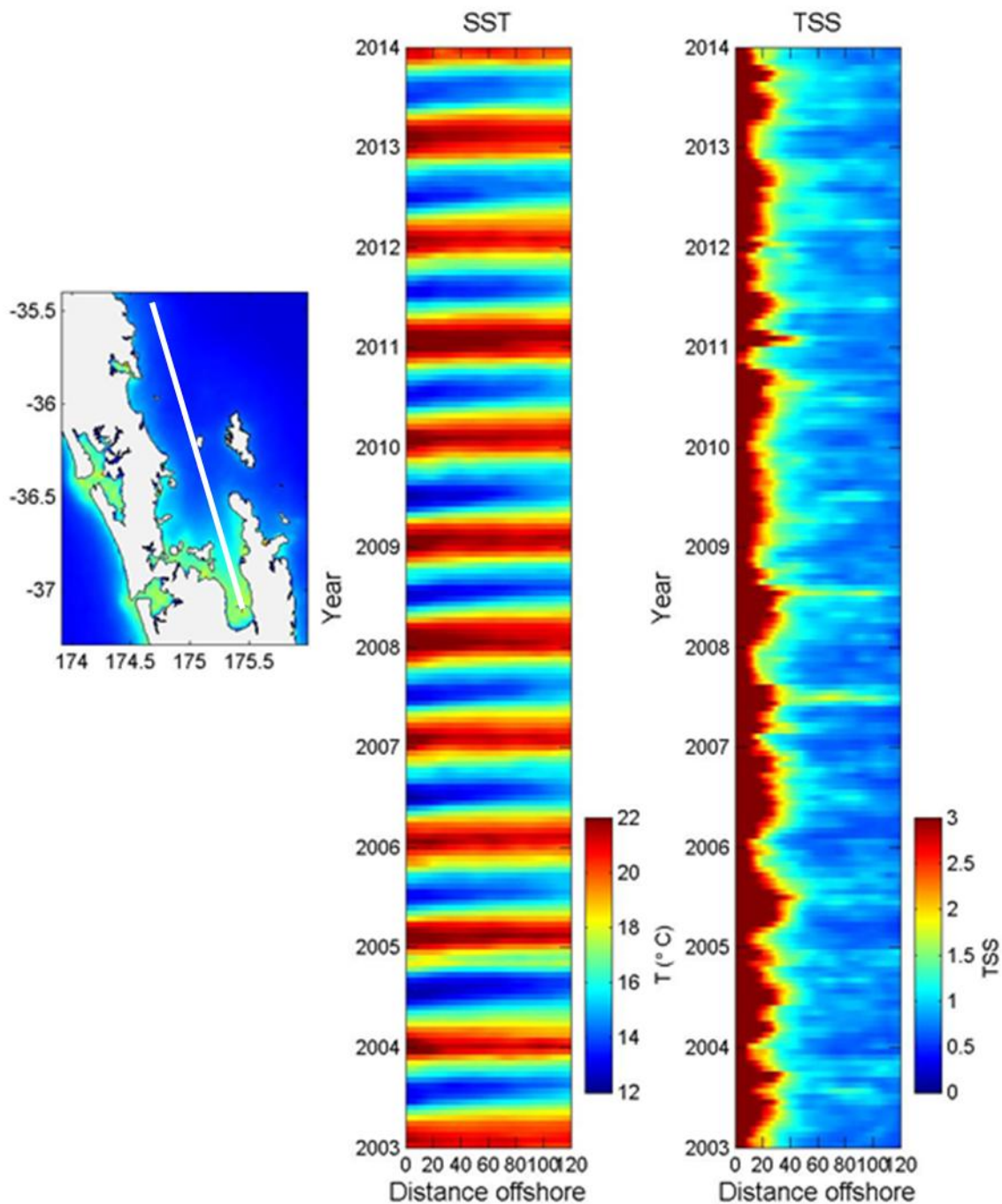
Figure 4-23: Time series of remotely sensed sea surface temperature (degrees C) and total suspended sediment (mg L^{-1}) from MODIS/Aqua satellite data. Data were composited into 3.5-km spatial bins and 15-day time bins before plotting in distance-by-time space along the indicated transect (inset), extending from the inner Firth of Thames to the inner continental shelf. The southern end of the transect is marked by a faint cross that indicates zero distance offshore. Values of SST and TSS are indicated by scales to the right of each plot.

Based on the comparison between satellite-derived and *in situ* measurements of TSS (Figure 4-24), we estimate that the satellite data are likely to be accurate to within about a factor of 2. The root-mean square log difference was 0.7374, which is equivalent to differences of a factor of 0.48 – 2.09. The mean log difference (ln[MODIS TSS] – ln[*in situ* TSS]) was -0.2530, indicating a mean underestimate of 22%. This analysis is likely to overestimate the uncertainty because the match-up

criteria allowed for potentially large changes in bio-optical conditions to have occurred between the *in situ* and satellite sampling (namely up to 10 days difference and coefficients of variation within the 3 extracted satellite data points of up to 50%).
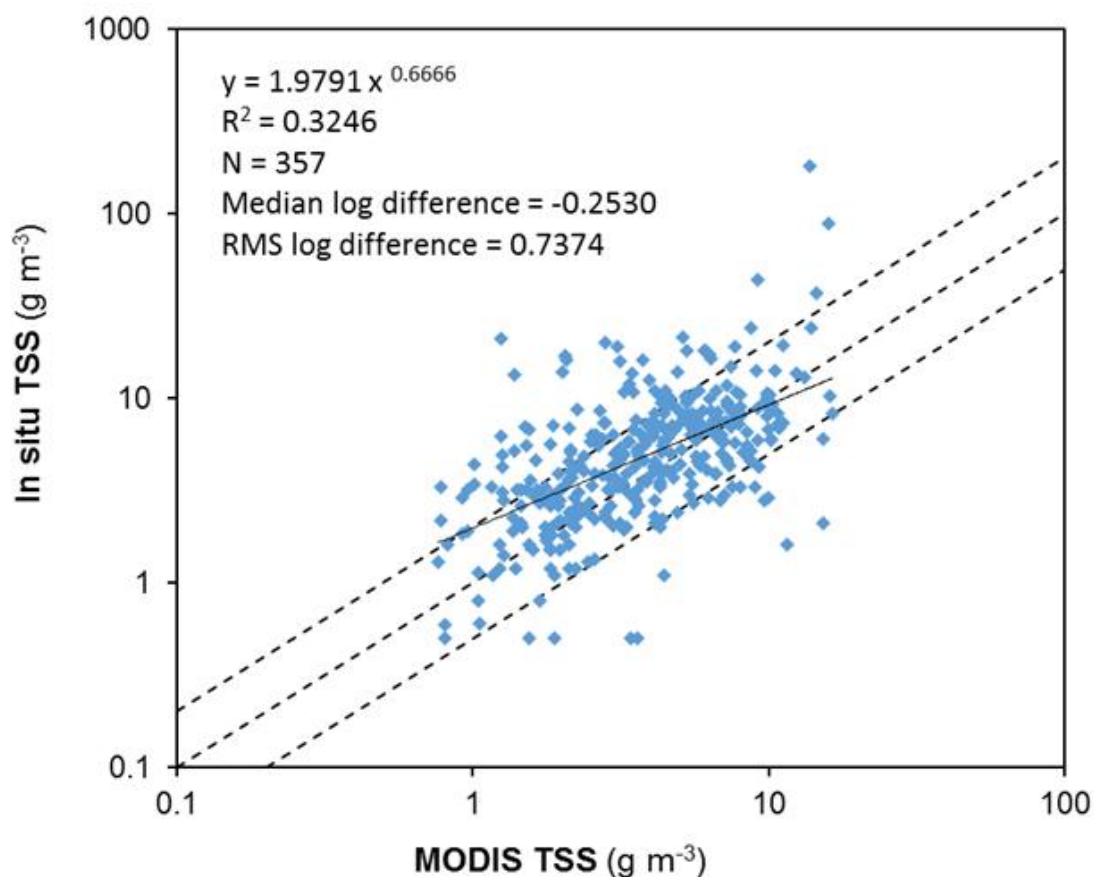

Figure 4-24. Testing algorithms for TSS against *in situ* data. *In situ* measurements of gravimetric total suspended sediment ("*in situ* TSS") (Wilson Bay monitoring data) and scaled particulate backscatter at 488 nm from the MODIS-Aqua quasi-analytic algorithm (BBP_{QAA}) (m^{-1}). The solid line is the least-squares *y*-on-*x* regression line, for which the equation and coefficient of determination (R^2) is shown (*N* = 357). The dashed lines show 1:1, 1:2 and 2:1 correspondence.

4.10   Sediment dispersal and deposition modelling

4.10.1 Overview and approach

To gain insight into the dispersal of freshwater and sediment discharged from river sources into the Firth of Thames, numerical modelling has been employed.

A near-field modelling approach was used, which focused on the relatively close vicinity (i.e., order of less than 10 km) of the major river mouths, describing in detail the deposition of sediment to the benthic environment in these areas. The near-field modelling used the Deltares Delft3d hydrodynamic, SWAN wave and sediment-transport modelling suite.

The main aim of the Deltares modelling was to determine the potential sediment deposition foot-print associated with sediment discharged from specific rivers during a flood event.

4.10.2 Deltares model

The Deltares model was driven at the ocean open boundaries by the tide, a wind stress from a specific direction, and an idealised time series of freshwater discharge and sediment flux from specific river sources into the model. The details of the model set up and implementation are given in Appendix B; the overall approach, results and interpretations are presented below.

Note that the sediment-transport module of the Deltares modelling suite has not been calibrated. Had the model been calibrated, the results would be more reliable. It is not possible to quantify precisely the extra reliability to be expected from calibration.

In addition to tidal forcing at the ocean boundaries, a wind stress was added to some of the scenarios to mimic the passage of a weather system. An increase in wind stress can potentially drive surface transport of a combined brackish water and sediment-laden plume, and it can also generate local wind waves. Wind waves in shallow water have the potential to resuspend previously deposited seabed sediments.

Some simplifying assumptions were made:

- There are no deposits of sediment on the bed at the start of the simulation.

- Sediments have a single class size of 20 μm (fine silt).

- Freshwater and suspended sediment discharge are limited to three separate sources in the inner Firth: the Waihou, Kauaeranga and Piako Rivers. Freshwater and sediment source inputs are based on historical hydrological records. Of course, in reality, the discharge of all rivers that drain to the Firth (and Gulf) will be elevated during typical rainstorms.

- The sediment deposition footprint results are presently separately for sediment from each single source.

- The wind speeds and directions are: 0 km h^{-1} (i.e., calm) 40 km h^{-1} from the SW, 40 km h^{-1} from the NE. As explained in Appendix B, these are calm conditions or no wind, the prevailing southwest (SW) wind and a northeast (NE) wind. The SW wind mimics the influence of oceanic weather systems propagating northward from lower latitudes, and the NE wind mimics the passage of tropical lows southward from the equator.

- There is no surface heat flux at the ocean surface; all variations in salinity through the model domain are driven by the freshwater discharge and mixing.

- Salinity and temperature flux at the open ocean boundaries are set at constant values.

- Ocean boundary conditions are driven only by the astronomical tide.

- Wind waves are locally generated and the predicted wave field does not take into account ocean swell.

- Simulations are terminated 15 days after the peak of the discharge event.

The number of scenarios is limited to the 11 simulations shown in Table 4-6. The "event" is an approximate 6-month ARI (annual return interval) rainstorm and the "large event" is an approximate 1-year ARI (annual return interval) rainstorm.

Table 4-6:   Event conditions for the 11 model simulations.

Source	Calm	SW	NE
Waihou River (Event)	x	x	x
Waihou River (Large Event)		x	x
Piako River (Event)	x	x	x
Kauaeranga River (Event)	x	x	x

The results from the model simulations are presented as a series of regional maps (Figure 4-25 to Figure 4-28) showing both the maximum SSC (mg L^{-1}) that occurred during the simulation and the final sediment deposition footprint (mm deposited) predicted by the simulation.

The fact that the sediment-transport model is uncalibrated, the simplifying assumptions, and the limited number of scenarios modelled, mean that the modelling results should be treated as "indicative" only.
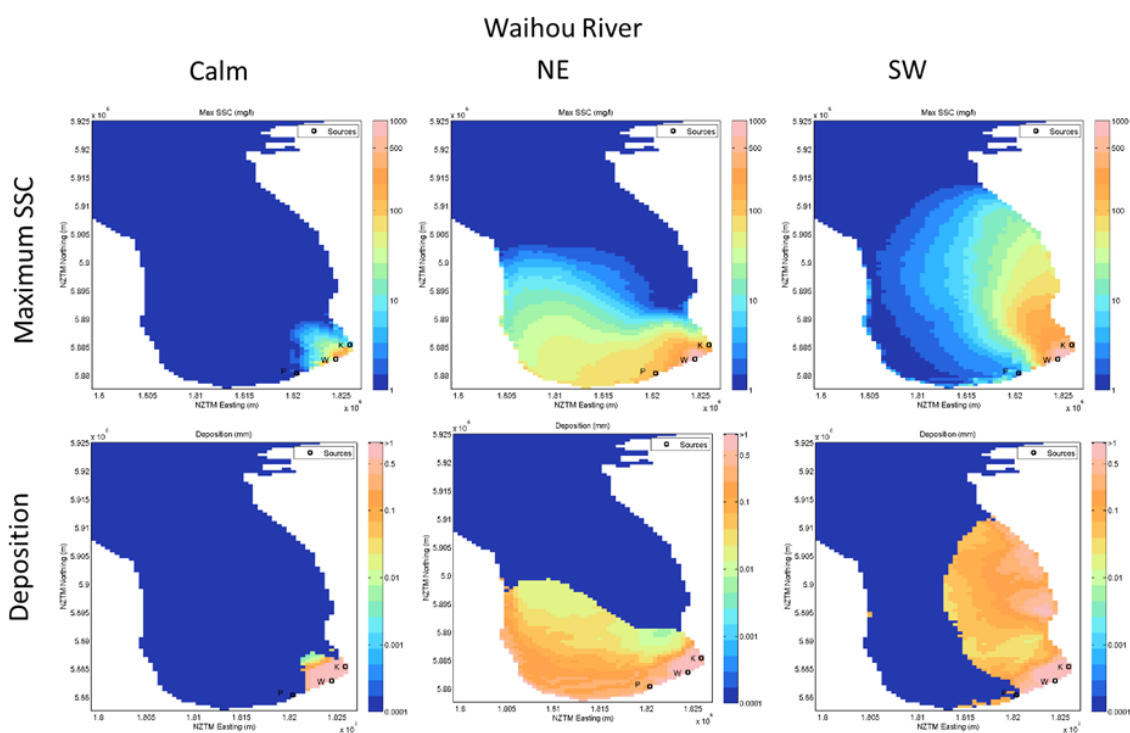

Figure 4-25:   Maximum SSC (mg L^{-1}) and sediment deposition footprint (mm) extracted from the model for 3 wind conditions for the "event" (i.e., approximate 6-month ARI rainstorm) discharge from the Waihou River (W).
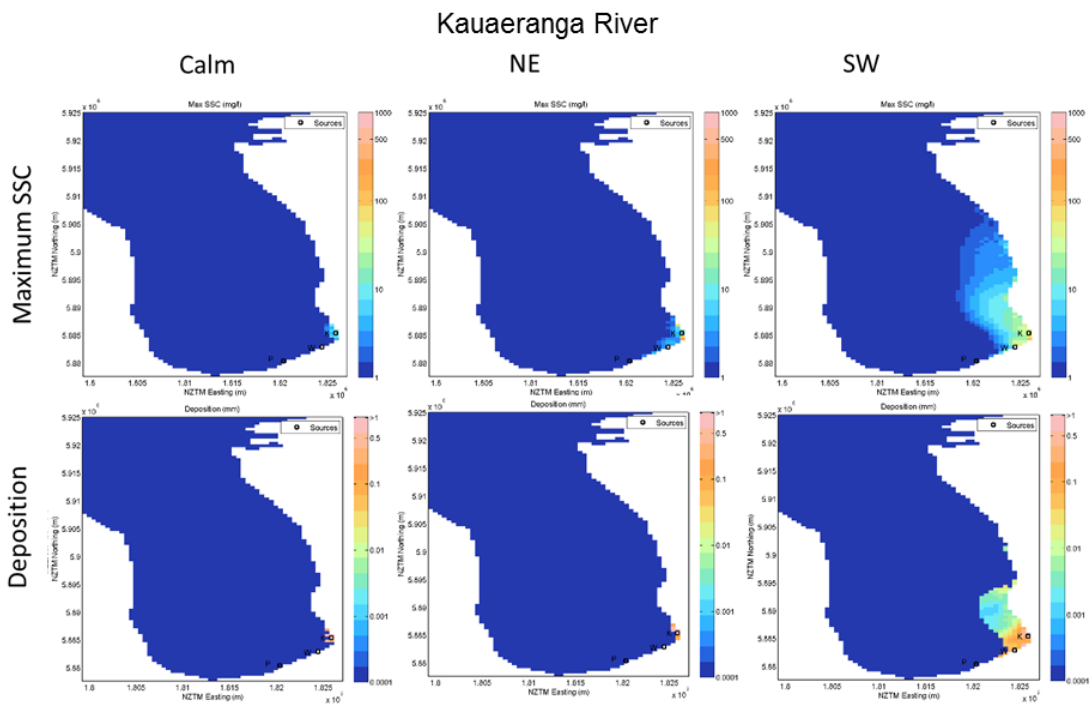
Figure 4-26: Maximum SSC (mg L^{-1}) and sediment deposition footprint (mm) extracted from the model for 3 wind conditions for the "event" (i.e., approximate 6-month ARI rainstorm) discharge from the Kauaeranga River (K).
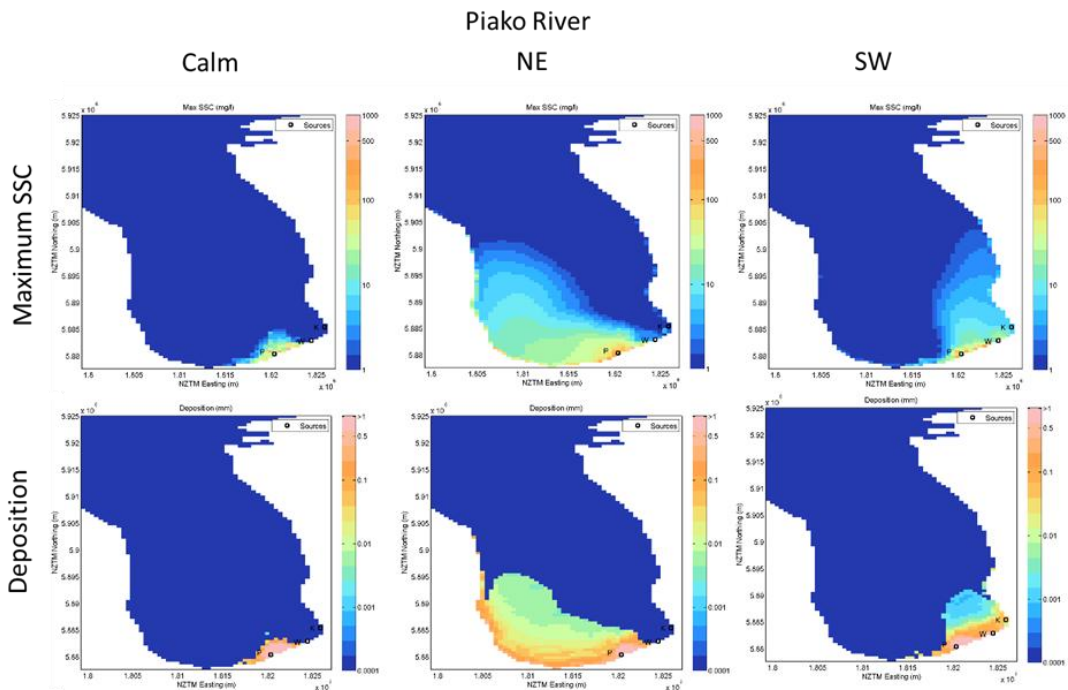

Figure 4-27: Maximum SSC (mg L^{-1}) and sediment deposition footprint (mm) extracted from the model for 3 wind conditions for the "event" (i.e., approximate 6-month ARI rainstorm) discharge from the Piako River (P).
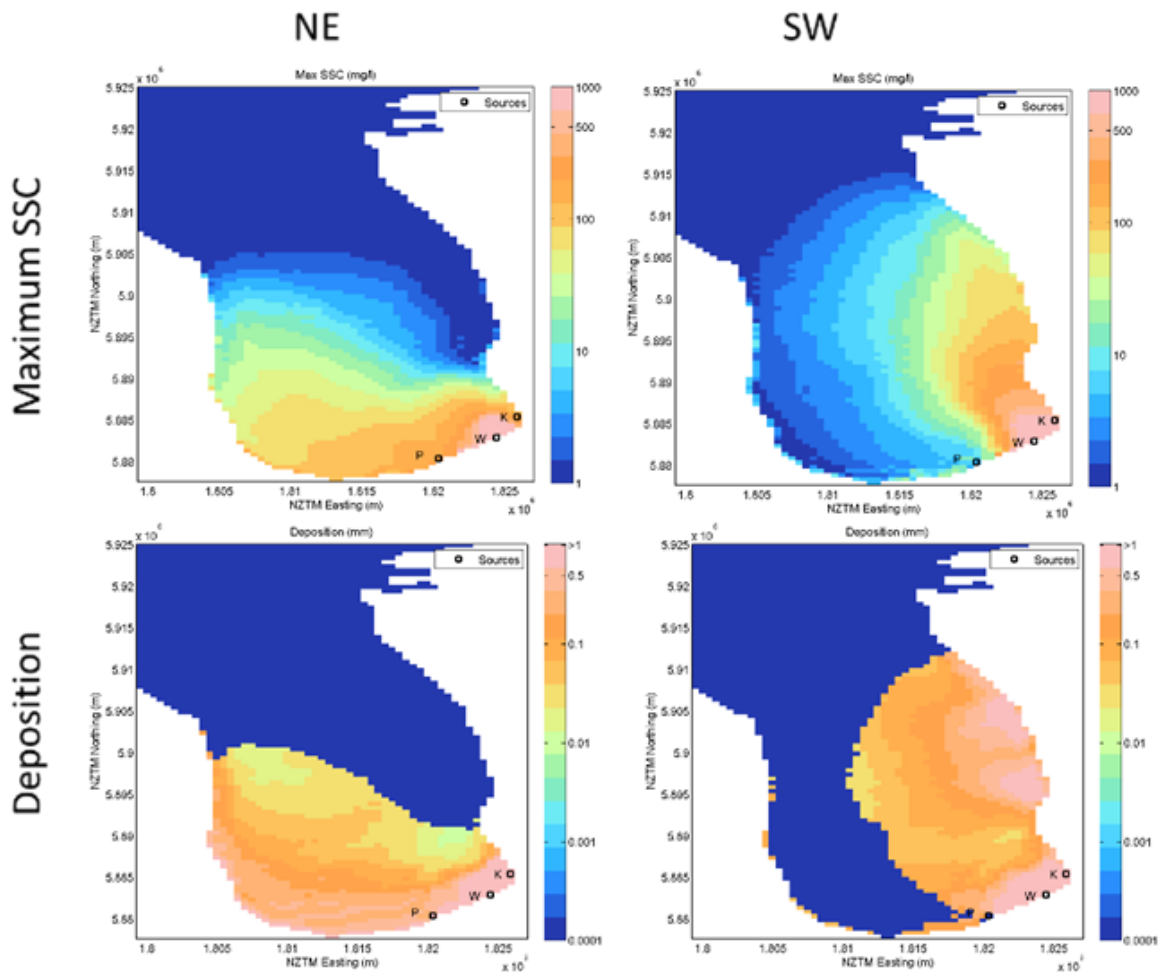
Figure 4-28: Maximum SSC (mg L^{-1}) and sediment deposition footprint (mm) extracted from the model for 3 wind conditions for "large event" (i.e., approximate 1-year ARI rainstorm) discharge from the Waihou River (W).

Generally, both the maximum SSC and the bed deposition after a flood event are scaled in relation to the size of the sediment/freshwater source. Consequently, the largest sediment footprint is associated with inflow from the Waihou River, followed by the Piako and the Kauaeranga Rivers.

The simulations predict that under calm conditions, all three rivers deposit sediment in the lower region of the Firth close to their respective mouths, where the freshwater discharge decelerates and particles drop out of suspension. Consequently, deposition lobes form intertidal flats outside the river mouths, either side of a deeper main subtidal channel. The present model grid resolution of 500 m does not produce the exact geomorphological form (as seen, for example, in Google Earth) but the maps in Figure 4-25 to Figure 4-28 do show the predicted near-source deposition.

The introduction of a surface wind stress increases the lateral dispersion of the river plume. A NE wind stress forces the plume up against south and southwest coasts of the Firth and, accordingly, most of the suspended sediment is deposited in this region.

A SW wind stress drives the river plume down-wind from the sources, and the highest SSC and levels of deposition in those conditions are found along the eastern shore of the Firth adjacent to the

Coromandel Peninsula. However, the model indicates that even the 1-year ARI discharge from the Waihou River, combined with a SW wind stress, results in very little sediment escapes to the extended Firth or the wider Hauraki Gulf. Suspended-sediment concentrations greater than 5–10 mg L^{-1} (the lowest concentration that it is practical to measure) do not extend beyond the northern entrance to the Firth.

This Delft3d model of the Hauraki Gulf suggests that fine sediments discharged by the three rivers under scrutiny are unlikely to be transported out of the inner Firth in large quantities. Simulations suggest that under calm conditions most of the sediment is deposited near the respective source; under SW winds sediment is deposited north of Thames alongside the Coromandel Peninsula; and during a NE wind, sediment is deposited on the southern and southwestern shore of the Firth.

4.11   References

Anderson, L.A., Sarmiento, J.L. (1994) Redfield ratios of remineralization determined by nutrient data analysis. *Global Biogeochemical Cycles*, 8: 65–80.

Augustinus, P.G.E.F. (1980) Actual development of the chenier coast of Suriname (South America). *Sedimentary Geology,* 26: 91–113.

Beaglehole, J.C. (1968) The journals of Captain James Cook on the voyages of discovery. *The voyage of Endeavour 1768–1771*. Cambridge University Press.

Brownell, B. (2004) *Muddy feet: Firth of Thames RAMSAR-site update 2004*. Ecoquest Education Foundation, Pokeno, New Zealand: 198.

Carter, L., Eade, J.V. (1980) Hauraki sediments. *New Zealand Oceanographic Institute (now NIWA) Chart, Coastal Series*, 1: 200 000.

de Baere, B.J.M. (2006) Silica diagenesis in New Zealand and Antarctic continental shelf sea sediments. *Unpublished MSc dissertation,* School of Ocean and Earth Science, Faculty of Science, University of Southampton, United Kingdom, 103 pp.

Eidem, E.J., Landmark, K. (2013) Acoustic seabed classification using QTC IMPACT on single-beam echo sounder data from the Norwegian Channel, northern North Sea. *Continental Shelf Research,* 68: 1–14.

Findlay, R.H., King, G.M., Watling, L. (1989) Efficacy of phospholipid analysis in determining microbial biomass in sediments. *Applied and Environmental Microbiology*, 55(11): 2888–2893.

Giles, H., Pilditch, C.A., Nodder, S.D., Zeldis, J., Currie, K. (2007) Benthic oxygen fluxes and sediment properties on the northeastern New Zealand continental shelf. *Continental Shelf Research,* 27 (18): 2373–2388, doi:10.1016/j.csr.2007.06.007.

Gladstone-Gallagher, R.V., Lundquist, C.J., Pilditch, C.A. (2014) Mangrove (*Avicennia marina* subsp. *australasica*) litter production and decomposition in a temperate estuary. *New Zealand Journal of Marine and Freshwater Research*, 48(1): 24–37, DOI:10.1080/00288330.2013.827124.

Hicks, D.M., Shankar, U., McKerchar, A., Basher, L.R., Lynn, I, Page, M., Jessen, M. (2011) Sediment yield from New Zealand Rivers. *Journal of Hydrology (NZ),* 50(1): 81–142.

Hope, G., Kershaw, A.P., van der Kaars, S., Xiangjun, S., Liew, P-M., Heusser, L.E., Takahara, H., McGlone, M., Miyoshi, N., Moss, P.T. (2004) History of vegetation and habitat change in the Austral-Asian region. *Quaternary International,* 118–119: 103–126.

Lancelot, C., Billen, G. (1985) Carbon-nitrogen relationships in nutrient metabolism of coastal marine ecosystems. In: Jannasch, H.W., Williams. P.J.leB., (Eds.) *Advances in Aquatic Microbiology,* 3. Academic Press, 263–321.

Manighetti, B., Carter, L. (1999) Across-shelf sediment dispersal, Hauraki Gulf, New Zealand. *Marine Geology,* 160: 271–300.

McGlone, M.S., Wilmshurst, J.M. (1999) Dating initial Maori environmental impact in New Zealand. *Quaternary International*, 59: 5–16.

Mehta, A.J. (2002) Mud-shore dynamics and controls p 19–60. In: Healy, T., Yang, J.-A. Healy (eds). *Muddy coasts of the world: processes, deposits and function*.

Meyers, P.A., Teranes, J.L. (2001) 9. Sediment organic matter. In: Last, W.M., Smol, J.P. (eds.), *Tracking Environmental Change Using Lake Sediments*. Volume 2: Physical and Geochemical Methods. Kluwer Academic Publishers, Dordrecht, The Netherlands: 239–269.

Mildenhall, D.C., Orpin, A.R. (2010) Terrestrial palynology from marine cores as an indicator of environmental change for the Waipaoa Sedimentary System and north-eastern New Zealand. *Marine Geology*, 270: 227–234.

Morrisey, D.J., Swales, A., Dittmann, S., Morrison, M.A., Lovelock, C.E., Beard, C. M. (2010) Ecology and Management of Temperate Mangroves. *Oceanography and Marine Biology: an Annual Review,* 48: 43–160.

Nodder, S.D., Duineveld, G.C.A., Pilditch, C.A., Sutton, P.J., Probert, P.K., Lavaleye, M.S.S., Witbaard, R., Chang, F.H., Hall, J.A., Richardson, K.M. (2007) Focusing of phytodetritus deposition beneath a deep-ocean front, Chatham Rise, New Zealand. *Limnology and Oceanography*, *52*: 299–314.

Nodder, S.D., Pilditch, C.A., Probert, P.K., Hall, J.A. (2003) Variability in benthic biomass and activity beneath the Subtropical Front, Chatham Rise, SW Pacific Ocean. *Deep-Sea Research I*, 50(8): 959–985.

Pocknall, D.T., Gregory, M.R., Greig, D.A. (1989) Palynology of core 80/20 and its implications for understanding Holocene sea level changes in the Firth of Thames, New Zealand. *Journal of the Royal Society of New Zealand* 19(2): 171–179.

Redfield, A.C., Ketchum, B.H., Richards F.A. (1963) The influence of organisms on the composition of sea-water. In: *The Sea, Volume 2*, M.N. Hill, editor, Interscience Publishers, John Wiley & Sons, 26–77.

Sikes, E.L., Uhle, M.E., Nodder, S.D., Howard M.E. (2009) Sources of organic matter in a coastal marine environment: Evidence from n-alkanes and their ◻13C distributions in the Hauraki Gulf, New Zealand. *Marine Chemistry*, 113: 149–163, doi:10.1016/j.marchem.2008.12.003.

Smith, A.M., Nelson, C.S. (1994) Calcification rates of rapidly colonising bryozoans in Hauraki Gulf, northern New Zealand. *New Zealand Journal of Marine and Freshwater Research*, 28(2): 227–234.

Sommerfield, C.K., Nittrouer, C.A., Alexander, C.R. (1999) [7]Be as a tracer of flood sedimentation on the Northern California margin. *Continental Shelf Research,* 19: 335–361.

Swales, A., Bell, R.G., Ovenden, R., Hart, C., Horrocks, M., Hermansphan, N., Smith, R.K. (2007) Mangrove-habitat expansion in the southern Firth of Thames: sedimentation processes and coastal-hazards mitigation. *Environment Waikato Technical Report,* 2008/13, www.ew.govt.nz/Publications/Coastal/.

Swales, A., Bentley, S.J., Lovelock, C., Bell, R.G. (2007b) Sediment processes and mangrove-habitat expansion on a rapidly-prograding muddy coast, New Zealand. Proceedings of the Sixth International Symposium on Coastal Engineering and Science of Coastal Sediment Processes (New Orleans, May 2007). *Coastal Sediments '07,* (Volume 2): 1441–1454.

Swales, A., Gibbs, M., Pritchard, M., Budd, R., Olsen, G., Ovenden, R., Costley, K., Hermanspahn, N., Griffiths, R. (2013) Whangarei Harbour sedimentation. Sediment accumulation rates and present-day sediment sources. *NIWA Client Report* HAM2013–143, prepared for Northland Regional Council.

Vernet, M., Lorenzen, C. J. (1987) The relative abundance of pheophorbide *a* and pheophytin *a* in temperate marine waters. *Limnology and Oceanography*, 32: 352–358.

Wells, J.T., Coleman, J.M. (1981) Physical processes and fine-grained sediment dynamics, coast of Surinam, South America. *Journal of Sedimentary Petrology,* 51: 1053–1068.

Yang, B.C., Dalrymple, R.W., Chun, S.S. (2005) Sedimentation on a wave-dominated, open-coast tidal flat, south-western Korea: summer tidal flat – winter shoreface. *Sedimentology,* 52: 235–252.

5 Nutrients

5.1 Overview of data sources

In this section we list sources of data presented in this chapter. Unless otherwise specified data were collected and are owned by NIWA.

- 15 years (1998–2013) of measurements every 3 months at the extended-Firth monitoring site. Measurements by CTD containing a rosette sampler lowered from a research vessel. Samples typically from 6 levels in the water column.

- Surveys of the Firth in spring, summer, autumn and winter of 2003 and also during 2012–13.

5.2 Data from the extended-Firth monitoring site

The figures in this chapter are all presented, in order, at the end of the chapter in order to facilitate reading of the text.

Nutrients have been measured at the extended-Firth monitoring site (Figure 5-1) seasonally (every 3 months) over the 15-year period 1998–2013. (Surveys were suspended during July 2001 to December 2002 when the research was transferred to Nelson Bays.) Samples were collected by a CTD containing a rosette sampler lowered from a research vessel. On each sampling occasion, samples were typically obtained from 6 levels in the water column.

Figure 5-1 shows plots of nutrient species.

Note that neither total nitrogen (TN) nor total phosphorus (TP) has been measured as single analytes. Measurement of particulate nitrogen, which could be summed with total dissolved nitrogen to give a measure of total nitrogen, only stated in 2008. We have not measured particulate phosphorus.

Time series of temperature, salinity and DIN at the extended-Firth monitoring site are shown in Figure 5-2.

The 15-year measurements of the different nutrient species reveal that dissolved inorganic nitrogen (DIN; the sum of nitrate and ammonium) is often most abundant in the upper water column during winter and early spring (indicated by times when temperatures are low: Figure 5-2A). The most likely reason is that uptake of DIN by primary production is limited by low light at those times. In summer and autumn, when there is plenty of light and seasonal production is well-developed, DIN in the upper water column is reduced because of uptake by primary production.

5.3 Trend analyses

The measurements of nutrients over the 15-year (1998–2013) period at the extended-Firth monitoring site (Figure 5-1) were analysed for trends using the non-parametric seasonal Kendall trend test (Jowett, 2004). The seasonal Kendall trend test tests for a monotonic trend in data. It is a nonparametric test, meaning that data are not required to be normally distributed for the test to be valid. "Monotonic" means the data consistently increase or decrease over time. Any trend may or may not be linear. "Seasonality" implies that the data are differently distributed in different seasons. A "season" may or may not be a season in the normally understood sense; for example, three 8-hour periods in a day may constitute different seasons.

Nutrient concentrations integrated over the water column were subjected to the trend test, calculated as:

$$I = \frac{\sum_{i=1}^{n-1} \Delta Z_{i,i+1} 0.5(B_i + B_{i+1})}{\sum_{i=1}^{n-1} \Delta Z_{i,i+1}}$$

where I denotes a sample level number (incrementing from 1 at the sea surface), B_i denotes concentration at sample level I, and $\Delta Z_{i,i+1}$ is the thickness (m) of the layer between sequential sampling depths.

The results are shown in **Error! Reference source not found.**, and the Kendall trends are plotted gainst the data in Figure 5-3. The estimate of the percentage annual change is statistically significant at the 95% confidence level if $p < 0.05$.

Table 5-1: **Non-parametric seasonal Kendall tests for time trends in water-column-integrated nutrient concentrations (mmole m^{-2}) and ratios.** Data from the extended-Firth monitoring site, October 1998 to July 2013. Data are grouped by season (seasons used were: Sep – Nov, Dec – Feb, Mar – May, Jun – Aug for spring, summer, autumn and winter, respectively).

Nutrient variable	Sample size	Median value	p	Median slope (annual)	5 % confidence limit for slope	95 % confidence limit for slope	Percent annual change
DIN	57	43.3	0.01	2.22	0.78	3.26	5.14
NO$_3$- N	57	24.7	0.10	0.83	-0.1	1.91	3.37
NH$_4$ -N	57	18.6	0.03	0.85	0.11	1.45	4.55
DIP	57	14.6	0.69	-0.1	-0.31	0.17	-0.68
DIN/DIP	57	3.1	0.04	0.13	0.05	0.24	4.15
DRSi	47	408.0	0.25	-8.69	-18.23	3.49	-2.13
DON	53	278.7	0.02	4.92	1.49	8.31	1.76
DOP	51	6.9	0.04	-0.38	-0.7	-0.08	-5.48

These results are for water-column-integrated data and therefore represent the entire inventory of each dissolved nutrient at the extended-Firth monitoring site through time.

The seasonal Kendall trend test of the water-column-integrated data is a first step towards identifying and understanding trends. The nutrient data exhibit significant vertical structure over the water column, that is, the water chemistry is markedly different between top and bottom water, which is lost by depth-integrating the data. For example, simple visual inspection of panel C in Figure 5-2 suggests that DIN has mostly changed in the water column at levels below about 20 m below the water surface. Furthermore, the change in DIN in the lower water column appears to have been driven by stronger "pulses" of DIN occurring later in the monitoring period. Specifically:

- There is a period between about 2007 and 2011 when DIN was greater in the lower water column compared to the years on either side of that period. That increase in DIN was not manifest as a steady higher concentration throughout the entire period: instead there were

intervals during that period when DIN was elevated. The intervals of elevated DIN appear to have been about 3–6 months in duration, and they appear to have occurred in the last half of each calendar year. There was no elevation in the calendar year 2007.

- Sometimes the elevated DIN in the lower water column seems to have "leaked into" the upper water column (e.g., 2006) and sometimes it does not (e.g., 2008).

This all suggests that there are complex drivers of the nutrient system, including potentially multiple different sources of DIN to the water column, with significant control on the system being exerted by the physical oceanography (specifically, the water-column stratification).

Analysis is required to verify these casual observations.

5.4   Survey data

Surveys of nutrients and chlorophyll *a* concentration which traversed the Firth in spring, summer, autumn and winter of 2003 and also during 2012–13 are shown in Figure 5-4. Seasonal rates of primary productivity averaged across the Firth from the 2003 data are also shown (note 'pp' values in Figure 5-4).

It is in winter, when production becomes strongly light-limited (Broekhuizen and Zeldis, 2007) and less nutrient-limited that the "conservative" spatial pattern of nutrient loading and concentration in the Firth is evident: inner Firth nitrate concentrations are high and decrease seaward.
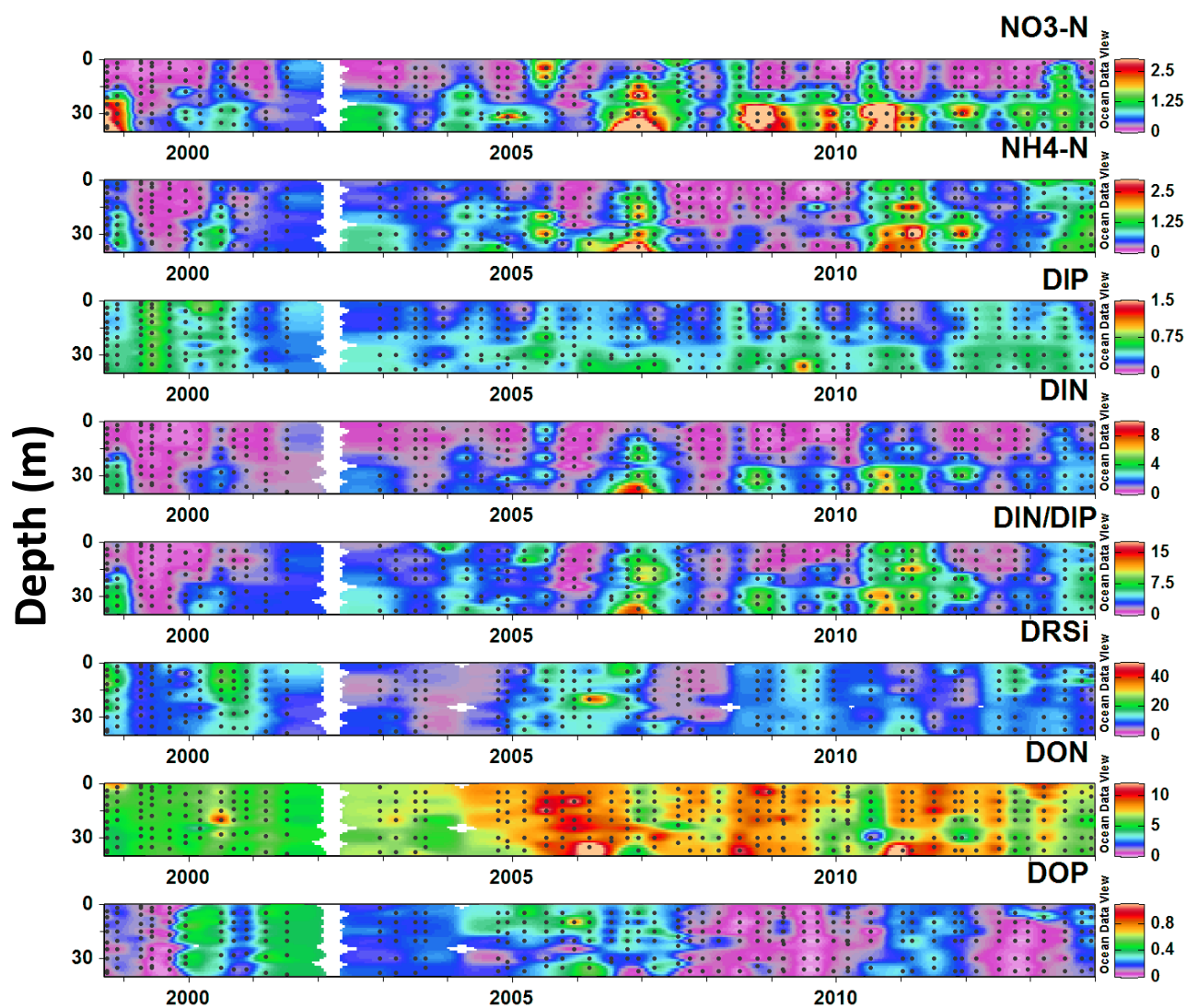
Figure 5-1: **Concentrations and ratios of nutrients plotted by depth and time at the extended-Firth monitoring site, 1998–2013.** Concentrations are in µmol L^{-1}. Ticks on the x-axis correspond to 1 January of each year.
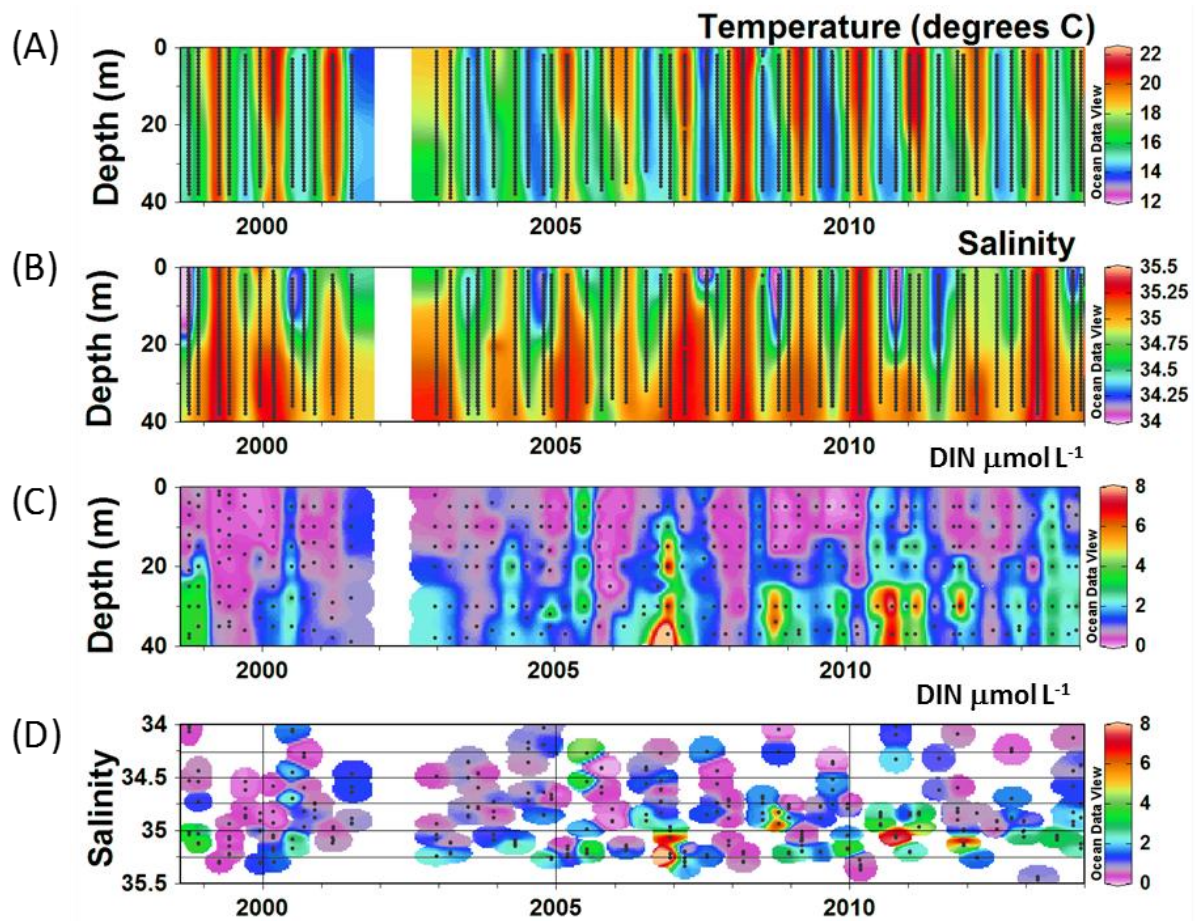
Figure 5-2: **Time series of (A) temperature with depth, (B) salinity with depth, (C) DIN with depth, (D) DIN with salinity at the extended-Firth monitoring site, 1998–2013.** Ticks on the x-axis correspond to 1 January of each year.
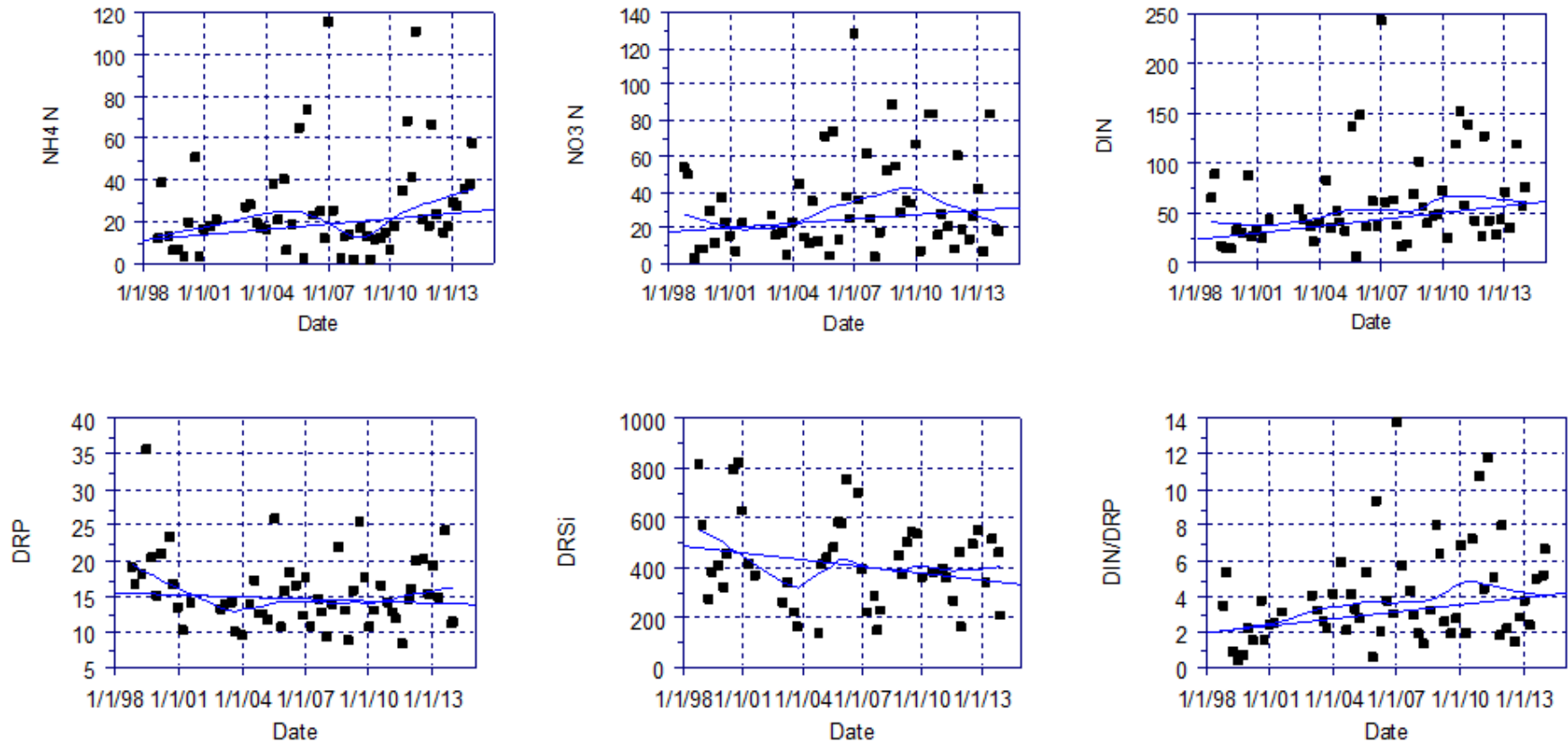
Figure 5-3: **Time series of water-column-integrated nutrient concentrations (units of mmole m^{-2}) at the extended-Firth monitoring site.** The blue curves show the fitted linear Kendall trend (the straight line) and a LOWESS moving average fit (the other line) that used 40% of the points in its fitting window.
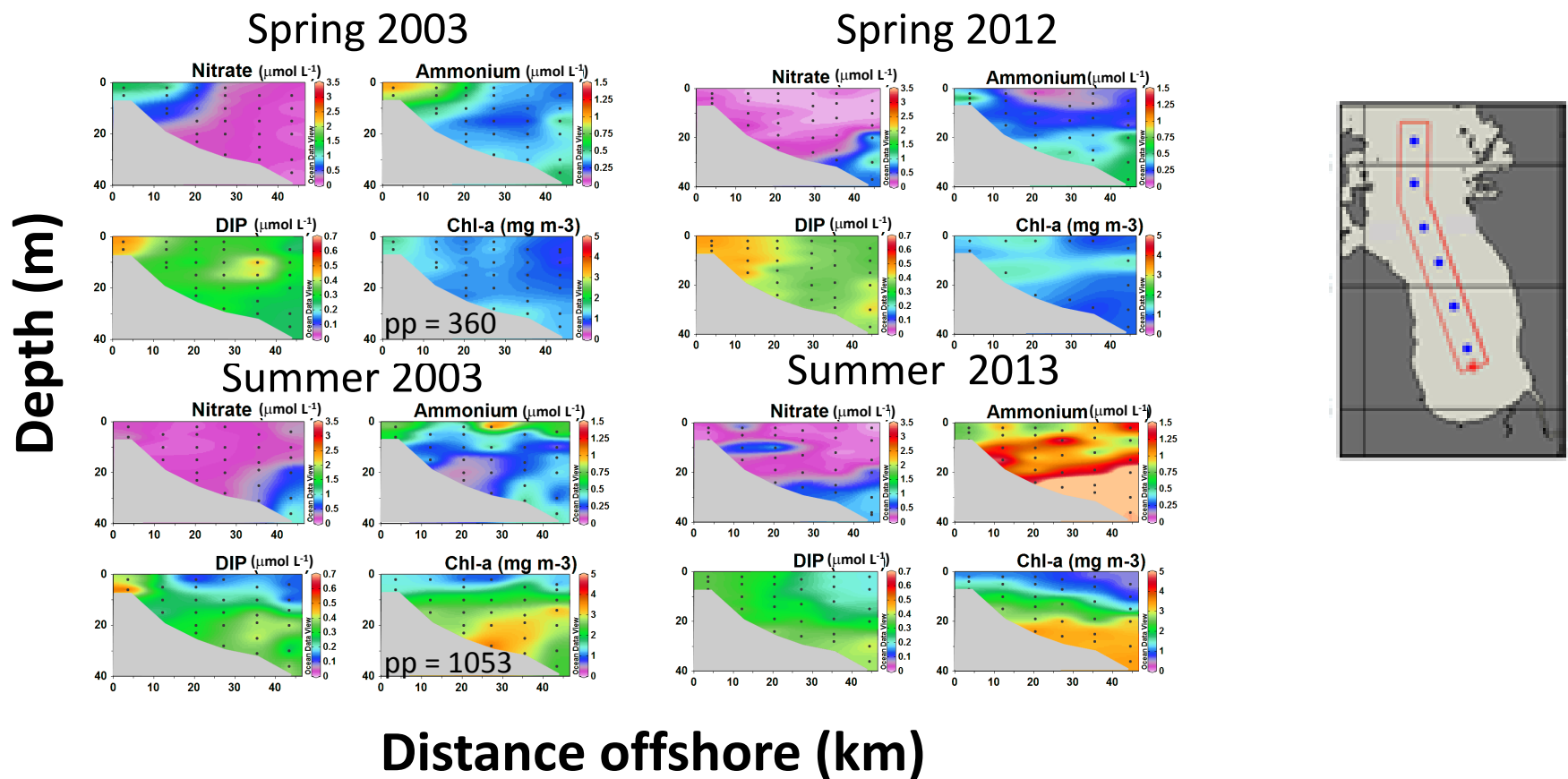
Figure 5-4: **Transects of nutrient and chlorophyll *a* concentration from the inner Firth to the extended Firth (inset), by depth and season during seasonal voyages made in 2003 and 2012–13.** Rates of primary production averaged across the Firth ('pp': mg C fixed m^{-2} d^{-1}) during the 2003 surveys are annotated on the 2003 chlorophyll *a* plots (see Figure 6-4). <u>**This page: spring and summer. Next page: autumn and winter.**</u>
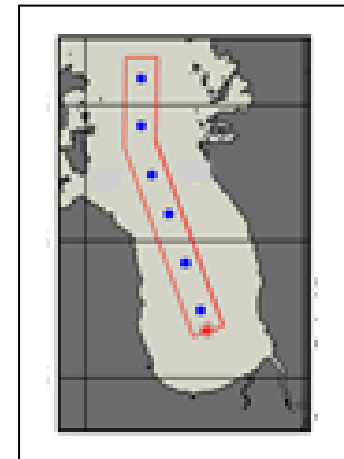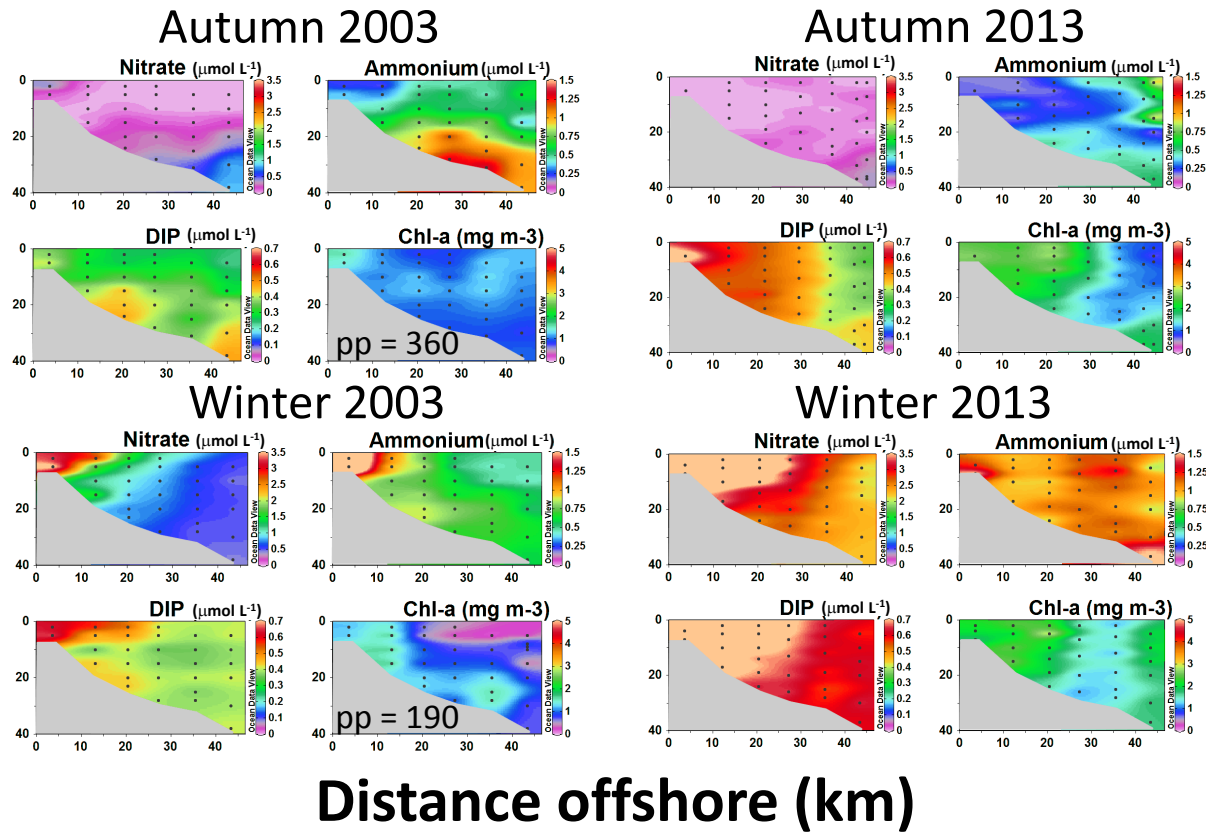
Figure continued from previous page. **This page**: autumn and winter. **Previous page**: spring and summer.

5.5   References

Jowett, I. (2014) Time Trends Software. http://www.jowettconsulting.co.nz/home/time-1

Broekhuizen, N., Zeldis, J. (2007) Forecasts of possible phytoplankton responses to elevated riverine nitrogen delivery into the southern Firth of Thames. *NIWA Client Report* HAM2005-131.

6 Phytoplankton and bacteria

6.1 Overview of data sources

In this section we list sources of data presented in this chapter. Unless otherwise specified data were collected and are owned by NIWA.

- Phytoplankton pigment (chlorophyll *a* and phaeopigment) has been measured and microphytoplankton cells (>2 μm cell size) have been collected at the extended-Firth monitoring site seasonally (every 3 months) over the 15-year period 1998–2013. Water samples for analysis by CTD containing a rosette sampler lowered from a research vessel. Samples typically from 6 levels in the water column. Picophytoplankton (<2 μm cell size) and bacteria cells have been collected at the extended-Firth monitoring site since December 2002

- Chlorophyll *a* samples at CTD sites in the greater Hauraki Gulf and Firth that have been occupied at various times, dating from 1996. This includes chlorophyll *a* measurements from a grid pattern of stations from the inner Firth to the extended Firth occupied in December (summer) 2002, March (autumn), July (winter), October (spring) and December (summer) 2003.

- Photosynthesis–irradiance determinations made onboard ship during primary-production experiments over 6 voyages from spring 1999 to summer 2000 at the extended-Firth monitoring site and at a site on the continental shelf.

- Data from two Integrating Natural Fluorometers (INFs) at the extended-Firth monitoring site. INFs positioned at 7 m and 20 m below the surface. Data were first collected in mid–2004, but most consistently after mid–2005.

- Chlorophyll *a* determined spatially using underway fluorometry during 4 seasonal voyages, 2012–13.

    o Spring – voyage KAH1209. Summer – voyage KAH1311. Autumn – voyage KAH1304. Winter – voyage KAH1306.

6.2 Data

6.2.1 Extended-Firth monitoring site

Phytoplankton pigment (chlorophyll *a* and phaeopigment) has been measured and microphytoplankton cells (>2 μm cell size) have been collected at the extended-Firth monitoring site (Figure 2-1) seasonally (every 3 months) over the 15-year period 1998–2013. (Surveys were suspended during July 2001 to December 2002 when the research was transferred to Nelson Bays.) Samples were collected by a CTD containing a rosette sampler lowered from a research vessel. On each sampling occasion, samples were typically obtained from 6 levels in the water column.

Picophytoplankton (<2 μm cell size) and bacteria cells have been collected at the extended-Firth monitoring site since December 2002.

Chlorophyll *a* and phaeopigment: Water (250 mL) was filtered through GFF filters (7 Hg vacuum) onboard the research vessel and the filters were immediately frozen in liquid nitrogen. In the laboratory, filters were acetone-extracted using the methods of Strathman (1967) and Strickland and

Parsons (1972) to determine total chlorophyll *a*, and then acidified and re-read to determine phaeopigment (degraded chlorophyll) concentrations by subtraction.

Micro- and nano-plankton: Unfiltered water samples (200 mL) were preserved in Lugol's Iodine solution (1% final concentration) onboard the research vessel. In the laboratory, samples were settled for >48 h before removing the supernatant and resettling in 10 mL Utermöhl chambers for at least 8 h. Phytoplankton >2 μm were identified and enumerated using a Leica DMI3000B inverted microscope at 100x to 600x magnification. Where possible, all abundant organisms were identified to genus and/or species level and then counted. The dimensions of taxa were measured and the biovolume estimated from approximated geometric shapes (spheres, cones, ellipsoids) following Rott (1981), Hillebrand et al. (1999) and Olenina et al. (2006). Phytoplankton biovolumes were then used to calculate cell carbon (mg C m^{-3}) using the conversion equations of Strathman (1967), Eppley et al., (1970) and Menden-Deuer and Lessard (2000) applied to different algal groups (diatoms, dinoflagellates and an 'others' category, which included silicoflagellates, raphidophytes, prymnesiophytes, cryptophyceae, chrysophyceae, euglenoids and monads).

Picophytoplankton and bacteria: Triplicate 1.8 mL water samples for picophytoplankton and bacteria were pre-filtered through 2.0 μm Nuclepore filters and immediately frozen in liquid nitrogen onboard the research vessel. In the laboratory, the abundances of eukaryotic and prokaryotic picophytoplankton (<2 μm) were measured using flow cytometry on a FACSCalibur instrument (Becton Dickinson, Mountain View, Cal.) reading natural fluorescence. Bacterial samples were stained with SYBRII stain (Molecular Probes Inc.) at a concentration of 10^{-4} of stock solution and incubated in the dark for 10–15 min before being analysed (Lebaron et al., 1998). Analysed volumes for all counts were calculated using Trucount^{TM} beads (Becton Dickinson, Mountain View, Cal.) as a tracer. Cell carbon for eukaryotic picophytoplankton was estimated from the literature then converted to biomass following Buitenhuis et al. (2012) for picophytoplankton and Fukuda et al. (1998) for bacteria.

6.2.2   Estimates of primary production

Chlorophyll *a* samples have been collected at CTD sites in the greater Hauraki Gulf and Firth that have been occupied at various times, dating from 1996. These data have been used to estimate primary production, as follows.

Depth-integrated primary production was determined using the approach of Behrenfeld and Falkowski (1997):

$$\sum PP = P^b{}_{opt} \times f[E_0] \times DL \times C_{avg} \times Z_{eu}$$

where the optimum chlorophyll-specific carbon fixation rate of the productivity profile, $P^b{}_{opt}$ (mg C mg chl^{-1} h^{-1}), is combined with a nonlinear irradiance dependent function ($f[E_0]$, dimensionless), day length (*DL*, h), average water-column chlorophyll *a* (*C$_{avg}$*) and euphotic zone depth (*Z$_{eu}$*) to calculate integrated production (ΣPP, mg C m^{-2} day^{-1}).

$P^b{}_{opt}$ data were obtained from photosynthesis–irradiance determinations made onboard ship during primary-production experiments over 6 voyages from spring 1999 to summer 2000 at the extended-Firth monitoring site and at a site on the continental shelf (Figure 6-1) (see Gall and Zeldis, 2011). *Z$_{eu}$* was taken as the depth where light fell to 1% of the surface value, determined using log–linear fitting of water-column measurements of the attenuation of photosynthetically active radiation. The parameter $f[E_0]$ was from Behrenfeld and Falkowski (1997).

Primary production was also estimated using data from a grid pattern of stations from the inner Firth to the extended Firth occupied in December (summer) 2002, March (autumn), July (winter), October (spring) and December (summer) 2003. In these surveys C_{avg} was the water-column average chlorophyll *a* determined over water-column profiles (*n* = 10 to 17 profiles per voyage; each profile with 2 to 6 chlorophyll *a* values, depending on bottom depth). The mean ΣPP value from the two summer voyages was averaged with the other seasonal values to calculate the annual mean ΣPP.

6.2.3   Chlorophyll from moored fluorometry

The mooring at the extended-Firth monitoring site carries two Integrating Natural Fluorometers (INFs), positioned at 7 m and 20 m below the surface (in the 40-m deep water column). These are serviced quarterly, when they are retrieved, downloaded and redeployed. Their optical sensors (photosynthetically active radiation [PAR] and solar-stimulated fluorescence [LuChl]) were kept clear of biofouling using an antifouling system. The ratios of PAR and LuChl were converted to chlorophyll *a* units using the methods of Yoshikawa and Furuya (2004) after processing with extracted chlorophyll *a*-specific absorption coefficients (a^*_{ph}) of phytoplankton sampled on each mooring servicing voyage. Data were first collected in mid–2004, but most consistently after mid–2005.

6.2.4   Chlorophyll from underway fluorometry

Chlorophyll *a* was determined spatially using underway fluorometry, which consisted of pumping near-surface water onto the ship and diverting it through an Ecotriplet fluorometer. This was done during the 4 seasonal voyages made during 2012–13 to monitor the carbonate system (see section 8.2).

6.3   Results

Figure 6-1 shows chlorophyll *a* data averaged from NIWA voyages made between 1996 and 2012. Phytoplankton biomass was concentrated in the inner Gulf coastal areas and was highest in the Firth.
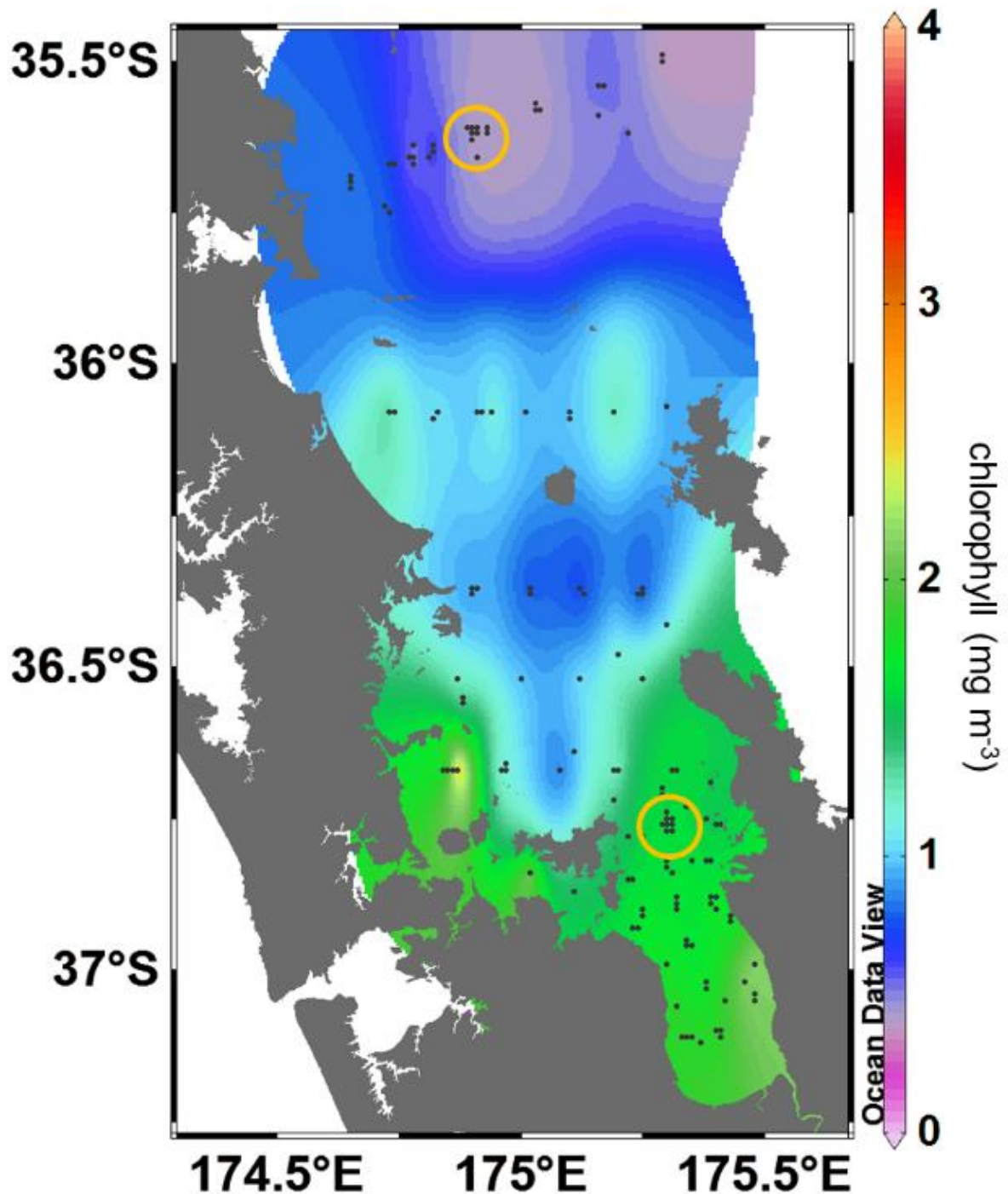
Figure 6-1: **Phytoplankton biomass in the greater Hauraki Gulf region.** Chlorophyll *a* data were averaged from NIWA voyages made between 1996 and 2012. Values are averages for all values in the upper 15 m of the water column, corresponding to the mixed layer depth over the region (Zeldis et al., 2004; authors' unpublished data), with sampling sites shown by black dots (Zeldis et al., 2013), many of which are overlaid. Orange rings show locations of the extended-Firth and shelf primary-production experiment sites occupied by Gall and Zeldis (2011).

Phytoplankton biomass varied seasonally, being generally greatest in spring and least in winter (Figure 6-2). Biomass was widely distributed in spring, but became progressively restricted to inshore

areas (especially the Firth) from summer through winter. In the extended Firth, biomass was greatest in the upper water column in spring, but increased noticeably at depth in autumn.
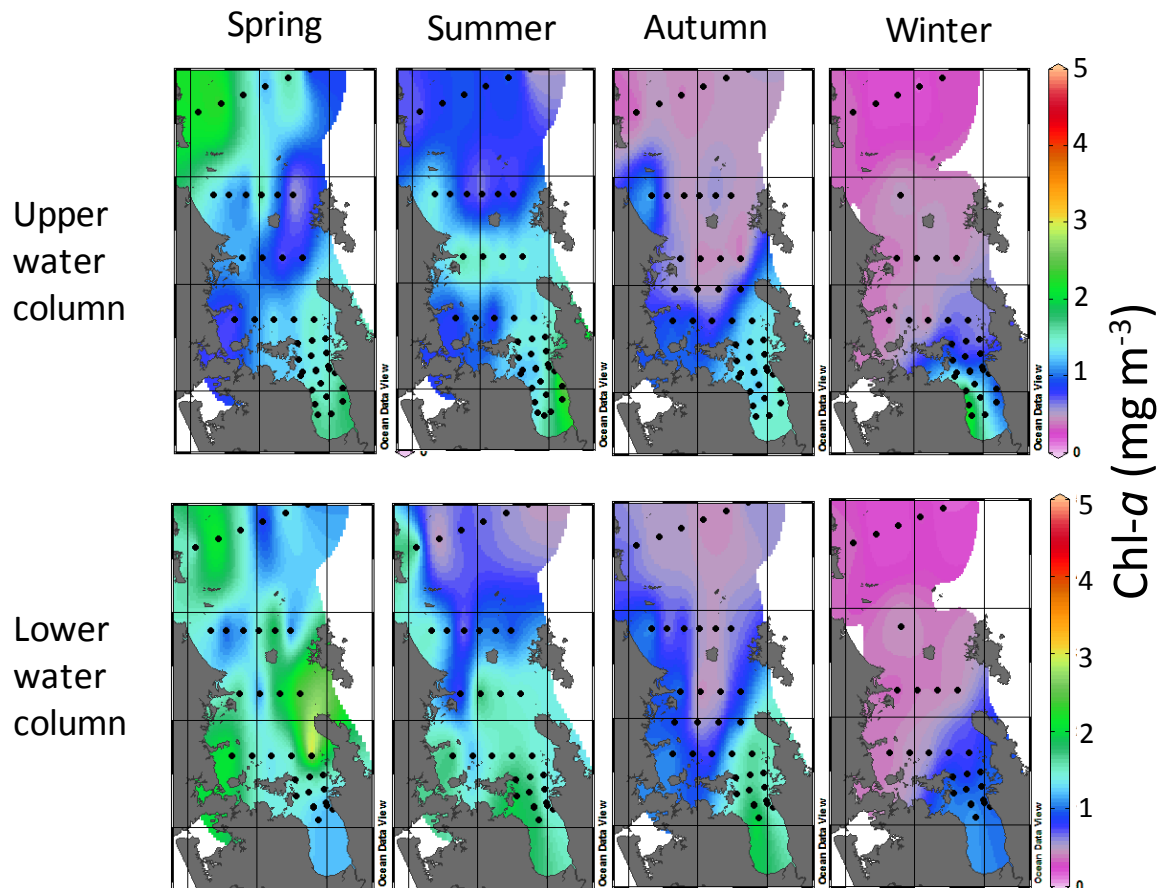

Figure 6-2:   Seasonal phytoplankton distributions in the greater Hauraki Gulf region in spring, summer autumn and winter. Chlorophyll *a* data were compiled from NIWA voyages made between 1996 and 2012. Values are averages for the upper water column (upper 15 m of the water column) and the lower water column (16–50 m), with sampling sites shown by black dots (Zeldis et al., 2013). Note that the inner Firth is shallower than 15 m hence no lower water column samples were estimated.

The concentrations of phytoplankton are shown in more detail by surface chlorophyll *a* maps made from data collected by underway sampling during the 4 seasonal voyages, 2012–13 (Figure 6-3). Except in spring, concentrations were consistently highest in the inner Firth especially in autumn, when a large area had values > 5 mg m^{-3}.
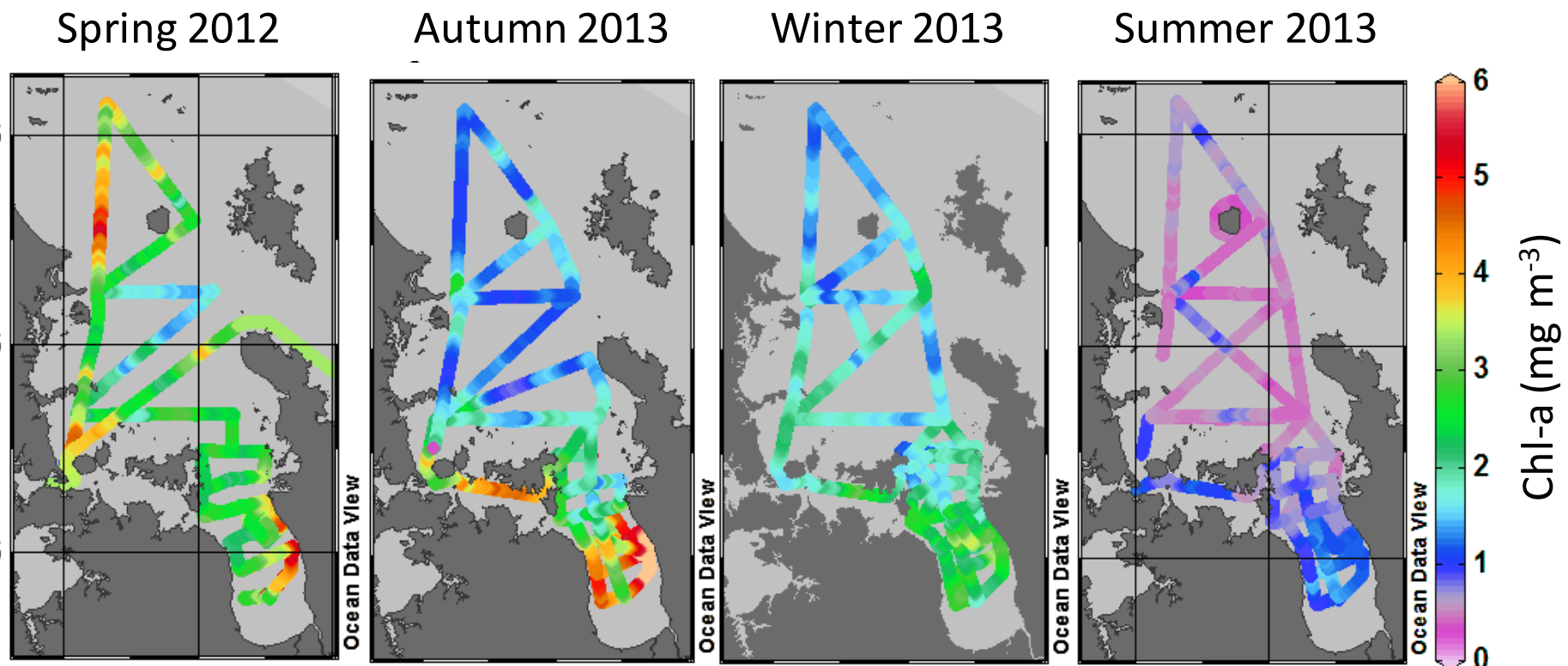
Figure 6-3: Surface chlorophyll *a* concentration mapped using underway sampling 2012–2013.

The greater phytoplankton biomass in the inner Hauraki Gulf/Firth drives higher primary productivity there compared to offshore on the shelf (Table 6-1).

Table 6-1: **Phytoplankton productivity (carbon fixation rate: mg C m^{-3} d^{-1}).** Values are for each season at the extended-Firth and shelf sites shown in Figure 6-1. Experiments and results are described in Zeldis and Willis (2014).

C Fixation (mg C m^{-3} d^{-1})	Extended Firth	Shelf
Spring	24	8
Summer	66	7
Autumn	27	12
Winter	19	9

Phytoplankton production was determined in detail across the Firth during voyages in 2002–03 (Figure 6-4). The first column in the figure shows the proportion of the water column receiving more than 1% of surface light irradiance (which is a commonly used measure of the depth of light-limitation of primary production). The light-limitation depth was equal to or shallower than the bottom depth over much of the Firth in summer, but shoaled further into the Firth in autumn and winter as seasonal light decreased. Although water column-integrated chlorophyll *a* (mg chlorophyll *a* m^{-2}) was often highest in the extended Firth because of its greater depth, volumetric chlorophyll *a* concentration (mg chlorophyll *a* m^{-3}) was often highest in the inner Firth (Figure 6-3), particularly around the Firth margins. Primary production rates in the Firth were greatest in summer, intermediate in spring and autumn, and reached minima in winter as light became limiting. Again, water column-integrated production was greatest in the extended Firth, because of its greater depth. Between-year variation was evident, with higher values of light penetration, chlorophyll *a* and production in summer 2003 compared to summer 2002.
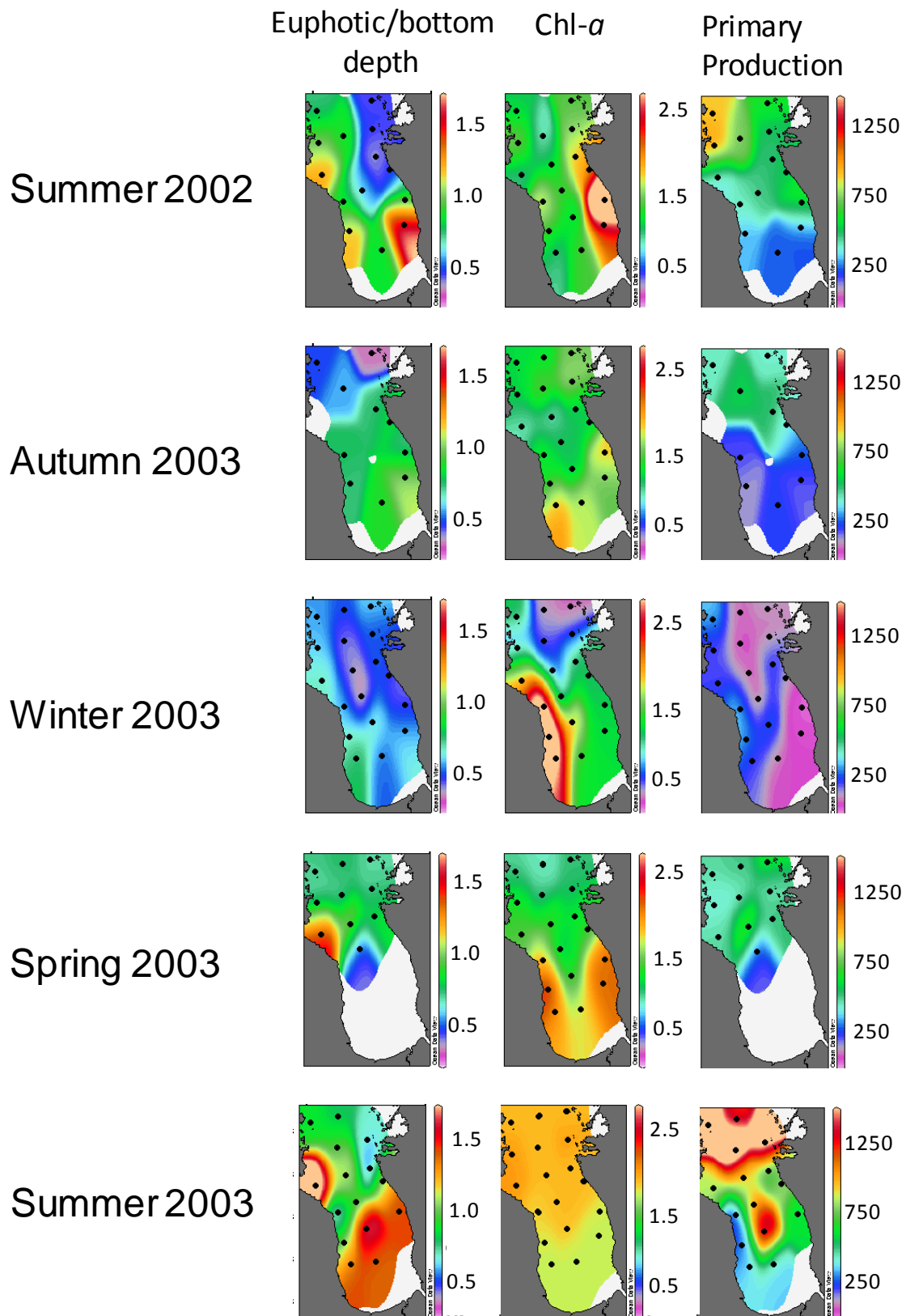
Figure 6-4: **Primary production in Firth over 5 seasonal voyages, summer 2002–summer 2003.** The columns show (left to right) the depth of light penetration relative to bottom depth, depth-integrated chlorophyll a concentration (mg m^{-2}) and primary production rate (mg C m^{-2} d^{-1}). Some light penetration data were lost in the spring voyage.

The primary production averaged over all seasons from the dataset of Figure 6-4 was about 460 mg C $m^{-2} d^{-1}$ averaged across the Firth and extended Firth (or about 191 g C $m^{-2} y^{-1}$).

The seasonal variation in phytoplankton distribution by depth noted above (Figure 6-2) reflects cycles of phytoplankton growth and senescence. In particular, the deepening of the phytoplankton in autumn indicates the exhaustion of upper-water-column nutrients and redistribution of phytoplankton under nutrient stress.

Seasonal events are shown clearly in the INF (Integrating Natural Fluorometer) data from the extended-Firth monitoring site. The deeper INF (20 m below the water surface, in a water depth of 40 m) shows a clear seasonal increase (~3–4-fold) from late spring/early summer to autumn each year (Figure 6-5B). Data collected using CTD (Figure 6-5C) showed these deep distributions and their differences between two autumns, with 2010 having a stronger deep maximum of chlorophyll than 2013.

Chlorophyll *a* and its breakdown product, phaeopigment, at the extended-Firth monitoring site over the period 1998–2013 are shown in Figure 6-6.

Cell counts of total micro-phytoplankton and its functional group components (diatoms, dinoflagellates and 'others'[43]) at the extended-Firth monitoring site over the period 1998–2013 are shown in Figure 6-7.

Biomasses of total micro-phytoplankton and its functional group components (diatoms, dinoflagellates, and 'others') at the extended-Firth monitoring site over the period 1998–2013 are shown in Figure 6-8. Also shown are biomasses of eukaryotic (nucleated) and prokaryotic (non-nucleated) pico-phytoplankton, which are among the smallest, but numerically most abundant phytoplankton taxa. Bacterial biomasses are also shown.

---

[43] The "Others" category included silicoflagellates, raphidophytes, prymnesiophytes, cryptophyceae, chrysophyceae, euglenoids and monads.
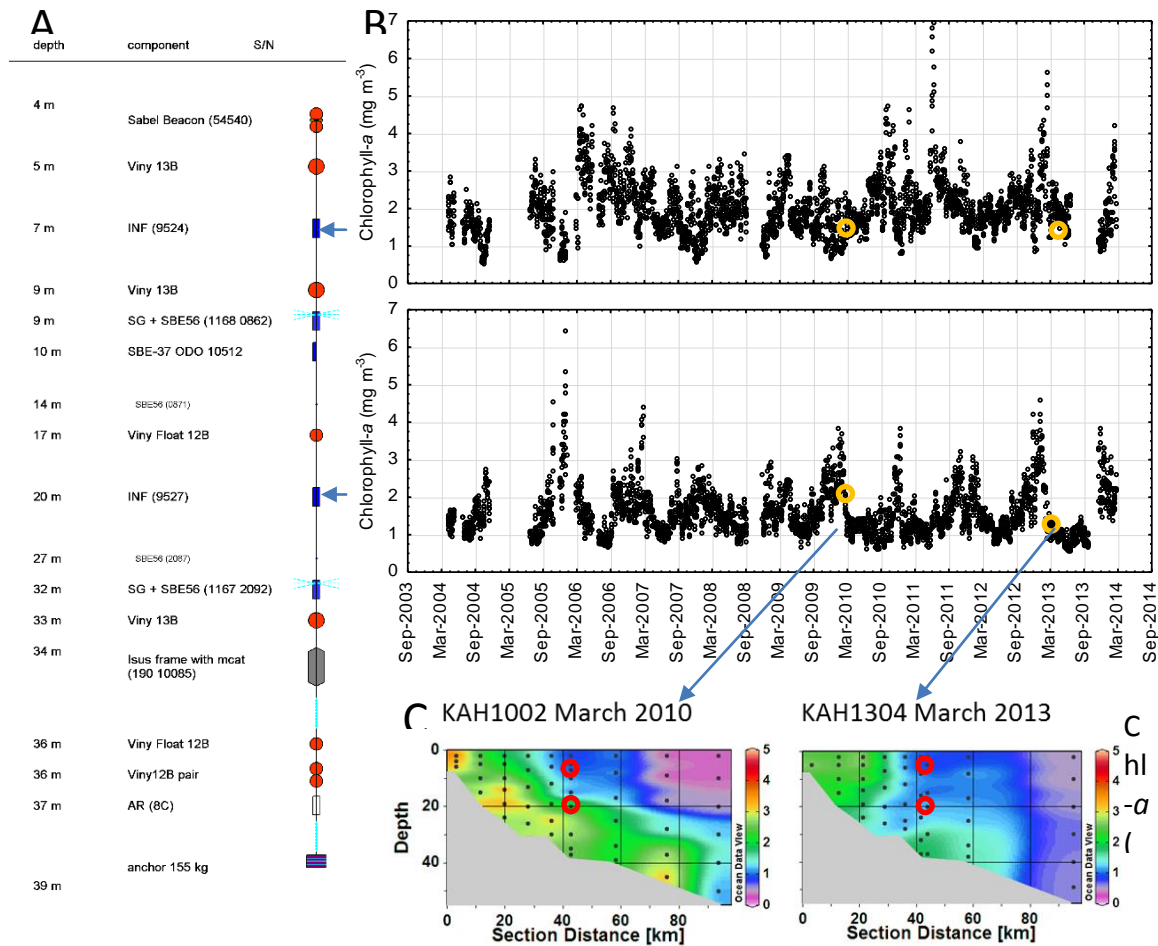
Figure 6-5: Time series of chlorophyll *a* measured by INFs and CTD at the extended-Firth monitoring site from 2004 to 2014. (A) Schematic of the mooring: INFs (arrows) are deployed 7 m below the surface and 20 m below the surface. Arrows point to (B) time series of daily average chlorophyll *a* determined by the two INFs from 2004 to 2014. Orange circles indicate INF data collected in March 2010 and March 2013 at the mooring. (C) Chlorophyll *a* data collected by CTD in March 2010 and March 2013 on a transect extending from the inner Firth to the outer Hauraki Gulf, with red circles indicating CTD-collected chlorophyll *a* at the depths of the INFs on the Firth mooring.
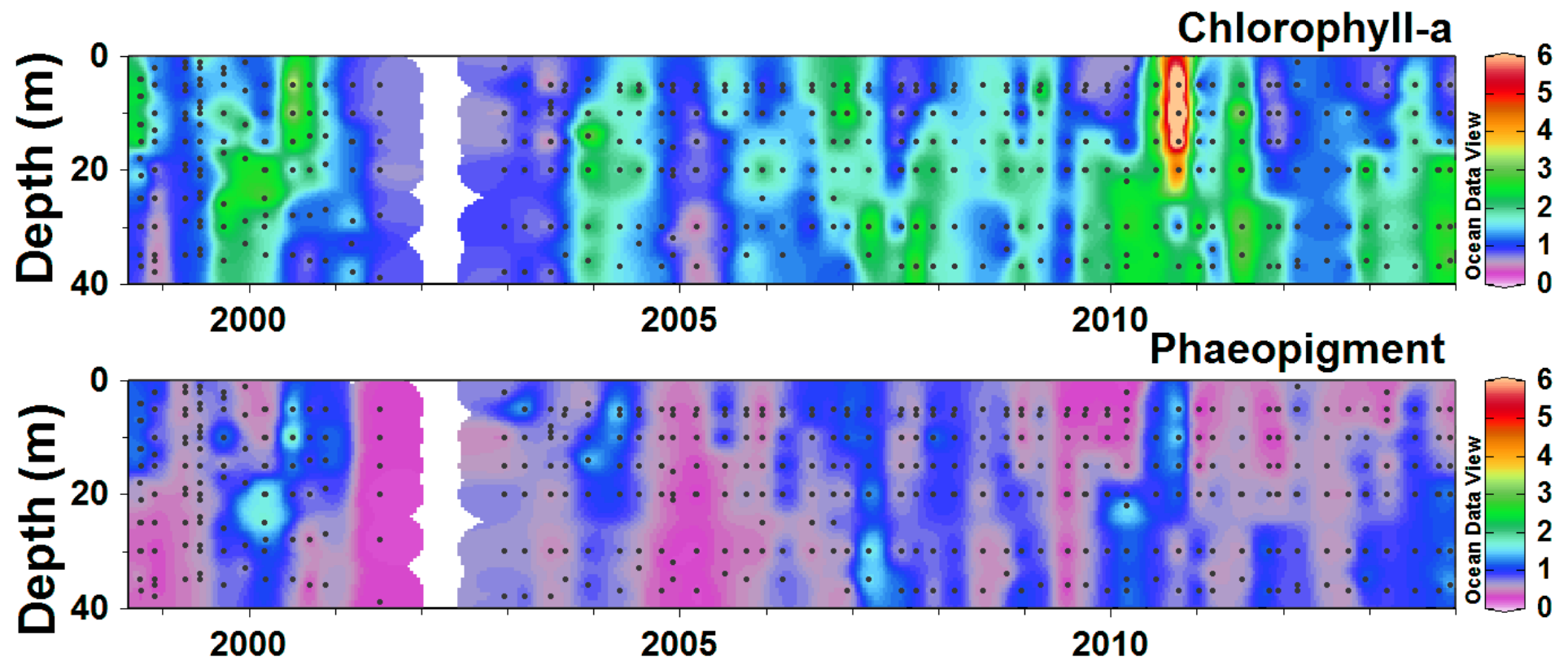
Figure 6-6: **Phytoplankton pigment concentrations (mg m^{-3}) plotted by depth and through time at the extended-Firth monitoring site, 1998–2013.** Ticks on the x-axis correspond to January 1 of each year.
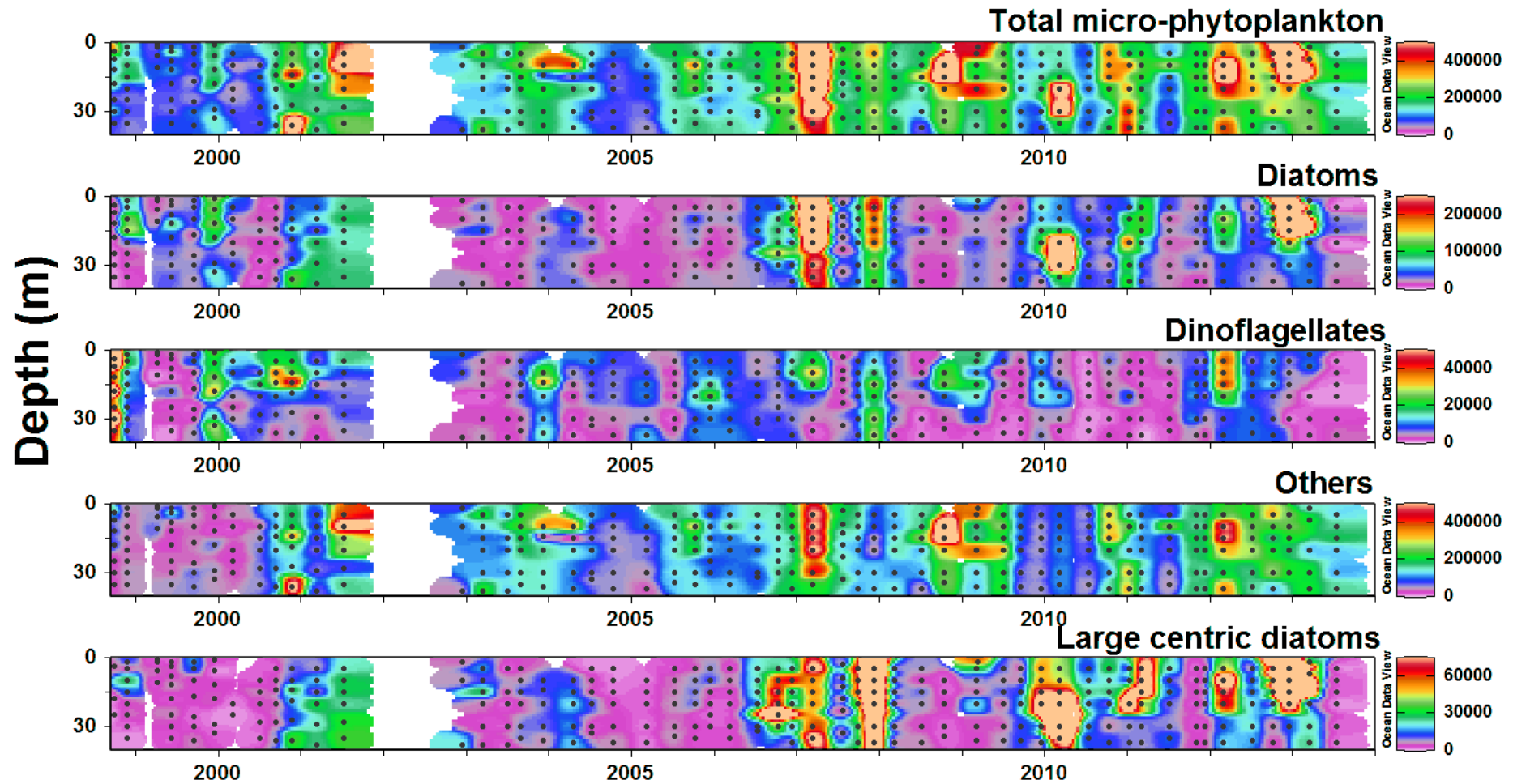
Figure 6-7: **Counts of phytoplankton and bacteria plotted by depth and through time at the extended-Firth monitoring site, 1998–2013.** Counts for phytoplankton are in units of cells L^{-1}. Counts for picoplankton and bacteria are in units of cells mL^{-1}. Ticks on the x-axis correspond to 1 January of each year.
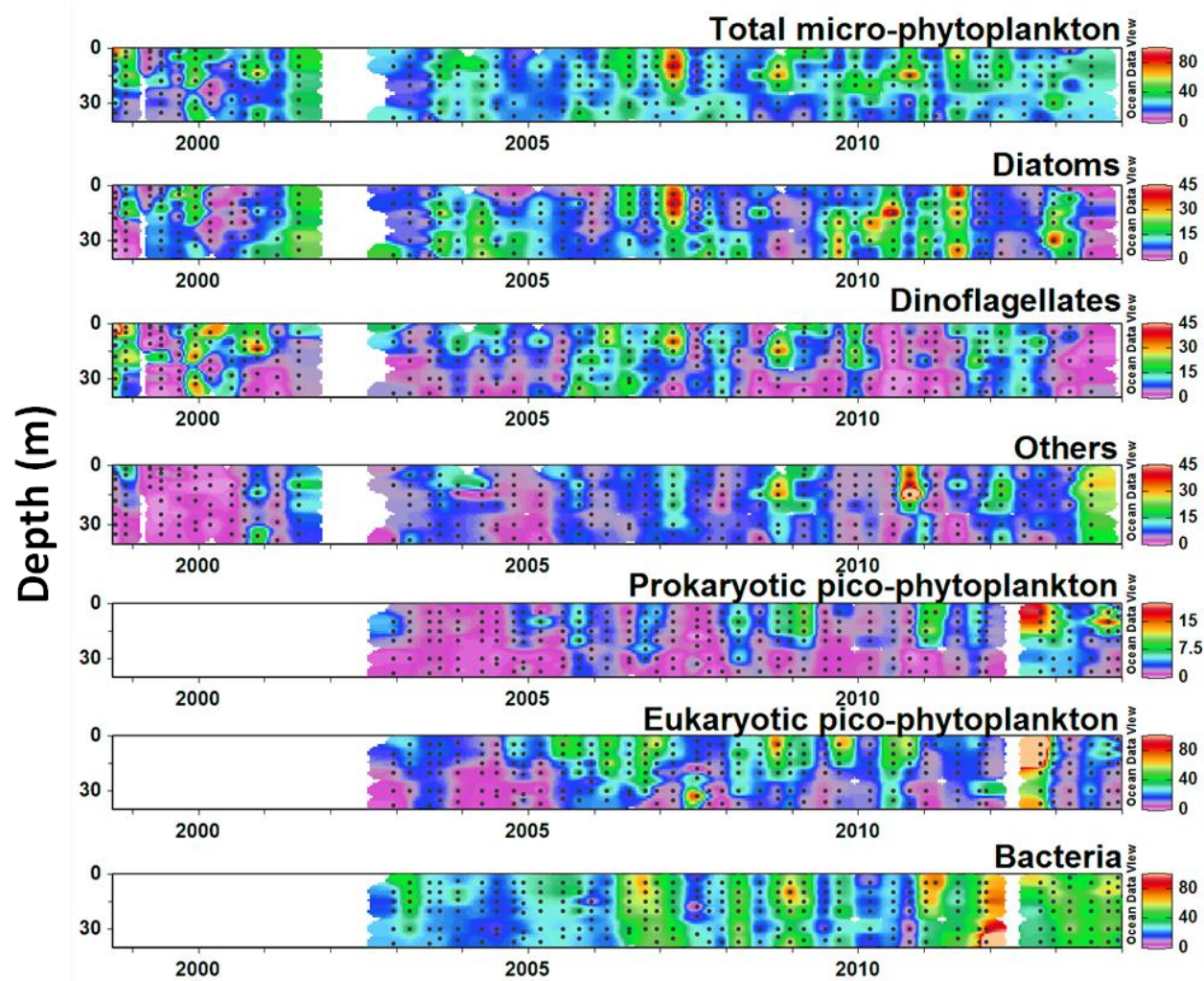
Figure 6-8: **Biomasses of phytoplankton and bacteria (mg C m^{-3}) plotted by depth and through time at the extended-Firth monitoring site, 1998–2013.** Biomasses are in units of mg C m^{-3}. Ticks on the x-axis correspond to January 1 of each year.

6.4 Trend analyses

The measurements of chlorophyll *a* and phaeopigment over the 15-year (1998–2013) period at the extended-Firth monitoring site (Figure 6-6) were analysed for trends using the non-parametric seasonal Kendall trend test (Jowett, 2004). The measurements were integrated over the upper water column (from the surface to 20 m below the surface) and the lower water column (20 m below the surface to 40 m below the surface).

The results are shown in Table 6-2, and the Kendall trends are plotted against the data in Figure 6-9. The estimate of the percentage annual change (the "trend") is statistically significant at the 95% confidence level if $p < 0.05$.

Table 6-2: **Non-parametric seasonal Kendall tests for time trends in chlorophyll *a* and phaeopigment concentrations (mg m^{-2}) integrated over the water column.** Data from the extended-Firth monitoring site, October 1998 to July 2013. Data are grouped by season (seasons used were: Sep – Nov, Dec – Feb, Mar – May, Jun – Aug for spring, summer, autumn and winter, respectively).

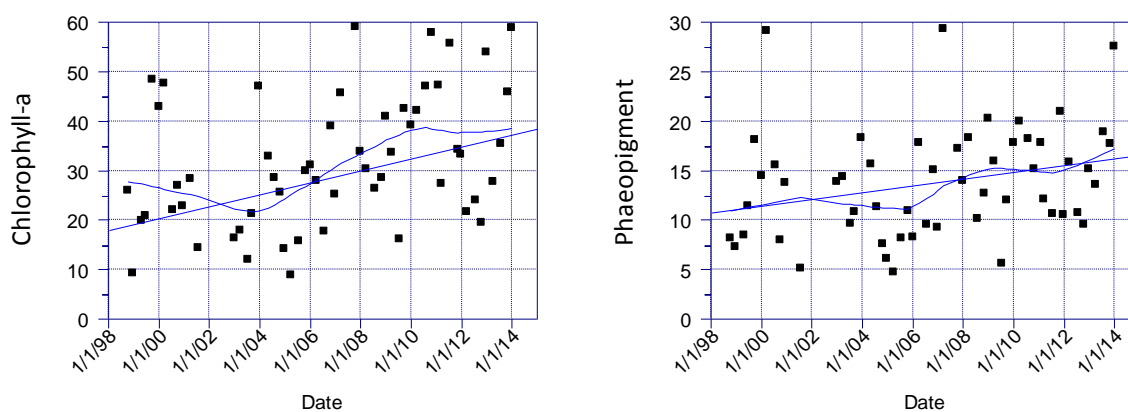| Chlorophyll variable	Sample size	Median value	*p*	Median Slope (annual)	5 % confidence limit for slope	95 % confidence limit for slope	Percent annual change
Chl-*a* >= 20 m	56	28.50	0.00	1.20	0.58	1.87	4.22
Chl-*a* < 20 m	56	24.08	0.51	-0.22	-1.02	0.46	-0.91
Phaeo >= 20 m	55	13.78	0.02	0.34	0.07	0.64	2.49
Phaeo < 20 m	55	12.79	0.11	-0.37	-0.73	0.02	-2.92

Figure 6-9: **Time series of chlorophyll *a* and phaeopigment concentrations (mg m^{-2}) at ≥ 20m depth in the water column.** The blue curves show the fitted linear Kendall trend (the straight line) and a LOWESS moving average fit (the other line) that used 40% of the points in its fitting window.

The cell counts of total micro-phytoplankton and its functional group components (diatoms, dinoflagellates, "others", and large centric diatoms) over the 15-year (1998–2013) period at the extended-Firth monitoring site (Figure 6-7) were analysed for trends using the non-parametric seasonal Kendall trend test (Jowett, 2004). The measurements were integrated over the water column.

The results are shown in Table 6-3, and the Kendall trends are plotted against the data in Figure 6-10. The estimate of the percentage annual change (the "trend") is statistically significant at the 95% confidence level if $p < 0.05$.

Table 6-3:   **Non-parametric seasonal Kendall tests for time trends in cell counts (cells m^{-2} x 10^{-3}) integrated over the water column.** Data from the extended-Firth monitoring site, October 1998 to July 2013. Data are grouped by season (seasons used were: Sep – Nov, Dec – Feb, Mar – May, Jun – Aug for spring, summer, autumn and winter, respectively).

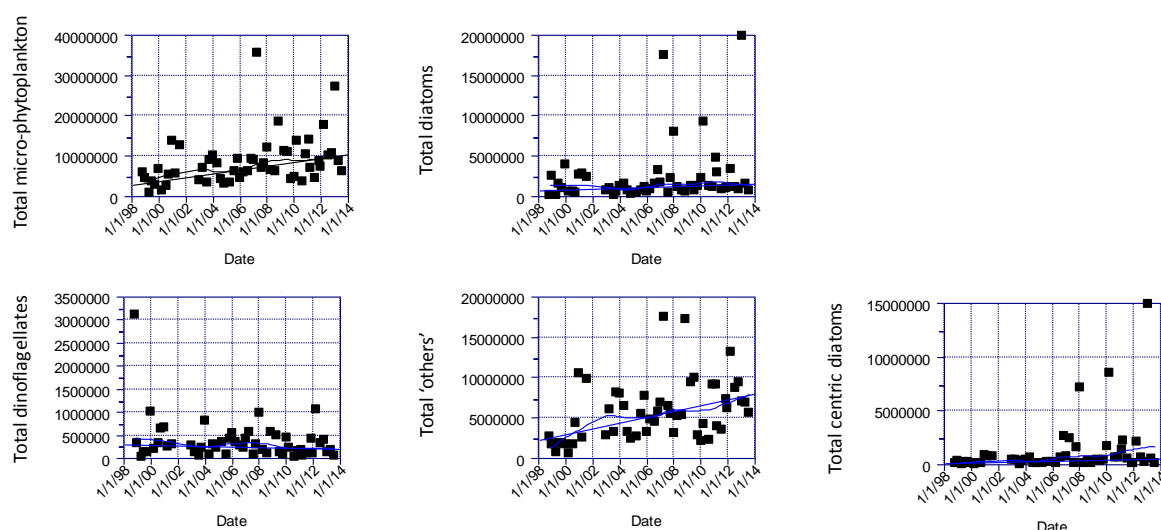| Counts	Sample size	Median value	p	Median slope (annual)	5 % C.L. for slope	95 % C.L. for slope	Percent annual change
All micro phyto	53	6938291	0.00	477211	223557	646149	6.9
Diatoms	53	1129149	0.03	51870	14361	96930	4.6
Dinoflagellates	53	237451	0.39	-5096	-18291	4258	-2.2
Others	53	5374044	0.00	361234	175643	477743	6.7
Large centric diatoms	53	341824	0.01	30252	8796	55277	8.9

Figure 6-10:   Time series of taxa counts (cells m^{-2} x 10^{-3}) integrated over the water column. The blue curves show the fitted linear Kendall trend (the straight line) and a LOWESS moving average fit (the other line) that used 40% of the points in its fitting window.

The biomasses of total micro-phytoplankton and its functional group components (diatoms, dinoflagellates, "others", and large centric diatoms, plus eukaryotic [nucleated] and prokaryotic [non-nucleated] pico-phytoplankton and bacteria) over the 15-year (1998–2013) period at the extended-Firth monitoring site (Figure 6-8) were analysed for trends using the non-parametric seasonal Kendall trend test (Jowett, 2004). The measurements were integrated over the water column.

The results are shown in Table 6-4, and the Kendall trends are plotted against the data in Figure 6-11. The estimate of the percentage annual change (the "trend") is statistically significant at the 95% confidence level if $p < 0.05$.

Table 6-4: **Non-parametric seasonal Kendall tests for time trends in cell biomass (mg C m^{-2}) integrated over the water column.** Data from the extended-Firth monitoring site, October 1998 to July 2013. Data are grouped by season (seasons used were: Sep – Nov, Dec – Feb, Mar – May, Jun – Aug for spring, summer, autumn and winter, respectively).

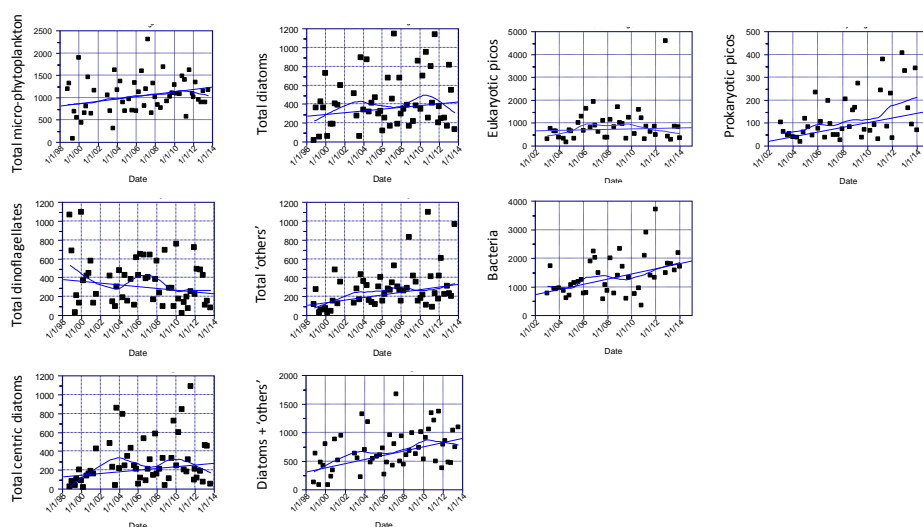| Biomass	Sample size	Median value	p	Median slope (annual)	5 % C.L. for slope	95 % C.L. for slope	Percent annual change
All micro phyto	53	1050	0.07	26.33	0.98	42.67	2.51
Diatoms	53	358	0.36	9.4	-6.17	21.84	2.62
Dinoflagellates	53	301	0.33	-9.45	-25.17	4.74	-3.15
Others	53	232	0.01	13.94	6.98	21.43	6.02
Eukaryotic picos	42	724	0.65	10.64	-25.95	50.2	1.47
Prokaryotic picos	42	83	0.01	10.19	4.91	19.85	12.34
Bacteria	42	1287	0.01	90.53	35.77	140.11	7.03
Centric diatoms	53	207	0.07	8.8469	0.6135	21.8612	4.27

Figure 6-11: **Time series of taxa biomasses (mg C m^{-2}) integrated over the water column.** The blue curves show the fitted linear Kendall trend (the straight line) and a LOWESS moving average fit (the other line) that used 40% of the points in its fitting window.

Potentially toxic genera were broken down into three groups; (toxic) dinoflagellates, (toxic) diatoms, and (toxic) "others". The dinoflagellates included the more prominent genera *Karenia*, *Alexandrium*, *Dinophysis*, *Gonyaulax*, *Lingulodinium*, and the less common *Ostreopsis*, and *Gambierdiscus*. Toxic diatoms were limited to the genus *Pseudo-nitzschia*, which is capable of dominating the entire phytoplankton population at times. The "others" group consisted of the raphidophytes including *Heterosigma*, *Fibrocapsa*, and *Chattonella,* as well as the occasionally observed *Oscillatoria/Trichodesmium* and *Prymnesium*.

The non-parametric seasonal Kendall trend test (Jowett, 2004) was applied to the toxic diatom cell counts and biomass integrated over the water column.

The results are shown in Table 6-5, and the Kendall trends are plotted against the data in Figure 6-12. The estimate of the percentage annual change (the "trend") is statistically significant at the 95% confidence level if *p* < 0.05.

Table 6-5: **Non-parametric seasonal Kendall tests for time trends in toxic diatom cell counts (cells m^{-2} x 10^{-3}) and biomass (mg C m^{-2}) integrated over the water column.** Data from the extended-Firth monitoring site, October 1998 to July 2013. Data are grouped by season (seasons used were: Sep – Nov, Dec – Feb, Mar – May, Jun – Aug for spring, summer, autumn and winter, respectively).

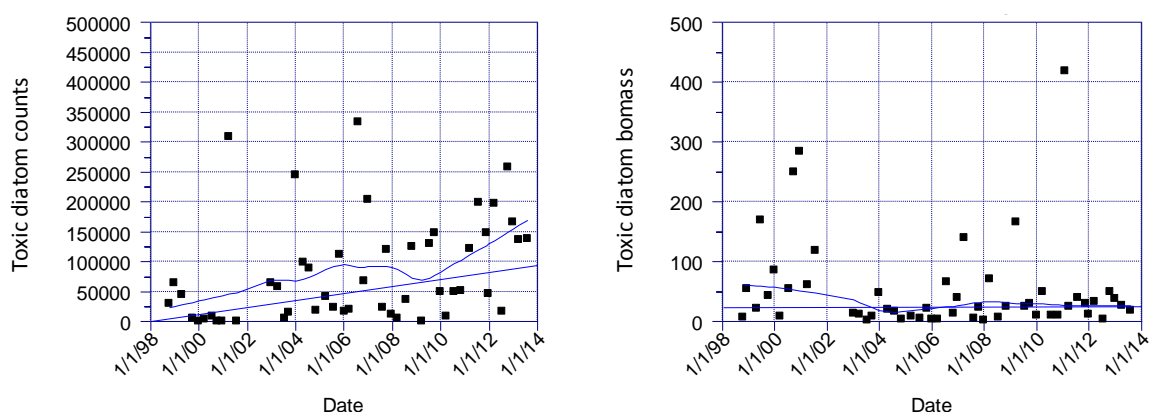| Toxic Counts/Biomass	Sample size	Median value	*p*	Median slope (annual)	5 % C.L. for slope	95 % C.L. for slope	Percent annual change
Diatom counts	53	51012	0.00	5777	3126	10726	11.33
Diatom biomass	53	23.79	0.88	0.18	-2.18	1.42	0.75
Dinoflagellate counts	53	88289	0.06	-5868	-10661	-490	-6.65
Dinoflagellate biomass	53	52.4	0.30	-2.1	-4.94	0.88	-4.01

Figure 6-12: Time series of toxic diatom counts (cells m^{-2} x 10^{-3}) and biomasses (mg C m^{-2}) integrated over the water column. The blue curves show the fitted linear Kendall trend (the straight line) and a LOWESS moving average fit (the other line) that used 40% of the points in its fitting window.

6.5　References

Behrenfeld, M., Falkowski, P. (1997) Photosynthetic rates derived from satellite-based chlorophyll concentration. *Limnology and Oceanography*, 42: 1–20.

Buitenhuis, E.T., Li, W.K.W., Vaulot, D., Lomas, M.W., Landry, M.R., Partensky, F., Karl, D.M., Ulloa, O., Campbell, L., Jacquet, S., Lantoine, F., Chavez, F., Macias, D., Gosselin, M., McManus, G.B. (2012) Picophytoplankton biomass distribution in the global ocean. *Earth Syst. Sci. Data,* 4:37–46.

Eppley, R.W.R., Reid, F.M.H., Strickland, J.D.H. (1970) Estimates of phytoplankton crop size, growth rate and production. *Bulletin of the Scripps Institution of Oceanography*. 17. 33-42.

Fukuda, R., Ogawa, H., Nagata, T., Koike, I. (1998) Direct determination of carbon and nitrogen contents of natural bacterial assemblages in marine environments. *Appl. Environ. Microbiol.,* 64: 3352–3358.

Gall, M., Zeldis, J. (2011) Phytoplankton biomass and primary production responses to physico-chemical forcing across the northeastern New Zealand continental shelf. *Continental Shelf Research,* 31: 1799–1810.

Hillebrand, H., Dürselen, C.D., Kirschtel, D., Pollingher, U., Zohary, T. (1999) Biovolume calculation for pelagic and benthic microalgae. *Journal of phycology,* 35: 403–424.

Lebaron, P., Parthuisot, N., Catala, P. (1998) Comparison of blue nucleic acid dyes for flow cytometric enumeration of bacteria in aquatic systems. *Appl. Environ. Microbiol.*, 64: 1725–1730.

Menden-Deuer, S., Lessard, E. (2000) Carbon to volume relationships for dinoflagellates, diatoms and other protist plankton. *Limnology and Oceanography,* 45: 569–579.

Olenina, I., Hajdu, S., Andersson, A., Edler, L., Wasmund, N., Busch, S., Göbel, J., Gromisz, S., Huseby, S., Huttunen, M., Jaanus, A., Kokkonen, P., Ledaine, I., Niemkiewicz, E. (2006) Biovolumes and size-classes of phytoplankton in the Baltic sea. *Baltic Sea Environment Proceedings* 106. 144 pp.

Rott, E. (1981) Some results from phytoplankton counting intercalibrations. *Schweizerische Zeitschrift für Hydrologie*, 43: 34–62.

Strathman, P. (1967) Estimating the organic carbon content of phytoplankton from cell volume or plasma volume. *Limnology and oceanography Limnology and Oceanography*, 12: 411–488.

Strickland, J., Parsons, T. (1972) *A practical handbook of seawater analysis Fisheries Research Board of Canada Bulletin.* 167. 311 pp.

Yoshikawa, T., Furuya, K. (2004) Long-term monitoring of primary production in coastal waters by an improved natural fluorescence method. *Marine Ecology Progress Series*, 273: 17–30.

Zeldis, J., Willis, K. (2014) Biogeographic and trophic drivers of mesozooplankton distribution on the n.e. continental shelf and in Hauraki Gulf, New Zealand. *New Zealand Journal Marine and Freshwater Research*. DOI: 10.1080/00288330.2014.955806

Zeldis, J., Walters, R.A., Greig, M.J.N, Image, K. (2004) Circulation over the northeastern New Zealand continental slope, shelf and adjacent Hauraki Gulf, from spring to summer. *Continental Shelf Research*, 24: 543–561.

Zeldis, J., Bind, J., Roulston, H., Sykes, J., Walkington, M. (2013) Visualising nutrients and phytoplankton in the Hauraki Gulf marine park using GIS July 2013. *NIWA Client Report.* CHC2013-080. 17 pp.

7 Dissolved oxygen

7.1 Overview of data sources

In this section we list sources of data presented in this chapter. Unless otherwise specified data were collected and are owned by NIWA.

- 15 years (1998–2013) of measurements every 3 months at the extended-Firth monitoring site. Measurements by CTD lowered from a research vessel.

- Spatial surveys of DO conducted in autumn of each of three years.

- Measurements every 15 minutes at two depths in the water column on a fixed mooring at the extended-Firth monitoring site over the period 2005–2014.

- Measurements every 15 minutes at the Wilson B site at 5 m below the water surface over the period January to April, 2013

7.2 Methods

7.2.1 CTD measurements

Dissolved oxygen (DO) has been measured at the extended-Firth monitoring site seasonally (every 3 months) over the 15-year period 1998–2013. (Surveys were suspended during July 2001 to December 2002 when the research was transferred to Nelson Bays.) The measurements were made using a CTD deployed from a research vessel.

Electronic CTD instrumentation (Seabird SBE 43 oxygen sensors) was used. Sensors were calibrated regularly within the recommended calibration interval (2 years) at the Seabird factory. The initial sensor accuracy is 2% of saturation with typical stability of 0.5% per 1000 h of operation (on time).

Spatial CTD surveys of oxygen have also been conducted across the Firth and Hauraki Gulf in the autumn of each of three years.

7.2.2 Moorings

Dissolved oxygen has been measured using moored oxygen sensors at the two locations shown in Figure 7-1. These locations are the extended-Firth monitoring site (36 45.6 S, 175 18.0 E; 40 m depth) and the Wilson B site (adjacent to the Wilson Area B marine farm zone; 36 58.297 S, 175 24.116 E; 16 m depth).
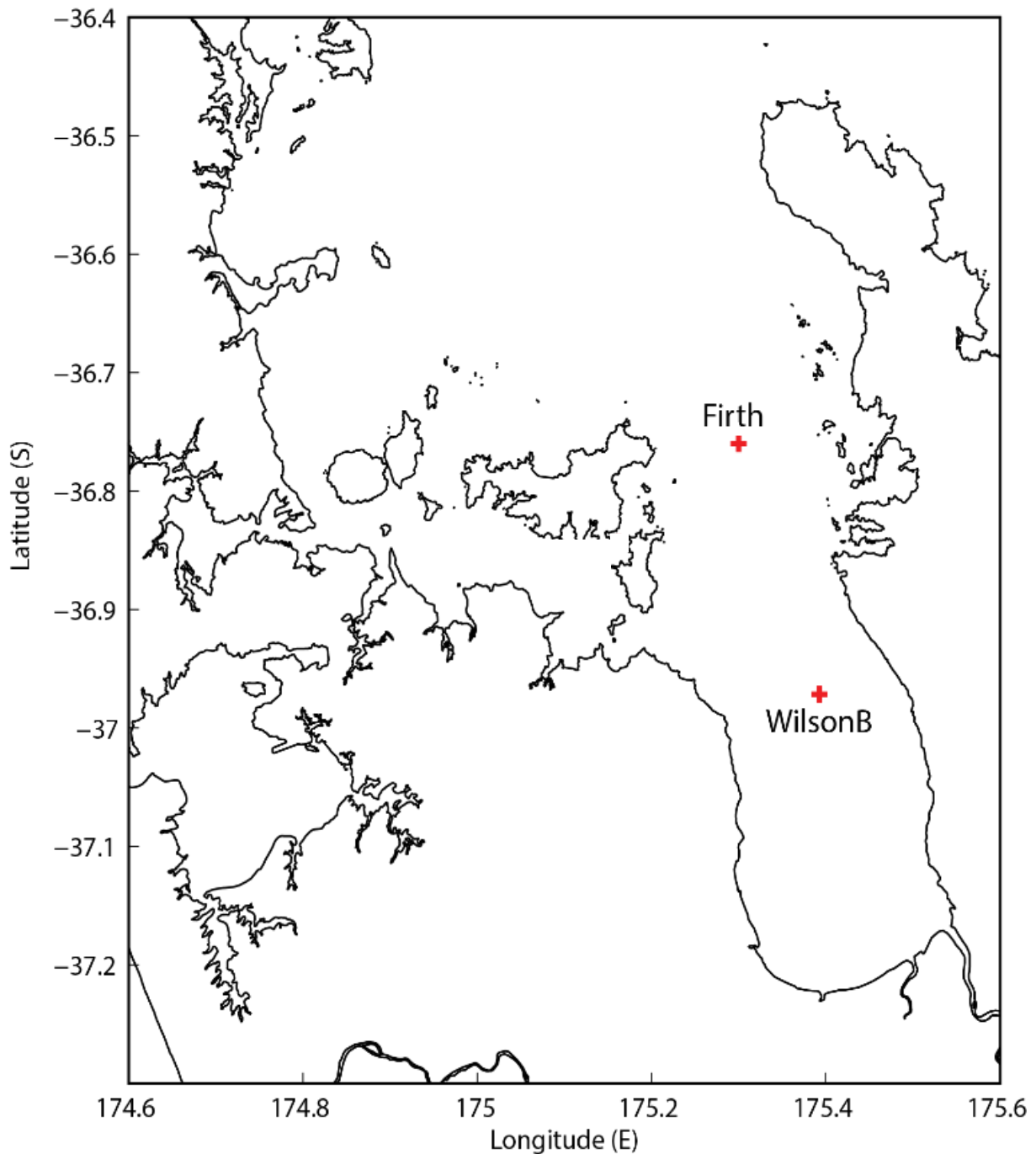
Figure 7-1: **Locations of moorings deployed in the Firth of Thames.** The "Firth" mooring is at the extended-Firth monitoring site (36 45.6 S, 175 18.0 E; 40 m depth). The "Wilson B" site was adjacent to the Wilson Area B marine farm zone (36 58.297 S, 175 24.116 E; 16 m depth).

The extended-Firth data were collected with DO sensors mounted in the upper and lower water column at mean depths below the water surface of 10 and 33 m. Measurements were made over the period 2005–2014 at a 15-minute interval. DO measurements on the mooring began in October 2005 with Aanderaa optodes installed on Aanderaa current meters. These were accompanied by Seabird's SBE-37 CT sensor to record salinity and temperature. In July 2011 the Aanderaa sensors were replaced with Seabird SBE-37 CT sensors with integrated dissolved oxygen.

The Firth mooring has been visited quarterly (winter, spring, summer, autumn) by ship to download data, clean hardware and instrumentation, and redeploy the mooring. During each visit the Aanderaa optodes were recalibrated. The SBE-37s were cleaned according to the manufacturer's instructions and returned to the Seabird factory every 2–3 years for calibration. During the mooring turnaround a Seabird CTD with rosette was deployed twice, once before the recovery of the mooring and again after its redeployment (usually 1–2 days apart) to record temperature, salinity and oxygen down through the water column. Sensor drift affected the mooring DO sensors, which required corrections to be applied to the data. The methods used for this are given in Appendix D.

The Wilson B mooring was 25 km to the south of the extended-Firth monitoring site. The mooring was deployed to observe changes in temperature, salinity, DO and current flow, and its location was selected to capture the near-field response to a dominant river source (Waihou River) as part of the NIWA Region of Freshwater Influence (ROFI) project. The Wilson B data, which were collected using a Seabird IDO MicroCAT (#9022) at 5 m below the water surface, are from the period January to April, 2013[44]. Measurements were made at a 15-minute interval. Calibration is described in Appendix D.

7.3   Results

The remaining figures in this chapter are all presented, in order, at the end of the chapter in order to facilitate reading of the text.

Time series of 3-monthly CTD-derived oxygen profiles at the extended-Firth monitoring site over the period 1998–2013 are shown in Figure 7-2.

The data in Figure 7-2 show:

- The upper 20 m of the water column at the extended-Firth monitoring site was generally well oxygenated (panels A and B), with greater than 90% DO saturation for much of the year.

- In summer and autumn (the higher temperatures in panel C), when the water column was stratified[45], DO typically reduced to about 60–70% saturation (4.9 and 5.7 mg L^{-1}, respectively) at levels in the water column greater than 20 m below the surface.

Time series of 15-minute data from the extended-Firth monitoring site at the two depths on the mooring (10 m below the water surface and 33 m below the water surface) during the period 2005–2014 are shown in Figure 7-3 to Figure 7-5.

The data in Figure 7-3 to Figure 7-5 show:

- In two of six years where the 15-minute record is complete, subsurface DO remained below 60% saturation for several weeks. The lowest recorded subsurface DO was about 40% saturation (2.7 mg L^{-1}).

- Generally, the upper water column was well oxygenated but, on rare occasions, and for periods of only a few days, surface DO dropped as low as 40% saturation; DO was low

---

[44] Another sensor type was also deployed at Wilson B: the "miniDOT" (Precision Measurement Engineering). We have subsequently determined that the miniDOT sensors were unacceptably affected by biofouling that rendered that data invalid. See Appendix E.

[45] Panel D shows the Brunt Väisälä frequency (*N*, units of cycles h^{-1}), which is indicative of water-column stratification: higher *N* means more strongly stratified.

(<60–70% saturation) at the surface less often and for shorter periods (maximum of about two weeks) than it was in the subsurface.

The Wilson B 15-minute data (January to April, 2013) are shown in Figure 7-6 and Figure 7-7 (detail). They show:

- At 5 m below the water surface, DO reached a minimum of 70–75% saturation. At these times the water was colder and more saline, and subsurface DO at the extended-Firth monitoring site was also low (60% saturation).

Low DO water (60% saturation) at the lower instrument at the extended-Firth monitoring site had temperatures between 18 to 19 °C and salinity of 35.2, corresponding to a density of about 1025.4 kg m^{-3} (Figure 7-8). This low-oxygen water is a seasonal feature of the lower extended Firth water column, occurring in late summer and autumn. Although the signature is slightly fresher at Wilson B (34.8–35.0) and warmer (20 °C) than at the extended-Firth monitoring site, the low-oxygen water between these two locations appear to be part of the same formation.

Spatial plots of oxygen (Figure 7-9) sampled in autumn in 3 separate years show a number of features:

- Oxygen depletion was variable in strength from year to year, with more depletion in 2009 and especially 2010, compared to 2013. This is consistent with the patterns seen in the moored oxygen time series at the extended-Firth monitoring site (Figure 7-3 to Figure 7-5).

- Oxygen depletion at the extended-Firth monitoring site was contiguous with that at Wilson B, but the magnitude of oxygen depletion became progressively smaller moving into the southern Firth. This is most likely due to rapid equilibration of low-oxygen water with the atmosphere in shallow water depths, where density stratification is not sustained.

- The spatial distribution of the strong autumn oxygen minimum in 2010 was similar to that of the deep phytoplankton maximum. The weaker oxygen minimum of 2013 had considerably less phytoplankton associated with it (chlorophyll data were not available for 2009).

- Water with O$_2$ as low as 4.9 mg L^{-1} or 60% saturation was present at the extended-Firth monitoring site in autumn 2010.

Oxygen data acquired in autumn in 3 separate years at 3 latitudes across the Gulf and Firth (Figure 7-10):

- Oxygen concentrations were lower in 2009 and 2010 than in 2013 (as also shown in longitudinal sections in Figure 7-9).

- Lower-oxygen waters were present during all sampling years at the Hauraki Gulf G line at its western end (see top line of panels in Figure 7-10), where upwelled water enters the Gulf (Zeldis et al., 2004).

- Oxygen concentrations decreased toward the inner Gulf (H line) and into the Firth (FoT line) in 2009 and 2010. These waters were not present in the Firth in autumn 2013.

- Water with O_2 as low as 4.2 mg L^{-1} was present in the vicinity of Wilson Bay Areas A and B in autumn 2010, near the seabed. In 2009, water with O_2 of 5.4 mg L^{-1} was recorded near the seabed. The O_2 depletion of autumn 2010 was moderate intensity in the context of the 1998–2014 time series at the extended-Firth monitoring site (Figure 7-2).

7.4 Trend analyses

The measurements of dissolved oxygen over the 15-year (1998–2013) period at the extended-Firth monitoring site (Figure 6-6) were analysed for trends using the non-parametric seasonal Kendall trend test (Jowett, 2004). The measurements were integrated over the upper water column (from the surface to 20 m below the surface) and the lower water column (everything below that).

The results are shown in Table 7-1. The estimate of the percentage annual change (the "trend") is statistically significant at the 95% confidence level if $p < 0.05$.

Table 7-1: **Non-parametric seasonal Kendall tests for time trends in oxygen concentrations (mg L^{-1}).** Data from the extended-Firth monitoring site, October 1998 to July 2013. Data are grouped by season (seasons used were: Sep – Nov, Dec – Feb, Mar – May, Jun – Aug for spring, summer, autumn and winter, respectively).

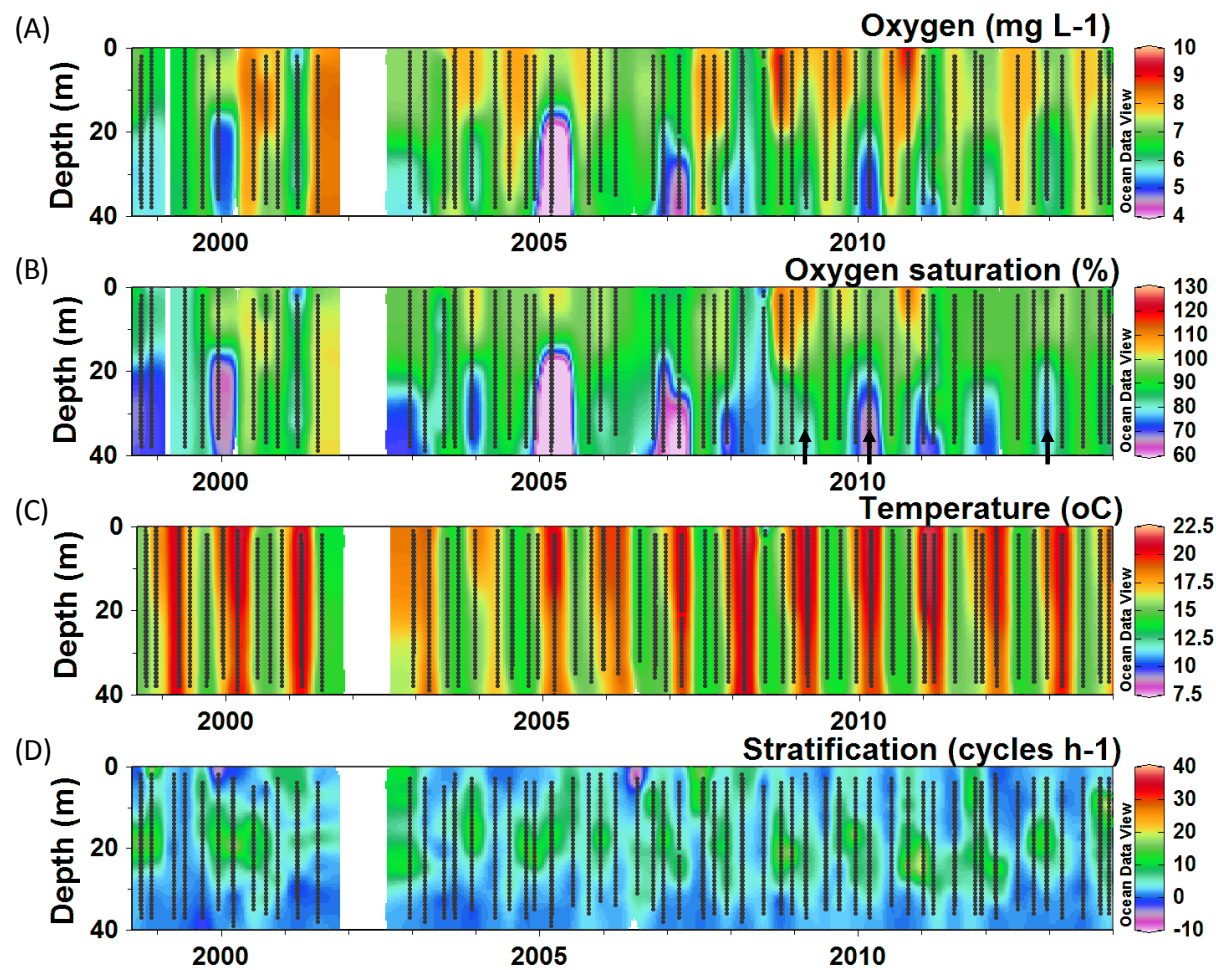| Oxygen variable	Sample size	Median value	p	Median slope (annual)	5 % C.L. for slope	95 % C.L. for slope	Percent annual change
Oxygen <20 m depth	53	224.6	0.98	-0.05	-1.10	1.18	-0.03
Oxygen ≥ 20 m depth	53	198.2	0.66	0.21	-0.60	0.98	0.11

Figure 7-2: **Oxygen and physical properties plotted by depth and time from 3-monthly CTD sampling at the extended-Firth monitoring site over the period 1998–2013.** Oxygen is shown (A) as concentration (mg O_2 L^{-1}) and (B) as percent surface O_2 saturation. Also shown are (C) temperature (^oC) and (D) stratification calculated as the Brunt Väisälä frequency (N, units of cycles h^{-1}) which is a measure of the strength of density stratification at each depth in the water column (higher values mean more strongly stratified). Vertical lines of black dots are 1-m interval CTD values. Ticks on the x-axis correspond to 1 January of each year. Black arrows in (B) in 2009, 2010 and 2013 indicate data signified in Figure 7-4.
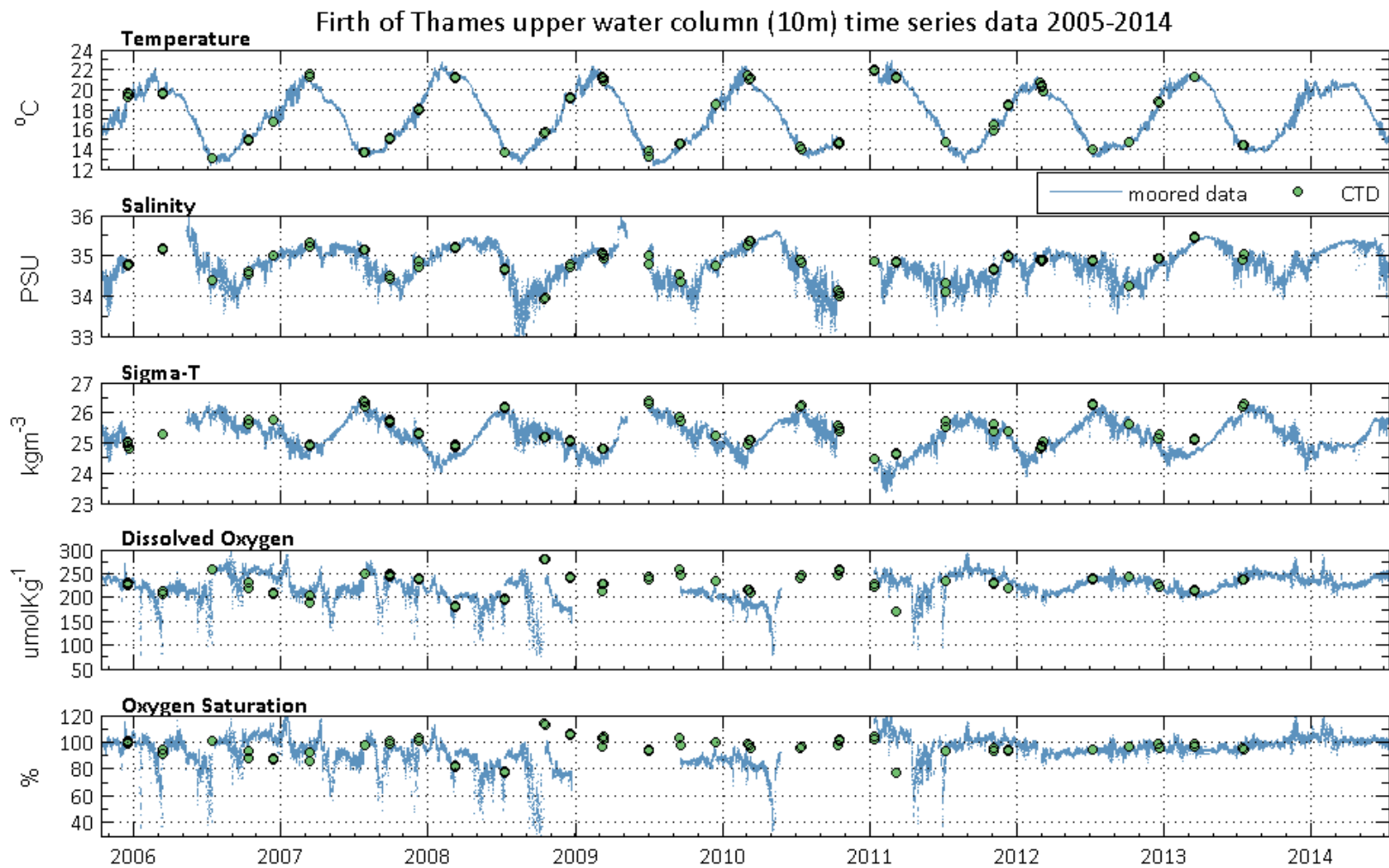
Figure 7-3: **Time series of 15-minute data from the extended-Firth monitoring site, 2005–2014.** The data are from the upper water column (10 m below the surface).
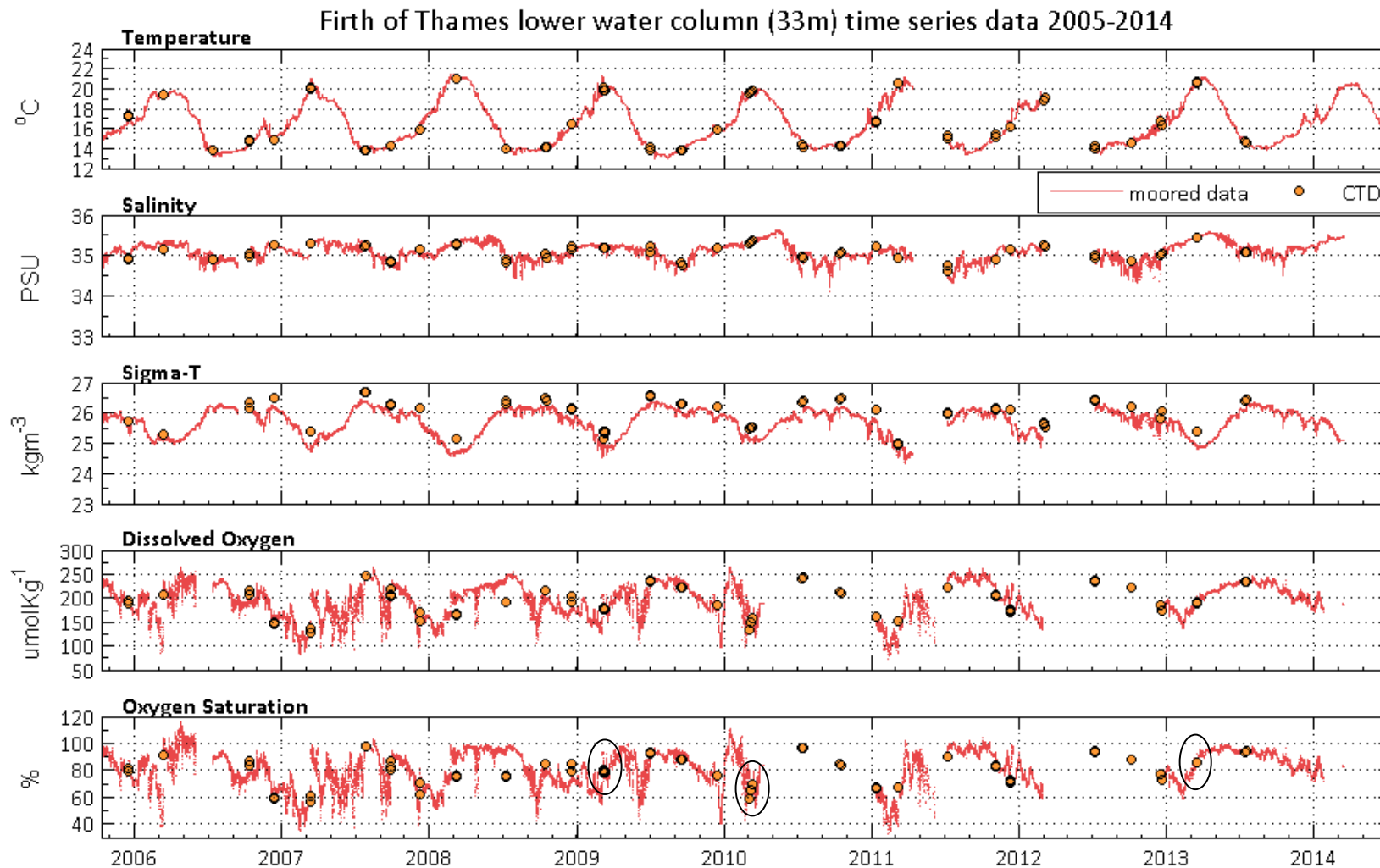
Figure 7-4: **Time series of 15-minute data from the extended-Firth monitoring site, 2005–2014.** The data are from the upper water column (10 m below the surface). The circled data in the % saturation plot are coincident with the CTD oxygen data arrowed in Figure 7-2.
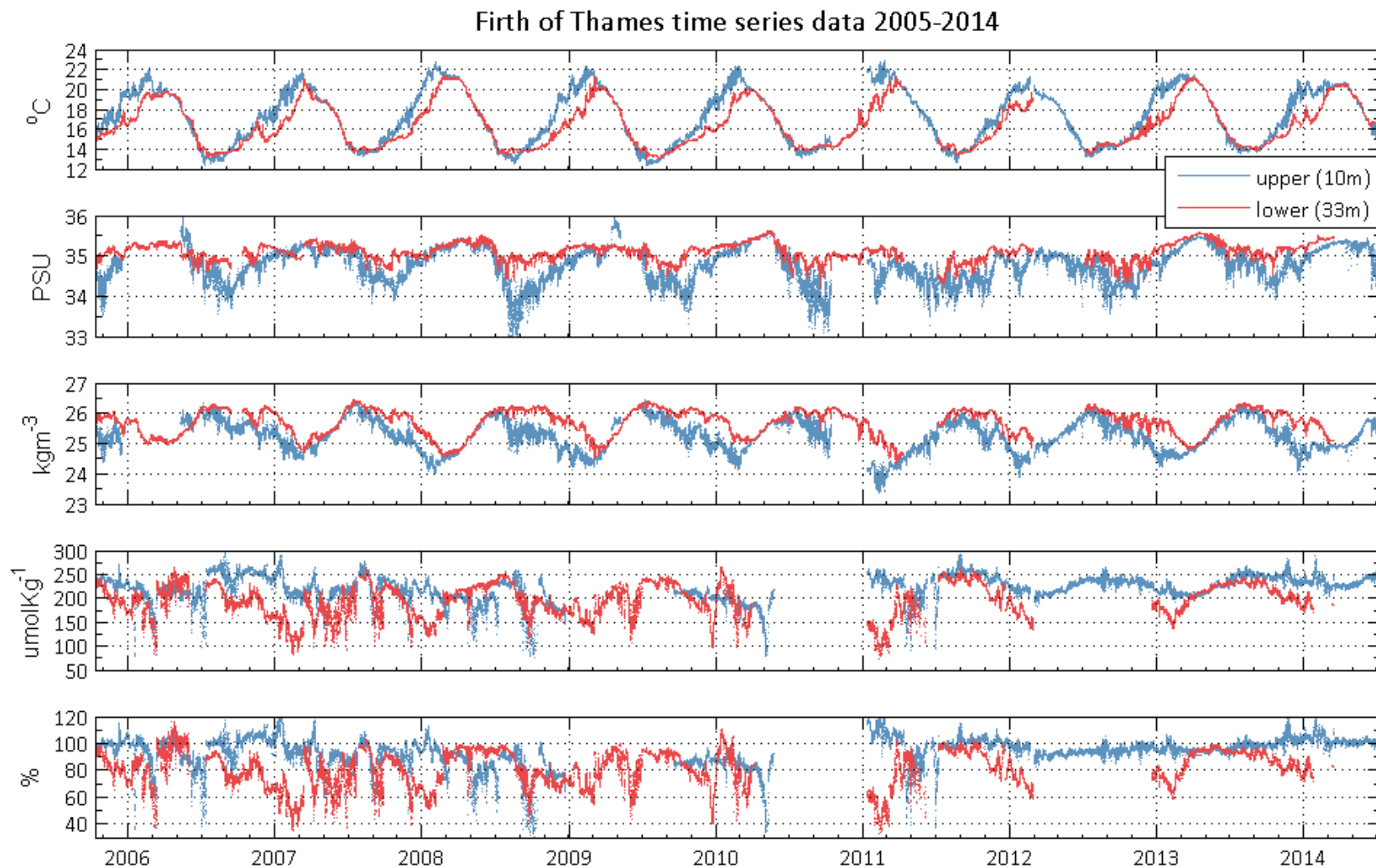

Figure 7-5: **Time series of 15-minute data from the extended-Firth monitoring site, 2005–2014.** The blue data are from the upper water column (10 m below the surface) and the red data are from the lower water column (33 m below the surface).
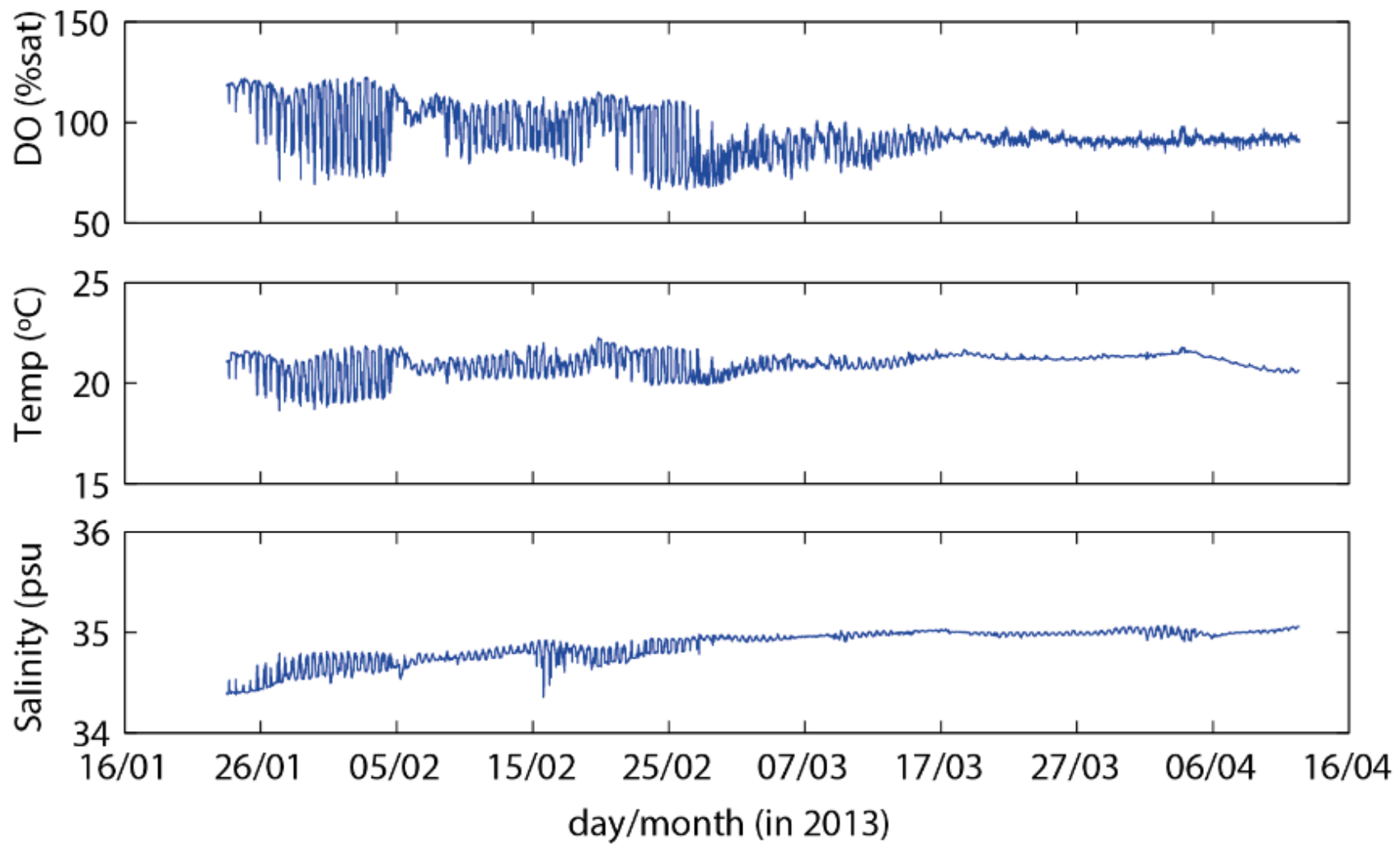
Figure 7-6:   DO, temperature and salinity at Wilson B (5 m) from January to April, 2013.
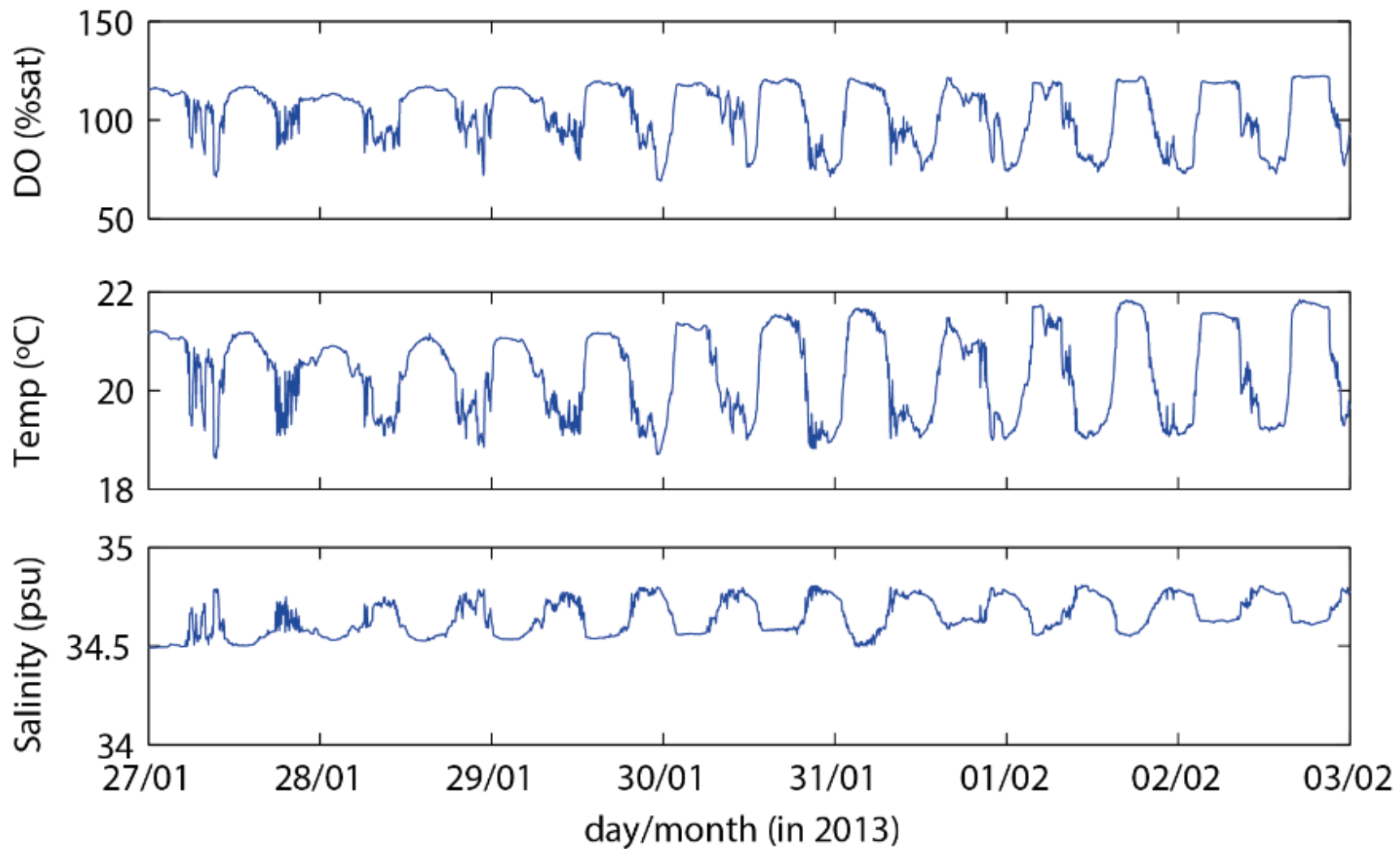
Firth of Thames Water Quality and Ecosystem Health – Data Report

Figure 7-7: **DO, temperature and salinity at Wilson B (5m) from January 27 to February 3, 2013.** This shows detail of Figure 7-6.
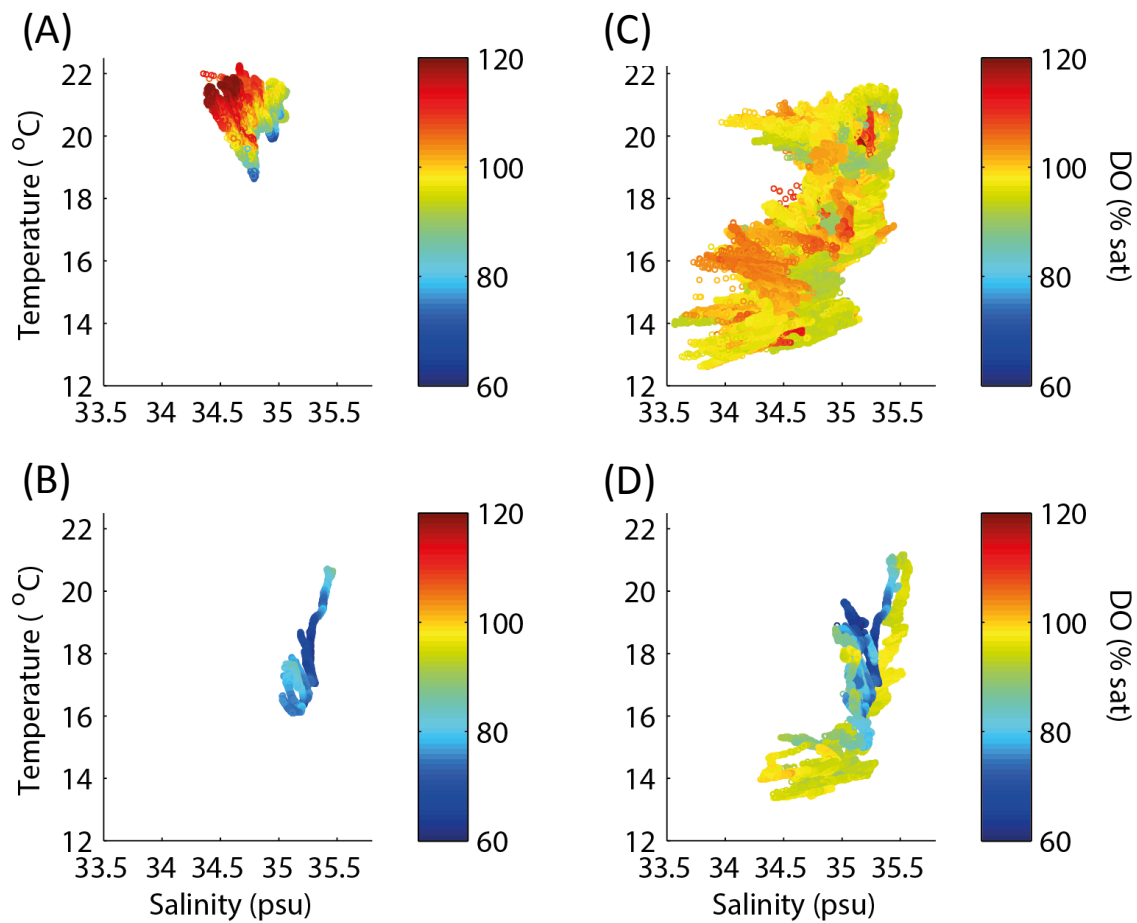
Figure 7-8: **Temperature–salinity plots coloured by oxygen (% saturation).** (A) Wilson B, 5 m below surface, January to April 2013. (B) Extended-Firth monitoring site, 33 m below surface, December to April 2013. (C) Extended-Firth monitoring site, 11 m below surface, all data 1998–2013. (D) Extended-Firth monitoring site, 33 m below surface, all data 1998–2013.
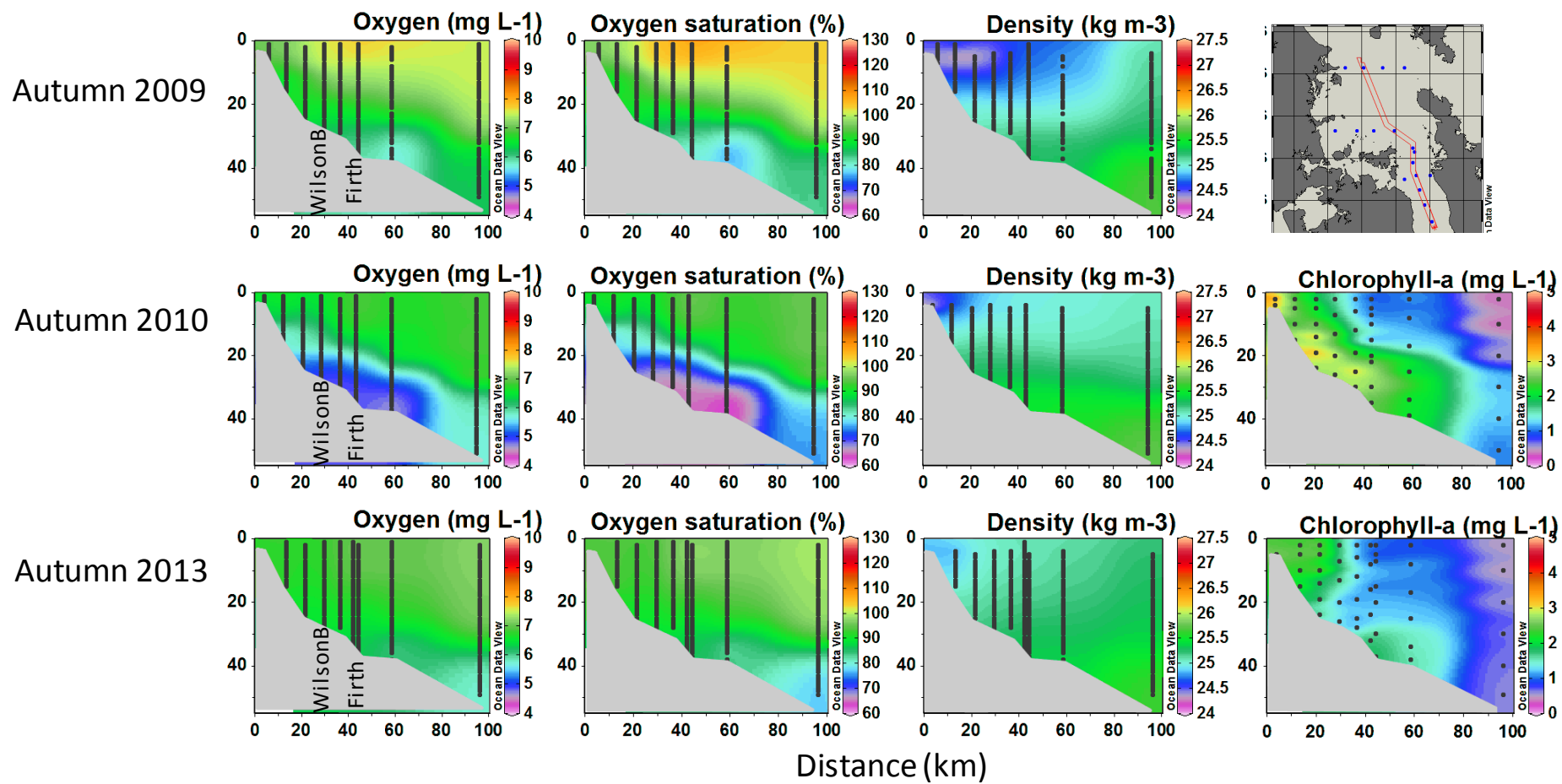
Firth of Thames Water Quality and Ecosystem Health – Data Report

Figure 7-9: **Oxygen, physical structure and phytoplankton in the Firth of Thames and Hauraki Gulf in autumn 2009, 2010 and 2013.** Shown are oxygen concentration, oxygen saturation, seawater density and chlorophyll *a* at stations indicated in the inset map. The extended-Firth monitoring site and Wilson B mooring site are labelled in the left panels.
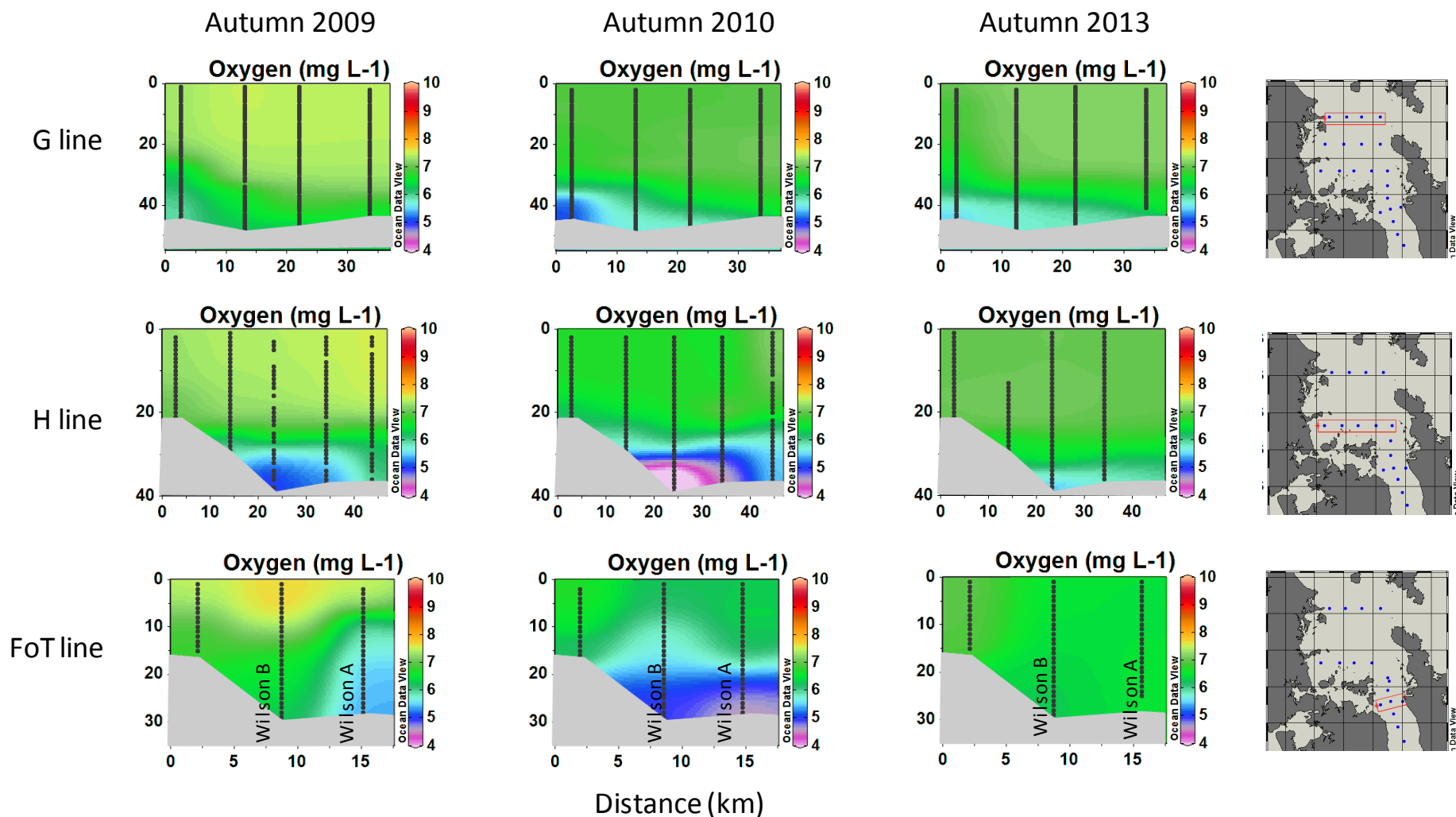
Figure 7-10:   Oxygen in the Firth and Hauraki Gulf in autumn 2009, 2010 and 2013. Shown are oxygen concentrations (mg O_2 L^{-1}) for 3 latitudinal sections, at stations within red rectangles on the maps. The Wilson B mooring site and the station at the northern end of Wilson Bay Area A are labelled in the FoT line panels.

8 pH

Atmospheric carbon dioxide (CO_2) and CO_2 generated by the respiration of organic matter in the ocean enter the aqueous carbonate system. As CO_2 concentration in the ocean increases (due to, for instance, increasing atmospheric CO_2 or an increase in primary productivity that leads to a higher organic matter loading in the water column) pH decreases, signifying acidification. This reduces the concentration of carbonate ions available for calcification, thus lowering calcium carbonate saturation state (Sunda and Cai, 2012; Waldbusser and Salisbury, 2014). From the perspective of an organism that requires calcium carbonate, decrease in saturation state is potentially deleterious as it demands that more energy be diverted to building shell at the expense of other key metabolic processes (Provoost et al., 2010; Capson and Guinotte, 2014). Negative effects of acidification also include direct effects on metabolism (Kroeker et al., 2010) and behaviour (Munday et al., 2010).

8.1 Overview of data sources

In this section we list sources of data presented in this chapter. Unless otherwise specified data were collected and are owned by NIWA.

- Voyage in autumn 2010 (KAH1002), comprising underway sampling and sampling with a CTD at stations.

- 4 seasonal voyages in 2012–13, comprising underway sampling and sampling with a CTD at stations.

  o Spring – voyage KAH1209. Summer – voyage KAH1311. Autumn – voyage KAH1304. Winter – voyage KAH1306.

8.2 Methods

Carbonate system parameters (pH, partial pressure of CO_2 [pCO_2], dissolved inorganic carbon [DIC] and total alkalinity) were surveyed over the Firth and Hauraki Gulf during voyages in autumn 2010, and during 4 seasonal voyages in 2012–13.

The voyage dates were:

- Autumn 2010 (KAH1002) 9-12 March 2010

- Spring 2012 (KAH1209) 5-8 October 2012

- Summer 2013(KAH1311) 12-15 December 2013

- Autumn 2013 (KAH1304) 17-20 March 2013

- Winter 2013 (KAH1306) 15-18 July 2013

Two sampling methods were used:

- underway mapping of the properties near the sea surface (2 m) while the ship steamed over the region and

- CTD sampling of properties within the water column at grids of stations over the region.

The underway sampling (Figure 8-1) included temperature, salinity, chlorophyll *a*, coloured dissolved organic matter and turbidity (backscatter measured at 660 nm) sampled at the same rates as pCO_2

(10-s intervals). The former variables were sampled using a Seabird thermo-salinograph and a Wet Labs EcoTriplet fluorometer. During these surveys the ship stopped at 17 stations for the discrete CTD sampling of the water column for DIC and alkalinity to resolve depth distributions of carbonate parameters.

Details of the analytical procedures for the carbonate system analysis are given in Appendix F. These include the calculation of underway alkalinity and pH from salinity and pCO_2. Discrete CTD samples were used to calculate surface and bottom water pCO_2, pH, aragonite saturation (Ω_a), as well as calcite saturation (Ω_c) from measured alkalinity and DIC using the CTD temperature, salinity and depth values.

Figure 8-1: **Underway sampling and shipboard laboratory.** (Left) Water was pumped aboard via a towfish and hose assembly, and (right) sent to the shipboard LiCor CO_2 analyser and filtration laboratory.

8.3 Results

8.3.1 Underway surveys

Water-quality properties measured in the underway sampling of surface waters during the 2012–13 4-season surveys are shown in Figure 8-2 to Figure 8-5, which show the following features:

- Temperature followed a predictable seasonal pattern, being low in spring, increasing through summer and autumn, and lowest in winter. Temperatures in the Firth of Thames were lower than in the Hauraki Gulf in winter, and warmer than in the Hauraki Gulf in summer and autumn.

- Salinity was relatively stable in the Hauraki Gulf, but varied widely in the Firth of Thames. In autumn, salinity was higher in the Firth of Thames than it was in other seasons, reflecting low river runoff prior to the survey.

- Coloured dissolved organic matter (CDOM) was higher in all areas in winter and spring but decreased in the Hauraki Gulf in summer and autumn. Firth of Thames CDOM was higher than it was in the Gulf in all seasons, with an increasing shoreward gradient reflecting riverine organic matter supply and higher inshore productivity patterns.

- Chlorophyll *a* was higher in spring than in other seasons across the region, reflecting the spring bloom. It decreased in the Hauraki Gulf in other seasons, again creating an increasing gradient towards the Firth of Thames (strongest in autumn). Chlorophyll *a* was lowest across the region in summer.

- Backscatter (turbidity) varied relatively little by season, but always had a marked increasing gradient toward the southern Firth of Thames. In the Firth of Thames, turbidity was highest in autumn when chlorophyll *a* was highest and in winter when river runoff increased.

- The partial pressure of CO_2 (pCO_2) was near or below atmospheric pressure (~ 390 µatm) in spring, reflecting spring-bloom drawdown by actively growing phytoplankton. pCO_2 started to increase in summer and then peaked in autumn, with maximum values in the Firth of Thames (about 550 µatm). Values were lowest in winter, being under-saturated with respect to the atmosphere over most of the region, when the water column was well mixed and phytoplankton were moderately abundant.

- In summer and especially in autumn, there was a consistent decreasing seaward gradient in surface pCO_2, with maximal DIC oversaturation in the Firth of Thames, moderate oversaturation in the extended Firth of Thames, and values near neutral (atmospheric) in the Hauraki Gulf.

- pH showed similar seasonal and spatial gradients as pCO_2. pH was near oceanic values (~8.05–8.1) in spring over the whole region, but started dropping in summer in the Firth of Thames. pH reached minimum values of ~7.92 in the Firth of Thames in autumn. pH increased in winter toward oceanic values. There was a decreasing gradient (corresponding to increasing acidity) from the Hauraki Gulf into the Firth of Thames in all seasons, strongest in autumn.

An underway survey was also conducted in autumn 2010. In that survey, pCO_2 was higher than in autumn 2013 (by 25–50 µatm), but otherwise the two surveys showed an almost identical pCO_2 gradient from the Hauraki Gulf into the Firth of Thames (Figure 8-6).
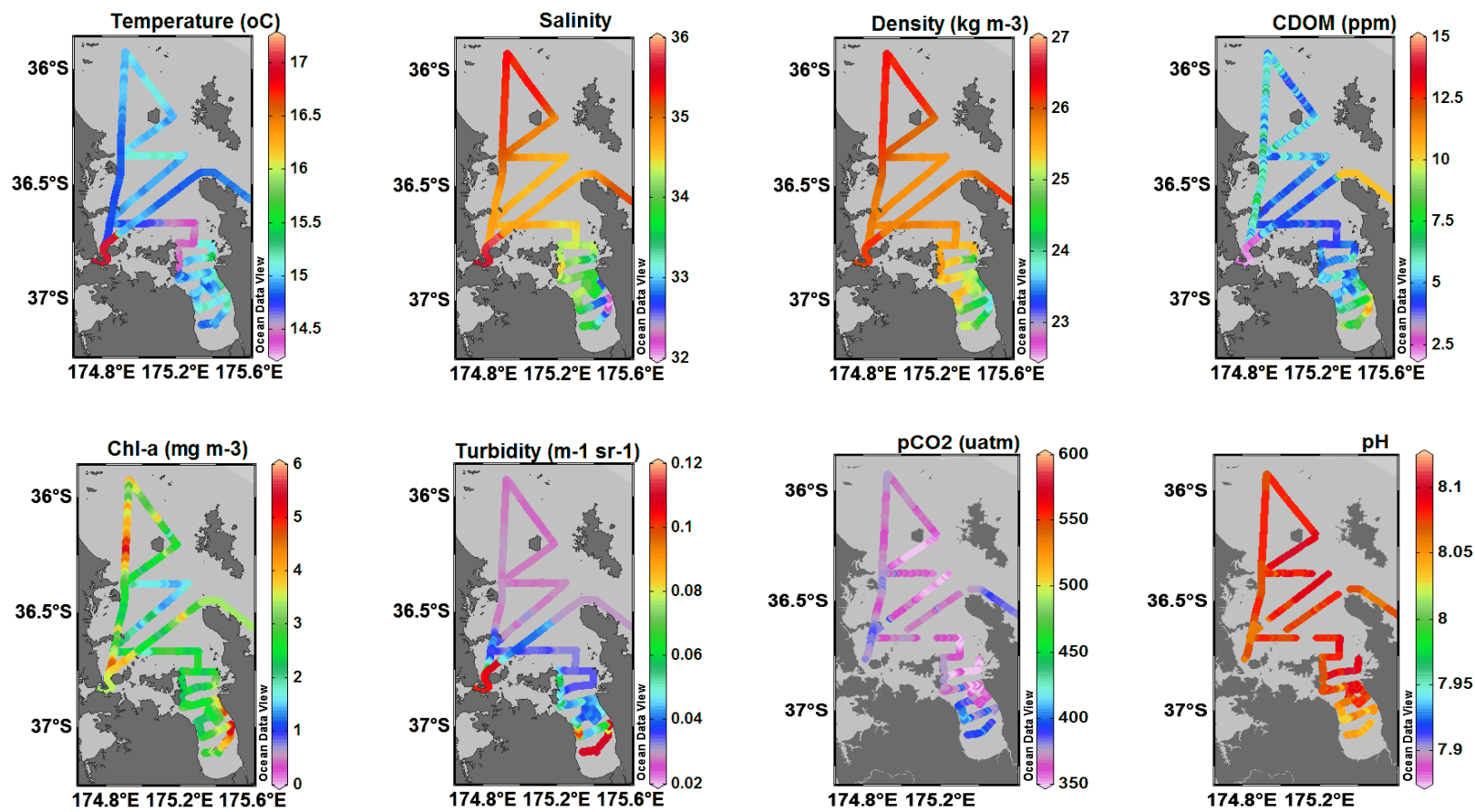
- pH in autumn 2010 was generally lower than in 2013.

Figure 8-2: **Spring (KAH1209) underway sampling results.** Ribbon plots of surface water properties for temperature, salinity, water density, coloured dissolved organic matter (CDOM), chlorophyll *a*, turbidity (backscatter), partial pressure of CO_2 and pH.

Figure 8-3: **Summer (KAH1311) underway sampling results.** Ribbon plots of surface water properties for temperature, salinity, water density, coloured dissolved organic matter (CDOM), chlorophyll *a*, turbidity (backscatter), partial pressure of CO_2 and pH.
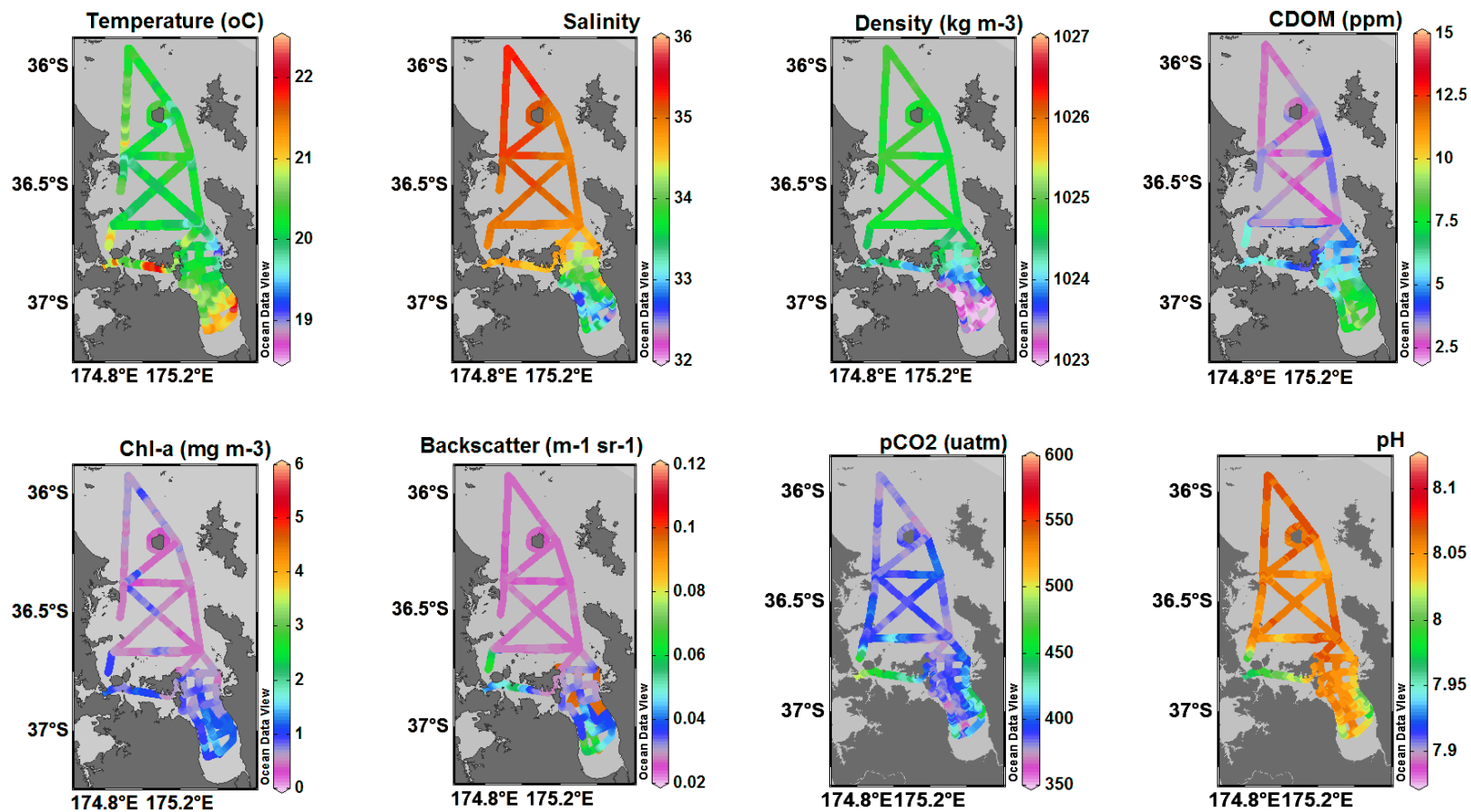
Figure 8-4: **Autumn (KAH1304) underway sampling results.** Ribbon plots of surface water properties for temperature, salinity, water density, coloured dissolved organic matter (CDOM), chlorophyll *a*, turbidity (backscatter), partial pressure of CO_2 and pH.

Firth of Thames Water Quality and Ecosystem Health – Data Report

Figure 8-5: Winter (KAH1306) underway sampling results. Ribbon plots of surface water properties for temperature, salinity, water density, coloured dissolved organic matter (CDOM), chlorophyll *a*, turbidity (backscatter), partial pressure of CO_2 and pH.
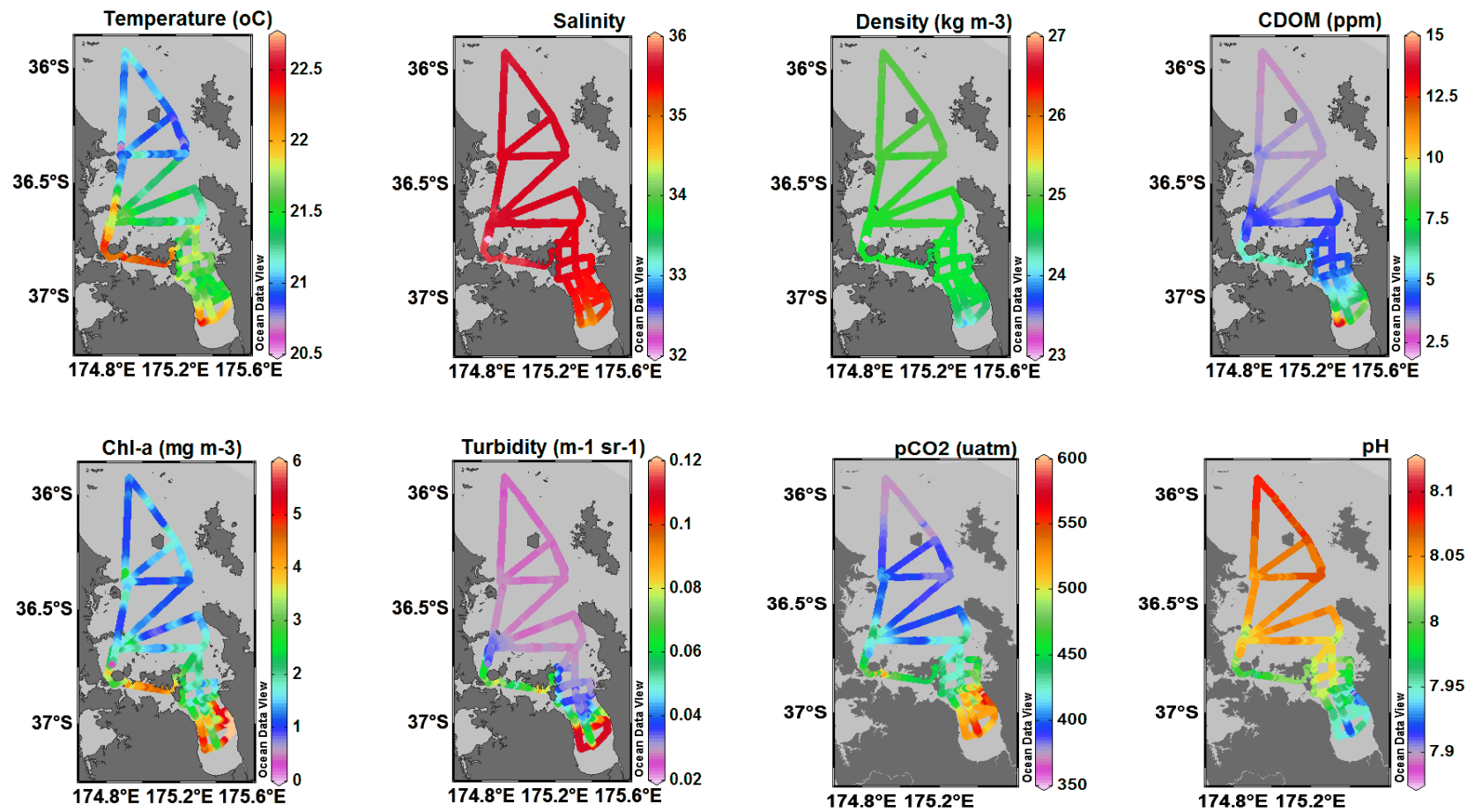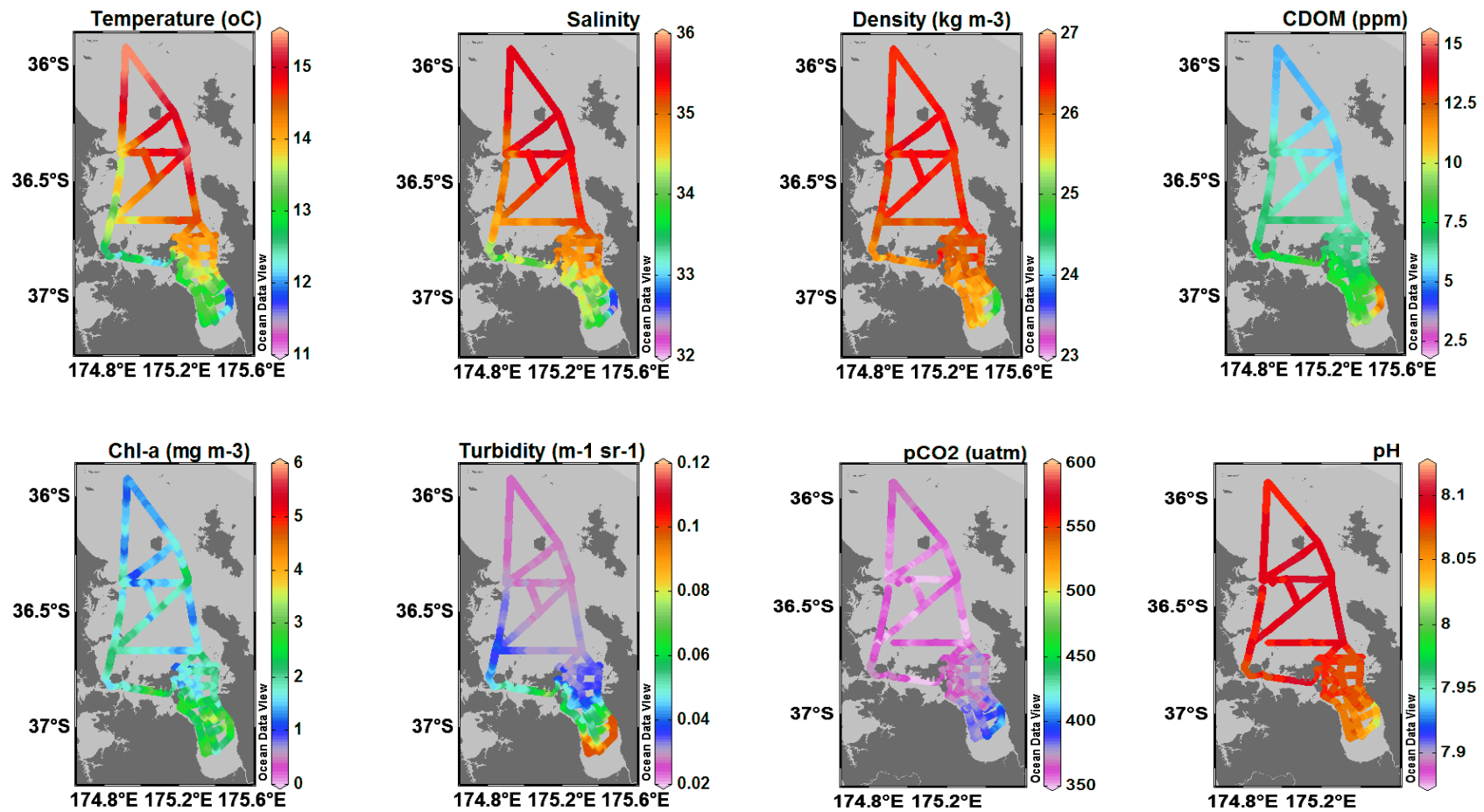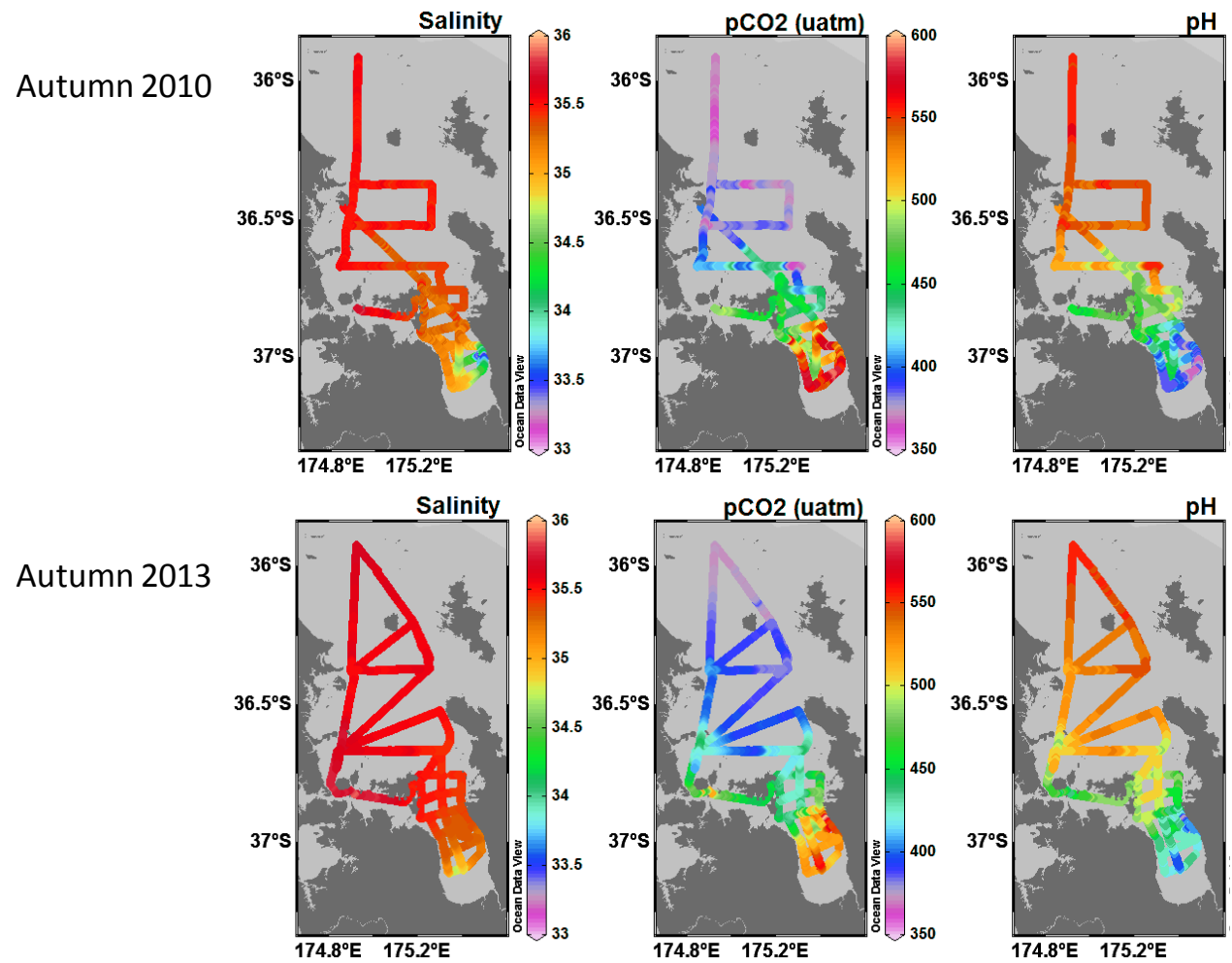
Figure 8-6: Salinity, pCO$_2$ and pH compared in two autumn surveys, 2010 (KAH1002) and 2013 (KAH1304).

8.3.2 Discrete surveys

Carbonate system parameters were discretely sampled using a CTD near the surface and near the seabed during the 4-season surveys (Figure 8-7). The samples allowed for the calculation of the saturation state of aragonite (Ω_{Ar}), which is a measure of the thermodynamic stability of calcium carbonate ($CaCO_3$).

The results show:

- Discrete pCO_2 samples followed the pattern shown by the underway sampling, with highest values in autumn (up to 550 µatm) and highest values in the Firth of Thames.

- pCO_2 was about 25 to 100 µatm higher near the seabed than near the sea surface in spring and summer. Near-seabed and near-surface values were similar to each other in autumn and winter.

- Discrete pH also followed these seasonal patterns, with contrast between the upper and lower water column being less in autumn and winter.

- The contrasts in vertical distribution of pCO_2 and pH with season were probably sustained by higher phytoplankton concentrations/abundance in spring and summer, which reduced CO_2 (and increased pH) in the upper water column.

- Saturation state (Ω_{Ar}) showed less contrast among the seasons than did pCO_2 or pH. There was a decreasing gradient in Ω_{Ar} from the Hauraki Gulf into the Firth of Thames. Offshore, Ω_{Ar} was in the range 2.8–3.0, and in the Firth Ω_{Ar} was in the range 2.3–2.4.

- Ω_{Ar} sampled in autumn 2010 (Figure 8-8) was lower than in autumn 2013, reaching minimal values of ~1.8. Ω_{Ar} was typically ~2.1–2.3 in the Firth.

8.3.3 Trend analyses

The time series measurements of pH data are not long enough to conduct trend analysis.
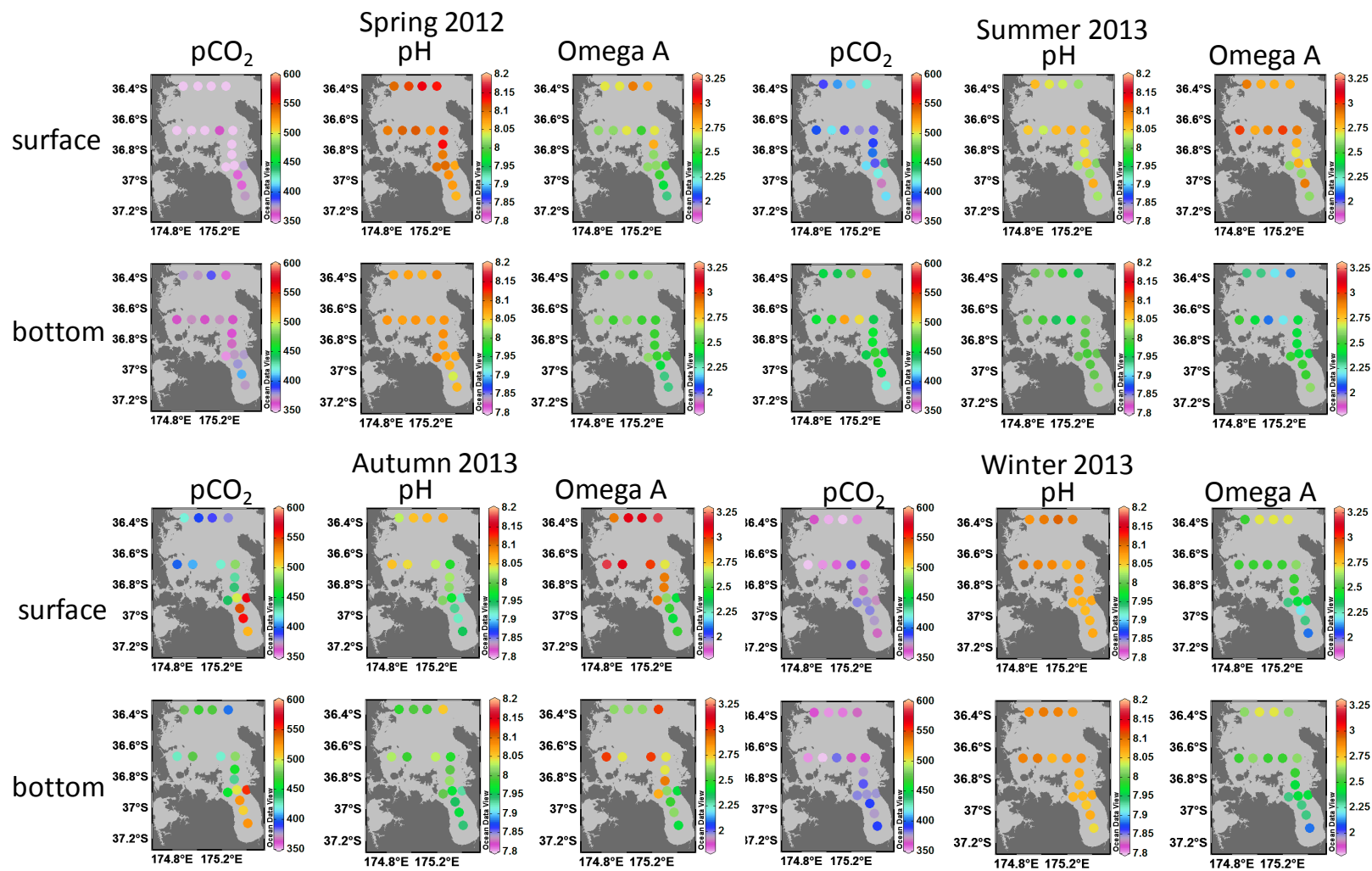
Figure 8-7: **Partial pressure of CO₂ (pCO₂), pH and saturation state of aragonite (Ω_Ar) during the 4-season survey.** Data are shown for near-surface and near-seabed.

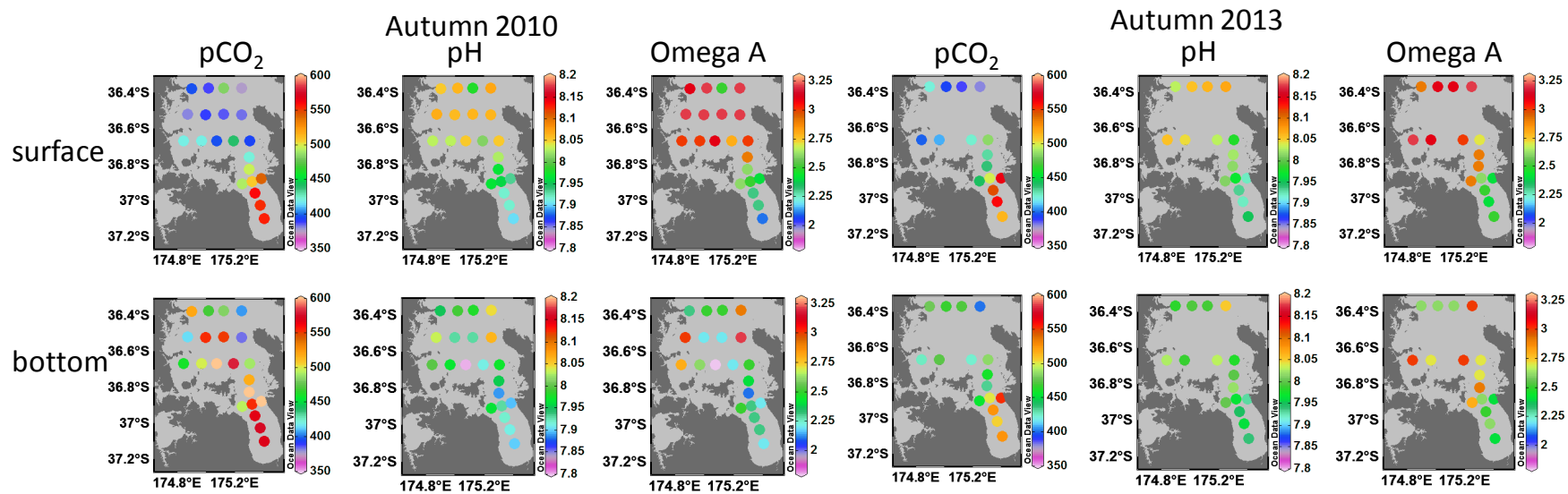Firth of Thames Water Quality and Ecosystem Health – Data Report

Figure 8-8: Partial pressure of CO_2 (pCO_2), pH and saturation state of aragonite (Ω_{Ar}) during autumn 2010 and autumn 2013 surveys. Data are shown for near-surface and near-seabed.

9 Benthic and pelagic mineralisation

9.1 Overview of data sources

In this section we list sources of data presented in this chapter. Unless otherwise specified data were collected and are owned by NIWA.

- Voyages KAH0310 in December 2003 and KAH1202 in March 2012 visiting subtidal sites around the Firth and extended Firth.

- Voyage TAN9915 north of the Mokohinau Islands in a water depth of 125 m (site 5, 35° 48.83'S, 175° 1.83'E).

- NIWA biogeochemical study in the Firth in May 2012, sites in the inner and extended Firth.

9.2 Benthic mineralisation

Shipboard sediment community oxygen consumption (SCOC[46]) measurements have been undertaken at several subtidal sites and times throughout the Firth and wider Hauraki Gulf since 1999. These include the NIWA voyages KAH0310 in December 2003 and KAH1202 in March 2012 around the Firth and extended Firth (Figure 9-1), and NIWA voyage TAN9915 north of the Mokohinau Islands.

---

[46] Sediment community oxygen consumption has become a standard approach for estimating carbon and energy requirements of sediment-dwelling organisms within aquatic sediments. It is generally assumed that SCOC at shallow depths is a direct estimate of the coupling between benthic and pelagic processes. Rowe, G. et al. (2008), Deep Sea Research Part II, Topical Studies in Oceanography, 55: 2686–2691.
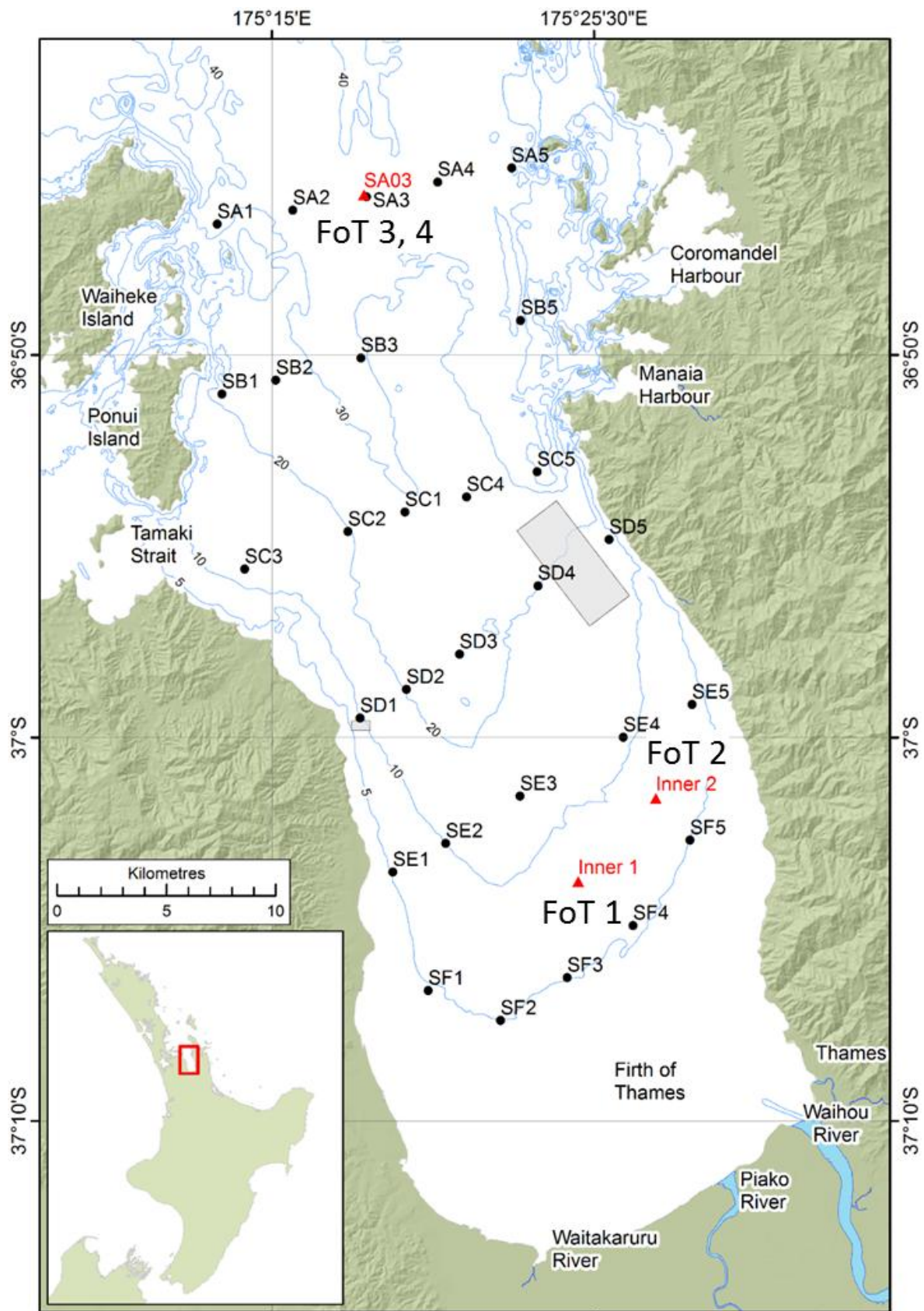
Figure 9-1: **Locations of sites sampled in December 2003 (black dots) and March 2012 (red triangles) in Firth of Thames.** Note that sites FoT1 and FoT2 are at locations inner 1 and 2, respectively, and sites FoT3 and FoT4 are both at location SA03. Mussel farms are depicted as grey boxes.

On KAH0310, samples were obtained using an Ocean Instruments MC-800 multi-corer with eight 10 cm diameter sampling tubes, which is designed to sample the sediment–water interface with minimal disturbance. On KAH1202, a similar diameter mini-multi-corer (KC Denmark Model 71.000) was used. Figure 9-2 shows some images of shipboard handling of cores.

Figure 9-2:   Sediment sampling in the Firth. Multi-coring device retrieved onto the ship with sediment cores. Upper right: sediments being extruded to incubation cores. Lower right: core surface showing intact surface faunal structure.

After siphoning off the overlying seawater, sediment samples were then either:

- sliced at set intervals (0.5 or 1 cm thick slices) for analysis of physical and biogeochemical parameters (e.g., grainsize, total organic matter, calcium carbonate content, organic carbon, nitrogen, phosphorus and phytopigments);

- subsampled for biological components of the seabed community (e.g., meiofauna, macro-infauna); and/or

- extruded into chambers and used in shipboard incubation experiments to derive fluxes of key biogeochemical elements (e.g., oxygen, nutrients, dissolved inorganic carbon).

An additional sample was collected on the shelf during NIWA voyage TAN9915 north of the Mokohinau Islands in a water depth of 125 m (site 5, 35° 48.83'S, 175° 1.83'E).

For information on the KAH0310 sediment core oxygen consumption (SCOC) incubations refer to Giles et al. (2007). As far as practicable, the same methods for SCOC determinations were employed on KAH1202, with additional analyses also undertaken to determine dissolved inorganic nutrient fluxes, which focused on nitrate + nitrite (NO_x-N), ammoniacal nitrogen (NH_4-N) and dissolved reactive phosphorus (DRP). Assay methods for nutrient incubations were conducted using the standard laboratory protocols of the NIWA Hamilton Water Quality Laboratory. Seawater samples from the sediment incubation chambers were filtered immediately (1.2 μm pore size GF/F glass micro-fibre filter) and then frozen until analysis for NH_4-N, NO_x-N, DRP and Total Dissolved Nitrogen using standard methods for seawater (Grasshoff et al., 1983). Nutrient and dissolved oxygen fluxes were derived from the differences in solute concentrations in the seawater overlying the sediment before and after the incubation period.

Data collected in December 1999 (voyage TAN9915) and December 2003 (voyage KAH0310) were summarised by Giles et al. (2007), who showed that there was a distinct gradient of decreasing SCOC progressing from the Firth out into the Gulf and onto the northeast shelf and slope (Figure 9-3). These results showed that benthic remineralisation of organic matter is most active inshore.
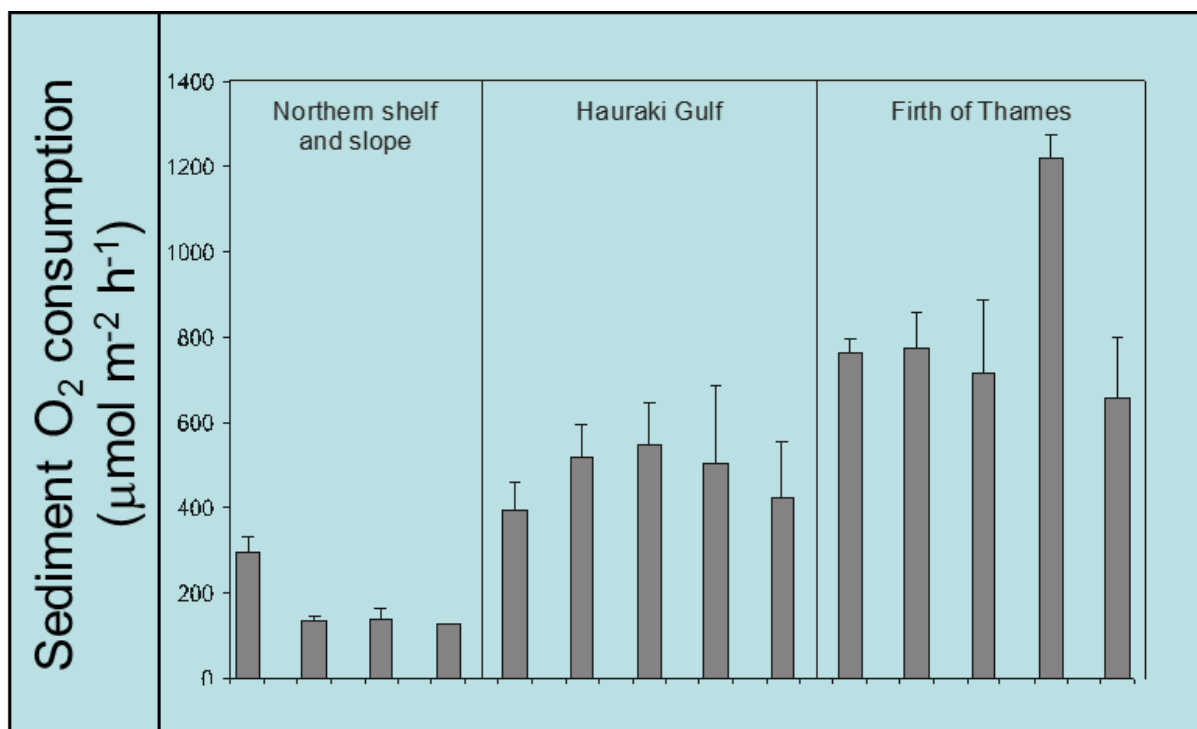

Figure 9-3: **Dark sediment oxygen consumption across the Firth, Hauraki Gulf, shelf and slope.** From Giles et al. (2007), data collected in December 1999 and December 2003.

The data collected in the Firth in December 2003 (transects SF, SD and SA: Figure 9-1) showed that dark SCOC rates were similar across the Firth, typically varying between 600 and 800 μmol O_2 m^{-2} h^{-1}, with values up to 1200. The highest value was measured at shallow site SF2. Data collected in March 2012 (voyage KAH1202) revealed similar trends, with highest values of between 1200 and 1800 μmol O_2 m^{-2} h^{-1} at the inner Firth sites, decreasing to 750–830 at the extended Firth (site SA3: Figure 9-4). These values were similar to those found by Giles et al. (2006) at reference sites in the central Firth, used in a study of sedimentation effects at mussel farms.
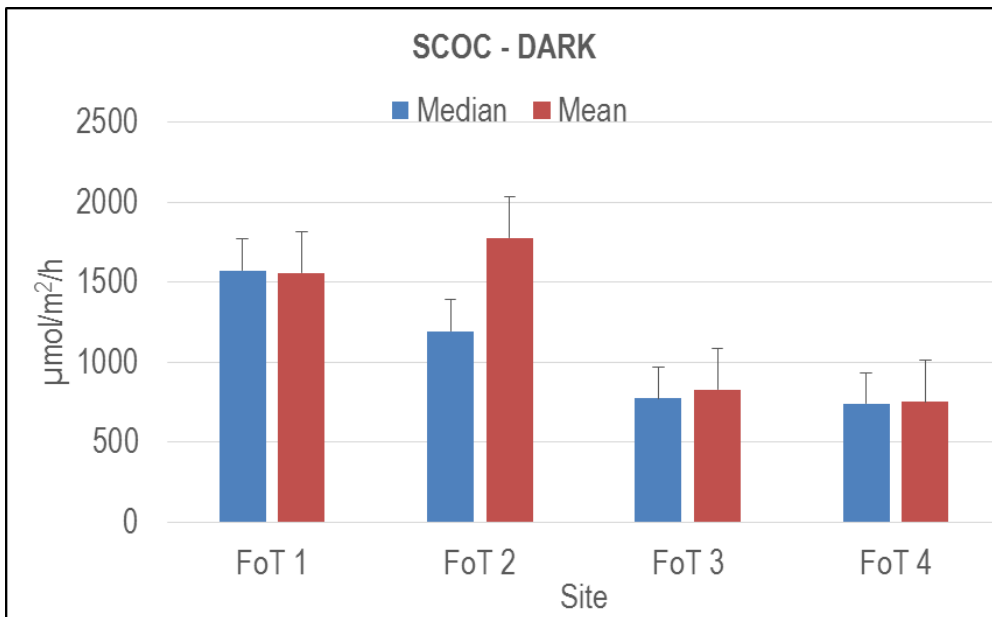
Figure 9-4: **Sediment community oxygen consumption (SCOC) during dark incubations at sites in the inner (FoT1 and FoT2) and extended (FoT3 and FoT4) Firth in March 2012 (voyage KAH1202).** Shown are medians (blue, ± 1 median absolute deviation from median) and means (red, ±1 standard deviation). Note that values are negative, i.e., fluxes are into the sediments. Refer to Figure 9-1 for site locations.

Both light and dark SCOC incubations were undertaken during March 2012, enabling the production and consumption of oxygen to be measured. Oxygen production is largely a function of the benthic micro-algal (BMA) activity, and was highest at the inner Firth sites (median 507 ± 212 μmol O_2 m^{-2} h^{-1} at inner FoT1 and 182 ± 42 at inner FoT2, compared to 81 ± 17 at FoT3 and 125 ± 38 at FoT4). These estimates were used to calculate the net diurnal oxygen flux, which showed that at all sites there was net oxygen consumption by the sediments (i.e., respiration exceeded production). Net daily oxygen consumption by sediments was typically two times higher at the inner Firth sites, compared to the extended Firth (Figure 9-5).
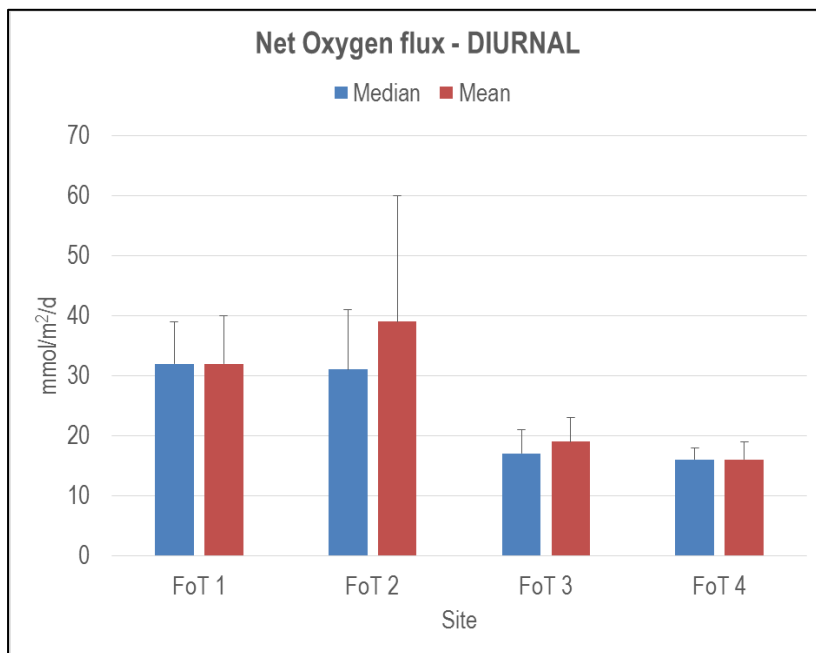
Figure 9-5: **Daily net oxygen fluxes at sites in the inner (FoT1 and FoT2) and extended (FoT3 and FoT4) Firth in March 2012 (voyage KAH1202).** Shown are medians (blue, ±1 median absolute deviation from median) and averages (±1 standard deviation). Note that positive values indicate fluxes into the sediments. Refer to Figure 9-1 for site locations.

Nutrient fluxes measured during SCOC incubations in March 2012 showed that ammonium fluxes were 2–4 times higher at the shallower inner Firth sites compared to the extended Firth (Figure 9-6). Dark ammonium fluxes were similar in magnitude and identical in sign (i.e., efflux) to the light incubations (data not shown), showing the minor influence that BMA had on exchange of nutrients across the sediment–water interface (Giles et al., 2006). This was not unexpected, given the relatively small benthic production that was measured under light incubations (not shown). The inner Firth fluxes were similar to those recorded by Giles et al. (2006) in the mid-Firth at their reference sites.
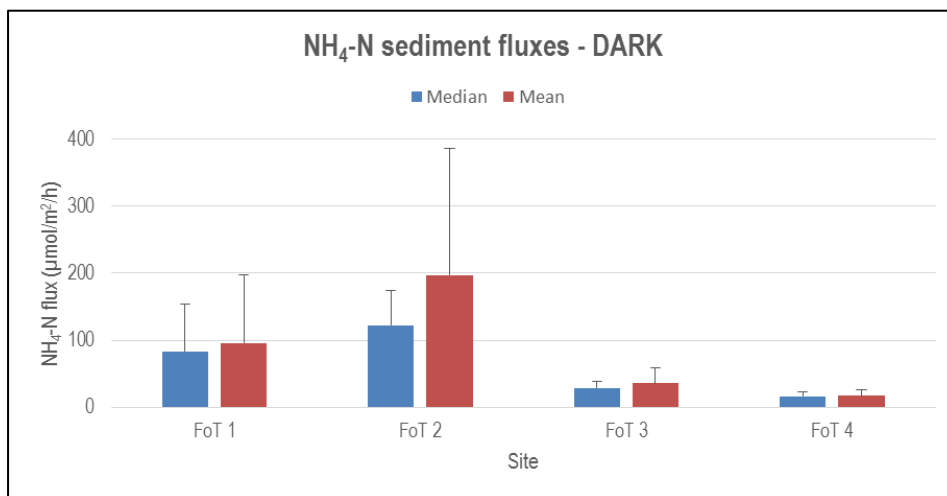
Figure 9-6: **Ammonium (NH$_4$-N) fluxes during dark incubations at sites in the inner (FoT1 and FoT2) and extended (FoT3 and FoT4) Firth in March 2012 (voyage KAH1202).** Shown are medians (blue, ±1 median absolute deviation from median) and averages (±1 standard deviation). Note that positive values indicate fluxes into the sediments. Refer to Figure 9-1 for site locations.

Porewater concentrations of ammonium at both inner and extended Firth sites increased down to a depth of 50 mm, whereupon ammonium concentrations continued to increase at the shallow sites to a maximuim measured concentration of 140 µmol L^{-1}. In comparison, ammonium concentrations at the extended Firth sites remained constant at ~40 µmol L^{-1}, down to 100 mm sediment depth (Figure 9-7).

Figure 9-7: **Down-core porewater ammonium concentrations in the inner and extended Firth (denoted by "outer (Hauraki Gulf)" in the figure), measured during KAH1202**. Refer to Figure 9-1 for site locations.

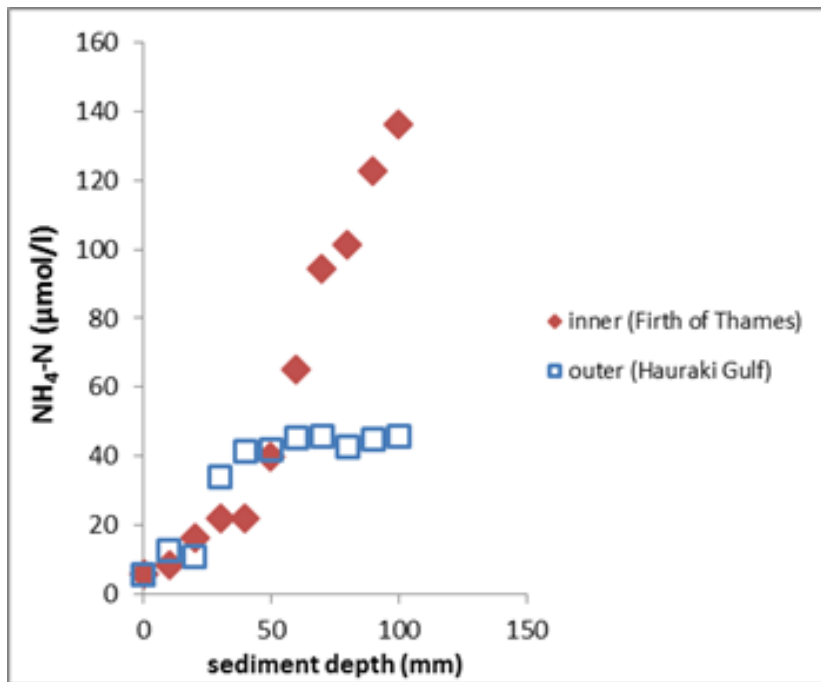Nitrate and dissolved reactive phosphate (DRP) fluxes were also measured during the shipboard sediment core incubations. Median nitrate fluxes were between 2±2 and 5±6 μmol m^{-2} h^{-1}, while DRP fluxes were more variable, ranging from 0.2±0.5 to 7±3 μmol m^{-2} h^{-1} at the inner and extended Firth sites (data not shown). These fluxes were comparable those measured by Giles et al. (2006). The daily fluxes of these nutrients were small and similar in magnitude with a maximum rate of only 0.1 mmol DRP m^{-2} d^{-1}.

Giles et al. (2007) showed that across the NE shelf SCOC rates were significantly negatively correlated with water depth ($p < 0.01$ for dark SCOC; $p < 0.05$ for light SCOC), being highest at shallow Firth sites and lowest at outer shelf and upper slope depths (Figure 9-3). Because of this gradient, dark SCOC was also negatively correlated with CaCO$_3$ content ($p < 0.01$), and positively correlated with POC ($p < 0.01$), PON ($p < 0.01$), sediment chlorophyll *a* ($p < 0.001$), phaeopigments ($p < 0.001$) and silt/clay fraction ($p < 0.05$) all of which had clear on–offshore gradients. Light SCOC was correlated positively only with sediment chlorophyll *a* concentration ($p < 0.05$).

BMA have been shown to contribute significantly to primary production in shallow systems, often up to 60%, (e.g., Underwood and Kromkamp, 1999). On the March 2012 voyage, the degree of benthic primary production by BMA was measured using gross oxygen production (light oxygen production minus dark oxygen production, and assuming that dark respiration levels are the same as light respiration levels). Figure 4-14 shows that considerably more BMA exist in the inner Firth (sites FoT1, FoT2) than at the deeper extended Firth (sites FoT3, FoT4), which is consistent with the gradient in benthic light availability between these areas (Figure 6-4). Irrespective, inner Firth BMA gross production was minimal in light, and oxygen fluxes under light and dark conditions were similar. This was likely due to the high turbidity in the inner Firth subtidal water column: water column light attenuation measured during primary-production experiments (see section 6.3) showed high light attenuation in the inner Firth (0.8 m^{-1}) compared to the extended Firth (0.2 m^{-1}).

As such, the inner Firth sediments showed a net consumption of oxygen overall (i.e., net heterotrophy). Across all Firth sites, production to respiration ratios (P:R) were less than 0.2 (Figure

9-8: based on 12:12 h light:dark incubations). It is therefore apparent that the Firth benthos is strongly respiration-dominated (Cook et al., 2004), regardless of water depth and/or sediment characteristics. In comparison, net oxygen production is commonly found in other estuarine systems in New Zealand known to host significant microalgal populations, e.g., Ngamahau Bay, Tory Channel, Marlborough Sounds (Gillespie et al., 2000) and Avon-Heathcote Estuary (C. Depree, NIWA, unpublished data).
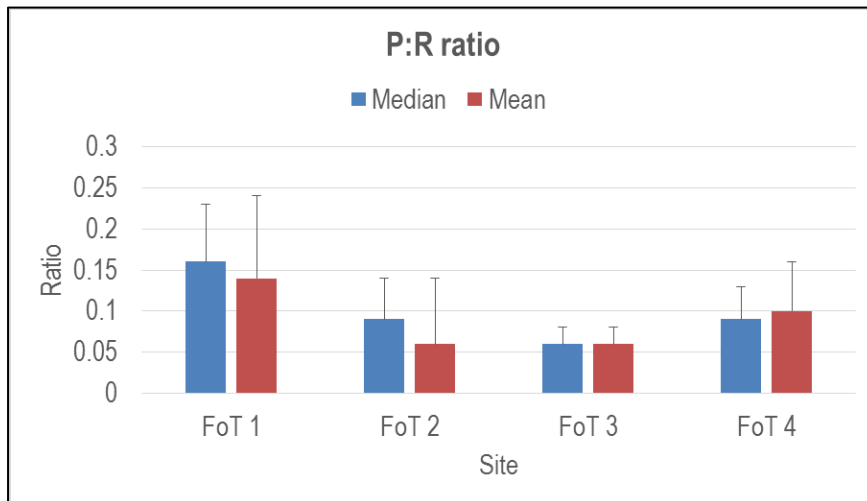

Figure 9-8: **Production to respiration ratios (P:R) from shipboard incubations at sites in the inner (FoT1 and FoT2) and extended (FoT3 and FoT4) Firth in March 2012 (voyage KAH1202).** Shown are medians (blue, ±1 median absolute deviation from median) and averages (±1 standard deviation). Ratios < 1 indicate net heterotrophy and ratios > 1 indicate net autotrophy. Refer to Figure 9-1 for site locations.

During a separate NIWA biogeochemical study in the Firth in May 2012, inner and extended Firth sites were sampled and the sediments were analysed for numerous parameters including porewater (e.g., nutrients, Fe/Mn, sulphide) and sediment sulphide phases (chromium reducible sulphides [CRS] and acid volatile sulphide [AVS]), reactive iron and general bulk sediment properties (Clearwater and Depree, NIWA, unpublished data). Differences between inner and extended Firth sediments were apparent from the visual appearance of sediment cores (Figure 9-9). The inner site sediments were largely composed of mud-sized particles, consistent with previous observations in the vicinity (see section 4.8.2) and, at time of sampling (autumn), a pronounced apparent redox potential discontinuity (aRPD) layer was evident (at about 50 mm below surface). Above this discontinuity the sediment had the characteristic orange colour of Fe(III) and below this layer the sediment was dark grey to black, indicative of sulfidic phases (e.g., iron monosulfide [FeS] and pyrite [FeS_2]). These sulphide phases are formed from the reaction of sulphide (formed from anoxic sulphate reduction of organic matter) and Fe(II) present in the sediment. Typically, the higher the loading of organic matter, the greater the 'shortfall' of oxygen for oxic respiration, and hence the greater the proportion of organic matter that is mineralised via anoxic pathways (Canfield et al., 2005).
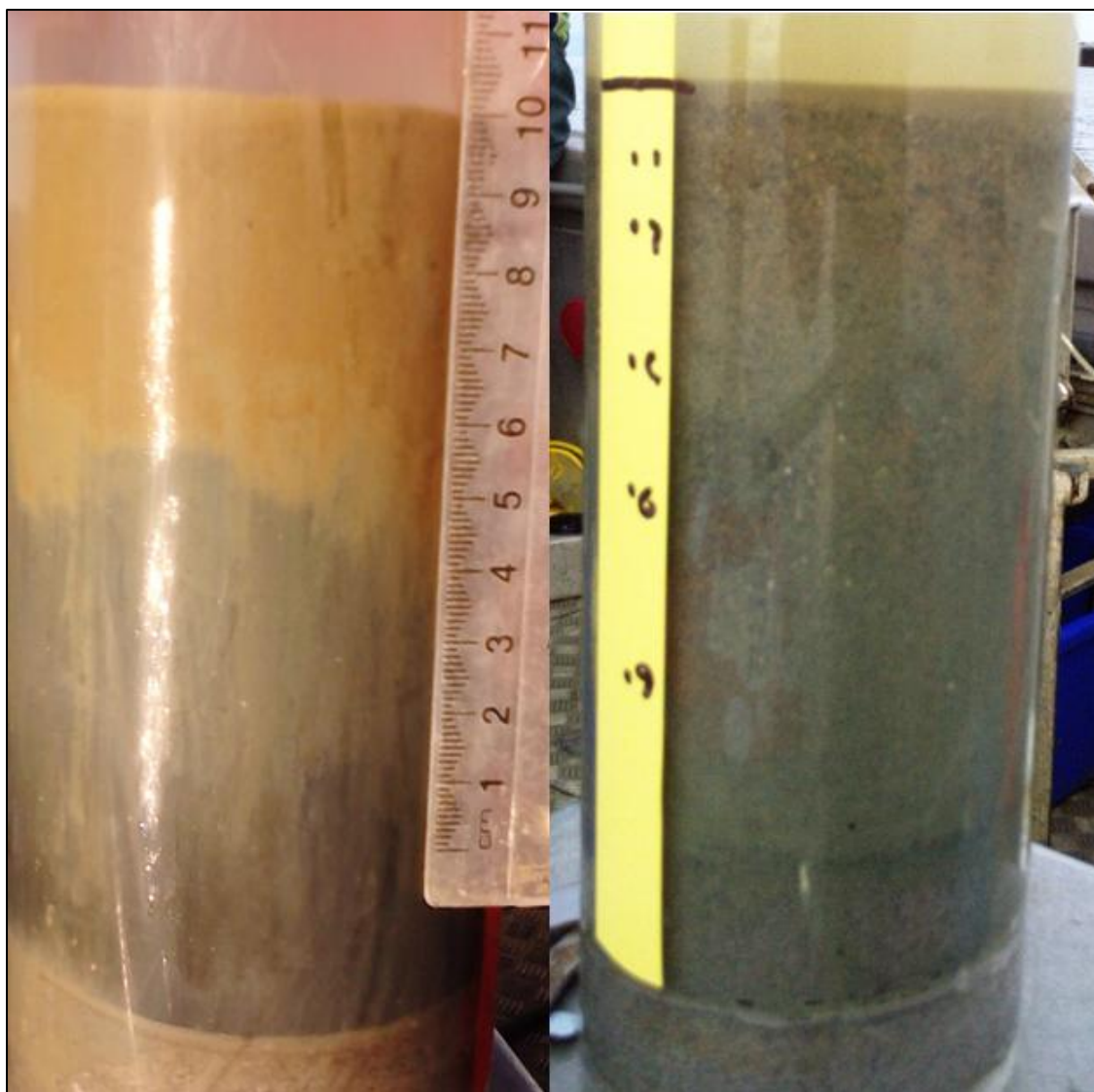
Figure 9-9: **Photographs comparing sediment cores from inner (left) and extended (right) Firth of Thames sites.** Samples were collected and analysed in May 2012 (Clearwater and Depree, NIWA, unpublished data).

In contrast to the inner Firth, the extended Firth sediments were dominated by sand-sized particles and an absence of an aRPD boundary, indicating much lower organic matter loading rates and hence lower sediment oxygen demand, which is consistent with measured SCOC rates (Figure 9-4). These results confirm that there were biogeochemical differences between the extended and the inner Firth sediments, with inner-Firth sites having higher concentrations of reduced species (i.e., sulphides) and elevated ammonium concentrations compared to extended-Firth sites (Figure 9-10). Consistent with the aRPD layer in inner Firth sediments occurring at a sediment depth of approximately 50 mm, sulphide was only detected in the 80 mm-deep sediment layer and not in the surface sediments (20 mm depth). The concentrations of porewater sulphides at 80 mm depth in these inner Firth sediments were very low (14 µmol). It appears that the large sediment pool of reactive Fe (and Mn) in the inner Firth sediments may provide considerable capacity to immobilise toxic soluble sulphides via reaction with Fe(II) to form insoluble sulphides (e.g., iron monosulfides and pyrites).
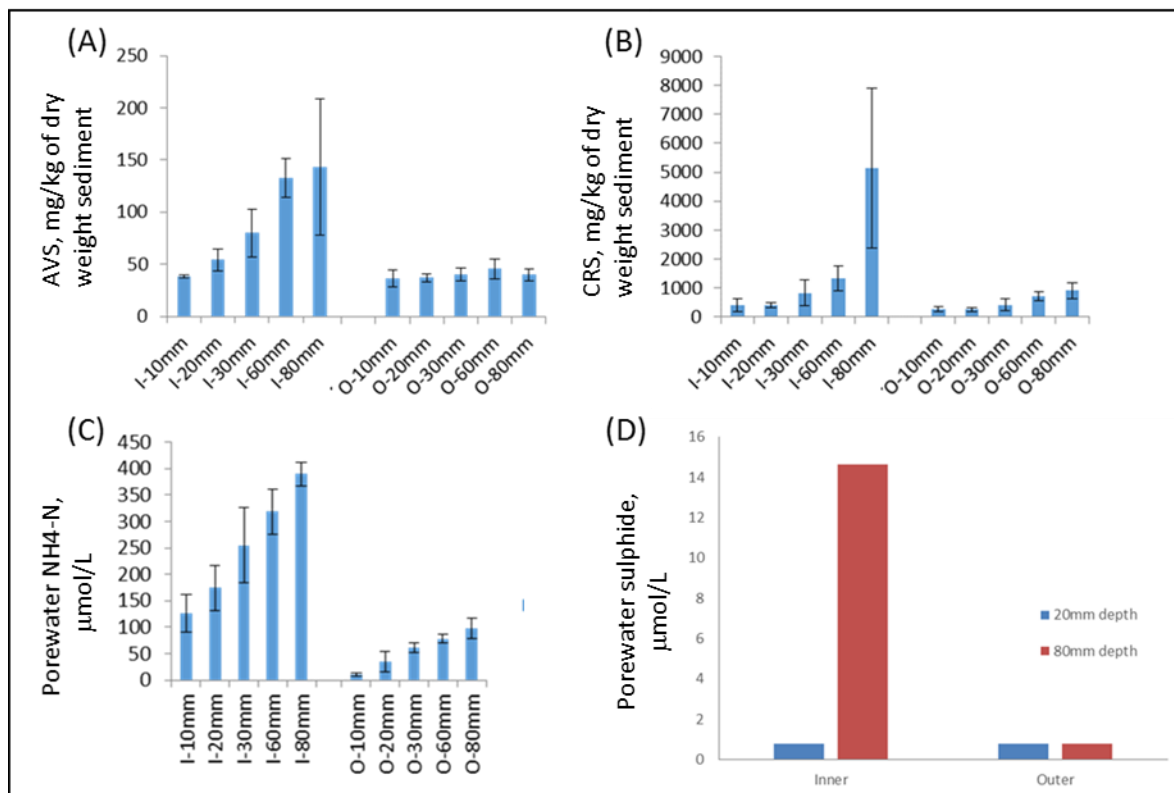
Figure 9-10:   Various biogeochemical metrics of organic matter loading in Firth of Thames sediments. (a) Acid volatile sulphides (AVS); (b) chromium reducible sulphides (CRS); (c)) porewater ammoniacal-nitrogen (NH_4-N); (d) porewater sulphides. I = inner, O = extended Firth sites, with five sediment depth fractions of 10, 20, 30, 60 and 80 mm.

9.3   Pelagic mineralisation

During March 2012 (voyage KAH1202), measures of oxygen evolution and uptake were made in shipboard incubations at the inner and extended Firth sites (FoT 1-4: see Figure 9-1). Upper water-column (euphotic zone) water and deep water-column (just above bottom) water were examined separately. Samples were dispensed into 25 mL vials and their oxygen levels monitored over the following 24 h, starting at 07:00 with 3 h sampling until 19:00, followed by a 12 h dark period and final sampling. Five seawater samples and one distilled water (control) sample were incubated for each light and dark treatment, for each water type (upper and deep).

Fluorescent lights suspended 300 mm above the incubator gave an immersed light intensity between 60 and 70 µmol m^{-2} s^{-1}. The vials were held in plastic boxes in two layers: a top layer (light) and a bottom layer (dark) separated by plastic plates. Each incubation vial contained an oxygen sensitive spot (PreSens SP-SPt3-NAU-DS-YOP, 0835-01-PSt3-0804-02, made 03-09-2008) attached to the inside of each vial with silicone. The vials were fitted with conical lid inserts to allow the removal of all air bubbles. Each spot was calibrated (0 and 100% O_2 saturation) prior to the voyage. Incubations were made in a constant temperature (21°C) water bath. At each sampling time each vial was assayed at least 10 times (1 s pulses of light) using a bare-ended fibre optic cable from the FIBOX 3 LCD v3 measurement unit (PreSens).

Incubations were also made using natural light, with light levels reduced to a daily average value of about 80 µmol m^{-2} s^{-1} using shade cloth. Otherwise methods were identical to the artificial light incubations.

The results (Figure 9-11) showed:

1. All incubations drew down O_2, whether in light or dark, indicating net heterotrophy in this autumn period.

2. Net O_2 drawdown (respiration) rates were greater at the inner-Firth sites than the extended-Firth sites by about twofold. This indicates greater heterotrophy in the water column at the inner-Firth sites.

3. The extended-Firth sites had lower water-column O_2 saturation at the start of the incubations than the inner-Firth sites.

4. In almost all experiments, light incubations drew O_2 down more slowly than dark incubations, indicating O_2 production in light. The O_2 production during the 12 h light periods (minus dark; i.e., gross O_2 production in light) was about 2–3% at inner-Firth sites compared to 1–2% at extended-Firth sites, indicating a more productive inner-Firth phytoplankton community compared to the extended Firth.

5. The exceptions were at depth at the extended-Firth sites, where O_2 drawdown in light was either similar to or greater than drawdown in the dark. This could be explained if the phytoplankton were senescing and had become unproductive at depth.

6. Inner-Firth sites had O_2 drawdown rates over 24 h of about 0.2% h^{-1}, while extended-Firth sites had about 0.1% h^{-1} drawdown. To calculate the total daily O_2 consumption in the water column, the drawdown rates were integrated over their respective water columns (7 and 40 m depth). The integrated values were compared with the benthic daily net O_2 consumptions measured in sediment core incubations at the inner-Firth and extended-Firth sites on this voyage (Figure 9-5). It was found that the ratios of water column-to-sediment respiration were 50:50 at inner-Firth sites and 90:10 at extended-Firth sites, i.e., evenly balanced between the water column and benthos at the inner sites and dominated by the water column at deep extended-Firth sites.
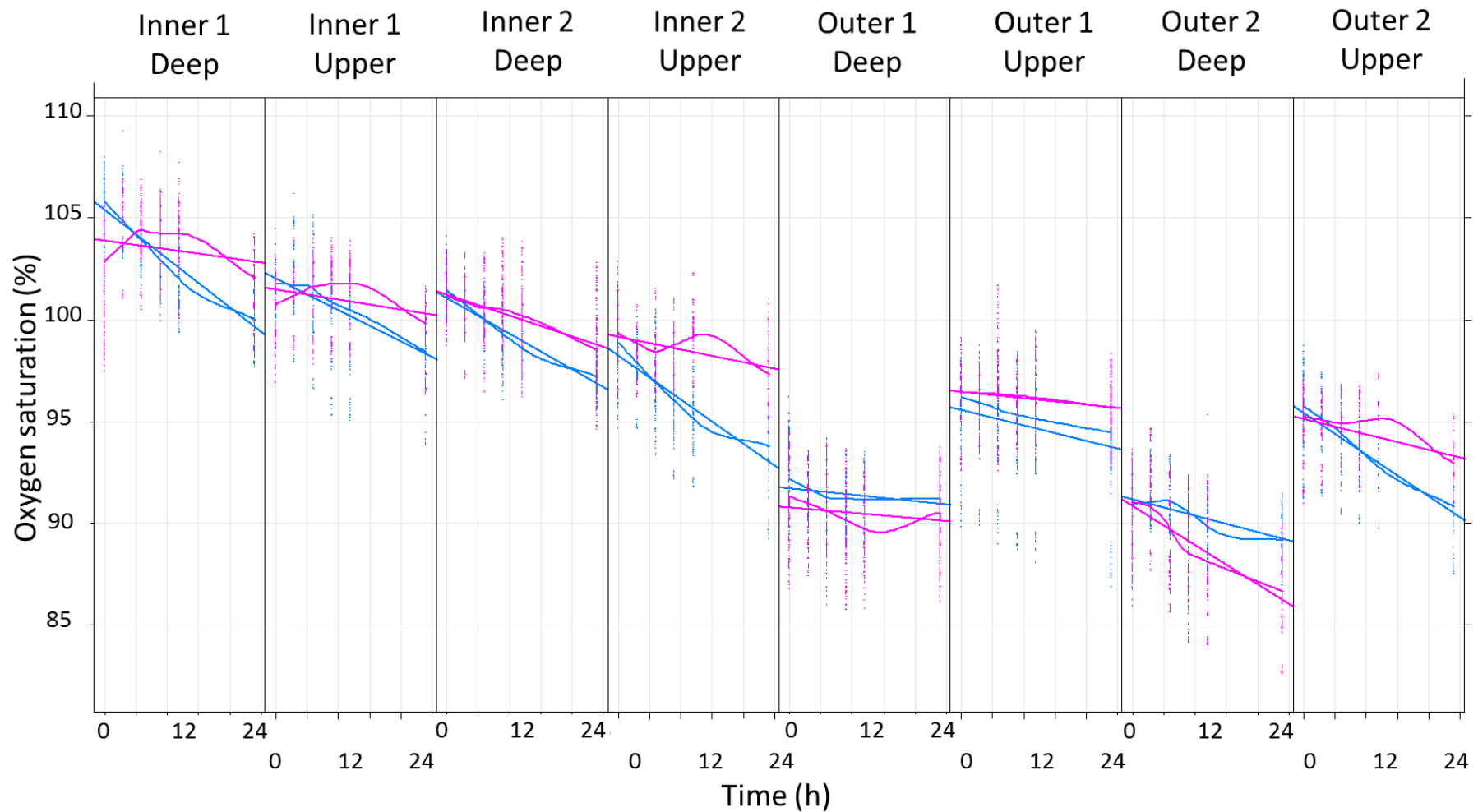
Figure 9-11:   Oxygen percent saturation during oxygen uptake experiments in March 2012 at inner and extended ("outer" in the figure) Firth sites. Deep and upper water-column treatments are incubated under light (pink) and dark (blue) conditions. The natural and artificial light data were pooled in this analysis (dots) and were fitted with LOWESS and linear regression lines.

9.4   References

Canfield, D., Thamdrup, B., Kristensen, E. (2005) *Aquatic geomicrobiology.* Elsevier Academic Press.

Cook, P., Butler, E., Eyre, B. (2004) Carbon and nitrogen cycling on intertidal mudflats of a temperate Australian estuary: I. Benthic metabolism. *Marine Ecology Progress Series,* 280: 25–38.

Giles, H., Pilditch, C.A., Nodder, S.D., Zeldis, J., Currie, K. (2007) Benthic oxygen fluxes and sediment properties on the northeastern New Zealand continental shelf. *Continental Shelf Research,* 27 (18): 2373–2388, doi:10.1016/j.csr.2007.06.007.

Giles, H., Pilditch, C.A., Bell, D.G. (2006) Sedimentation from mussel (*Perna canaliculus*) culture in the firth of Thames, New Zealand: Impacts on sediment oxygen and nutrient fluxes. *Aquaculture*, 261: 125–140.

Gillespie, P., Maxwell, P., Rhodes, L. (2000) Microphytobenthic communities of subtidal locations in New Zealand: Taxonomy, biomass, production, and food-web implications. *New Zealand Journal of Marine and Freshwater Research,* 34: 41–53.

Grasshoff, K., Ehrhardt, M., Kremling K. (editors) (1983) *Methods of seawater analysis.* Verlag-Chemie, Berlin.

Underwood, G., Kromkamp, J. (1999) Primary production by phytoplankton and microphytobenthos in estuaries. *Advances in Ecological Research,* 29: 93–153.

10 Water, salt and carbon/nutrient budgets

10.1 Introduction

A water budget, a salt budget and a carbon/nutrient budget for the Hauraki Gulf and Firth of Thames were constructed using the Land-Oceans Interaction in the Coastal Zone (LOICZ) biogeochemical budgeting procedure (Gordon et al., 1996; Swaney, 2011; http://nest.su.se/mnode/). Each budget divides the region into 3 boxes, with the Firth of Thames box inshore of the Hauraki Gulf box, and the Hauraki Gulf box inshore of the Continental shelf box (Figure 10-1).

The difference between the Firth box in the budget and the definition of the Firth of Thames used otherwise in this report should be noted.

The validity of assumptions and the precision of estimates are described in Appendix C.

The water and salt budgets are "conservative" meaning that water and salt do not change form. In contrast, the carbon and nutrient budgets are non-conservative, reflecting the biogeochemical processes that transform these elements (e.g., assimilation of carbon into organic matter by autotrophs and the breakdown of organic matter into carbon dioxide by heterotrophs).

Because of data limitations, the budgets for the Gulf are valid for spring, summer and winter, while those for the Firth are valid for spring, summer and autumn. The budgets represent the conditions that prevailed during 2000–2001 surveys; at this time river flows were either close to average (for spring and autumn) or about 60% of average (for summer and winter). Sampling did not include conditions of strong upwelling.
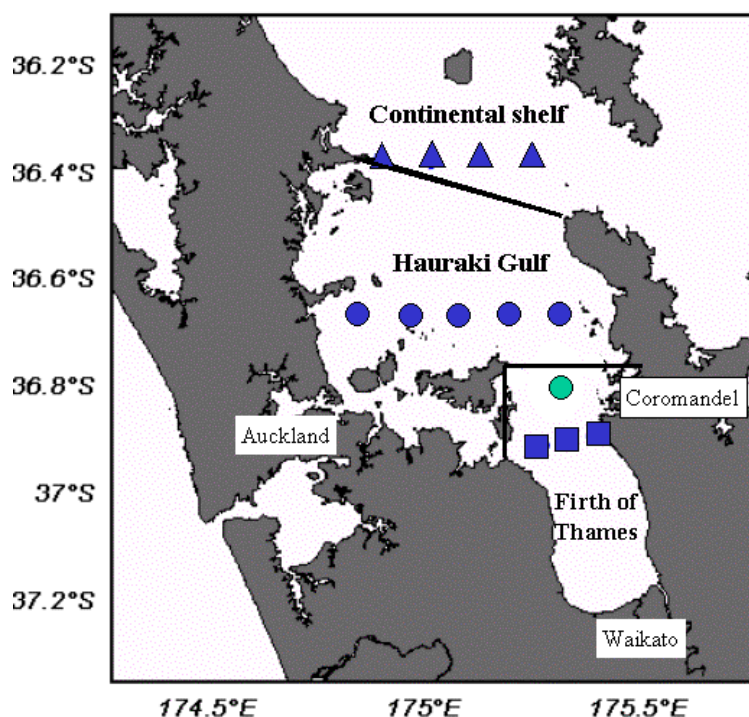
Figure 10-1: Firth of Thames, Hauraki Gulf and shelf boxes (or "compartments") used in the budgets. Black lines show compartment boundaries. Blue symbols are locations of CTD sampling used for estimating salt and nutrient concentrations. The green symbol is the location of the extended-Firth monitoring site. The difference between the Firth box in the budget and the definition of the Firth of Thames used otherwise in this report should be noted.

10.2 Water budget

A budget was established of freshwater flows into and out of each box comprising river runoff, groundwater, wastewater, precipitation and evaporation (Figure 10-2).

Assuming a steady state, water volume is conserved. For each box, there is an outflow to the adjacent offshore box to balance the net freshwater volume flowing into the box. This is the residual flow of water, V_R, calculated as:

$$V_R = -(V_Q + V_O + V_G + V_P + V_E) \qquad (10.1)$$

where subscripts R, Q, O, G, P and E denote volumes of residual flow, river runoff, wastewater, groundwater, precipitation, and evaporation, respectively. Because residual flow is out of each box, V_R is negative.
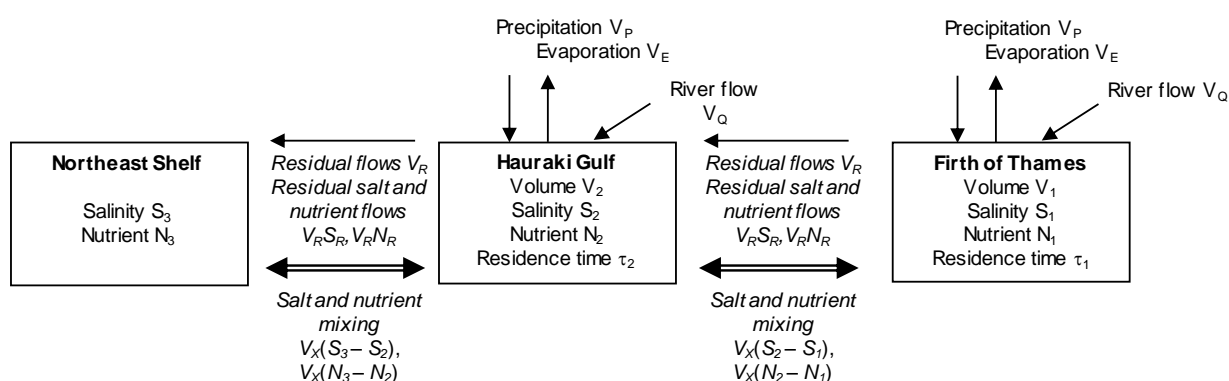

Figure 10-2: Boxes used in the budget for Hauraki Gulf and Firth of Thames. Flows of freshwater, salt and nutrients between boxes are shown, with terms defined in the text.

10.3 Salt budget

Assuming a steady state, salt is conserved. Therefore, salt removed from each box by the residual flow to the adjacent offshore box is replaced by mixing between the boxes to sustain the salinity difference observed between the boxes (Figure 10-2).

The steady-state balance of salt between the boxes is defined by:

$$0 = V_R S_R + V_X (S_1 - S_2) \qquad (10.2)$$

where the salinity of the residual flow (S_R) is the average salinity of the inshore box (S_1) and the adjacent offshore box (S_2). Rearrangement of equation (10.2) allows calculation of V_X, which is the mixing between boxes required to balance the residual flow of salt.

The implementation of the Hauraki Gulf / Firth of Thames budget as a 3-box model in series meant that residual flow from the Gulf box to the shelf box was calculated as the sum of the absolute value of the residual flow between the Firth box and the Gulf box and the freshwater terms affecting the Gulf box (Zeldis, 2005). Also, the exchange term for the Gulf box was determined using the exchanges across both the inner and outer boundaries of the Gulf box (http://nest.su.se/mnode/); Swaney, 2011).

The mean residence time τ of water in each box is calculated as:

$$\tau = V / \left(V_X + |V_R| \right) \qquad (10.3)$$

where *V* is the volume of water.

10.4   Carbon/nutrient budgets

Exchanges of dissolved carbon (C), nitrogen (N) and phosphorus (P) between the boxes deviate from the conservative exchanges described above for salt because of non-conservative release and uptake (biogeochemical processing) of C, N and P.
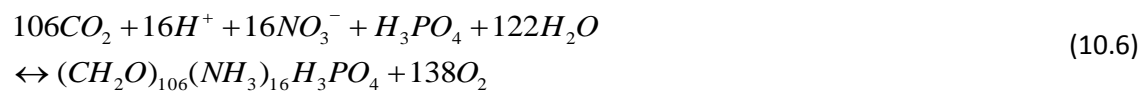
Exchanges of C, N and P are described with an additional term, ΔY, to account for the net non-conservative fluxes:

0 = *freshwater +residual+ mixing +ΔY* $\qquad (10.4)$

Net ecosystem metabolism (NEM) is the balance between net primary production and decomposition of organic material by the system, as represented by a relationship that describes the net community production of the system (Gordon et al., 1996; Swaney, 2011):

CO_2 + inorganic nutrients + water $\leftrightarrow$ organic matter + O_2 $\qquad (10.5)$

which has the following stoichiometry among its elements:

$$106CO_2 + 16H^+ + 16NO_3^- + H_3PO_4 + 122H_2O$$
$$\leftrightarrow (CH_2O)_{106}(NH_3)_{16}H_3PO_4 + 138O_2 \qquad (10.6)$$

Equation (10.6) shows the relationships among C, N, P and oxygen (O) typical of Redfield molar ratios, which apply to typical organic material found within the plankton of the coastal system.

Carbon has both aqueous and gas phases, including dissolved inorganic and organic carbon (DIC, DOC) and CO_2, which exchanges across the air–sea interface. This means that NEM cannot be estimated from measurements of dissolved materials only. However, because there is no gas phase for P, it may be used as a proxy for NEM by using the Redfield relationship between C and P. That is, the non-conservative net fluxes of dissolved inorganic P *(ΔDIP)* can be considered approximations of net C metabolism, at the scale of the ecosystem (Swaney, 2011).

Via the net DIP fluxes, the net rates at which C is either produced or consumed by the system may be estimated, and from that the system NEM, or the difference between system production and respiration (*p-r*), may be estimated. When the estimated net dissolved C fluxes are added to independent estimates of the primary production (carbon fixation) rate of the ecosystem, the absolute rate of ecosystem respiration can be estimated.

Nitrogen also has a major gas flux pathway through denitrification (i.e., evolution of N_2 gas) and its back-reaction, N fixation. The expected flux of N *(ΔDIN$_{exp}$)* can be predicted from *ΔDIP* by using the Redfield N:P composition ratios. The deviation of the observed flux (i.e., budgeted from the water samples for *DIN, ΔDIN$_{obs}$*) from that expected (based on *ΔDIP*) gives an estimate of the net rate at which the system is either denitrifying or fixing N (*nfix-denit*). Since fluxes of dissolved organic N *(ΔDON)* are also measured, an estimate of net denitrification corrected for dissolved organic N metabolism is possible (Smith et al., 1991; Swaney, 2011).

Overall, because the budgeting provides information on both loading and metabolic processing of C and N in the system, the estimated rates of NEM and net denitrification can be related to the

sources, intensity and speciation of the dissolved nutrient loading the system receives from the land and from the sea offshore. Although the metabolism of particulate materials is not budgeted (Smith et al., 1991; Gordon et al., 1996) results for deficits or surpluses of dissolved N loading with respect to N required to sustain the estimated denitrification provide information on particulate loading.

10.5 Data used in budget construction

10.5.1 Ocean surveys

Information selected from salinity and nutrient samples collected in quarterly oceanographic voyages in spring (September), summer (November–December), autumn (March) and winter (July) of 2000–01 was used to construct the Hauraki Gulf and Firth of Thames budgets. This involved totals of 96, 108 and 50 salinity and nutrient samples in shelf, Gulf and Firth boxes, respectively, divided nearly equally amongst the four voyages.

Salinities and nutrients were collected using a CTD (Figure 10-3). Nutrients (NO_3^-, NH_4^+, DIP, Total Dissolved N [TDN] and P [TDP]) were assayed using the methods of Pickmere (1998). Dissolved organic N (DON) and P (DOP) were determined by difference between TDN and TDP and the respective inorganic dissolved forms. Mean salinity and nutrients in each system and adjacent offshore waters were calculated using arithmetic averaging of data from all depths and stations to estimate annually-averaged salt and nutrient concentrations.

Figure 10-3:   The conductivity–temperature–depth (CTD) instrument about to be deployed from the stern of NIWA RV *Kaharoa*. It is lowered though the water and used to sample parameters including temperature, salinity, oxygen and light, at various depths in the water column, using the electronic sensors at the base of the package. The bottles can be shut at specified depths to capture water for later laboratory analysis for nutrients.

10.5.2 Freshwater and nutrient loadings

River flow data needed for each seasonal budget were acquired from the NIWA hydrometric database (sourced from Waikato Regional Council and Auckland Council). The Waihou and Piako Rivers, three smaller rivers and the many streams and drains that flow to the Firth of Thames from the Waikato District and the Coromandel region were included. The flows were estimated for all gauged catchments draining inside the land boundaries of each box and summed, then pro-rated by catchment area to scale the gauged flows to total catchment outflow using NIWA Tideda software. The annual inflow to the Firth of Thames (109 m^3 s^{-1}) accounted for most of the total Hauraki Gulf / Firth of Thames inflow (160 m^3 s^{-1}).

Multi-year-mean nutrient concentrations at gauging sites for the five Firth rivers were obtained from Vant and Wilson (1998) and B. Vant (Environment Waikato, pers. comm., June 2004), which were multiplied by monthly mean flows for the 2000–01 period and then summed to obtain annual loads at the gauging sites[47]. Summed dissolved and particulate organic N and P concentrations were determined as the difference between TN and DIN and the difference between TP and DRP concentrations, respectively. The data did not allow separation of dissolved and particulate organic forms in river loads, so for the purposes of budgeting their sums were used as the riverine organic concentrations (DON and PON).

Total nitrogen (TN) annual loads at terminal reaches (i.e., at the coast) for all inflows to the Firth of Thames and Hauraki Gulf were estimated using SPARROW (SPAtially Referenced Regressions On Watershed attributes), which accumulates TN loads down-catchment based on catchment characteristics, landuse and in-river parameters, and which is calibrated against upstream TN gaugings (S. Elliott, NIWA, pers. comm., January 2008). The ratio of the Firth-wide SPARROW terminal-reach TN load to the summed SPARROW estimates at the gauging sites for the 5 rivers was 1.92. This factor was applied to the loads of all the nutrient species measured at the gauging sites to estimate nutrient loads at terminal reaches. Flows and loads for each quarterly budget were estimated by determining quarterly flow values as the mean of daily flows averaged over the month of each survey and the preceding month, to allow a one month lead-in time. The terminal-reach loads were then scaled by the quarterly flows to estimate the loads corresponding to each survey. The implementation of SPARROW terminal-reach estimates for all catchment inflows to the respective boxes has meant that the flux estimates reported here diverge from those of Vant (2013), which were calculated by summing data from major-river gauging sites rivers only.

Nutrient concentrations for the rivers and streams draining to the western Gulf were estimated from the means of Wilcock and Stroud (2000), and concentrations for rivers and streams draining to the eastern Gulf were estimated using the means for the Kauaeranga River (Vant and Wilson, 1998) because, like the Kauaeranga, they largely drain forested catchments. Terminal-reach values for smaller streams were not estimated because the gauging sites in these cases were generally near the coast and their loads were much smaller than those of the Firth rivers. DON+PON values were estimated as the difference between the DIN loads of Wilcock and Stroud (2000) and the SPARROW TN loads. These were again pro-rated by the quarterly flows to estimate loads corresponding to each survey.

---

[47] It was assumed that a simple multiplication of annual mean concentration by flow was an adequate estimator of load as there was relatively little variation in monthly mean concentrations of nutrients in outflows. For instance, between 1989 and 1998, NO_3^- concentrations in the Waihou River averaged 88 mmol m^{-3} (s.d. = 17, n =120) and DIP averaged 1.8 mmol m^{-3} (s.d. = 0.5) (Vant and Wilson, 1998).

Groundwater was considered to be a negligible contributor to inflow to the Hauraki Gulf and Firth of Thames coastal regions because the land is composed largely of relatively impermeable sandstones (A. Smaill, Auckland Regional Council, pers. comm., November 1998).

Rainfall was evaluated using annual averages of data collected between 1986 and 1996 at 4 sites around the Hauraki Gulf region.

Over-water evaporation was estimated for the same period using mean evaporation data from two terrestrial sites, and was assumed to be 0.7 times the terrestrial evaporation (M. Duncan, NIWA, pers. comm., November 1998).

Discharges of treated sewage effluent, predominately from the North Shore (Auckland) but also other smaller discharges further up the west coast of the Hauraki Gulf, were obtained from M. Shipton (North Shore Regional Council, pers. comm., November 1998) and input to the Hauraki Gulf box.

Urban wastewater to the Firth of Thames was neglected as the Firth drains a predominately rural region.

Wet and dry atmospheric P and N deposition to the Hauraki Gulf and Firth of Thames boxes was neglected as these are likely to be small given the relatively clean air.

10.6 Results

Table 10-1 shows elemental fluxes for the Firth of Thames and Hauraki Gulf boxes, averaged across the seasonal surveys used to construct the budget.

Table 10-2 shows fluxes of nitrogen and carbon for the Firth of Thames and Hauraki Gulf boxes, averaged across the seasonal surveys used to construct the budget.

A limiting factor in the calculation of the mixing term V_x is that there be a reasonably strong salinity gradient between adjacent boxes (Swaney, 2011). In the winter seasonal budget the salinity gradient between the Firth of Thames box and the Hauraki Gulf box was very small (0.02), resulting in unrealistic estimates of residence time (<1 day) for the Firth of Thames box. This problem also affected the autumn budget for the Hauraki Gulf box, with a salt contrast with the continental shelf box of only 0.07, resulting in an unrealistically short residence time of 11 days for the Hauraki Gulf box. Consequently, these seasonal budgets were not considered in the calculation of the annual means shown in Table 10-1.[48]

The residual and exchange terms for the Gulf budget in winter were enabled by considering the Gulf/Firth system to be a single box (river flow inputs for the two boxes were summed in this case). This adjustment was consistent with the lack of salinity contrast between the Gulf and Firth in that season. The resulting Gulf residence time (32 days) for winter was realistic.

The budgets represent the conditions that prevailed during the 2000–2001 surveys; at this time river flows were either close to average (for spring and autumn) or about 60% of average (for summer and winter). Sampling did not include conditions of strong upwelling (which occur about 11% of the time) (MacDiarmid et al., 2009).

---

[48] This development of the model was made subsequent to (Zeldis 2005) and (Zeldis 2008a) and has changed some of the flux estimates given in those earlier studies. Also, an error in estimation of terrestrial organic matter fluxes in the earlier studies has been corrected here.

Table 10-1: **Dimensions and fluxes for the Firth of Thames and the Hauraki Gulf boxes.** A positive flux is directed out of the box.

Box	Area (km^2)	Volume (km^3)	Residual flow V$_r$ (10^9 m^3 y^{-1})	Mixing flow V$_x$ (10^{11} m^3 y^{-1})	Residence time (d)	ΔDIP (mmol m^{-2} y^{-1})	ΔDIN (mmol m^{-2} y^{-1})	ΔDOP (mmol m^{-2} y^{-1})	ΔDON (mmol m^{-2} y^{-1})
Firth of Thames	1100	16	3.5	-3.2	20	54	-280	-29	150
Hauraki Gulf	2800	82	5.7	-5.8	32	-2	-240	-1	200

Table 10-2: **Fluxes of nitrogen and carbon for the Firth of Thames and the Hauraki Gulf boxes.** Units for nitrogen and carbon fluxes are t y^{-1}. Positive values signify fluxes out of the box. 'Catchment' means fluxes from land. For the Firth of Thames box, 'Marine' means fluxes with respect to the Hauraki Gulf. For the Hauraki Gulf box, 'Marine' means fluxes with respect to the Firth of Thames or the continental shelf.

Box	Catchment DIN	Catchment DON+PON	Marine DIN	Marine DON	Marine PON	Net DIC flux	Net denitrification
Firth of Thames	-3700	-920	-570	3200	-6100	75000	8100
Hauraki Gulf	-760	-150	-8200	10400	-2000	-8600	700

Some findings are:

- Mean water residence time of the Firth, or the average time required for the summed residual and mixing flows to exchange the water volume of the Firth with the Gulf, was 20 days. The exchange time of the Gulf with the shelf and the Firth was 32 days.

- Fluxes of DIP and DIN were highly non-conservative, indicating strong internal processing. The DIP flux reflected the net decomposition of organic matter to inorganic nutrients and the evolution of dissolved inorganic carbon (DIC) (see equation 10.6). For the Firth, primary production (p) is slower than respiration (r) of organic matter. Average net ecosystem metabolism (NEM) was therefore negative (heterotrophic), with (p - r) = -5700 mmol C m^{-2} y^{-1}. In contrast, the Hauraki Gulf is net productive with (p - r) slightly positive (820 mmol C m^{-2} y^{-1}) (i.e., nearly balanced between autotrophy and heterotrophy). The seasonal estimates of NEM were -5600, -2300 and -9200 mmol C m^{-2} y^{-1} in spring, summer and autumn, respectively.

- For the Firth, the excess of oxidation over production must be subsidised by net import of substantial amounts of labile organic carbon from the land and from offshore, and its subsequent oxidation in the Firth (Table 10-2).

- Firth respiration exceeds planktonic primary production by 16 mmol C m^{-2} d^{-1}. Firth primary production is 44 mmol C m^{-2} d^{-1} (from Figure 6-4), so gross Firth respiration r is 44 +16 = 60 mmol C m^{-2} d^{-1}.

- The deviations between observed and expected fluxes of DIN in the Firth indicate that it denitrifies large amounts of nitrogen gas to the atmosphere on a net basis (estimated from equation 10.2 as 1.5 mmol N m^{-2} d^{-1} or 60 μmol N m^{-2} h^{-1}, for the Firth).

- About 73% of the total N export from the Firth (total = denitrification plus DON export) was as denitrified N_2 gas (deduced from Table 10-2).

- The planktonic primary production is 520 mg C m^{-2} d^{-1} or 31,000 t N y^{-1}, incorporated into organic material. Denitrification is 8,100 t N y^{-1} or about 26% of primary production. This indicates that N, once introduced into the Firth by net N import, cycles about four times through the production–decomposition cycle on average, before being lost to denitrification or (to a lesser extent) hydrographic export.

- The behaviour of the Firth as a source of DIP and sink of DIN is indicated by the contrasts in these properties across the survey area (Figure 10-4). Dissolved organic phosphorus (DOP) and nitrogen (DON) had less spatial contrast, showing more conservative transport and a more refractory nature.

- The (*p - r*) value (defined in Figure 10-5) for the Firth places it amongst the more heterotrophic values derived from 70 LOICZ budgets in the global LOICZ budget database (Figure 10-5) compiled by Buddemeier et al. (2002). The (*nfix - denit*) values from the Firth are near the mode of net denitrifying values tabulated by Buddemeier et al. (2002).

- The balance between catchment-derived and offshore-derived nutrient loading for the Firth was estimated by:

  river inputs / (river inputs + mixing flow inputs + residual flow losses)

  which revealed that the Firth rivers contributed 57% of total N inputs (DIN + DON + PON) and 87% of DIN inputs to the total Firth N load, with the remainder coming from offshore.
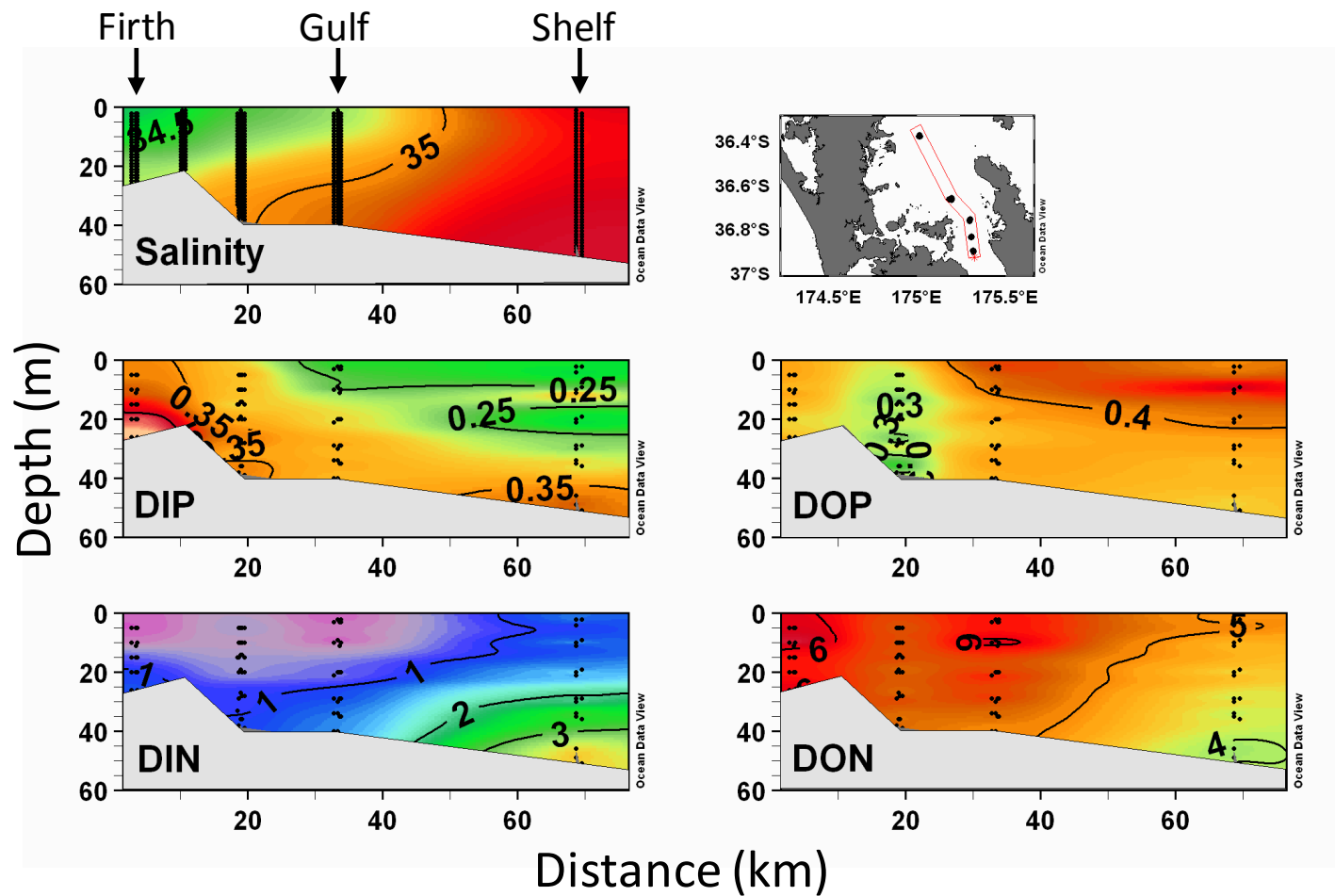
Figure 10-4: Vertical sections of properties with increasing distance offshore, from the Firth, through the Gulf, to the shelf, from the 2000–2001 surveys undertaken to obtain data to construct the budgets. Shown are the means across all 4 surveys of salinity, and (in µmol), dissolved inorganic nitrogen (DIN), dissolved inorganic phosphorus (DIP), dissolved organic nitrogen and dissolved organic phosphorus (DOP). The map shows station positions and arrows show profiles in Firth, Gulf and shelf boxes.
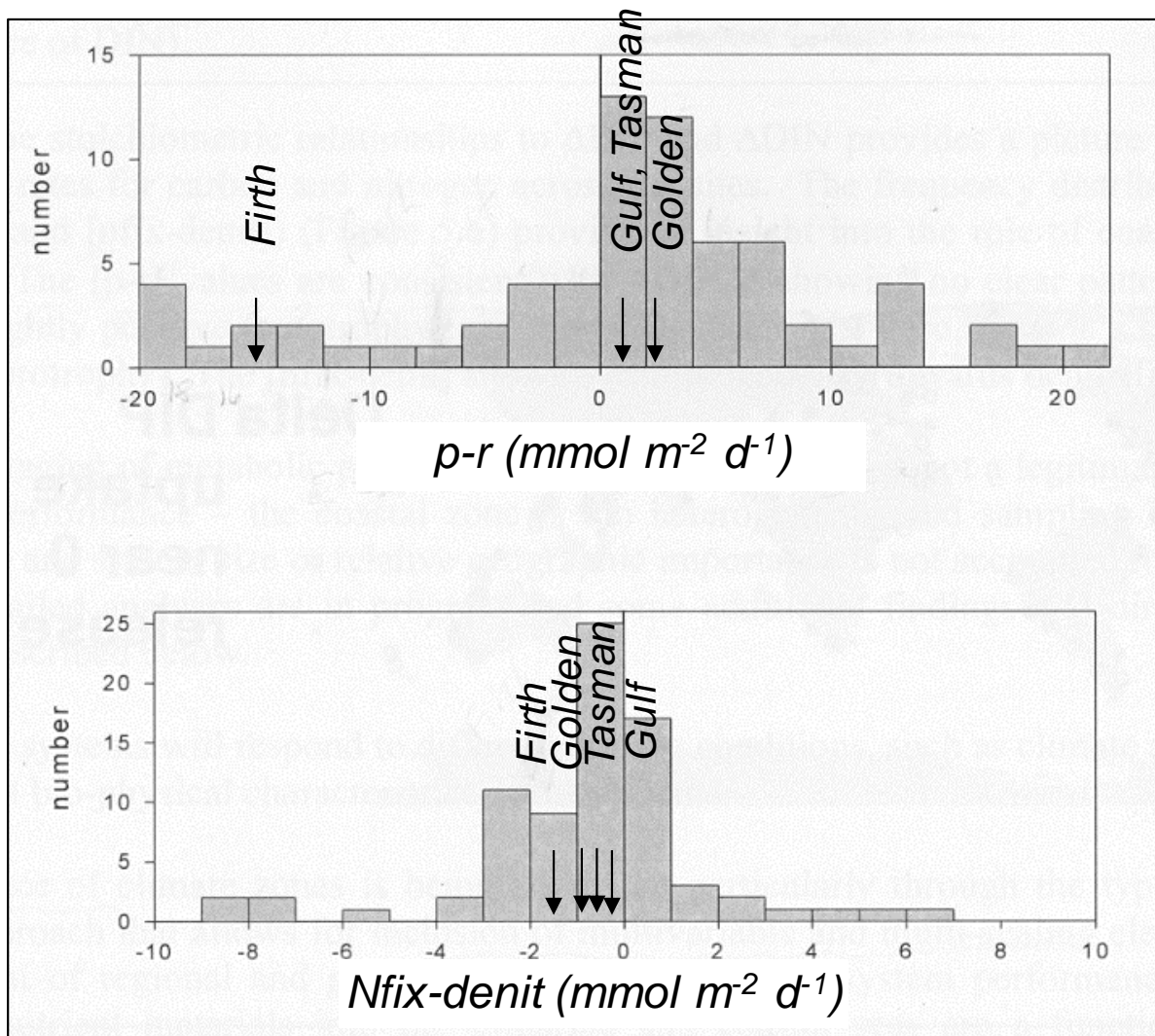
Figure 10-5: Histograms of production - respiration (*p - r*) and N fixation - Ndenitrification (*nfix - denit*) (both as mmol m^{-2} d^{-1}) from the global LOICZ database of Buddemeier et al. (2002). Values for the Firth, the Hauraki Gulf and Tasman and Golden Bays (Zeldis, 2008) are indicated.

10.7 References

Buddemeier, R., Smith, S., Swaney, D., Crossland, C. (2002) The role of the coastal ocean in the disturbed and undisturbed nutrient and carbon cycles. *LOICZ Reports & Studies*. LOICZ Texel, The Netherlands.

Gordon, D.J., Boudreau, P., Mann, K., Ong, J.-E., Silver, W., Smith, S., Wattayakorn, G., Wulff, F., Yanagi, T. (1996) *Loicz biogeochemical modelling guidelines*. Texel. LOICZ/RandS/95-5, 96 pp.

Pickmere, S. (1998) Biological effects of cross-shelf water transfer programme nutrient report. *NIWA Internal Report.* 98/04: 5.

MacDiarmid, A., Sutton, P., Chiswell, S., Stewart, C., Zeldis, J., Schwarz, J., Palliser, C., Harper, S., Maas, E., Stevens, C., Taylor, P., Thompson, D., Torres, L., Bostock, H., Nodder, S., MacKay, K., Hewitt, J., Halliday, J., Julian, K., Baird, S., Hancock, N., Neil, K., D'Archino, R., Sim-Smith, C., Francis, M.,

Leathwick, J., Sturman, J. (2009) OS2020 Bay of Islands Coastal Project: Phase 1 – Desktop study. NIWA Client Report, WLG2009-3, 396 pp.

Smith, S., Hollibaugh, J., Dollar, S., Vink, S. (1991) Tomales Bay metabolism: C-n-p stoichiometry and ecosystem heterotrophy at the land-sea interface. *Estuarine, Coastal and Shelf Science*, 33: 223–257.

Vant, B., Wilson, B. (1998) Trends in river water quality in the Waikato region, 1980–97. *Environment Waikato technical report 1998/13.* Environment Waikato.

Vant, B. (2013) Trends in river water quality in the Waikato region, 1993-2012*. Waikato Regional Council Technical Report 2013/20.* Environment Waikato.

Wilcock, R., Stroud, M. (2000) Review of the long-term baseline water quality programme for freshwater streams 1992-2000. *NIWA Client Report* ARC00259/1. 126pp

Zeldis, J.R. (2005) Magnitudes of natural and mussel farm-derived fluxes of carbon and nitrogen in the Firth of Thames. NIWA Client Report. CHC2005-048 35 pp.

Zeldis, J. (2008) Exploring the carrying capacity of the Firth of Thames for finfish farming: a nutrient mass-balance approach. NIWA Client Report, CHC2008-02: 25 pp.

11 Acknowledgements

Appendix A   Radioisotope dating

Radioisotopes, such as caesium-137 (^{137}Cs, ½-life 30 years) and lead-210 (^{210}Pb, ½-life 22.3 years), and plant pollen can be used to reconstruct the recent sedimentation history of an estuary.

Dating of estuarine sediments using independent methods offsets the limitations of any one approach. This is particularly important when interpreting sediment profiles from lakes and estuaries, given the confounding effects of physical and biological mixing (Robbins and Edgington, 1975; Sharma et al. 1987; Alexander et al. 1993; Valette-Silver, 1993; Benoit et al. 1999). A description of the various methods of dating sediments follows. The S.I. unit of radioactivity used in this study is the Becquerel (Bq), which is equivalent to one radioactive disintegration per second.

^{137}Cs dating

^{137}Cs was introduced to the environment by atmospheric nuclear weapons tests in 1953, 1955–1956 and 1963–1964. Peaks in annual ^{137}Cs deposition corresponding to these dates are the usual basis for dating sediments (Wise, 1977; Ritchie and McHenry, 1989). Although direct atmospheric deposition of ^{137}Cs into estuaries is likely to have occurred, ^{137}Cs is also incorporated into catchment soils, which are subsequently eroded and deposited in estuaries (Figure A-1). In New Zealand, ^{137}Cs deposition was first detected in 1953 and its annual deposition was been measured at several locations until 1985. Annual ^{137}Cs deposition can be estimated from rainfall using known linear relationships between rainfall and Strontium-90 (^{90}Sr) and measured ^{137}Cs/^{90}Sr deposition ratios (Matthews, 1989). Experience in Auckland estuaries shows that ^{137}Cs profiles measured in estuarine sediments bear no relation to the record of annual ^{137}Cs deposition (i.e., 1955–1956 and 1963–1964 ^{137}Cs-deposition peaks absent), but rather preserve a record of direct and indirect (i.e., soil erosion) atmospheric deposition since 1953 (Swales et al., 2002). The maximum depth of ^{137}Cs occurrence in sediment cores (corrected for sediment mixing) is taken to coincide with the year 1953, when ^{137}Cs deposition was first detected in New Zealand. We assume that there is a negligible delay in initial atmospheric deposition of ^{137}Cs in estuarine sediments (e.g., ^{137}Cs scavenging by suspended particles) whereas there is likely to have been a time-lag (i.e., <1 year) in ^{137}Cs inputs to estuaries from topsoil erosion, which would coincide with the occurrence of floods.

If a surface mixed layer (SML) is evident in a core, as shown by an X-ray image and/or a tracer profile (e.g., ^{7}Be, ^{210}Pb) then ^{137}Cs is likely to have been rapidly mixed through the SML. Therefore, to calculate time-averaged sedimentation rates, the maximum depth of ^{137}Cs occurrence is reduced by the maximum depth of the SML.

Uncertainty in the maximum depth of ^{137}Cs results from: (1) the depth interval between sediment samples and (2) minimum detectable concentration of ^{137}Cs, which is primarily determined by sample size and counting time. The 1963–1964 ^{137}Cs deposition peak was about five times greater than the deposition plateau that occurred between 1953 and 1972. Thus, depending on the sample size, there is uncertainty in the age of the maximum ^{137}Cs depth (i.e., 1953–1963). To reduce this uncertainty, we have maximised the sample mass that is analysed.
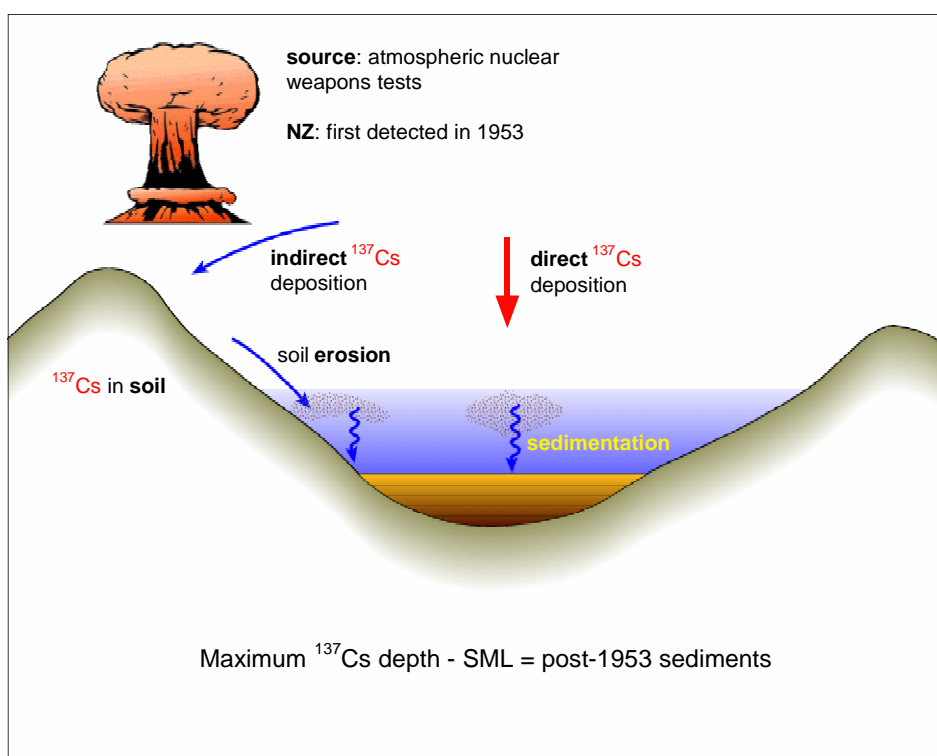
Figure A-1: [superscript]137[/superscript]Cs pathways to estuarine sediments.

[superscript]210[/superscript]Pb dating

^{210}Pb (half-life 22.3 y) is a naturally occurring radioisotope that has been widely applied to dating recent sedimentation (i.e., last 150 years) in lakes, estuaries and the sea (Figure A-2). ^{210}Pb is an intermediate decay product in the uranium-238 (^{228}U) decay series and has a radioactive decay constant (k) of 0.03114 y^{-1}. The intermediate parent radioisotope radium-226 (^{226}Ra, half-life 1622 years) yields the inert gas radon-222 (^{222}Rn, half-life 3.83 days), which decays through several short-lived radioisotopes to produce ^{210}Pb. A proportion of the ^{222}Rn gas formed by ^{226}Ra decay in catchment soils diffuses into the atmosphere where it decays to form ^{210}Pb. This atmospheric ^{210}Pb is deposited at the earth surface by dry deposition or rainfall. The ^{210}Pb in estuarine sediments has two components: supported ^{210}Pb derived from *in situ* ^{222}Rn decay (i.e., within the sediment column) and an unsupported ^{210}Pb component derived from atmospheric fallout. This unsupported ^{210}Pb component of the total ^{210}Pb concentration in excess of the supported ^{210}Pb value is estimated from the ^{226}Ra assay (see below). Some of this atmospheric unsupported ^{210}Pb component is also incorporated into catchment soils and is subsequently eroded and deposited in estuaries. Both the direct and indirect (i.e., soil inputs) atmospheric ^{210}Pb input to receiving environments, such as estuaries, is termed the unsupported or excess ^{210}Pb.

The concentration profile of unsupported ^{210}Pb in sediments is the basis for ^{210}Pb dating. In the absence of atmospheric (unsupported) ^{210}Pb fallout, the ^{226}Ra and ^{210}Pb in estuary sediments would be in radioactive equilibrium, which results from the substantially longer ^{226}Ra half-life. Thus, the ^{210}Pb concentration profile would be uniform with depth. However, what is typically observed is a reduction in ^{210}Pb concentration with depth in the sediment column. This is due to the addition of unsupported ^{210}Pb directly or indirectly from the atmosphere that is deposited with sediment particles on the bed. This unsupported ^{210}Pb component decays with age (k = 0.03114 y^{-1}) as it is buried through sedimentation. In the absence of sediment mixing, the unsupported ^{210}Pb

concentration decays exponentially with depth and time in the sediment column. The validity of ^{210}Pb dating rests on how accurately the ^{210}Pb delivery processes to the estuary are modelled, and in particular the rates of ^{210}Pb and sediment inputs (i.e., constant versus time variable).
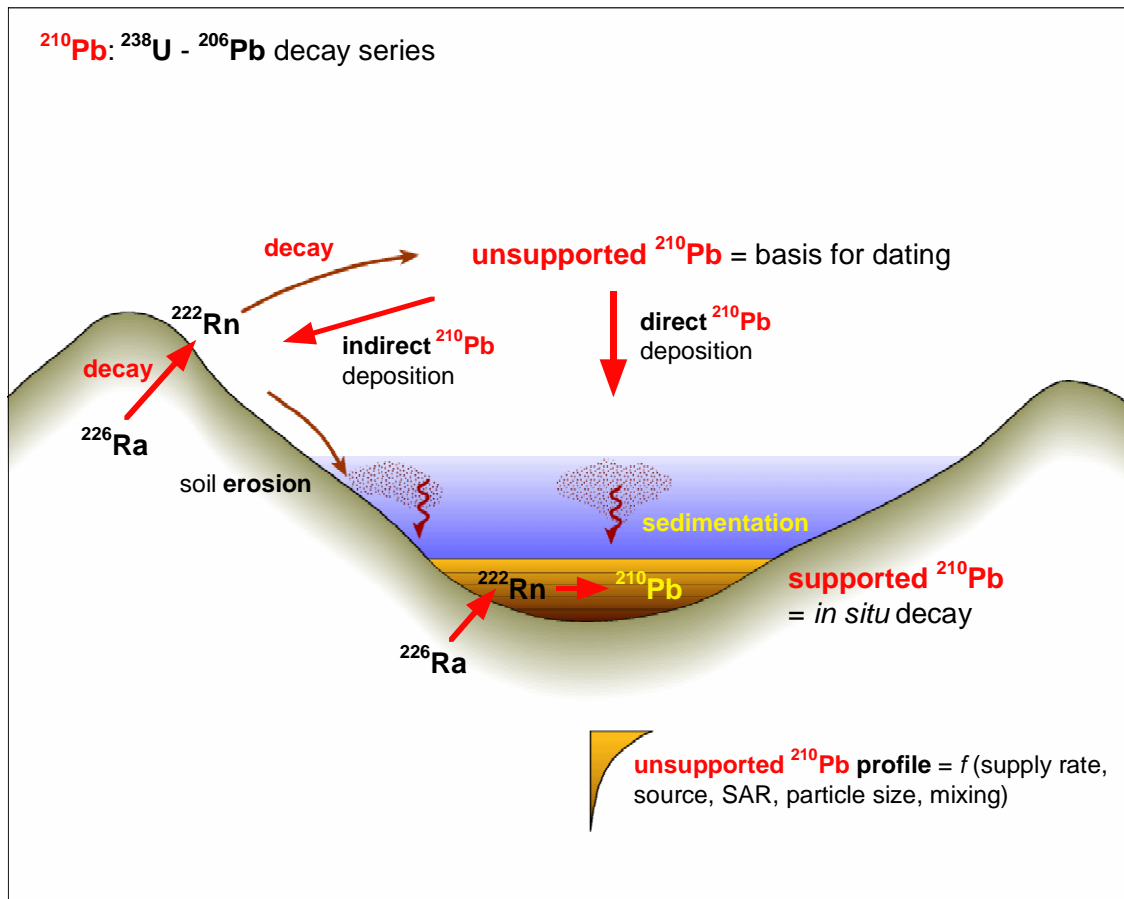
Figure A-2: ^{210}Pb pathways to estuarine sediments.

Sediment accumulation rates

Sedimentation rates calculated from cores are net average sediment accumulation rates (SAR), which are usually expressed as mm y^{-1}. These SAR are net values because cores integrate the effects of all processes, which influence sedimentation at a given location. At short time scales (i.e., seconds–months), sediment may be deposited and then subsequently resuspended by tidal currents and/or waves. Thus, over the long term, sedimentation rates derived from cores represent net or cumulative effects of potentially many cycles of sediment deposition and resuspension. However, less disrupted sedimentation histories are found in depositional environments where sediment mixing due to physical processes (e.g., resuspension) and bioturbation is limited. The effects of bioturbation on sediment profiles and dating resolution reduce as SAR increase (Valette-Silver, 1993).

Net sedimentation rates also mask the fact that sedimentation is an episodic process, which largely occurs during catchment floods, rather than the continuous gradual process that is implied. In large estuarine embayments, such as the Firth, mudflat sedimentation is also driven by wave-driven

resuspension events. Sediment eroded from the mudflat is subsequently re-deposited elsewhere in the estuary.

Although sedimentation rates are usually expressed as a sediment thickness deposited per unit time (i.e., mm y^{-1}) this statistic does not account for changes in dry sediment mass with depth in the sediment column due to compaction. Typically, sediment density (ρ = g cm^{-3}) increases with depth and therefore some workers prefer to calculate dry mass accumulation rates per unit area per unit time (g cm^{-2} y^{-1}). These data can be used to estimate the total mass of sedimentation in an estuary (tonnes y^{-1}) (e.g., Swales et al. 1997). However, the effects of compaction can be offset by changes in bulk sediment density reflecting layering of low-density mud and higher-density sand deposits. Furthermore, the significance of a SAR expressed as mm y^{-1} is more readily grasped than a dry-mass sedimentation rate in g cm^{-3} y^{-1}. For example, the rate of estuary aging due to sedimentation (mm y^{-1}) can be directly compared with the local rate of sea level rise.

The equations used to estimate time-averaged SAR from the excess ^{210}Pb and ^{137}Cs profiles are described below.

Estimating SAR using ^{210}Pb profiles

The rate of decrease in excess ^{210}Pb activity with depth can be used to calculate a net sediment accumulation rate. The excess ^{210}Pb activity at time zero (C_0, Bq kg^{-2}), declines exponentially with age (t):

$$C_t = C_0 e^{-kt}$$

Assuming that within a finite time period, sedimentation (S) is constant then $t = z/S$ can be substituted into the above equation and by re-arrangement:

$$\frac{\ln\left[\dfrac{C_t}{C_0}\right]}{z} = -k/S$$

Because excess ^{210}Pb$_{us}$ activity decays exponentially and assuming that sediment age increases with depth, a vertical profile of natural log(C) should yield a straight line of slope $b = -k/S$. A linear regression model is fitted to natural-log transformed excess ^{210}Pb data to calculate b. The SAR over the depth of the fitted data is given by:

$$S = -(k)/b$$

An advantage of the ^{210}Pb-dating method is that the SAR is based on the excess ^{210}Pb profile rather than a single layer or horizon, as is the case for ^{137}Cs were the maximum penetration depth of this radioisotope is used for dating. Furthermore, if the ^{137}Cs tracer is present at the bottom of the core then the estimated SAR represents a minimum value.

Estimating SAR using ^{137}Cs profiles

The ^{137}Cs profiles will also be used to estimate time-averaged SAR based on the maximum depth of ^{137}Cs in the sediment column, corrected for surface mixing. The ^{137}Cs SAR is calculated as:

$$S = (M - L)/T - T_0$$

where S is the ^{137}Cs SAR, M is the maximum depth of the ^{137}Cs profile, L is the depth of the surface mixed layer (SML) indicated by the ^{7}Be profile and/or X-ray images, *T* is the year cores were collected and T_0 is the year (1953) ^{137}Cs deposition was first detected in New Zealand.

Sediment mixing

Biological and physical processes, such as the burrowing and feeding activities of animals and/or sediment resuspension by waves (Figure A-3), mix the upper sediment column (Bromley, 1996). As a result, sediment profiles are modified and this limits the temporal resolution of dating. Various mathematical models have been proposed to take into account the effects of bioturbation on ^{210}Pb concentration profiles (e.g., Guinasso and Schink, 1975).
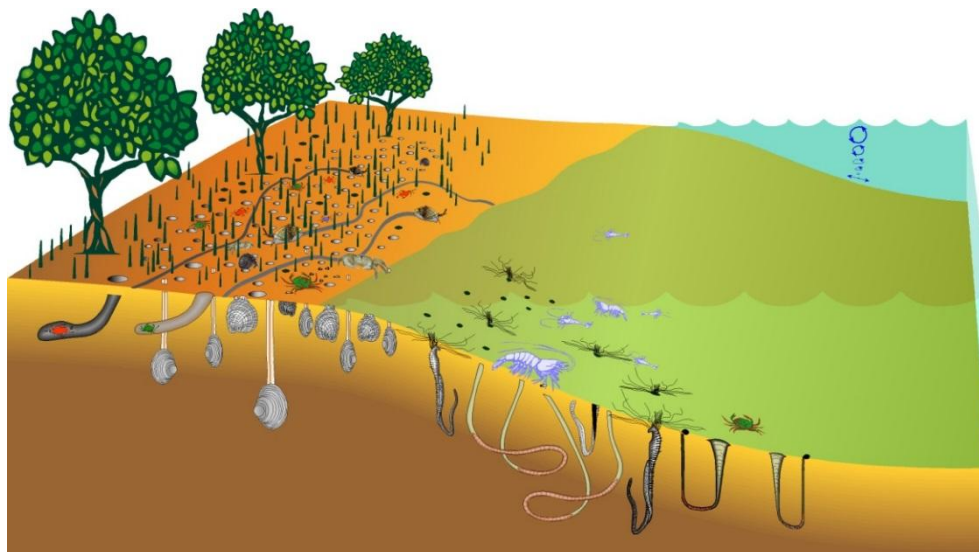

Figure A-1:   Biological and physical processes such as the burrowing and feeding activities of animals and/or sediment resuspension by waves, mix the upper sediment column. As a result, sediment profiles are modified and limit the temporal resolution of dating. The surface mixed layer (SML) is the yellow zone.

Biological mixing has been modelled as a one-dimensional particle-diffusion process (Goldberg and Kiode, 1962) and this approach is based on the assumption that the sum effect of 'random' biological mixing is integrated over time. In estuarine sediments exposed to bioturbation, the depth profile of unsupported ^{210}Pb typically shows a two-layer form, with a surface layer of relatively constant unsupported ^{210}Pb concentration overlying a zone of exponential decrease. In applying these types of models, the assumption is made that the mixing rate (i.e., diffusion co-efficient) and mixing depth (i.e., surface-mixed layer, SML) are uniform in time. The validity of this assumption usually cannot be tested, but changes in bioturbation process could be expected to follow changes in benthic community composition.

References

Alexander, C.R., Smith, R.G., Calder, F.D., Schropp, S.J., Windom, H.L. (1993) The historical record of metal enrichment in two Florida estuaries. *Estuaries,* 16(3B): 627–637.

Benoit, G., Rozan, T.F., Pattoon, P.C., Arnold, C.L. (1999) Trace metals and radionuclides reveal sediment sources and accumulation rates in Jordan Cove, Connecticut. *Estuaries,* 22(1): 65–80.

Bromley, R.G. (1996) *Trace fossils: biology, taphonomy and applications*, second edition. Chapman and Hall, London: 361.

Guinasso, N.L. Jr., Schink, D.R. (1975) Quantitative estimates of biological mixing rates in abyssal sediments. *Journal of Geophysical Research,* 80: 3032–3043.

Matthews, K.M. (1989) Radioactive fallout in the South Pacific, a history. Part 1. Deposition in New Zealand. *Report NRL* 1989/2*.* National Radiation Laboratory, Christchurch, New Zealand.

Ritchie, J.C., McHenry, J.R. (1989) *Application of radioactive fallout caesium-137 for measuring soil erosion and sediment accumulation rates and patterns: A review with bibliography*. Hydrology Laboratory, Agriculture Research Service, U.S. Department of Agriculture, Maryland.

Robbins, J.A., Edgington, D.N. (1975) Determination of recent sedimentation rates in Lake Michigan using ^{210}Pb and ^{137}Cs. *Geochimica et Cosmochimica Acta,* 39: 285–304.

Sharma, K., Gardner, L.R., Moore, W.S., Bollinger, M.S. (1987) Sedimentation and bioturbation in a saltmarsh revealed by ^{210}Pb, ^{137}Cs and ^{7}Be studies. *Limnology and Oceanography,* 32(2): 313–326.

Swales, A., Hume, T.M., Oldman, J.W., Green, M.O. (1997) Holocene sedimentation and recent human impacts in a drowned-valley estuary: 895–900. In: Lumsden, J. (Ed.). *Proceedings of the 13th Australasian Coastal and Ocean Engineering Conference,* Centre for Advanced Engineering, University of Canterbury, Christchurch, New Zealand.

Swales, A., Williamson, R.B., Van Dam, L.F., Stroud, M.J., McGlone, M.S. (2002) Reconstruction of urban stormwater contamination of an estuary using catchment history and sediment profile dating. *Estuaries,* 25(1): 43–56.

Valette-Silver, N.J. (1993) The use of sediment cores to reconstruct historical trends in contamination of estuarine and coastal sediments. *Estuaries,* 16(3B): 577–588.

Wise, S. (1977) The use of radionuclides ^{210}Pb and ^{137}Cs in estimating denudation rates and in soil measurement. *Occasional paper No. 7 University of London*, Kings College, Department of Geography, London.

Appendix B   Delft3d hydrodynamic flow and sediment transport model

Model suite description

Three-dimensional flows are solved in the Delft3d model using the three-dimensional nonlinear momentum equations derived from the Navier-Stokes equations. The solutions assume that flow is incompressible and that horizontal length scales are greater than vertical depth scales. This small aspect ratio thus reduces the vertical momentum equation to the hydrostatic pressure assumption and greatly simplifies the numerical solutions and computational times of simulations.

The transport of scalars i.e., salinity, temperature (density) and sediment, is solved using a coupled three-dimensional advection–diffusion (A–D) equation. Horizontal and vertical variations in density in the model caused by, for example, freshwater from rivers, are initially transported and mixed by the coupled advection and diffusion equation. The model solution assumes the Boussinesq approximation where the variations in the density are only dynamically accounted for in the pressure terms of the Navier-Stokes equation. In the Delft3d vertical sigma co-ordinate system, this reduces the immediate effects of buoyancy on vertical flows by assuming this is taken into account through the effects of the horizontal pressure gradient and vertical turbulence closure scheme (Deltares, 2011).

Cohesive suspended sediments are transported by the same A-D transport methodology where suspensions are advected by the flow and diffused vertically by turbulent mixing. In addition, sediment fractions have a specified settling velocity (related to particle size via the Stokes settling equation), bed power of erosion, critical bed erosion threshold and critical deposition threshold that may be varied through the model domain. The process of flocculation can be simulated by modifying the settling velocity of the localised sediment suspension through both suspension concentration and the effects of salinity in the water column (Deltares, 2011).

The SWAN model is a spectral wave model intended for shallow water applications in coastal and estuarine environments (Booij et al., 1999; Ris et al., 1999). It computes the evolution of the wave energy spectrum in position (x, y) and time (t), explicitly taking into account the various physical processes acting on waves in shallow water. These include the effects of refraction by currents and bottom variation, and the processes of wind generation, white-capping, bottom friction, quadruplet wave-wave interactions, triad wave-wave interactions and depth-induced breaking. The model can incorporate boundary conditions representing waves arriving from outside the model domain.

For all scenarios that include a surface wind stress, the SWAN wave model is 'online dynamically coupled' to the Delft3d flow module throughout a simulation.

Hauraki Gulf model development history

The Delft3d model of the Hauraki Gulf was developed under internal NIWA capability funding to replace the Regional Harbour Model (RHM) that was originally run on the DHI MIKE3 and even older 3DD model platforms (Oldman et al., 2004; Black et al., 2000). The new model domain shown in Figure B-1 has a regular orthogonal 500 m × 500 m resolution grid and the bathymetry used in the grid is derived from a combination of digitised chart data (LINZ: NZ53, NZ532 and NZ553) plus NIWA soundings.

The Delft3d model was set up with 10 equally spaced vertical sigma-layers although vertical resolution can be set much higher. Consequently, in the shallower coastal water of the model

domain, the vertical resolution of the water column is higher than in a deeper offshore water column. An increased vertical resolution effectively increases computational time by a factor of 2. Therefore, for practical applications some sacrifice has to be made between vertical resolution and overall run time. For this study we were mainly focused on regions in the Hauraki Gulf less than 50 m deep (~5 m model vertical resolution). This was reasoned as acceptable for this initial study where sediment transport processes in the relatively shallow Firth of Thames was of the main interest.

Model boundary conditions and inputs

Tides

Outer northern boundaries of the model are between the North Island east coast and Great Barrier Islan, and the model's eastern boundary is between Great Barrier Island and the northern tip of the Coromandel Peninsula as shown in Figure B-1. The model is forced at these two ocean boundaries with time series of tidal elevations generated by harmonic constituents extracted from the EEZY tidal model (Stanton et al., 2001). The horizontal component of salinity and temperature (and density) at the two boundaries is held constant through the simulation.

River Sources

The sites of the three river sources under investigation are shown in Figure B-1. Table B-1 shows the mean annual discharge rating according to the NIWA Water Resource Explorer (WRENZ) database. In addition, a time series of gauged discharge data recorded in the Waihou River dating back from the present to 1997 was used to determine the magnitude and duration of a typical flood event for the Waihou River. The mean and maximum peak discharge and duration of the event (over both the rising and falling limbs of the hydrograph) for the Waihou time series are shown in Table B-1. Data for the Piako and Kauaeranga Rivers when in flood are estimated from some recent floods captured and recorded in the Waikato Regional Council (WRC) Gauge network database and are shown in Table B-1.

Table B-1: **River discharge and SSC for the three river sources.**

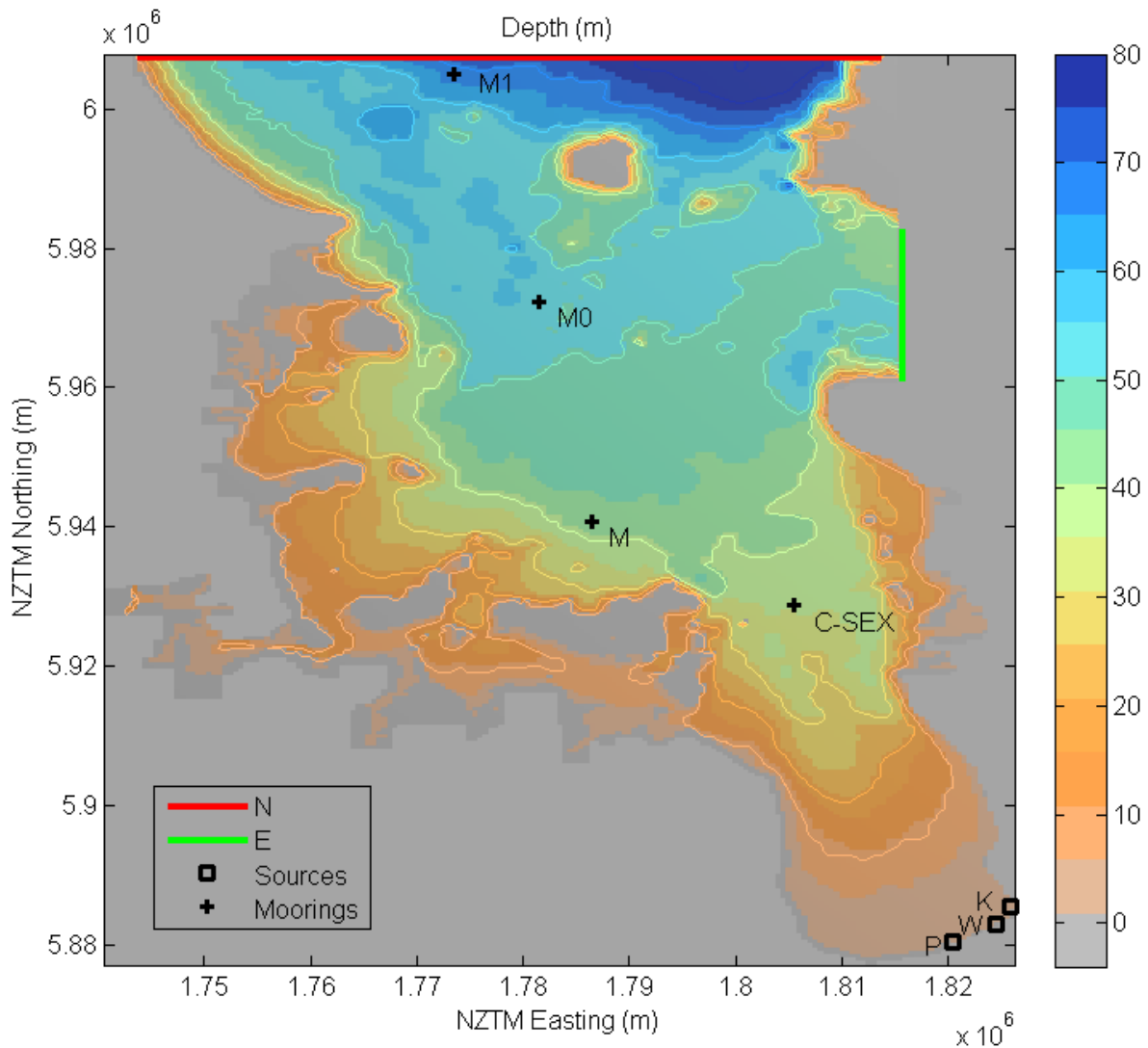| Source	Mean Q (m^3/s)	Storm Peak Q (m^3/s)	Large Storm Q (m^3/s)	Duration of event (days)	SSC (mg/l)	Peak SSC (mg/l)
Waihou	60	100	200	16	200	1200
Piako	20	30	N/A	2.5	200	1200
Kauaeranga	7	17	N/A	2.5	200	1200

Figure B-1: Hauraki Gulf model bathymetry, oceanic boundaries, mooring sites and freshwater source input locations. W = Waihou; P = Piako; K = Kauaeranga .

The asymmetric fast rising limb to a flood peak and slow falling limb that returns to a mean discharge are synthesised using a lognormal shape function that spans the period of an event. The shape function asymmetrically increases mean flow to the peak flows shown in Table B-1 and then returns back to mean flow. This effectively simulates an idealised hydrograph.

At the time of writing no conclusive analysis of sediment loading of the major rivers was available. A. Swales (pers. comm.) has measured SSC levels of up to 1700 mg/l during floods at an instrumented station on the 'Appletree' transect, which is situated in the mangroves in the southern Firth. These high levels of SSC are elevated mainly through wave resuspension of bed sediments. Therefore, based on some of these measurements, we assume a nominal background loading of 200 mg/l. This value is slightly arbitrary but representative of baseline (no storm/flood) concentrations in the sources included in the model. The same lognormal shape function is also used to synthesise the SSC time series increasing from background levels of 200 mg/l to 1200 mg/l during a storm.

Wind Speed and Direction

Three winds were used in the simulation. These are calm conditions or no wind, the prevailing southwest (SW) wind and a northeast (NE) wind. The SW wind mimics the influence of oceanic weather systems propagating northward from lower latitudes, and the NE wind mimics the passage of tropical lows southward from the equator.

Wind speed is ramped up from zero through the simulation to an asymptotic peak of 40 kph (11 m/s) that coincides with peak river discharg,e and then subsides back to zero. The ramp up of wind speed is to prevent the development of spurious shock waves and inertial currents in the model domain.

Salinity stratification and mixing

The modelling of salinity and stratification in the Hauraki Gulf includes only the 3 major identified freshwater sources to the southern Firth of Thames. The freshwater is transported and mixed in the model scheme through the A-D scheme and turbulence closure model.

Turbulence closure and vertical mixing in the model are handled by the Delft3d k-epsilon turbulence closure model. This solves two transport equations, the production (k) and the dissipation (epsilon) of turbulent kinetic energy (TKE). Solutions to the two transport equations in the k-epsilon closure model assume that the TKE production, buoyancy and TKE dissipation terms dominate vertical stability and mixing, and that horizontal flow scales are much larger than those in the vertical (Deltares, 2011).

Background horizontal eddy viscosity and eddy diffusivity are parameterised in the model and used to simulate the effects of horizontal shear and mixing due to, for example, larger eddies. This is used as an effective calibration parameter to tune the transfer of horizontal momentum (velocity) and mass (salinity) effects in the model. These can be produced as maps for the models and values geographically isolated/allocated to exact locations.

Suspended sediment transport model setup

The Delft3d cohesive sediment transport model requires information about sediment particle size, including Stokes fall velocity, critical shear stress thresholds for deposition and erosion of the particles, and power of erosion at the bed. An initial bed layer is specified in the model domain. The critical shear stress thresholds and power of erosion can be mapped into the model domain. This allows different flow regimes to be mimicked by the model, e.g., different thresholds can be specified for wetting and drying areas.

A particle grain size of 20 μm was used in the sediment-transport model, corresponding to a fine to medium silt.

Model validation

The model was validated using hydrographic data sets collected by NIWA during 1996 at the M0 and M1 sites and at the C-SEX mooring site (Figure B-12; Figure B-3). The current meters were moored in relatively deep water (60, 50 and 40 m, respectively). The model shows good agreement with tidal current periodicity and phase at the two sites. The model also simulates the effects of surface wind forcing (yearday 254), but there is more variation in the predicted currents than seen in the observations.

Figure B-4 shows the observed and modelled surface and bottom salinity and temperature time series at the C-SEX mooring site for the January 2006 time period. The model captures the effects of near-surface seasonal heating but the modelled bottom temperature field deviates from the observed. This is a possible result of not including the influence of shelf fluxes of temperature into

the model, e.g., upwelling/downwelling effects. The modelled salinity shows deviation from the observed and towards the end of the predicted time series overestimates the strength of salinity stratification. This could result from overestimating river inputs or underestimating the effects of mixing. These will need to be further investigated in future studies.
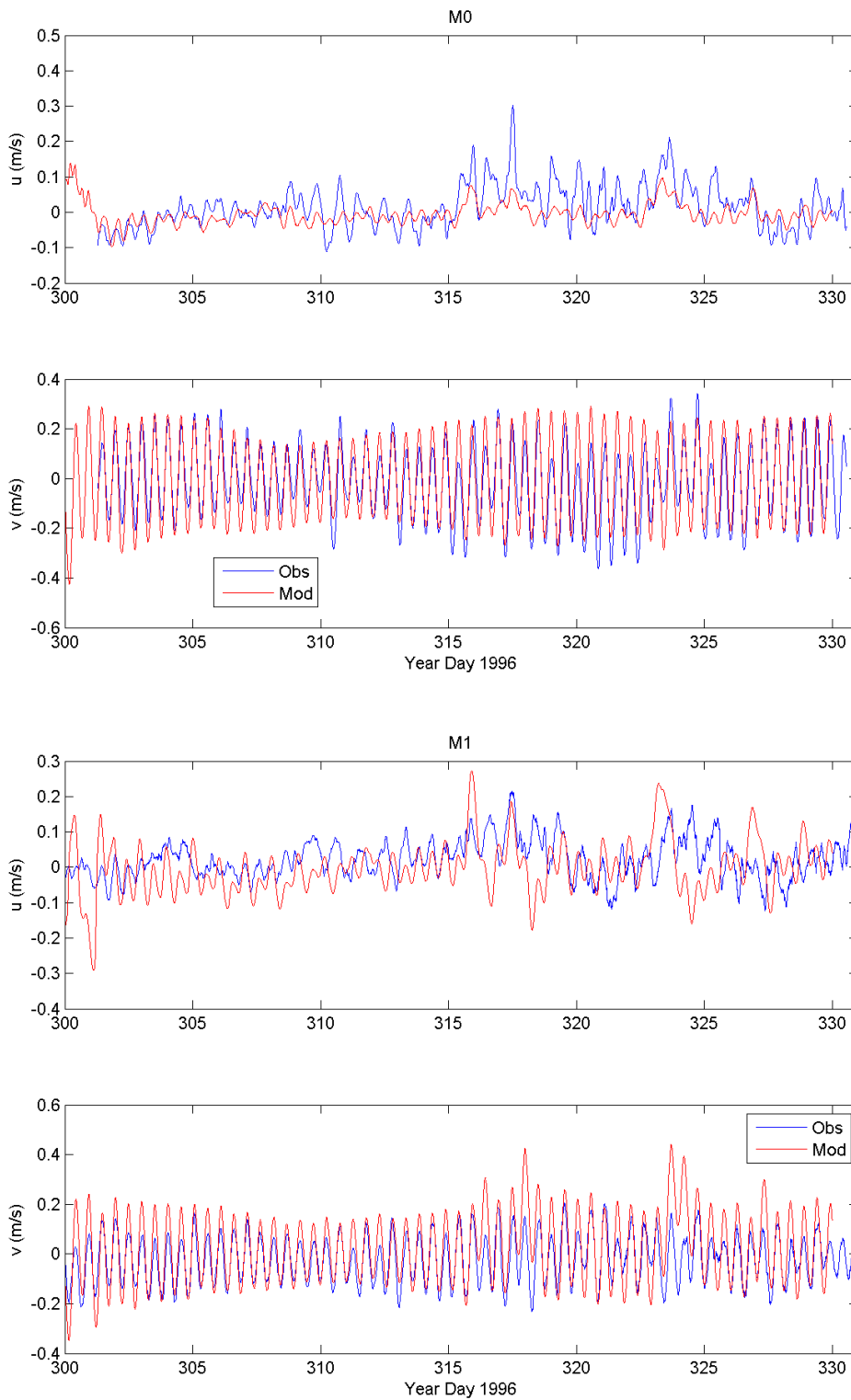

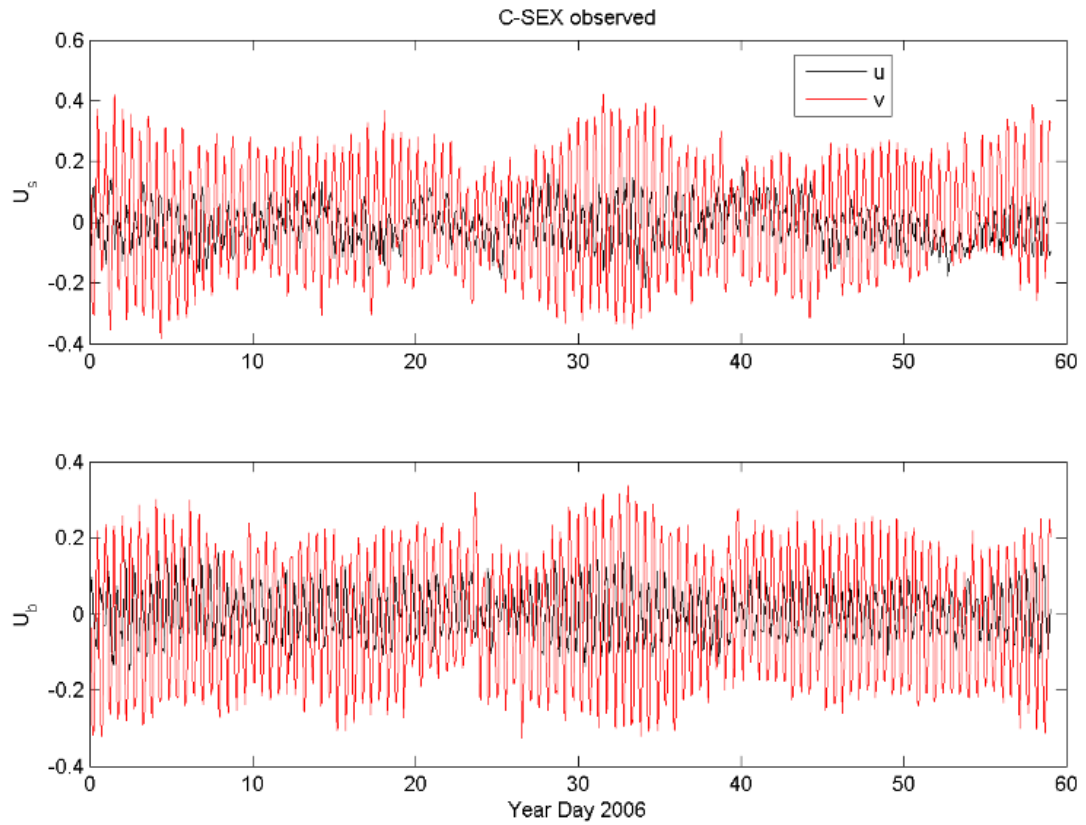**Figure B-2:   MO and M1 mooring data used to validate Deltares modelling.**

Figure B-3: Observed currents from Firth of Thames mooring current meters (upper) used to validate Deltares modelled currents (lower).
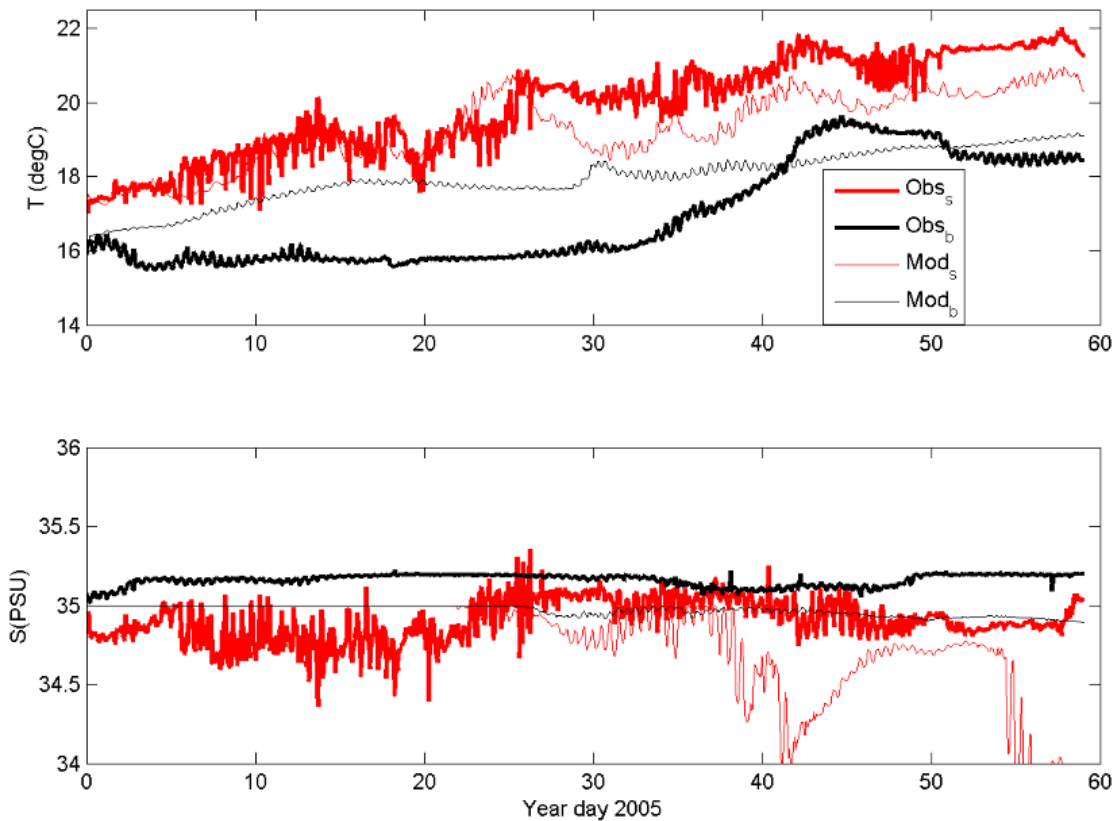
Figure B-4: Observed temperature and salinity from Firth of Thames mooring current meters (upper) used to validate Deltares modelled temperature and salinity (lower).

No SSC data were available to calibrate the sediment-transport model. Therefore, sediment-transport parameters were taken from the literature (e.g. Whitehouse et al., 2000).

References

Black, K.P., Bell, R.G., Oldman, J.W., Carter, G.S., Hume, T.M. (2000) Features of 3-dimensional barotropic and baroclinic circulation in the Hauraki Gulf, New Zealand. *New Zealand Journal of Marine and Freshwater Research,* 34(1): 1–28.

Booij, N., Ris, R.C., Holthuijsen. L.H. (1999) A third-generation wave model for coastal regions 1. Model description and validation. *Journal of Geophysical Research,* 104(C4): 7649–7666.

Capson, T., Guinotte, J. (2014) F*uture proofing New Zealand's shellfish aquaculture: monitoring and adaptation to ocean acidification.* ISSN 1179-6480 (online), ISBN 978-0-478-43763-8 (online).

Deltares (2011). Delft-3D-Flow: Simulation of multi-dimensional hydrodynamic flows and transport phenomena, including sediments. *User Manual Version* 3.15: 672.

Kroeker, K. J., Kordas, R.L., Crim, R.N., Singh, G.G. (2010) Meta-analysis reveals negative yet variable effects of ocean acidification on marine organisms. *Ecol. Lett.* 13: 1419–1434.

Munday, P.L., Dixson, D.L., McCormick, M.I., Meekan, M., Ferrari, M.C.O., Chivers, D.P. (2010) Replenishment of fish populations is threatened by ocean acidification. *Proceedings of the National Academy of Sciences,* 107: 12930–12934.

Oldman, J.W., Senior, A., Haskew, R., Ramsey, D. (2004) Hauraki Regional Harbour Model: Set-up, Calibration and Verification. *NIWA Client Report:* HAM2004-038: 49.

Provoost, P., van Heuven, S., Soetaert, K., Laane, R. W. P. M., Middelburg, J. (2010) Seasonal and long-term changes in pH in the Dutch coastal zone. *Biogeosciences*, 7: 3869–3878.

Ris, R.C., Holthuijsen, L.H., Booijm, N. (1999) A third-generation wave model for coastal regions 2. Verification. *Journal of Geophysical Research,* 104(C4): 7667–7681.

Stanton, B.R., Goring, D.G., Bell, R.G. (2001) Observed and modelled tidal currents in the New Zealand region. *New Zealand Journal of Marine and Freshwater Research,* 35(2): 397–415.

Sunda, W., Cai, W.-J. (2012) Eutrophication induced CO2-acidification of subsurface Coastal Waters: interactive effects of temperature, salinity and atmospheric pCO2. *Environmental Science and Technology*, 46: 10651–10659.

Waldbusser, G.G., Salisbury, J.E. (2014) Ocean acidification in the coastal zone from an organism's perspective: multiple system parameters, frequency domains, and habitats. *Ann. Rev. Mar. Sci*. 6: 221–247.

Whitehouse, R.J., Soulsby, R.L., Roberts, W., Mitchener, H. (2000) *Dynamics of estuarine muds.* Thomas Telford, UK.

Appendix C Accuracy and precision of nutrient budget

Webster et al. (1999) conducted sensitivity analyses on idealised LOICZ budgets of various temporal and spatial averaging schemes. High-inflow periods into the Firth are of much shorter duration than low-flow periods, and the overall range of salinities in the Firth under high and low flows is not large (~2 psu), indicating that ocean end-member mixing clearly dominates river flows in terms of the salt budget. The analysis of Webster et al. (1999) indicated that negligible bias in estimated mixing would be incurred by annual temporal averaging in this case.

Spatial averaging was also applied, in both horizontal and vertical dimensions. The Firth sampling stations were located in the central Firth, down-estuary of the riverine sources of freshwater and nutrients at its head. As described by Webster et al. (1999), these relative dispositions of sampling sites and freshwater and nutrient sources are unlikely to introduce bias in the estimation of fluxes. Similarly, the Gulf stations are located down-estuary of the dominant freshwater source for that compartment (the Firth), and other direct freshwater inputs to the Gulf are relatively small. The budget was also vertically averaged, rather than stratified into upper and lower water-column boxes. Webster et al. (1999) found that the assumption of vertical homogeneity incurred significant bias in flux estimates only if the estuary was in fact highly stratified (i.e., many psu in salinity). Vertical gradients in Firth of Thames salinity were not large (~1 psu) even when maximally stratified, justifying use of a vertically averaged model.

The Firth and Hauraki Gulf, being large and relatively deep systems, were assumed to be dominated in terms of their primary production regimes by phytoplankton. Hence the application of the classical "planktonic" Redfield stoichiometry was assumed to be appropriate for conversions among C, N and P (106:16:1) (Gordon et al., 1996; Swaney, 2011).

The annually averaged primary productivity of 166 g C m^{-2} y^{-1} assessed from seasonal surveys at the Firth monitoring site in 1999–2000 (Gall and Zeldis, 2011) was well within the range of typical productivity values for temperate coastal waters compiled by Bury et al. (2012) for shelf and coastal areas in Hauraki Gulf, elsewhere in New Zealand and overseas. For the elements of the LOICZ budget, it is noted that gross Firth respiration (r = 50 mmol C m^{-2} d^{-1}) was within the range for a number of European estuaries documented by Frankignoulle et al. (1998), while net metabolism (p - r = -12 mmol C $m^{-2}d^{-1}$) was well within the range of heterotrophic cases within the distribution of 70 LOICZ metabolic estimates obtained from budgets made around the world (Buddemeier et al., 2002) (Figure 10-5). The denitrification estimate (1.5 mmol N m^{-2} d^{-1}) was also near the mean of estimates from the 70 budgets tabulated by Buddemeier et al. (2002) (Figure 10-5) and was close to the mean of the literature summary of Seitzinger (1988) for 12 shelf and estuarine studies (1.8 mmol $m^{-2}d^{-1}$), as well as the estimate of Firth denitrification by Giles et al. (2007), which was predicted using oxygen consumption data from Firth benthic biogeochemical field surveys. Finally, the predictions of N loading and metabolism by the budget were used to assess the impacts of Firth mussel farming on ecosystem N removal. These predictions were similar to those of N removal estimates made by biophysical dynamic modelling (Broekhuizen et al., 2005), and converged on a similar conclusion (*viz.*, small impacts by farming). Overall, the primary production, respiration and denitrification values obtained appear reasonable in the context of similar estimates made elsewhere, made with the same, and made with other, methods.

The precision of the Firth nutrient budget estimates was estimated using a Monte Carlo approach (Swaney, 2011) that was similar to that implemented by Álvarez-Salgado and Gilcoto (2004) to

estimate error of oceanographic variables in budgetary analyses. Net metabolism (p - r) can be described as:

(residual P flux + mixing P flux + river P flux) x organic C:P (1)

Residual P flux error is considered to be composed of the errors associated with river gauging (estimated to be 8%; A. McKerchar, NIWA, pers. comm.) and the errors associated with CLUES predicted loads relative to gauged loads (estimated to be 10%; Elliott et al., 2005). Error on mean P for the Firth was 4% over all voyages. These errors were used to generate 100 normally distributed estimates of residual flux and mean P, and their product, residual P flux. Similarly, 100 mixing P flux estimates were created based on the error of salinity over all seasons (1%) and the residual salt flux (calculated from residual flux and salinity difference), and the error on P samples. Error on organic C:P estimates was set at 4%, based on Smith et al. (1991). The CV of 100 iterations of equation (1), above, was 24%. Thus, (p – r) was -12 $\pm$ 3 mmol C m^{-2} d^{-1}. Error of denitrification was assumed to be a similar relative magnitude, indicating that denitrification was 1.5 $\pm$ 0.4 mmol m^{-2} d^{-1}.

References

Álvarez-Salgado, X., Gilcoto, M. (2004). Inferring nitrification rates with an inverse method in a coastal upwelling system, Ría de Vigo (NW Spain). *Marine Ecology Progress Series*, 276: 3–17.

Broekhuizen, N., Oldman, J., Image, K., Gall, M., Zeldis, J. (2005) Verification of plankton depletion models against the Wilson Bay synoptic survey data. *NIWA Client Report.*

Buddemeier, R., Smith, S., Swaney, D., Crossland, C. (2002) The role of the coastal ocean in the disturbed and undisturbed nutrient and carbon cycles. *LOICZ Reports & Studies*. LOICZ Texel, The Netherlands.

Bury, S.J., Zeldis, J.R., Nodder, S.D., Gall, M. (2012) Regenerated primary production dominates in a periodically upwelling shelf ecosystem, northeast New Zealand. *Continental Shelf Research,* 32: 1–21.

Elliott, A., Alexander, R., Schwarz, G., Shankar, U., Sukias, J., McBride, G. (2005) Estimation of nutrient sources and transport for New Zealand using the hybrid mechanistic-statistical model SPARROW. J*ournal of Hydrology (New Zealand)*, 44: 1–27.

Frankignoulle, M., Abril, G., Borges, A., Bourge, I., Canon, C., Delille, B., Libert, E., Théate, J.-M. (1998) Carbon dioxide emission from European estuaries. *Science*, 282: 434–436.

Gall, M., Zeldis, J. (2011) Phytoplankton biomass and primary production responses to physico-chemical forcing across the northeastern New Zealand continental shelf. *Continental Shelf Research,* 31: 1799–1810.

Gordon, D.J., Boudreau, P., Mann, K., Ong, J.-E., Silver, W., Smith, S., Wattayakorn, G., Wulff, F., Yanagi, T. (1996) *Loicz biogeochemical modelling guidelines*. Texel.

Seitzinger, S. (1988) Denitrification in freshwater and coastal marine ecosystems: Ecological and geochemical significance. *Limnology and Oceanography,* 33: 702–724.

Smith, S., Hollibaugh, J., Dollar, S., Vink, S. (1991) Tomales Bay metabolism: C-n-p stoichiometry and ecosystem heterotrophy at the land-sea interface*. Estuarine, Coastal and Shelf Science*, 33: 223–257.

Swaney, D. (2011) Biogeochemical budgeting in estuaries. Pp. 343–362. In: Wolanski, E., McCluskey D.S., Uncles, R.J., editors. *Treatise on estuarine and coastal science*. Academic Press.

Webster, I., Parslow, J., Smith, S. (1999) Implications of spatial and temporal variation for LOICZ biogeochemical budgets. *Australasian Estuarine Systems: Carbon, Nitrogen and Phosphorus Fluxes*. 12, LOICZ IPO, Texel, The Netherlands.

Appendix D Corrections to moored DO sensors

The following provides information on the Aanderaa 3830 and SeaBird SBE-37s used on the mooring as well as how the data were validated and corrected.

Aanderaa Dissolved Oxygen Optode 3830

Documents used
http://www.aanderaa.com/media/pdfs/Oxygen-Optode-3835-4130-4175.pdf

Method for optode data processing
- Raw data files for each upper and lower RCM deployment are concatenated.
- A nominal depth value is obtained from the metadata header of the files.
- The optode outputs DO in µM (µmol/L) which is converted to µmol/Kg. As conductivity (and therefore salinity and Sigma-T) is not measured by most RCMs interpolate the Sigma-T values from the corresponding SBE-37.
  The following equation is used to convert oxygen from µmol/L to µmol/Kg:

$$DO\left[\mu\frac{mol}{Kg}\right] = DO\left[\mu\frac{mol}{L}\right] * \frac{1000}{Sigma\_theta(P=0,T,S)+1000}$$

Where:
  - µmol/L = micromoles per Kilogram (=µM), unit output from the optode
  - µmol/Kg = micromoles per Kilogram, the derived unit
  - Sigma_theta = potential density, is the density a parcel of water would have if it were raised adiabatically to the surface without change in salinity, calculated with pressure = 0.
  - T = temperature
  - S = salinity

- Flag all values below 70 µmol/Kg and above 350µmol/Kg. These cutoff points were chosen by looking at the CTD DO data and finding the max and mins.
- Reduce the noise of the DO signal by computing a fifth-order one-dimensional median filter of the dataset.
- The median is calculated using the following equation :

$$Y(k) = X\left(k - \frac{N-1}{2} : k + \frac{N-1}{2}\right) \qquad \text{for N odd}$$
$$Y(k) = X\left(k - \frac{N}{2} : k + \frac{N}{2} - 1\right) \qquad \text{for N even}$$
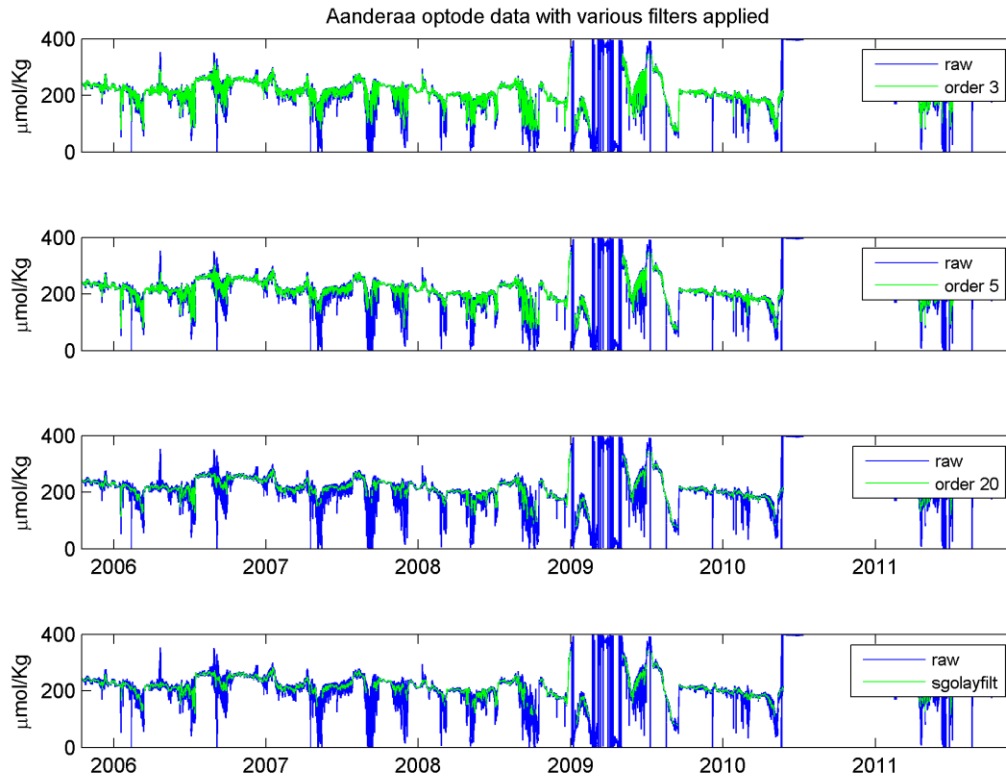
Figure D-1:   Raw Dissolved Oxygen data (blue line) with median filters of various orders (green line).
Subplot 1: DO data with a median filter of order 3 applied. Subplot 2: DO data with a median filter of order 5 applied. Subplot 3: DO data with a median filter of order 20 applied. Subplot 4: DO data with a Savitzky-Golay smoothing filter applied. A median filter of order 5 was chosen as the final data filter as it best smoothed the signal without losing significant detail.

- Calculate the theoretical saturation values based on the 100% oxygen saturation capacity of water at a given temperature and salinity.

$$Oxsol(T,S)\left[\frac{ml}{L}\right] = e^{\{A0+A1(Ts)+A2(Ts)^2+A3(Ts)^3+A4(Ts)^4+A5(Ts)5^5+S*[B0+B1(Ts)+B2(Ts)^2+B3(Ts)^3]+C0(s)^2\}}$$

$$Oxsol(T,S)\left[\mu\frac{mol}{Kg}\right] = \frac{(Oxsol(T,S)\left[\frac{ml}{L}\right] * 4460)}{(Sigma\_theta + 1000)}$$

Where:
- Oxsol(T,S) = oxygen saturation value = volume of oxygen gas at standard temperature and pressure conditions (STP) absorbed from humidity-saturated air at a total pressure of one atmosphere, per unit volume of the liquid at the temperature of measurement (mL/L)
- Ts = ln [(298.15 – T) / (273.15 + T)], scaled temperature
- S = salinity (psu)
- T = water temperature (ITS-90, °C)
- A0 = 2.00907, A1 = 3.22014, A2 = 4.0501, A3 = 4.94457, A4 = -0.256847, A5 = 3.88767
- B0 = -0.00624523, B1 = -0.00737614, B2 = -0.010341, B3 = -0.00817083
- C0 = -0.000000488682

- Calculate Oxygen Saturation for corrected and uncorrected DO values.
- Manually flag bad data.
- Interpolate data to hourly intervals, identify data gaps during turnaround times or when an instrument has failed, set these periods to NaN.

-   Create final 'upper' and lower' data sets containing depth, nominal depth, temperature, salinity, sigma-t, DO, DO % saturation from SBE-37s and current speed, current direction, DO, DO % saturation from the RCMs.

SeaBird SBE-37 with integrated dissolved oxygen sensor

https://www.seabird.com/application_notes/AN64-2.htm

http://www.seabird.com/application_notes/AN64.htm

http://www.seabird.com/application_notes/AN64-3.htm

http://www.seabird.com/products/spec_sheets/37smpododata.htm

http://www.seabird.com/products/spec_sheets/37smpidodata.htm

Seabird manufactures two types of dissolved oxygen sensor: the SBE43, a redesign of the Clark polarographic membrane, which is incorporated into the SBE37-IDO model, and the SBE 63, which is an optical oxygen sensor, incorporated into the SBE37-ODO model. Both instrument types have been used in this study. The SBE37-ODOs replaced the SBE37-IDOs mid-2013 because, although the optical sensors have a slower response time, they are proven to have better longer term stability, suffer from less instrument drift, and are better suited to mooring deployment. The CTD uses the fast responding SBE43 sensor.

Variables

XML files offloaded from the SBE37s were converted to engineering units using the Seabird software SBEdataproc.exe. The following values were output:

Temperature [ITS-90, deg C], Pressure Strain gauge [db], Conductivity [S/m], Oxygen SBE 43 [mg/l] *or* Oxygen SBE 63 [mg/l], Optional: Oxygen SBE 43 [% saturation] *or* Oxygen SBE 63 [% saturation], Salinity Practical [PSU].

If practical salinity or oxygen percent saturation were not output they were calculated using the IMOS seawater toolbox.

Oxygen variables

Oxygen, concentration (units of mg/l or micromoles/kg as selected) - measured SBE 43 or SBE 63 oxygen concentration.

Oxygen, theoretical saturation (units of mg/l or micromoles/kg, as selected) - theoretical saturation limit of the water at the local temperature and salinity, but with local pressure reset to zero (1 atmosphere). This calculation represents what the local parcel of water could have absorbed from the atmosphere when it was last at the surface.

Oxygen, percent saturation (percent) - ratio of measured oxygen concentration to oxygen saturation.

The following equation was used to convert oxygen from mg/l to micromoles/Kg:

[μmole/Kg] = [mL/L] * 44660 / (Sigma_theta(P=0,T,S) + 1000)

where:

[mL/L] = [mg/L] / 1.42903

Sigma_theta (potential density), is the density a parcel of water would have if it were raised adiabatically to the surface without change in salinity.

Comparison of CTD and moored data

DO collected from moored instrumentation typically had higher values than the corresponding points from the CTD casts (Figure D-2). There were a number of features that indicated that the DO data were affected by sensor drift over the length of the mooring deployments:

- There were apparent shifts in DO concentrations across some turnaround dates in both the upper and lower units (Figure D-3). The most obvious was between SBE37-IDO SN 9158, installed as the upper sensor from November 2012 – July 2013, and its replacement in the July 2013 turnaround, SBE37-ODO 10512. The difference was ~36 µmol/Kg.

- For the July 2013 turnaround there were lower than expected DO concentration and saturation values for instruments mounted at 10 m, as well as lower values compared to previous years (Figure D-4). Referring to Figure D-2, a value of 80% saturation in July 2013 was low for 10 m depth. The instrument was in the upper mixed layer, so it would be expected that saturation would be higher at this time of year.

- Lower than expected concentrations when compared to theoretical DO concentration at 100% saturation (discussed further below).
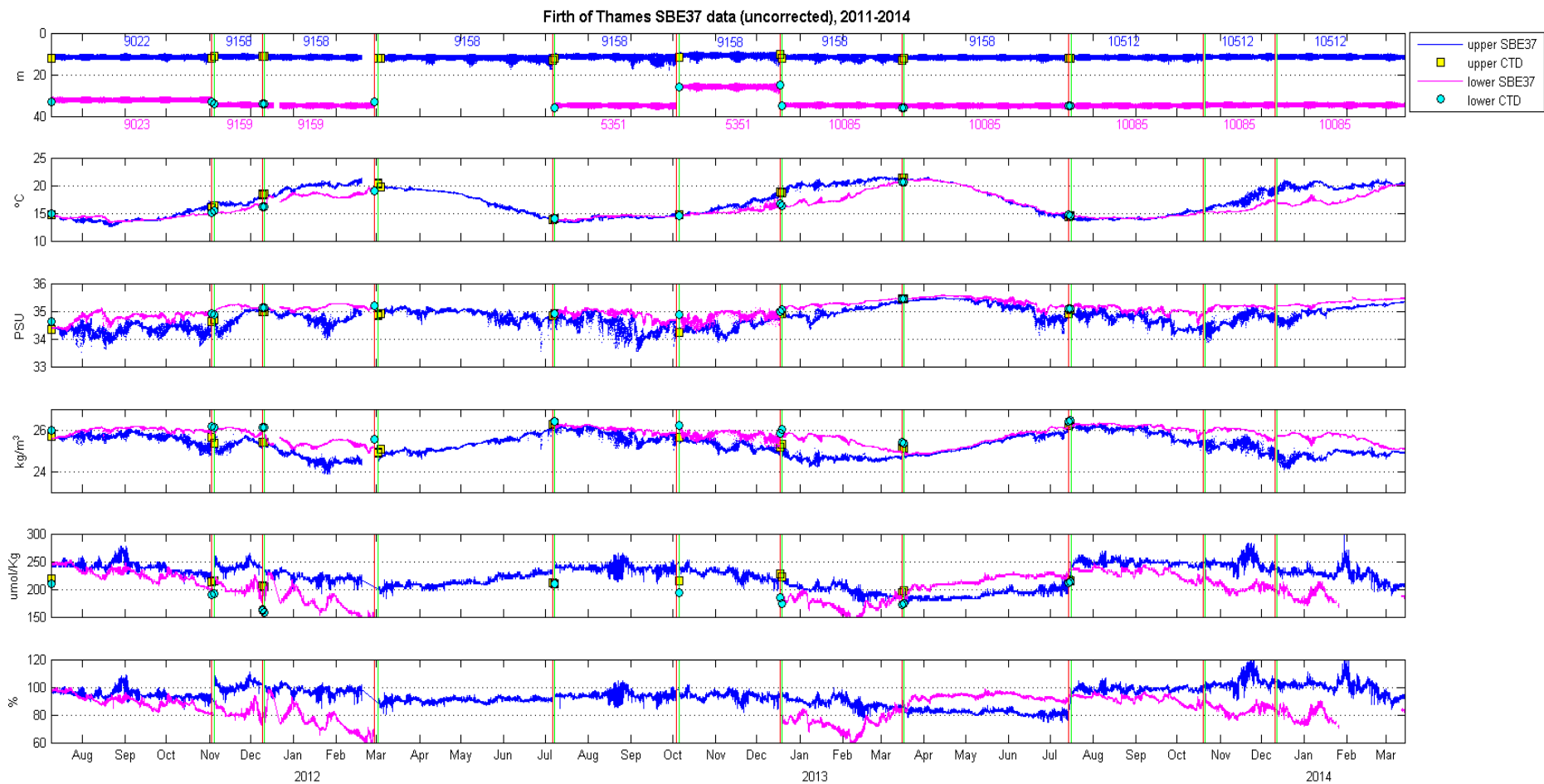
Figure D-2:   Uncorrected time series plot of the upper and lower SBE37s on the C-SEX mooring. The upper SBE37 is plotted in blue with corresponding CTD values represented by yellow squares, the lower SBE37 is plotted in magenta with corresponding CTD values represented by cyan circles. Green and red vertical lines show deployment turnarounds (when instruments will have been cleaned or replaced). Instrument serial numbers are displayed in the top axis.
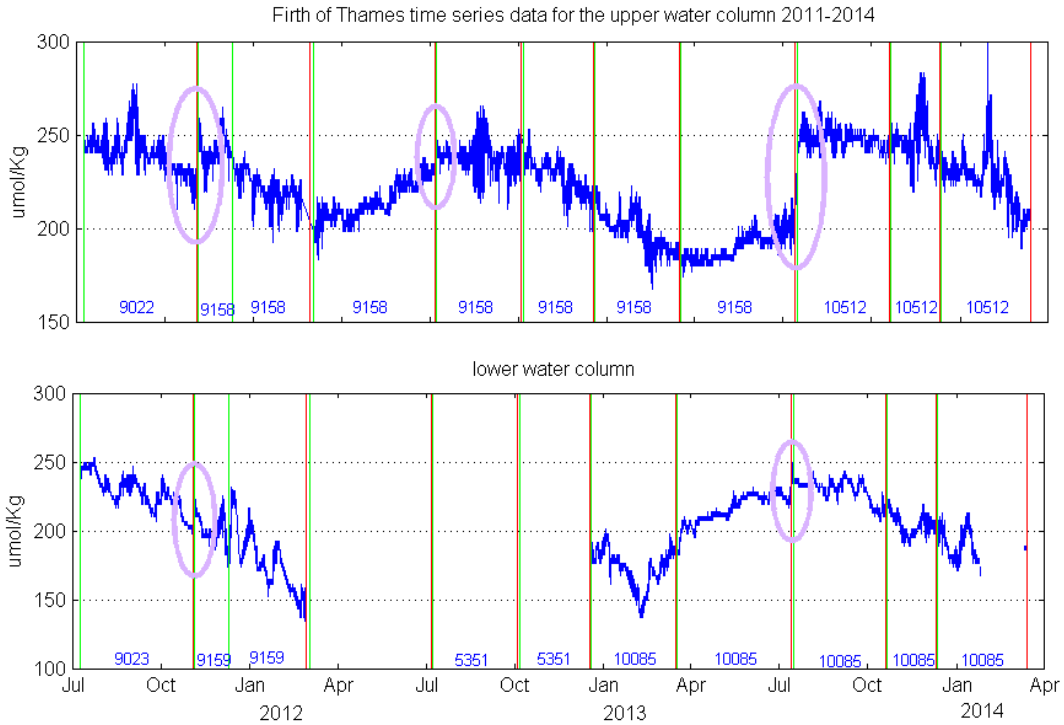
Figure D-3: Uncorrected time series plot showing DO concentration in the upper and lower SBE37s. Highlighted in lilac are offsets before and after turnaround (upper unit in Oct 2011, Jul 2012, and Jul 2013, and lower unit in Nov 2011, and Jul 2013). This occurs because the instrument is experiencing sensor drift and bio-fouling has built up during a deployment. Cleaning of the sensor during turnaround, or replacement of the instrument, has restored the sensors performance.
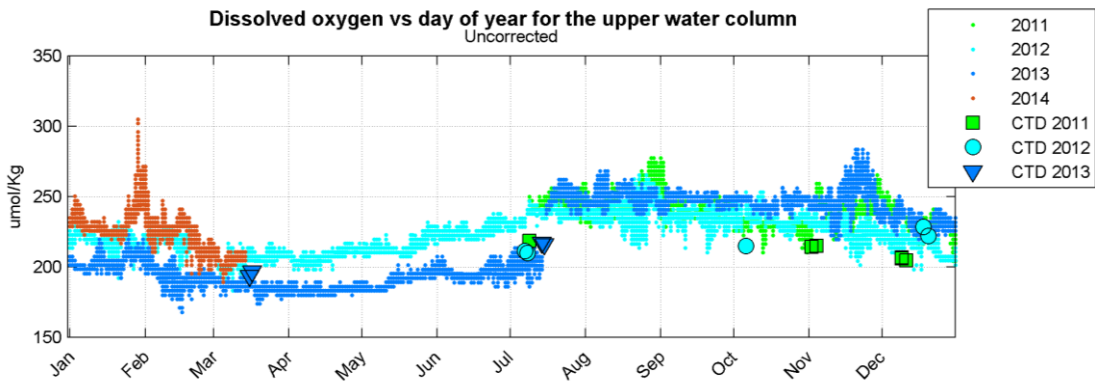
Figure D-4: DO plotted against the day of the year for the upper SBE37. DO concentrations in July 2013 were approximately 30 μmol/Kg lower than values in the same time period in the preceding two years.

Another way to examine sensor performance and water quality trends in time is by comparing values based on the 100% oxygen saturation capacity of the water (using measured temperature and salinity data) to the measured oxygen concentration (Figure D-5). These comparisons are useful for measurements made near the surface, where oxygen saturation in the water column is typically near 100%.

Figure D-5:	Actual concentrations (red line) for the upper unit compared to corresponding theoretical values (blue line) for the same temperatures and salinities. The two concentrations lined up again when the SBE37-ODO 10512 unit was substituted for SBE37-IDO 9158 at the July 2013 turnaround.
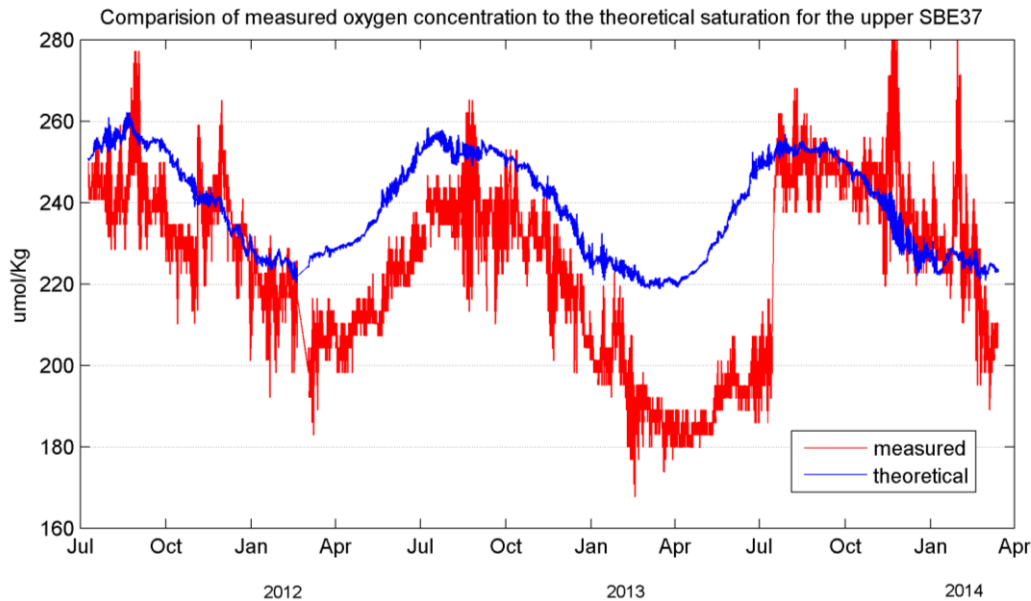
The measured oxygen concentration can be lower or higher than theoretical saturation (which never exceeds 100%) due to natural causes such as algal blooms or wind mixing/bubble injection from waves. If the saturation measured by the sensor does not match the theoretical saturation based on temperature and salinity alone, this does not mean the sensor is reporting incorrectly. However, it does provide a good indication of what we would typically expect to see with the measured temperature and salinity values.

Why do the sensors drift?

Though the sensing technology is very different between the SBE43 (SBE37-IDO) and SBE 63 (SBE37-ODO) oxygen sensors, both are optimized to measure actual DO concentration within spec of +/- 2%. It is not typical to see such a big difference between the SBE43 and 63 when they are working well, recently calibrated, and within spec. SBE37-IDO 9158 was due for recalibration June 2013 (1 month before the end of its deployment) while SBE-37-ODO 10512 was almost new (2 months old).

 Changes in sensor electronics and fouling (biological growth on a sensor, or coatings from oil and other materials in the water column) are the main causes of loss of accuracy in aquatic sensors. As the SBE 43 and 63 DO sensors have very stable electronics, any loss of accuracy is primarily due to fouling. Seabird have noted that the SBE43 sensor is more susceptible to drift than the SBE63.

Typically, the DO sensors will drift low of actual concentrations. As mentioned, the 37-IDO 9158 was due for calibration, so this could have resulted in the difference found as it had been about 2 years since calibration. Given that the SBE63 was more recently calibrated, the expectation was that this sensor was within spec and reporting correct oxygen values within 1 – 2%.

 It is standard procedure during NIWA mooring turnarounds to clean the SBE37s with a diluted Triton-X solution and flush with fresh water in order to reduce the effects of fouling on sensor output. In addition, antifoulant discs are mounted at the water intake and outtake points and these are replaced approximately once per year. According to SeaBird, cleaning the sensor (using Triton as

per their directions) will often remove bio fouling and restore the sensor's performance. If this was the case, one would expect to see an increase in measured DO concentrations after a mooring turnaround when the same sensor has been deployed. From Figure D-2, it is clear that this does not always occur, which indicates that sensor drift as well as biofouling was affecting performance. This drift was treated as increasing at a constant rate from the beginning to the end of the respective sensors deployment.

Correcting Oxygen data

Adverse fouling might take several weeks to occur. When the SBE 43 or 63 sensor starts to show drift from fouling, the effect on the sensor calibration is assumed linear, and therefore can be corrected by adjusting the linear slope term of the calibration equation:

*Oxygen (mL/L) = [Soc * (V + Voffset + tau(T,P) * dV/dt)} * Oxsol (T,S) * (1.0 + A*T + B*T^2 + C*T^3) * e$^{(E*P/K)}$

where:

- V = SBE 43 output voltage signal (volts)

- dv/dt = time derivative of SBE 43 output signal (volts/second), computed over a default window of 2 seconds

- T = temperature (°C)

- S = salinity (psu)

- P = pressure (dbars)

- K = temperature (°K = °C + 273.15)

- $tau(T,P)$ = sensor time constant at temperature and pressure

- $Oxsol(T,S)$ = oxygen solubility function (mL/L), which converts oxygen partial pressure (sensor measurement) to oxygen concentration (Garcia and Gordon, 1992). See Appendix A in [Application Note 64](): Background Information, Deployment Recommendations, and Cleaning and Storage for values at various temperatures and salinities.

- $Soc, Voffset, A, B, C, E,$ and $tau20, D1, D2$ [terms in calculation of tau(T,P)} are calibration coefficients

* Calculates DO from SBE43 output voltage, assumed equal to the SBE63 sensor.

Both the SBE 43 and 63 behave the same in terms of linear drift, the slope drifts rather than its offset. If the reference method for making the correction is as accurate as calibrating using Winkler's determinations or another clean/calibrated DO sensor from different instrument, the sensor can continue to report DO concentrations within factory specifications by applying an adjustment to *Soc*.

The following steps were carried out to derive a correction factor and adjust oxygen data

- Identify periods where DO has sharply changed due to sensor cleaning or instrument replacement (e.g., Figure D-3). Samples taken after the turnaround are more accurate as they have either been more recently calibrated or cleaning of the sensor during turnaround has restored the sensor's performance. These are the reference values.

- Compute the correction ratio between the reference value and the before turnaround SBE 37 sensor value (Ratio = Reference / Before)

- Multiply the correction ratio by the previous *Soc* in the latest calibration sheet.

NewSoc = BeforeSoc * Ratio

since:

BeforeOxygen = BeforeSoc * (V + Voffset) * φ

One can just multiply before DO values with Ratio:

CorrectedOxygen = BeforeOxygen * Ratio

- Correct recovered raw DO data by assuming a linear drift rate. Multiply the oxygen concentrations by the slope correction ratio determined by the time in the deployment that that particular sample was taken.

CorrectedOxygen = BeforeOxygen * Ratio * Rate

Note, to find before and after turnaround values, averages were taken over 1, 4, 24 and 48 hours. The residuals and ratios were calculated for all averages. Table D-1 shows the resulting data sets of all averaged values. 24 hours was considered to fit the data best so the final data set was compiled using those values.

Table D-1:   Correction ratios calculated from averaged time periods before and after mooring turnarounds.

Inst	Correction times		Drifted (before) instrument averages (μmol/Kg)				Reference (after) instrument averages (μmol/Kg)				Residual (Reference - Drifted) (μmol/Kg)				Ratio (Reference / Drifted)			
	start	end	1hr	4hr	24hr	48hr	1hr	4hr	24hr	48hr	1hr	4hr	24hr	48hr	1hr	4hr	24hr	48hr
s1	2011/07/09 10:45	2011/11/02 15:11	228.0	228.6	224.9	223.9	237.2	248.1	252.3	250.6	-9.2	-19.6	-27.5	-26.7	1.04	1.09	1.12	1.12
s1	2012/03/02 07:13	2012/07/06 09:13	230.3	231.1	232.4	231.9	235.3	238.2	238.6	239.8	-5.0	-7.0	-6.2	-7.9	1.02	1.03	1.03	1.03
s1	2012/10/05 13:25	2013/07/14 08:00	204.1	202.8	202.4	203.5	232.7	236.7	241.5	243.1	-28.6	-33.8	-39.1	-39.6	1.14	1.17	1.19	1.19
s2	2011/07/09 10:45	2011/11/02 15:11	205.9	203.7	201.5	201.5	211.4	217.2	218.4	216.5	-5.5	-13.5	-16.9	-15.0	1.03	1.07	1.08	1.07
s2	2013/03/17 13:10	2013/07/14 08:00	228.4	228.1	226.8	225.7	236.3	236.9	234.9	234.9	-7.9	-8.8	-8.1	-9.2	1.03	1.04	1.04	1.04

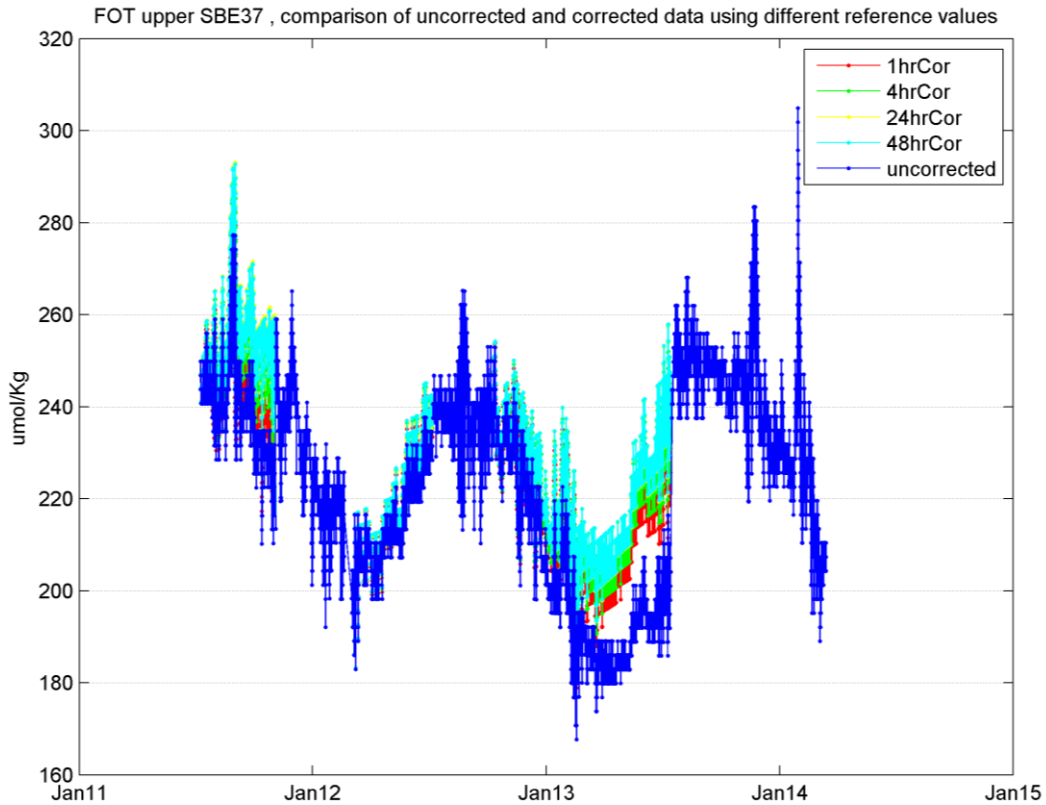**Figure D-6:** Uncorrected and corrected DO data calculated from correction ratios using averages of data 1, 4, 24 and 48 hours before and after mooring turnarounds Refer Table D-1.

The results of the corrections applied to the SBE data are shown in the following plots.

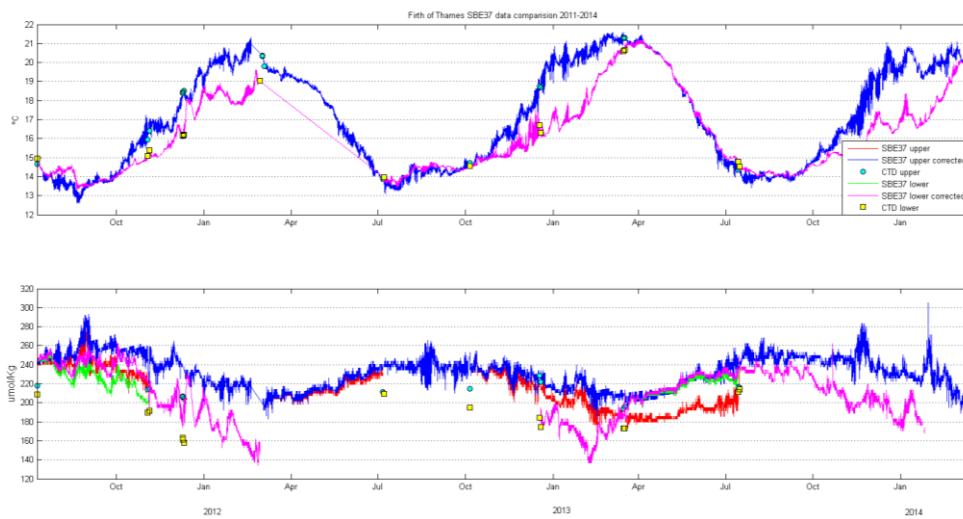**Figure D-7:** Corrected, uncorrected and CTD DO concentrations in the upper (upper axis) and lower (lower axis) water column.
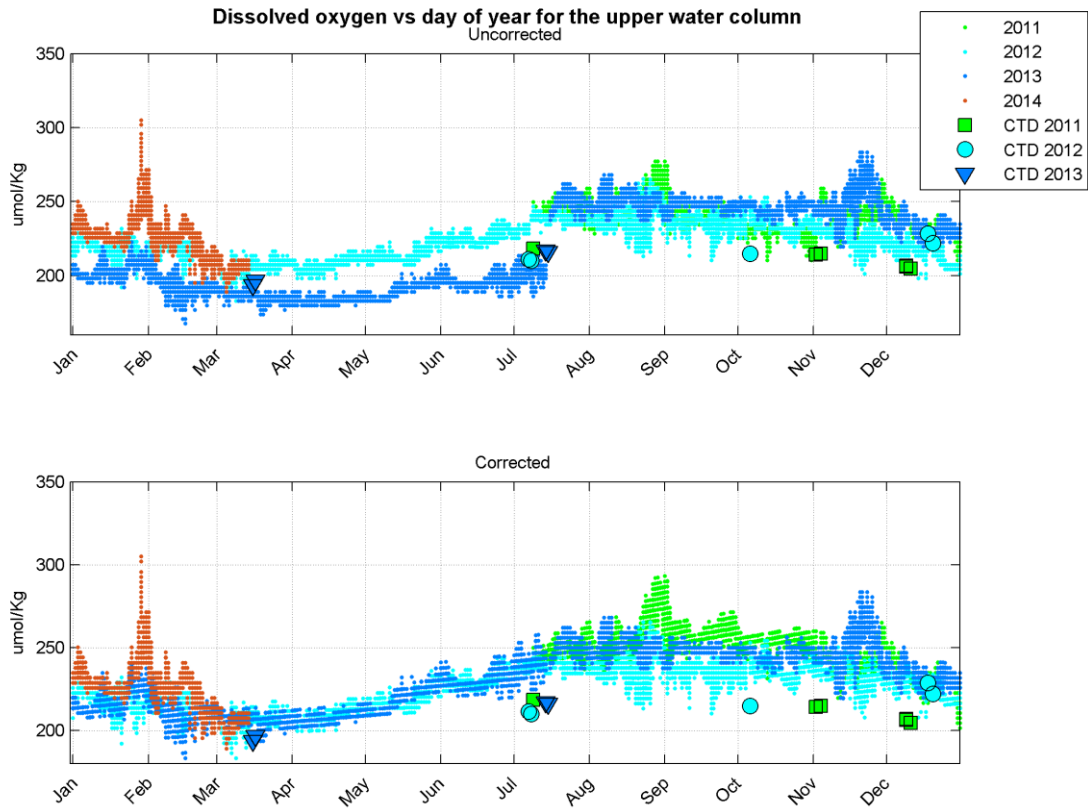
Figure D-8: Corrected and uncorrected oxygen concentration plotted against the day of the year for the upper SBE37. The plot shows the corrected DO concentration values in July 2013 are in better agreement with the values in the same time period in the preceding two years.
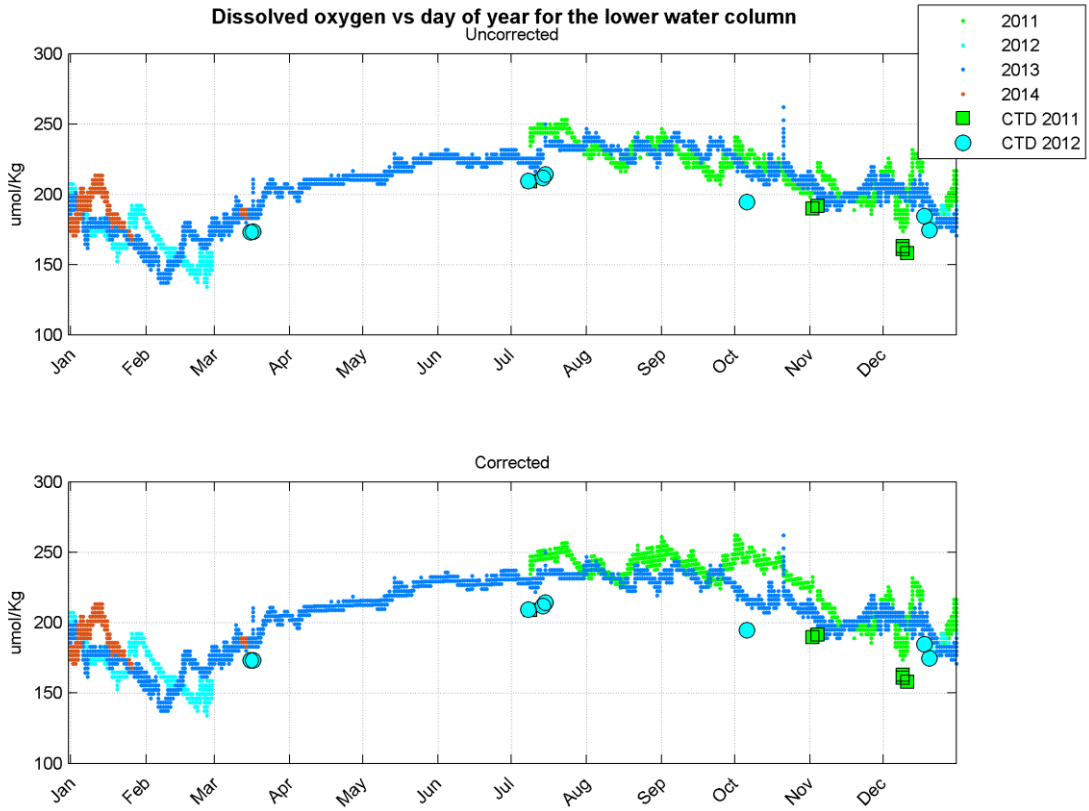
Figure D-9: Corrected and uncorrected oxygen concentration plotted against the day of the year for the upper SBE37.
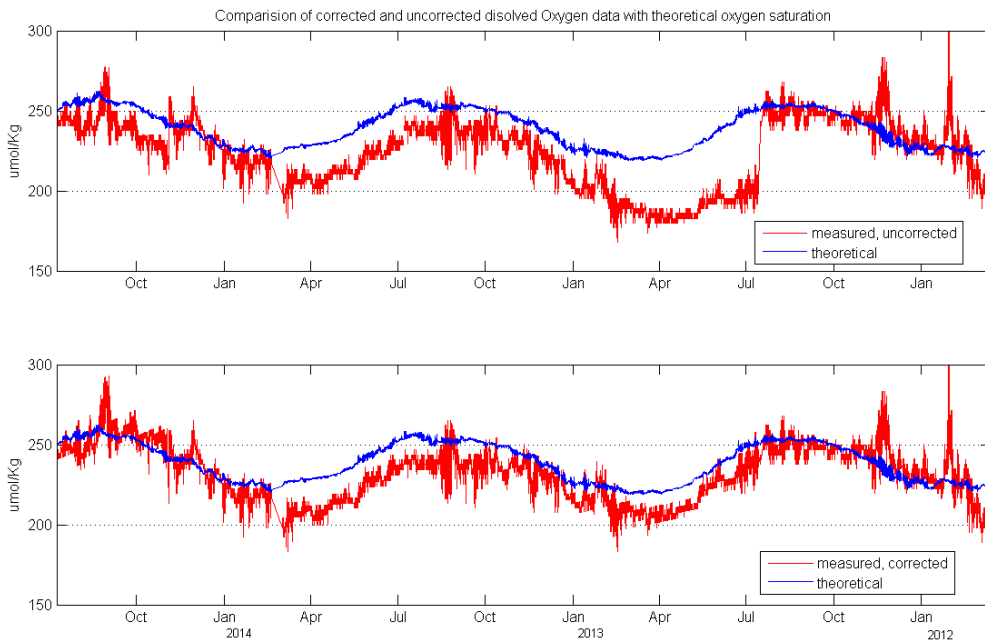
Figure D-10: Actual concentrations (red line) for the upper unit compared to corresponding theoretical values (blue line) for the same temperature and salinity measurements for (top) uncorrected and (bottom) corrected DO values.

Figure D-11: Time series plot of the upper and lower SBE37s on the C-SEX mooring with corrected oxygen concentration and oxygen saturation. The upper SBE37 is plotted in blue and the lower SBE37 in red.

Firth of Thames Water Quality and Ecosystem Health – Data Report

Table D-2: Files used in DO mooring analysis.

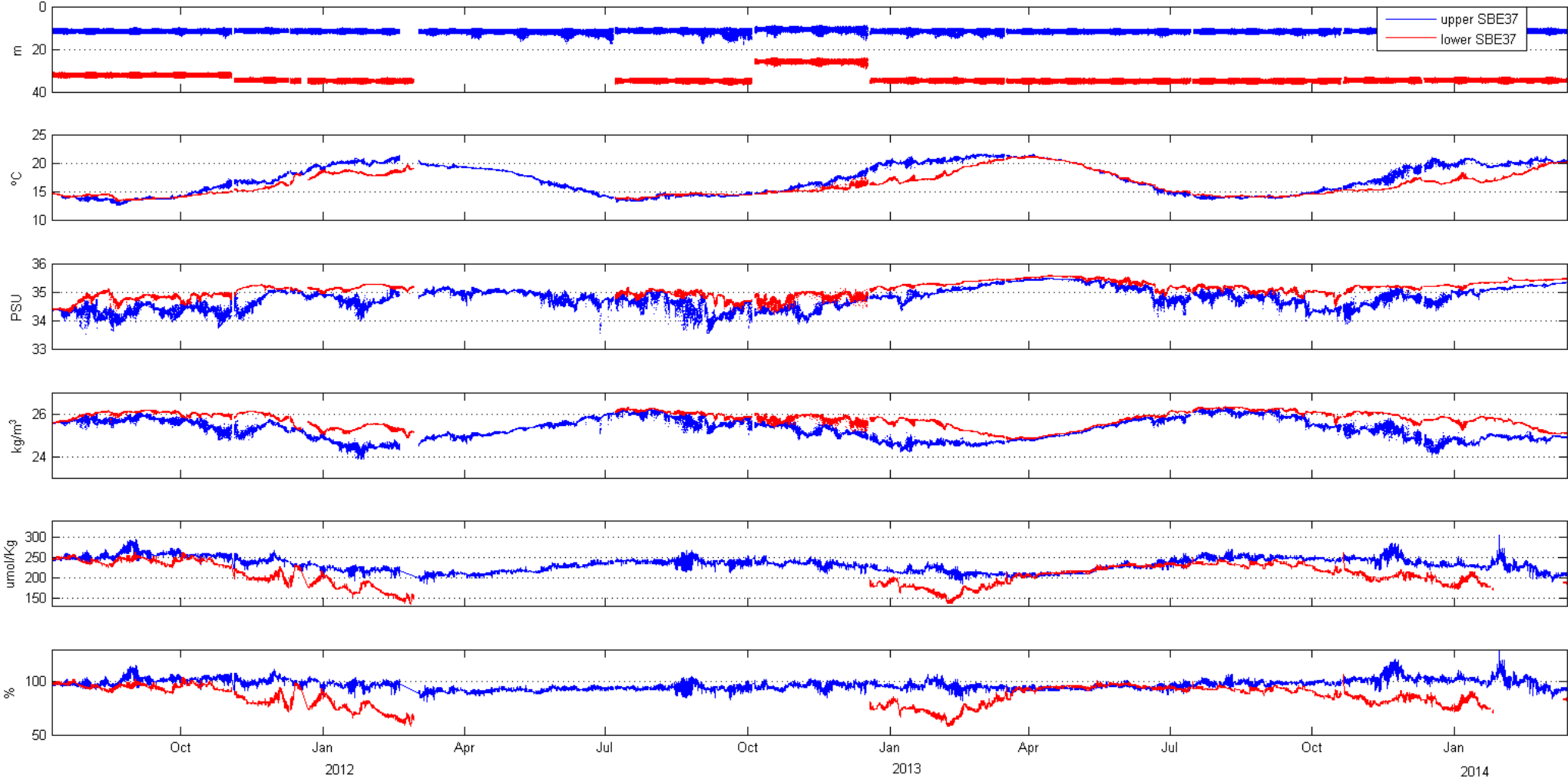|		
s0510fot1_2443_qc.mat	c0803fot1_1258_qc.mat	s1103fot1_2443_qc.mat
s0510fot2_2444_qc.mat	s0807fot1_2443_qc.mat	s1103fot2_5675_qc.mat
c0510fot2_1242_qc.mat	s0807fot2_2444_qc.mat	c1103fot1_647_qc.mat
c0510fot1_647_qc.mat	c0807fot2_1250_qc.mat	c1103fot2_847_qc.mat
s0512fot1_2443_qc.mat	c0807fot1_1258_qc.mat	s1107fot1_9022_qc.mat
s0512fot2_2444_qc.mat	s0810fot1_2443_qc.mat	s1107fot2_9023_qc.mat
c0512fot2_1242_qc.mat	s0810fot2_2444_qc.mat	c1107fot1_647_qc.mat
c0512fot1_647_qc.mat	c0810fot2_1250_qc.mat	c1107fot2_847_qc.mat
s0603fot1_2443_qc.mat	c0810fot1_1258_qc.mat	s1111fot1_9158_qc.mat
s0603fot2_2444_qc.mat	s0812fot1_2443_qc.mat	s1111fot2_9159_qc.mat
c0603fot2_1242_qc.mat	s0812fot2_2444_qc.mat	c1111fot1_647_qc.mat
c0603fot1_647_qc.mat	c0812fot2_1250_qc.mat	c1111fot2_847_qc.mat
s0607fot1_1689_qc.mat	c0812fot1_1258_qc.mat	s1112fot1_9158_qc.mat
s0607fot2_0376_qc.mat	s0903fot1_2443_qc.mat	s1112fot2_9159_qc.mat
c0607fot1_1250_qc.mat	s0903fot2_2444_qc.mat	c1112fot1_1242_qc.mat
c0607fot2_1258_qc.mat	c0903fot2_1250_qc.mat	c1112fot2_845_qc.mat
s0610fot1_2443_qc.mat	c0903fot1_1258_qc.mat	s1203fot1_9158_qc.mat
s0610fot2_2444_qc.mat	s0907fot2_2444_qc.mat	c1203fot1_1242_qc.mat
c0610fot1_1250_qc.mat	s0907fot1_4440_qc.mat	c1203fot2_845_qc.mat
c0610fot2_1258_qc.mat	c0907fot2_1250_qc.mat	s1207fot2_5351_qc.mat
s0612fot1_2443_qc.mat	c0907fot1_1258_qc.mat	s1207fot1_9158_qc.mat
s0612fot2_2444_qc.mat	s0909fot2_2444_qc.mat	s1210fot2_5351_qc.mat
c0612fot1_1242_qc.mat	s0909fot1_4440_qc.mat	s1210fot1_9158_qc.mat
c0612fot2_647_qc.mat	c0909fot2_1250_qc.mat	s1212fot2_10085_qc.mat
s0703fot1_2443_qc.mat	c0909fot1_1258_qc.mat	s1212fot1_9158_qc.mat
s0703fot2_2444_qc.mat	s0912fot1_2443_qc.mat	c1212fot2_1084_qc.mat
c0703fot1_1258_qc.mat	s0912fot2_2444_qc.mat	c1212fot1_1162_qc.mat
c0703fot2_647_qc.mat	c0912fot2_1250_qc.mat	s1303fot2_10085_qc.mat
s0707fot1_2443_qc.mat	c0912fot1_1258_qc.mat	s1303fot1_9158_qc.mat
s0707fot2_2444_qc.mat	s1003fot1_2443_qc.mat	c1303fot2_1084_qc.mat
c0707fot2_1250_qc.mat	s1003fot2_2444_qc.mat	c1303fot1_1162_qc.mat
c0707fot1_1258_qc.mat	c1003fot2_1250_qc.mat	s1307fot2_10085_qc.mat
s0709fot1_2443_qc.mat	c1003fot1_1258_qc.mat	s1307fot1_10512_qc.mat
s0709fot2_2444_qc.mat	s1007fot1_2443_qc.mat	c1307fot2_1167_qc.mat
c0709fot2_1250_qc.mat	s1007fot2_2444_qc.mat	c1307fot1_1168_qc.mat
c0709fot1_1258_qc.mat	c1007fot1_1258_qc.mat	s1310fot2_10085_qc.mat
s0712fot1_2443_qc.mat	s1010fot2_5675_qc.mat	s1310fot1_10512_qc.mat
s0712fot2_2444_qc.mat	c1010fot2_1228_qc.mat	c1310fot2_1167_qc.mat
c0712fot2_1250_qc.mat	c1010fot1_845_qc.mat	c1310fot1_1168_qc.mat
c0712fot1_1258_qc.mat	s1101fot1_2443_qc.mat	s1312fot2_10085_qc.mat
s0803fot1_2443_qc.mat	s1101fot2_5675_qc.mat	s1312fot1_10512_qc.mat
s0803fot2_2444_qc.mat	c1101fot1_647_qc.mat	c1312fot2_1167_qc.mat
c0803fot2_1250_qc.mat	c1101fot2_847_qc.mat	c1312fot1_1168_qc.mat

depth	component	S/N	length	rope
5 m	Sabel Beacon			
5 m	Viny 13B			
			1 m	3/16" wire jc
7 m	Fluor			
			2 m	3/16" wire jc
9 m	Viny 13B			
9 m	RCM9			
10 m	Microcat			
			4.2 m	3/16" wire jc
15 m	RBR t		3 m	3/16" wire jc
18 m	Viny Float 12B			
			2 m	3/16" wire jc
20 m	Fluor			
			7 m	3/16" wire jc
27 m	RBR t		5 m	3/16" wire jc
32 m	RCM9			
33 m	Viny 13B			
34 m	Isus frame with mcat			
			1 m	Chain 10mm
36 m	Viny Float 12B			
36 m	Viny12B pair			
37 m	AR			
			1 m	Chain 10mm
	anchor 155 kg			
39 m				

Figure D-12: Diagram showing the general layout of the NIWA FOT mooring. Instruments focused upon in this Appendix are highlighted in yellow.

Appendix E   Observations of depleted oxygen reported by O'Callaghan (2013)

Data from a miniDOT dissolved oxygen sensor deployed at Wilson B that were reported by O'Callaghan (2013) showed oxygen depletion in surface waters. This included the observation that during late winter through to spring 2012 surface waters in the Firth of Thames had dissolved oxygen levels of less than 4.1 mg L^{-1} over a period of 28 days.

We have subsequently determined that the miniDOT sensors were unacceptably affected by biofouling that rendered the data invalid.

As a result, we and do not stand by the miniDOT data and observations based on that data presented in O'Callaghan (2013).

Reference

O'Callaghan, J. (2013) Dissolved oxygen variability in Hauraki Gulf. NIWA Client Report, WLG2013-42, 21 p.

Appendix F   Carbonate Chemistry Methodology

Water Analysis
Discrete Samples – from CTD
Discrete samples were taken from the top (nominally 2 m depth) and bottom Nisken bottle at each CTD station. Either 1-L Schott bottles (combined DIC and alkalinity samples) or 250-mL Schott bottles (DIC) plus 1-L PET bottles (alkalinity) were filled using a sampling tube following standard water sampling protocols (Dickson et al. 2007). The samples were preserved with saturated mercuric chloride then analysed within 3 months.

Dissolved inorganic carbon concentration (DIC) was determined coulometrically using a SOMMA-based extraction system similar to that described by Dickson et al. (2007). The accuracy and precision of the method was estimated to be ± 1 μmol kg^{-1} based on the repeat analysis of Dickson Certified Reference Materials.

Total alkalinity was determined using a closed cell potentiometric titration (Dickson et al., 2007), and a curve fitting optimization with least squares analysis of the titration curve was used to obtain the total alkalinity. The accuracy and precision of the method was estimated to be ± 2 μmol kg^{-1} based on the repeat analysis of Dickson Certified Reference Materials.

Underway Sampling – continuous measurements of partial pressure of CO_2 in equilibrium with seawater (pCO_2)
Surface seawater was pumped through insulated garden-type hose to the analysis rig located in the wet lab of the RV Kaharoa, via a de-bubbler and a SBE21 thermosalinograph. The main water inlet was located about 2 m below the surface in a metal fish that was hung from a boom off the starboard deck. For voyages KAH1209 and KAH1304 a centrifugal pump was used. A mono pump was used for voyages KAH1306 and KAH1311.

Water was equilibrated with a closed air loop in a water-jacketed equilibration chamber vented to maintain atmospheric pressure in the headspace. The equilibrated air was then dried and analyzed by a LiCor 6251 infra-red gas analyser (irga). The irga was calibrated with 3 standard gases and a "zero-gas" (ambient air passed through soda lime).

The data work-up consisted of accounting for the drift and offset of the irga CO_2 mol fraction using the standard gases, the drying of the saturated equilibrated air, and the warming of the seawater between the surface ocean and the equilibrator. The accuracy of the method is estimated to be ± 3 μatm, based on an intercalibration experiment.

Calculated parameters
Underway pH
Surface water pH at the in situ temperature was calculated on the total scale (pH_T) from the measured pCO2 and calculated alkalinity. Alkalinity was calculated from salinity using a linear relationship determined for each cruise using the discrete bottle samples.

Discrete pH (bottom water), aragonite saturation (Ω_a), and calcite saturation (Ω_c) were calculated from measured alkalinity and DIC using the CTD temperature, salinity and depth values, and the Mehrbach dissociation constants (Mehrbach et al. 1973) as refitted by Dickson and Millero (1987).

Table F-1: CO$_2$ standard gases used to calibrate pCO2 system.

Cruise	Calibrations Standards used XCO_2 / ppmv
KAH1209	0.0, 334.6 (Kim), 425.6 (Cliff), 505.0 (Cliff)
KAH1304	0.0, 334.6 (Kim), 379.1 (Kim) 407.6 (Kim)
KAH1306	0.0, 334.6 (Kim), 379.1 (Kim) 407.6 (Kim)
KAH1311	0.0, 334.6 (Kim), 379.1 (Kim) 407.6 (Kim)

Table F-2: Alkalinity–salinity relationship, surface samples (2 m).

Cruise	AT- S relationship	R2	Notes
KAH1209	$A_T = 57.323 * Sal + 236$	0.98	Exclude one point
KAH1304	$A_T = 99.559 * Sal - 1203$	0.97	
KAH1306	$A_T = 45.974 * Sal + 691$	0.97	
KAH1311	$A_T = 53.227 * Sal + 433$	0.94	Exclude one point

Over-determination

pCO$_2$ calculated from measured DIC and alkalinity at each station (top Nisken, 2 m) can be compared with the pCO2 measured using the underway system. This gives an indication of the internal consistency of the measurements. The pCO$_2$ at each station was determined at the CTD start time ± 1 min. If this datum was not available (due to, for example, the station corresponding to a pCO2 calibration period) then a nearby time was used if possible.

The average and ranges of the offsets between the measured pCO$_2$ and calculated pCO$_2$ (= ΔpCO$_2$) for each cruise are given in Table F-3. The offsets could be due to errors in each measurement, inappropriate equilibrium constant being used, or the samples being compromised in some way. On several occasions the pCO$_2$ increased while on station, possiblely as the towfish settled in the water when the vessel was stationary.

Table F-3: Overdetermination:, ΔpCO$_2$ = pCO$_2$ (measured) - pCO$_2$ (calculated) / μatm

Cruise	mean	range
KAH1209	30	5 to- 54
KAH1304	4	-12 to 24
KAH1306	0	-24 to +27, but mostly -6 -6
KAH1311	11	-17 to +38

Data presentation
Underway data

The pCO$_2$ data were matched with latitude, longitude, temperature and salinity data using NZST, and averaged into 30 second bins. Ocean Data View was used to prepare ribbon plots of surface underway parameters for each cruise.

Discrete data

The bottle data are plotted using ODV as surface and "bottom" values, where "bottom" is the depth of the deepest CTD bottle.

References

Dickson, A., Millero, F. (1987) A comparison of the equilibrium constants for the dissociation of carbonic acid in seawater media. *Deep-Sea Research*, 34: 1733-1743.

Dickson, A., Sabine, C., Christian, J. (2007) *Guide to best practices for ocean CO$_2$ measurements*. PICES Special Publication 3 IOCCP Report, 3: 191.

Mehrbach, C., Culberson, C., Hawley, J., Pytkowicz, R. (1973) Measurement of the apparent dissociation constants of carbonic acid in seawater at atmospheric pressure. *Limnology and Oceanography*, 19(6): 897-907.